

*C.P. ...
Ved
for ...*

Outer Continental Shelf Environmental Assessment Program

Final Reports of Principal Investigators

Volume 39

May 1986



U.S. DEPARTMENT OF COMMERCE
National Oceanic and Atmospheric Administration
National Ocean Service
Office of Oceanography and Marine Assessment
Ocean Assessments Division
Alaska Office



U.S. DEPARTMENT OF THE INTERIOR
Minerals Management Service
OCS Study, MMS 86-0031

"Outer Continental Shelf Environmental Assessment Program Final Reports of Principal Investigators" ("OCSEAP Final Reports") continues the series entitled "Environmental Assessment of the Alaskan Continental Shelf Final Reports of Principal Investigators."

It is suggested that sections of this publication be cited as follows:

Kozo, T. L. 1984. Mesoscale meteorology of the Norton Sound region. U.S. Dep. Commer., NOAA, OCSEAP Final Rep. 39:1-102

Kozo, T. L. 1984. Short term prediction (newcasting) of net daily sea ice movement in the Bering Strait with a mesoscale meteorological network. U.S. Dep. of Commer., NOAA, OCSEAP Final Rep. 39:103-160

Kozo, T. L. 1985. Wave hindcast statistics for the Hope Basin, north Chukchi and south Chukchi areas. U.S. Dep. of Commer., NOAA, OCSEAP Final Rep. 39:161-262

Kozo, T. L. 1985. Headland modeling applied to the eastern Beaufort Sea coast. U.S. Dep. of Commer., NOAA, OCSEAP Final Rep. 39:263-312

Kozo, T. L. 1985. Superstructure icing in the north Chukchi, south Chukchi and Hope Basin areas. U.S. Dep. of Commer., NOAA, OCSEAP Final Rep. 39:313-360

OCSEAP Final Reports are published by the U.S. Department of Commerce, National Oceanic and Atmospheric Administration, National Ocean Service, Office of Oceanography and Marine Assessment, Ocean Assessments Division, Alaska Office, Anchorage, and primarily funded by the Minerals Management Service, U.S. Department of the Interior, through interagency agreement.

Requests for receipt of OCSEAP Final Reports on a continuing basis should be addressed to:

NOAA-OMA-OAD
Alaska Office
701 C Street
P. O. Box 56
Anchorage, AK 99513

OUTER CONTINENTAL SHELF
ENVIRONMENTAL ASSESSMENT PROGRAM
FINAL REPORTS OF PRINCIPAL INVESTIGATORS

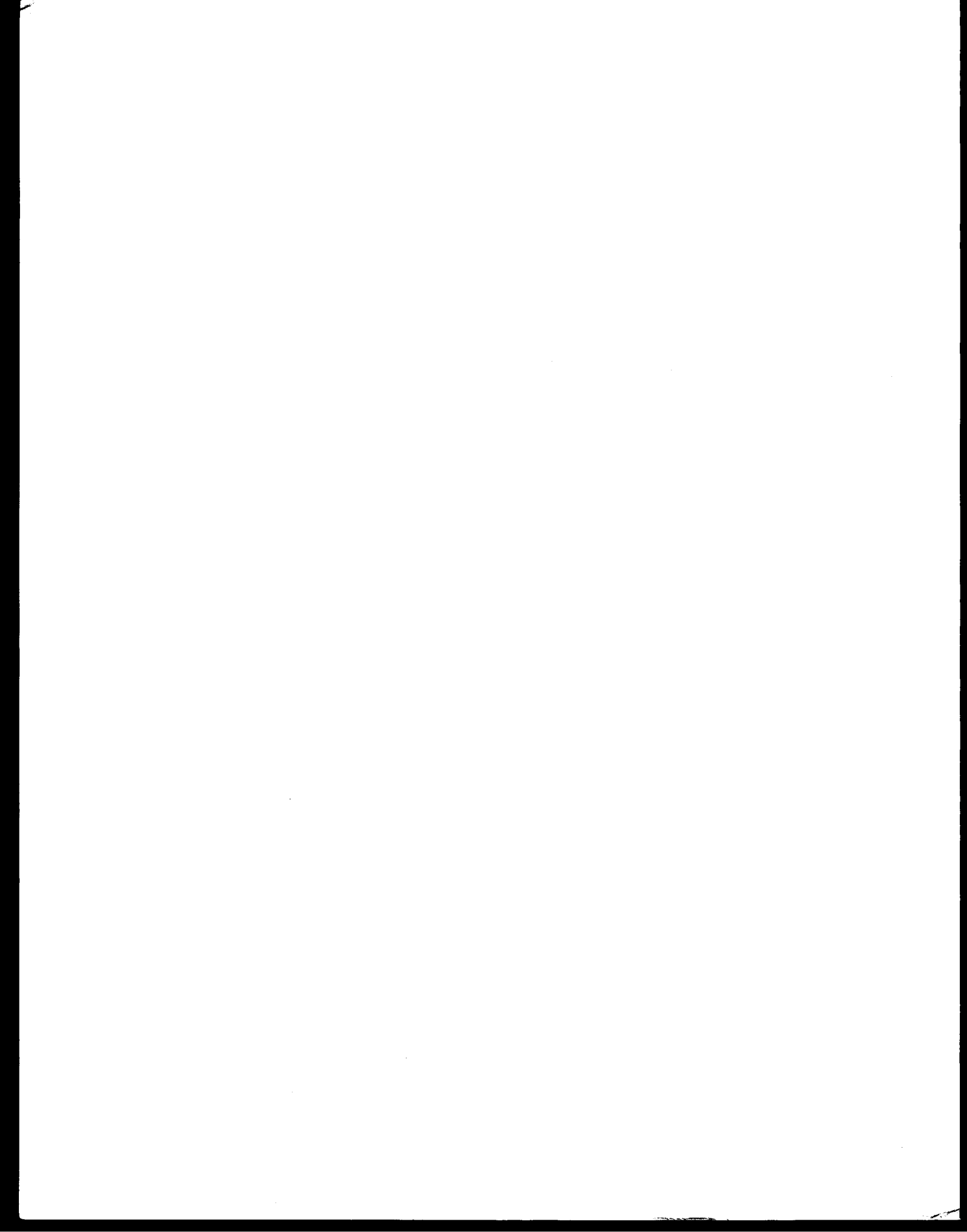
Volume 39

May 1986

U.S. DEPARTMENT OF COMMERCE
National Oceanic and Atmospheric Administration
National Ocean Service
Office of Oceanography and Marine Assessment
Ocean Assessments Division
Alaska Office

U.S. DEPARTMENT OF THE INTERIOR
Minerals Management Service
Alaska OCS Region
OCS Study, MMS 86-0031

Anchorage, Alaska



The facts, conclusions, and issues appearing in these reports are based on research results of the Outer Continental Shelf Environmental Assessment Program (OCSEAP), which is managed by the National Oceanic and Atmospheric Administration, U.S. Department of Commerce, and funded (wholly or in part) by the Minerals Management Service, U.S. Department of the Interior, through an Interagency Agreement.

Mention of a commercial company or product does not constitute endorsement by the National Oceanic and Atmospheric Administration. Use for publicity or advertising purposes of information from this publication concerning proprietary products or the tests of such products is not authorized.

Content of these reports has not been altered from that submitted by the Principal Investigators. In some instances, minor grammatical, spelling, and punctuation errors have been corrected to improve readability; some figures, charts, and tables have been enhanced to improve clarity in reproduction.



Outer Continental Shelf Environmental Assessment Program
Final Reports of Principal Investigators

VOLUME 39

MAY 1986

C O N T E N T S

T. L. KOZO: Mesoscale meteorology of the Norton Sound region	1
T. L. KOZO: Short term prediction (newcasting) of net daily sea ice movement in the Bering Strait with a mesoscale meteorological network	103
T. L. KOZO: Wave hindcast statistics for the Hope Basin, north Chukchi and south Chukchi areas	161
T. L. KOZO: Headland modeling applied to the eastern Beaufort Sea coast	263
T. L. KOZO: Superstructure icing in the north Chukchi, south Chukchi and Hope Basin areas	313

MESOSCALE METEOROLOGY OF THE NORTON SOUND REGION

by

Thomas L. Kozo, Ph.D.

VANTUNA Research Group

Occidental College

Final Report
Outer Continental Shelf Environmental Assessment Program
Research Unit 519

1984

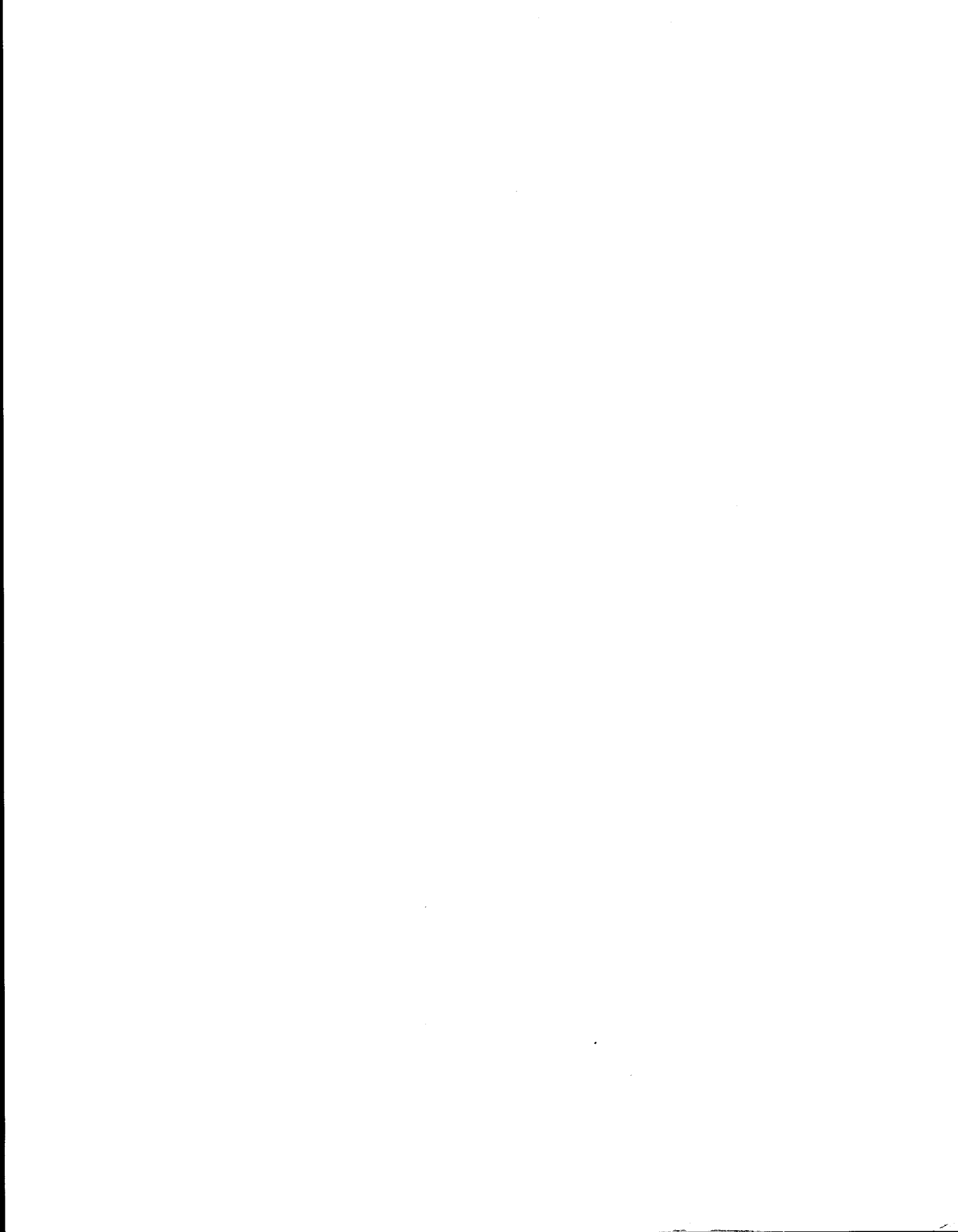


TABLE OF CONTENTS

LIST OF FIGURES.....	
LIST OF TABLES.....	
ABSTRACT.....	
1. INTRODUCTION.....	
2. STUDY AREA.....	
3. DATA.....	
a. Geostrophic Wind Data.....	
b. Surface Wind Data.....	
4. ANALYTICAL TOOLS.....	
a. Rotary Spectra.....	
b. Steadiness Tests.....	
c. Cross Correlation and Cross Spectrum Analysis.....	
d. Bivariate Distributions.....	
5. RESULTS WITH DISCUSSION.....	
a. General Characterisitcs (1964-1968 Data).....	
b. Large Scale Versus Mesoscale Winds.....	
c. Analysis of Surface Wind Time Series.....	
6. SUMMARY AND CONCLUSIONS.....	
7. REFERENCES.....	
8. APPENDIX A (Bivariate Distributions for Nome and Unalakleet).....	
9. APPENDIX B (Rotary Spectra from Northeast Cape, Unalakleet, and Nome).....	

.

LIST OF FIGURES

- Fig. 1. The triangular surface pressure network formed by the data stations at Nome, Unalakleet and Northeast Cape surrounding Norton Sound. The general summer surface wind directions at Nome and Unalakleet are shown by the small arrows. The general synoptic wind direction is shown by the large arrow. The Yukon Delta tip is designated Y. The dashed line represents the typical extent of mesoscale winds in the nearshore area.....
- Fig. 2. The same Norton Sound network as Fig. 1 is shown. The general winter surface wind directions are shown by the small arrows. The synoptic wind direction is shown by the large arrow. Y represents the tip of the Yukon Delta. The major ice movement in the Sound during winter is due to synoptic winds not local ones.....
- Fig. 3. The monthly average speeds at Nome (N), Unalakleet (U) and Northeast Cape (C) over a five year period (1964-1968).....
- Fig. 4. The monthly average air temperatures for Nome (N), Unalakleet (U) and Northeast Cape (C).....
- Fig. 5. Steadiness (decimal equivalent) of the surface winds at Unalakleet (U), Nome (N), and Northeast Cape (C).....
- Fig. 6. Average position of the ice edge in May (from Brower et al., 1977).....
- Fig. 7. Average position of the ice edge in November (from Brower et al., 1977).....

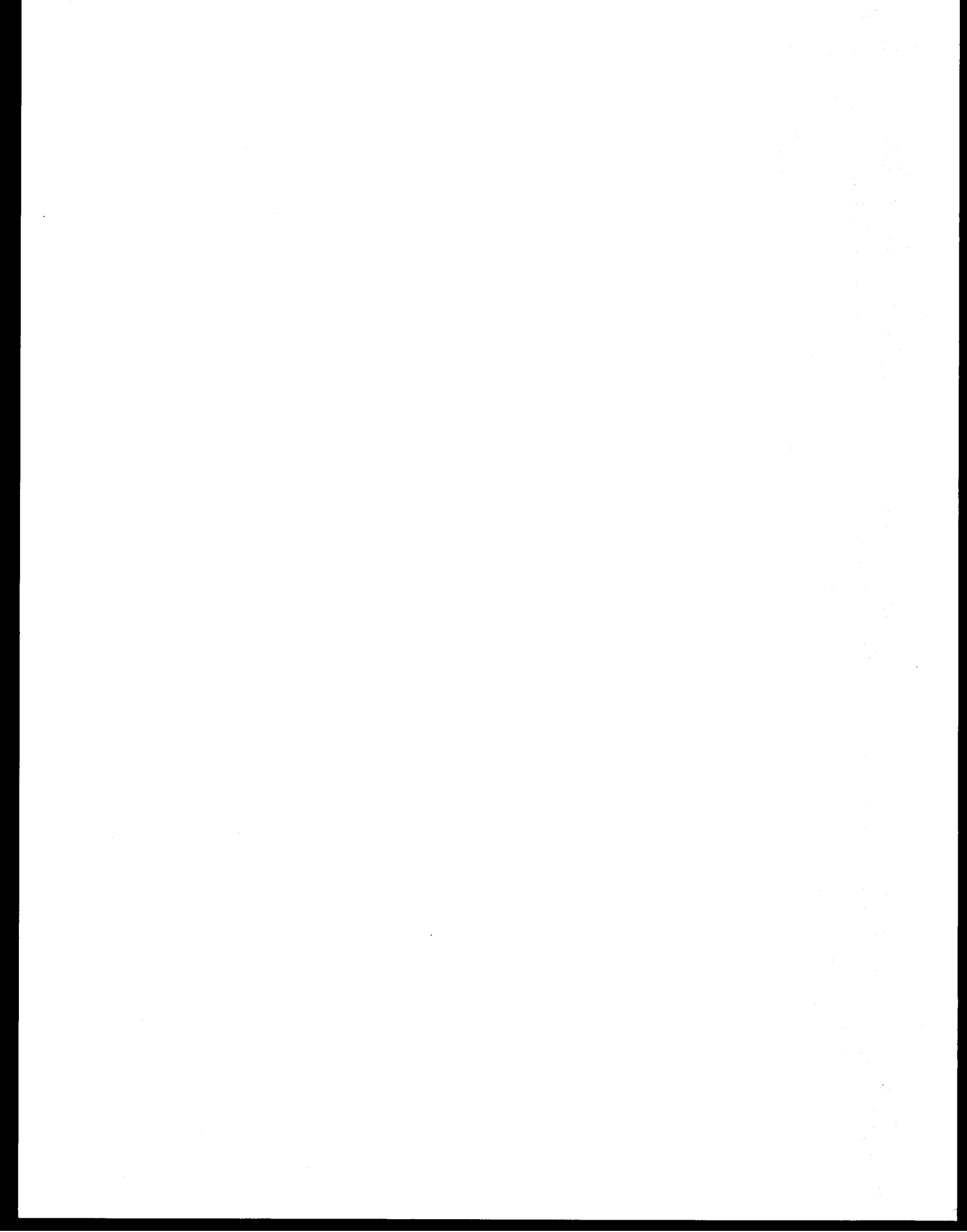
- Fig. 8. Cross correlation values for time series of wind velocity data from land surface wind stations versus distance of separation. The solid line was developed for stations on the Chukchi and Beaufort coasts as well as islands in the Bering Sea. The dashed line represents cross correlation wind data between Nome and Northeast Cape (N-C), Northeast Cape and Unalakleet (C-U), and Nome and Unalakleet (N-U)....
- Fig. 9. The average percentage directional distribution of the Nome (N), Unalakleet (U) and the calculated geostrophic (Vg) winds in January (1964-1968).....
- Fig. 10. The average percentage of occurrence for two types of corner effects at Unalakleet (U) and Nome (N). Seven months are shown for the 1964 to 1968 time period. The zero wind speed cases are designated B and the supergeostrophic wind cases are designated SG.....
- Fig. 11. The average occurrence percentage of cold air drainage (CAD) winds and sea breeze (SB) winds at Nome (N) and Unalakleet (U). Seven months are shown for the 1964 to 1968 time period.....
- Fig. 12. The average directional distribution (%) for Nome (N), Unalakleet (U) and the calculated geostrophic (Vg) winds in July (1964-1968).....
- Fig. 13. Major directions of offshore winds due to cold air drainage at Nome and Unalakleet.....

- Fig. 14. Major directions of onshore winds due to sea breeze influence at Nome and Unalakleet. The probable direction of these winds at the Yukon Delta are shown at the lowest arrow.....
- Fig. 15. The total amount of monthly mesoscale influence provided by mountain valley winds, sea breezes, corner effects and pure cold air drainage combined for Nome and Unalakleet (1964-1968).....
- Fig. 16. Time series rotary spectra of surface wind velocity data from Unalakleet, Northeast Cape, and Nome for (a) January, 1964 and (b) November, 1968.....
- Fig. 17. Time series rotary spectra of surface wind velocity data from Unalakleet, Northeast Cape, and Nome for (a) May, 1968 and (b) November 1968.....
- Fig. 18. The average monthly coherence (1964-1968) between sea breeze winds at Nome and Unalakleet. These winds have a one day period on the CW (-) side of spectral plots such as seen in Figs. 16 and 17. The dashed line represents the 1% coherence limit for 10 degrees of freedom.....
- Fig. 19. The normal diurnal variation of air currents in a valley (Fairbridge, 1967). (a-h): a. sunrise--onset of upslope winds (white arrows) and the continuation of mountain drainage winds (black arrows); b. forenoon--transition from down mountain to up valley winds; c. early afternoon--the fully developed valley wind with diminishing slope winds;

d. late afternoon--the valley wind; e. evening--the beginning of downslope winds and a diminishing valley wind; f. early night--the transition from valley to mountain winds showing well-developed downslope winds; g. middle of the night--continuing downslope winds and fully developed mountain winds; h. late night to morning--downslope winds ceasing with full mountain winds.....

LIST OF TABLES

- Table 1. Bivariate distribution of wind direction versus wind speed data (three hourly) for Unalakleet, Alaska in January, 1966. Winds above 14 ms^{-1} are considered gale class.....
- Table 2. Bivariate distribution of calculated geostrophic winds (V_g) versus Unalakleet simultaneous surface winds (U_s) for January, 1966. Horizontal directions represent the same sectors as the vertical except that 0 is the middle of the 348.5° - 11.0° sector instead of the minimum direction value..
- Table 3. Bivariate distribution of wind direction versus wind speed data (three hourly) for Unalakleet, Alaska in July, 1967. Winds above 14 ms^{-1} are considered gale class.....
- Table 4. Bivariate distribution of calculated geostrophic winds (V_g) versus Unalakleet simultaneous surface winds (U_s) for July, 1967. Horizontal directions represent the same sectors as the vertical except that 0 is the middle of the 348.5° - 11.0° sector instead of the minimum direction value.....



ABSTRACT

An analysis of the 1964-1968 surface winds, pressures and temperatures at weather stations surrounding Norton Sound was performed. The stations chosen for their network geometry were Northeast Cape (St. Lawrence Island), Nome, and Unalakleet. Surface pressure data from this network were used to calculate geostrophic wind velocities for the Sound center which are "immune" from orographic or thermally generated effects seen to exist only in a 20 km zone seaward of the coast. The stations were particularly suited for the mesoscale part of this study because Nome's coastline is perpendicular to Unalakleet's and each has small mountain ranges inland. Northeast Cape was outside the Sound on the tip of a small peninsula. This allowed for simultaneous comparison of sea breeze effects (summer) and orographic effects (mainly winter) on surface wind velocities at the three sites. The most important parts of this study are broken down into general characteristics, orographic effects, thermal effects and combined thermal and orographic effects.

The surface winds at the three coastal sites showed a higher steadiness when the sea in their vicinity was ice covered. The February average temperatures reached -19°C for all three stations and the July average temperature at Unalakleet reached 12°C (other two stations slightly lower). The Northeast Cape temperatures were moderated since it was on an island in the Bering Sea. Average wind speeds of 7.5 ms^{-1} were reached in the months of January and November for Unalakleet and Northeast Cape respectively. The average wind speeds recorded at Nome were generally lower than the other sites due to periods of 0 wind velocities caused by orographic blockage and

corner effects. This result and other data (particularly wind direction data) contained in this study indicate that Nome winds should not be used for Bering Sea transport models. Cross correlation values obtained from time series analysis of wind data from the above three stations were significantly less than that obtained in other areas of Alaskan Arctic. This points to a profound influence of orographic and thermal mesoscale effects.

Orographic effects at Nome and Unalakleet were most evident in the winter months. A major factor was cold air drainage down their respective river valleys which were oriented perpendicular to coastlines. Maximum cold air drainage winds recorded at Unalakleet were 16 ms^{-1} and 14.5 ms^{-1} at Nome. This effect alone occurred 20% of the time at Unalakleet in January. Ten percent of all wind velocities recorded at Nome for January and February were zero.

Thermal effects were seen as sea breezes in the Sound during open water months. The month of greatest occurrence (largest thermal contrast between land and water) was July at both Nome and Unalakleet when pure sea breeze effects controlled 23% of the measured wind velocities. The highest sea breeze velocities reached 10.8 ms^{-1} at both of the sites within Norton Sound during the local afternoons.

A discovery was made when examining summer rotary spectra of station wind time series from Unalakleet and Nome. A mountain valley wind system (combined thermal and orographic effect) was evident at both stations. This system produces up valley winds (enhances shoreward sea breeze flow) from the late morning to evening hours and down valley winds (creates an offshore wind) in the late evening and early morning hours. Therefore, a pseudo

summer land breeze can exist in the Arctic producing offshore winds in areas with river valleys. The maximum offshore winds due to this effect (hard to separate onshore sea breeze from onshore mountain valley wind) were 11.32 ms^{-1} at Nome and 10.8 ms^{-1} at Unalakleet and may reach 20 km offshore. Comparison of the network generated geostrophic winds with the coastal site surface winds showed pure orographic effects dominating in the months of total ice cover within the Sound. The thermal effects causing sea breezes and combined thermal-orographic effect of the mountain valley winds dominated in the open water months. The combined mesoscale effects in the open water months of July and August averaged 33% for Unalakleet and 26% for Nome. The geostrophic directions evident from this five year data base study showed that the Yukon Delta would be susceptible to large scale winds pushing contaminants from the west onshore in the open water months. The thermal contrast between the ocean and land would act in a 20 km coastal zone to push contaminants shoreward during weak large scale winds. The Delta does not have the orography to create a mountain valley wind system with periodic offshore winds and has a convex coastline which would further focus the onshore sea breeze effect.

1. Introduction

The prospect of oil development in the Norton Sound area has resulted in recent studies of the wind field both offshore and nearshore with a view to refining predictions of summer oil spill trajectories and winter ice movement. Histograms (Brower et al., 1977) of surface winds at coastal data sites surrounding the Sound show evidence of thermally driven local winds in the summer blowing toward the site shoreline. In other Alaskan areas Kozo (1982) has shown that sea breeze type winds can dominate a 20 km coastal zone at least 25% of the time during Arctic open water months. Winter surface wind velocity distributions (Brower et al., 1977) at coastal sites also show obvious orographic effects due to mountain channeling and cold air drainage (Katabatic type). The Sound is considered an ice factory supplying 10 times its area of ice to the Bering Sea (Thomas and Pritchard, 1981). The dominant winter wind directions measured at coastal sites would tend to move ice out of the Sound if these directions truly represented the synoptic wind directions rather than purely local winds.

The Yukon Delta region appears to be one of extreme vulnerability to oil spill and storm surge run-up during open water months. Unfortunately, only limited surface environmental data have been acquired there. Surface pressure data from coastal sites surrounding the Sound (Figs. 1 and 2) could be used to define a useful geostrophic wind to approximate the large scale wind field offshore and near the Delta. The Delta is subject to these synoptic winds with minimal orographic influence, but should have enhanced thermal influence in the summer due to sea breeze wind focusing caused by a convex coastline (McPherson, 1970).

The problem of differentiating between synoptic wind characteristics which would affect the Sound proper and the measured coastal wind characteristics which are often "contaminated" by mesoscale effects is always there. This masking (Kozo, 1984) is important in the summer since the thermally induced mesoscale effects perturb the coastal wind statistics and often do not characterize the winds beyond 20 km offshore. Masking is important in the ice covered months because the orographic drainage and corner effect winds (Kozo, 1984) at the coastal sites may be 180° off in direction from the "real" winds in the middle of the Sound which actually push the ice.

It is easy to see then, that the modeling of oil spill trajectories or ice movement cannot proceed without some offshore wind data or approximations to offshore wind data. Also, the monthly amount of mesoscale modification and threshold velocities for this modification must be quantified if shore station data are to be used in modeling.

2. Study Area

Norton Sound is a "peninsula" of water surrounded by mountains on all but its west flank. It can be seen in Fig. 1 with the general summer large scale wind direction (taken from this study) depicted within the triangle. The dashed line is the approximate seaward distance of onshore push created by sea breezes. The smaller wind arrows at Nome and Unalakleet (two of the three data sites used in this study) show their average summer wind directions. The orientation of the coastline at Nome and the typical onshore sea breeze influence are responsible for the difference in the average measured surface wind direction from the large scale direction.

The synoptic wind and the sea breeze wind are parallel at Unalakleet making pure directional tests bad for separating the two wind types at that site. There are three rivers intersecting at Nome, with at least two associated mountain valley systems to the north. Unalakleet has only one main river with a mountain valley system running east-west. These directions are evident during mountain valley wind events, particularly in the late evening to early morning, due to down valley winds. Y represents the tip of the Yukon Delta with its convex sea breeze focusing coast. Northeast Cape, the third station in our study network, was a United States Air Force Weather Station functioning only during the sixties. This convenient network geometry had not existed again until the eighties when Brown and Caldwell installed a satellite transmitting weather station on St. Lawrence Island for an EXXON sponsored study. Figure 2 shows the general winter large scale wind direction inside the triangle. The smaller arrows at Nome and Unalakleet again show their average wind directions during the winter. There is no sea breeze during this season, but mesoscale effects appear which can mask the real wind directions offshore. The surface station wind data arrows are influenced by cold air drainage through their inland river valleys. Again pure direction tests are not helpful to differentiate local winds from synoptic winds at Unalakleet, but are very revealing for Nome which can have average winds quite different in direction from the large scale winds affecting the Sound proper. Pure blockage of wind by mountain ranges and the corner effects (Kozo, 1984; Dickey, 1961) act to reduce wind velocities at Nome also.

3. Data

a. Geostrophic wind data

The wind arrows for the summer and winter in the above figures were computed from barometric pressure and temperature data provided by National Weather Service (NWS) approved stations at Nome, Northeast Cape and Unalakleet from 1964 through 1968. The accuracies of these temperature and pressure data are better than $\pm 1^\circ\text{C}$ and $\pm .25$ mb respectively. The atmospheric flow was assumed to be in geostrophic balance (1):

$$f(k \times V) + \frac{\nabla p}{\rho} = 0 \quad (1)$$

The first term is the Coriolis force, the second is the pressure gradient force. f is the Coriolis parameter ($1.31 \times 10^{-4} \text{ sec}^{-1}$ at 64°N), k is the vertical unit vector, V is the velocity vector, ∇p is the gradient of the atmospheric pressure and ρ is the temperature dependent air density. Using the above station grid (Fig. 1) and noting that pressure can be represented as a function of latitude (y) and longitude (x) on a plane surface, the following set of equations:

$$\begin{aligned} P_N(x,y) &= ax_N + by_N + c \\ P_U(x,y) &= ax_U + by_U + c \\ P_C(x,y) &= ax_C + by_C + c \end{aligned} \quad (2)$$

are generated, where the subscripts N, U, and C denote Nome, Unalakleet and Northeast Cape respectively. A matrix solution was applied to solve for the unknowns a , b , and c (Kozo, 1982). Since $\partial P/\partial x = a$, and $\partial P/\partial y = b$, the

pressure gradient (∇P) can be computed. The geostrophic velocity can now be calculated from (1) since f is known and ρ for dry air can be estimated from station temperatures. Station temperature errors of $\pm 1^\circ\text{C}$ will cause errors of less than 1% in velocity magnitudes since they only affect ρ estimates. With this network geometry (Fig. 1) errors in pressure of $\pm .25$ mb can cause maximum speed errors of 3 ms^{-1} and direction errors greater than $\pm 30^\circ$ for wind speeds below 5 ms^{-1} . Therefore, at wind speeds less than 5 ms^{-1} , wind directions should not be considered significant. Successful use of mesoscale networks to compute geostrophic winds and their increased resolution and predictive capabilities over NWS networks in the Arctic has been documented by Kozo (1980, 1984).

b. Surface wind data

Three hourly surface winds from coastal stations at Northeast Cape, Unalakleet and Nome were used for simultaneous comparison with the calculated geostrophic wind from the same network. Typical accuracies of Arctic type mechanical weather stations are $\pm 1\%$ of full scale (360°) for wind direction and $\pm 2\%$ of the measured value for wind speed (see Kozo 1982). The speed and direction data from Northeast Cape was important since it was out of the Sound proper and represented another "control" for testing the influence of mesoscale effects.

4. Analytical Tools

a. Rotary spectra

Surface wind data from the station network were examined with a rotary spectrum technique (Gonella, 1972). The variance for each frequency band is divided into clockwise (CW) rotating variance (negative frequency) and counterclockwise (CCW) rotating variance (positive frequency). The horizontal surface wind data time series were tested (O'Brien and Pillsbury, 1974) for the appearance of a significant peak on the CW rotating side of a rotary spectral plot corresponding to a one-day period characteristic of sea breezes.

b. Steadiness tests

Tropical trade winds have a steadiness greater than 90%. In the Arctic, wind steadiness tends to increase in the winter ice covered months and decrease in the summer (lower atmospheric stability) months. The definition can be seen in (3) from Halpern (1979):

$$ST = \frac{(\bar{u}^2 + \bar{v}^2)^{\frac{1}{2}}}{(u^2 + v^2)^{\frac{1}{2}}} \quad (3)$$

where the numerator is the magnitude of the mean wind vector and the denominator is the mean magnitude. The result is expressed in percent or decimal.

c. Cross correlation and cross spectrum analysis

Standard cross correlation techniques (Panofsky and Brier, 1968) were applied to the time series of wind velocities from the three network stations at both positive and negative time lags. Cross spectral analysis was used to determine whether the above correlations found were due to high frequency or low frequency components. Lastly, coherence tests were made to determine how good the relationship was between the different station wind time series at various significant periods.

d. Bivariate distributions

Tables of computed geostrophic wind directions and simultaneous surface wind directions and speeds were computed to determine mesoscale influences on the large scale wind field. The standard tables of surface wind direction versus surface wind speed were also constructed to match with the tables in Brower et al. (1977).

5. Results with Discussion

a. General characteristics (1964-1968 data)

Figure 3 is a monthly plot of the average wind speeds at Nome (N), Unalakleet (U) and Northeast Cape (C) over a five-year period. Only the key ice covered and open water months have been analyzed. These are January, February, April, May (transition month), July, August and November (transition month). The open water months showed lower wind speeds. The Nome wind speeds were less than the other two sites due to apparent periods of orographic blockage lasting up to two days (see below).

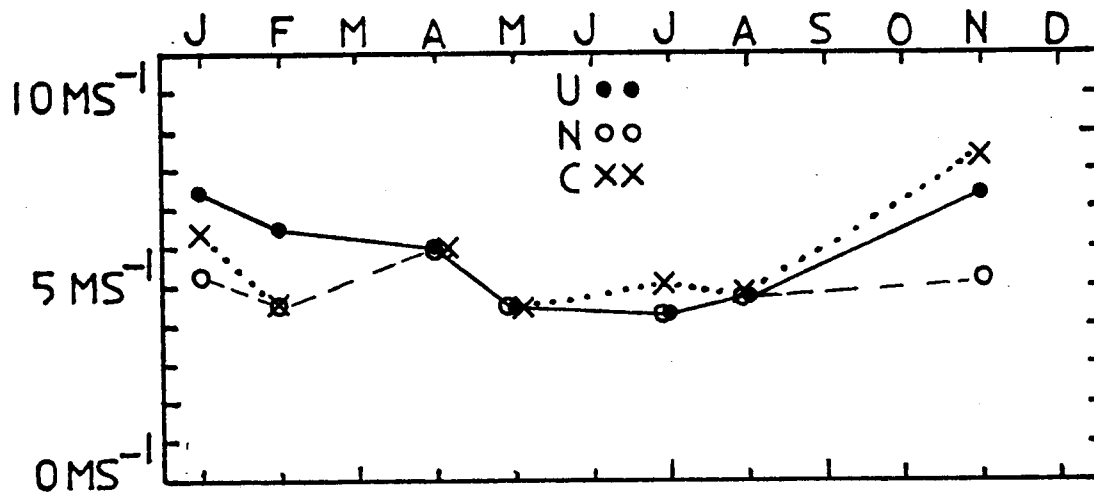


Fig. 3. The monthly average speeds at Nome (N), Unalakleet (U) and Northeast Cape (C) over a five year period (1964-1968).

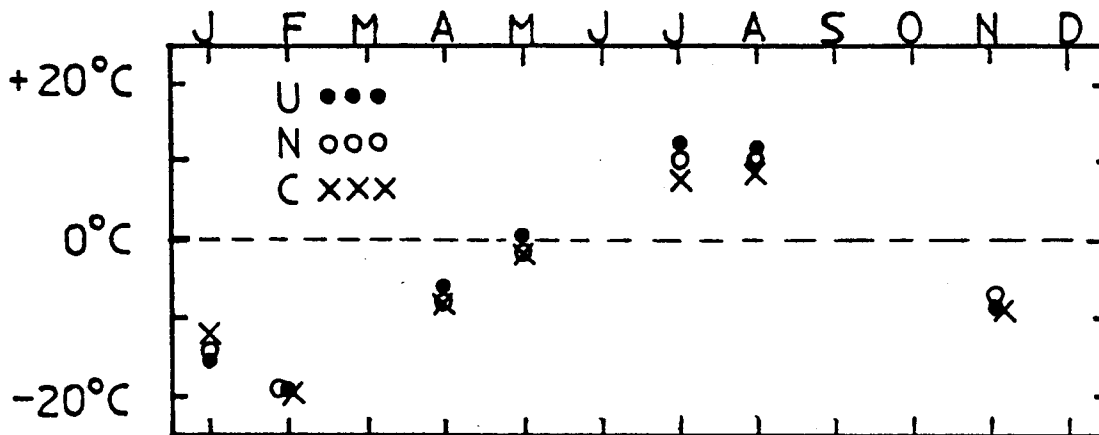


Fig. 4. The monthly average air temperatures for Nome (N), Unalakleet (U) and Northeast Cape (C),

Figure 4 shows a monthly plot of average air temperatures for Nome (N), Unalakleet (U) and Northeast Cape (C). The Northeast Cape temperatures were moderated since the site was on an island surrounded by Bering Sea water.

Figure 5 shows the steadiness (decimal equivalent) of the surface winds at the three designated study sites. The winds in the site vicinity were most steady when their respective offshore areas were ice covered. The ice covered months for Nome and Unalakleet were November through April while Northeast Cape was surrounded by ice from December through May (see Figs. 6 and 7). May and November represent periods of transition from solid ice cover to open water and open water to solid ice cover respectively. Unalakleet and Nome have a high steadiness (Fig. 5) in the winter months aided by orographic channelling but a low steadiness in the summer months due to the thermal contrast at the coast and mountain valley winds (see below). Northeast Cape is on a "tiny" peninsula with no preferred coastal orientation to produce a definite sea breeze direction or large system of mountain ranges to channel winds. It does, however, have some very local wind characteristics that are beyond the scope of this study.

Figure 8 is a plot of highest (lags from 0 to 15 hours) cross correlation values for time series of wind velocity data from land surface wind stations versus distance (km) of separation. The solid line was developed for stations on the Chukchi and Beaufort coasts as well as islands in the Bering Sea. None of these sites were subject to significant orographic modification, but all were subject to sea breeze effects. The coastlines of these previous land sites were usually parallel however, which improved the chances for higher correlations at 0 lags when synoptic winds were weak. The dashed line represents cross correlations between wind data from Nome and Northeast Cape (N-C), Northeast Cape and Unalakleet (C-U), and

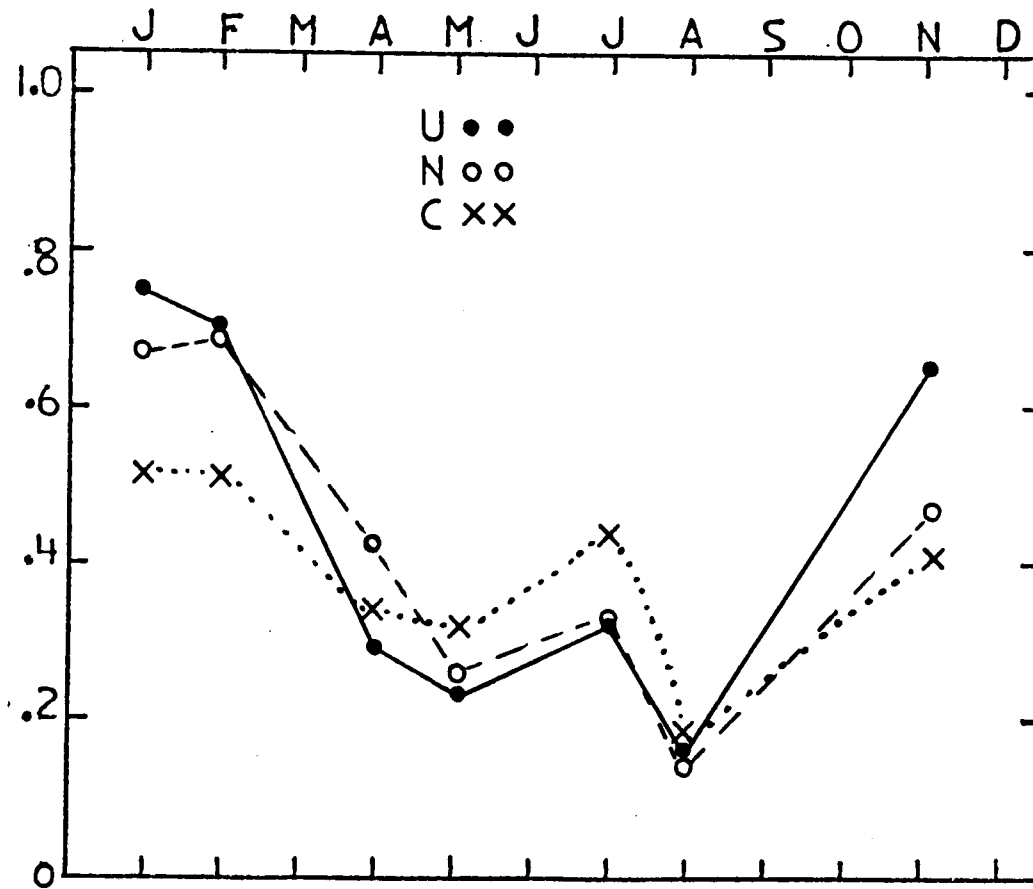


Fig. 5. Steadiness (decimal equivalent) of the surface winds at Unalakleet (U), Nome (N), and Northeast Cape (C).

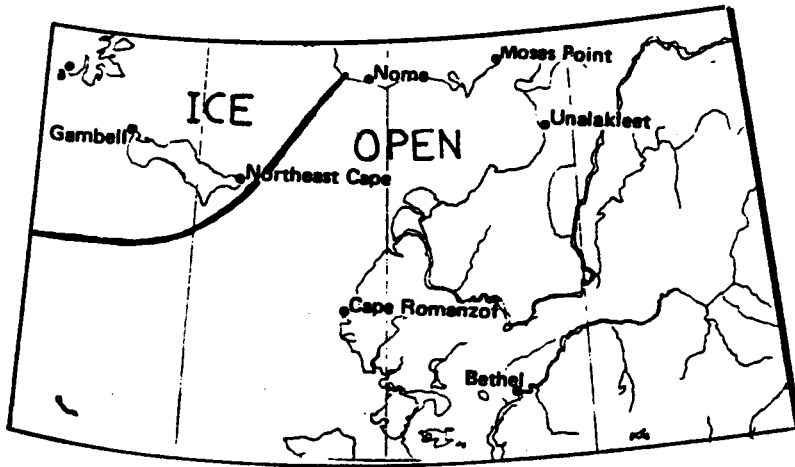


Fig. 6. Average position of the ice edge in May (from Brower et al., 1977).

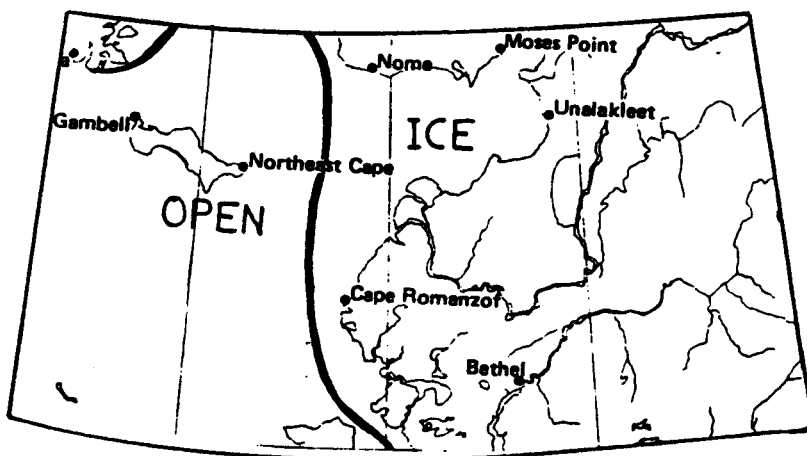


Fig. 7. Average position of the ice edge in November (from Brower et al., 1977).

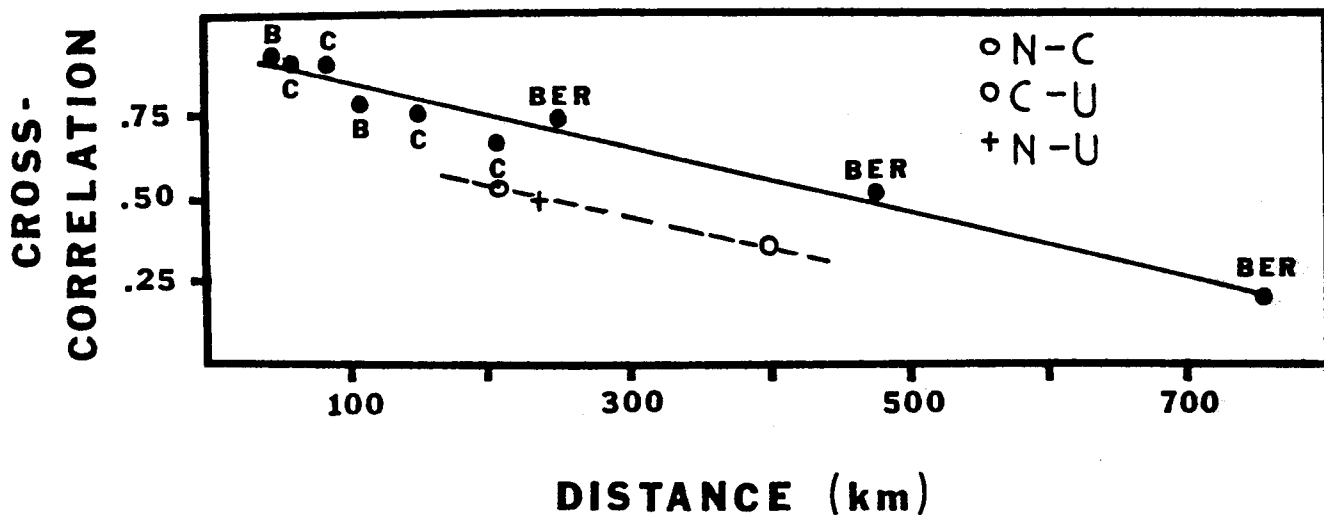


Fig. 8. Cross correlation values for time series of wind velocity data from land surface wind stations versus distance of separation. The solid line was developed for stations on the Chukchi and Beaufort coasts as well as islands in the Bering Sea. The dashed line represents cross correlation wind data between Nome and Northeast Cape (N-C), Northeast Cape and Unalakleet (C-U), and Nome and Unalakleet (N-U).

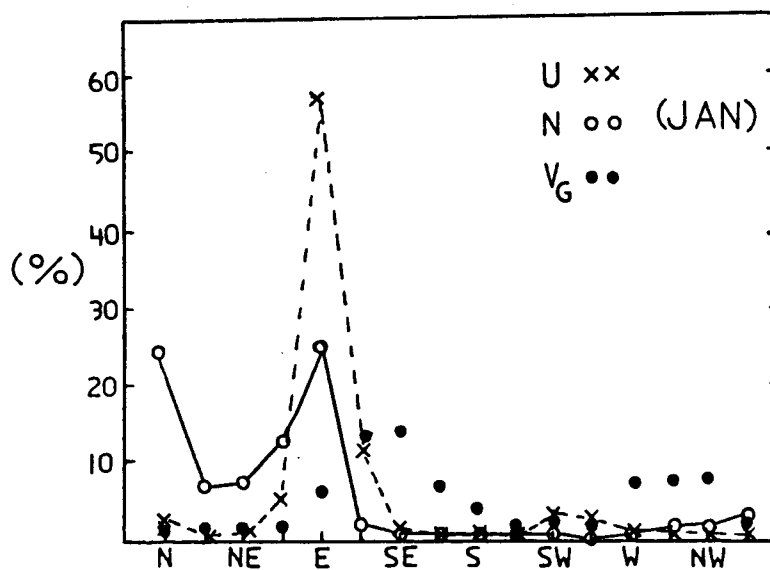


Fig. 9. The average percentage directional distribution of the Nome (N), Unalakleet (U) and the calculated geostrophic (V_g) winds in January (1964-1968).

Nome and Unalakleet (N-U). The correlation values are much lower than those previously obtained in other parts of the Alaskan Arctic. The influence of perpendicular coastline orientations (summer), perpendicular river valley cold air drainage systems (mainly winter) and preferred mountain blockage directions (winter) can easily be seen. Their effects on modifying the synoptic wind in the area are profound.

b. Large scale versus mesoscale winds

The geostrophic wind field in the Norton Sound area due to the atmospheric pressure gradient was calculated using standard techniques. The effect of land or water surface friction on this geostrophic wind should be a reduction in speed and 20° - 30° of CCW turning from the calculated direction (Kozo, 1984). Any turning of surface winds greater than this is a good indication of mesoscale influence. The surface winds at Nome and Unalakleet were compared simultaneously to the above calculated large scale wind to make quantitative estimates of these effects.

Table 1 is an extreme example of what winter orographic effects can do to the wind. In January 1966, 86% of the Unalakleet wind directions recorded were from 78.5° to 101.0° along with the highest wind speeds. Table 2 shows geostrophic wind (V_g) directions compared to simultaneous Unalakleet surface wind directions (U_s). The V_g direction distribution shows a large percentage of winds from at least four directions (78.5° - 101° , 101° - 123.5° , 123.5° - 146° , and 146° - 168.5°). The apparent wind turning from the calculated geostrophic direction to the surface is CW rather than "normal" CCW frictional turning and often more than 45° for a large number of cases. At least 30% of the surface winds in the 78.5° - 101° sector were due to some type of orographic

DIRECTION	S P E E D (ms ⁻¹)															(obs. 248)	
	0- 2	2- 4	4- 6	6- 8	8-10	10-12	12-14	14-16	16-18	18-20	20-22	22-24	24-26	26-28	28-30	TOTAL	PER
326.0-348.5	0	0	0	0	0	0	0	0	0	0	0	0	0	0	0	0	0.0
303.5-326.0	0	0	0	0	0	0	0	0	0	0	0	0	0	0	0	0	0.0
281.0-303.5	0	0	0	0	0	0	0	2	0	0	0	0	0	0	0	0	0.0
258.5-281.0	0	0	0	0	0	0	0	0	0	0	0	0	0	0	0	0	0.0
236.0-258.5	0	0	0	0	0	0	0	0	0	0	0	0	0	0	0	0	0.0
213.5-236.0	0	0	0	0	0	0	0	0	0	0	0	0	0	0	0	0	0.0
191.0-213.5	0	0	0	0	0	0	0	0	0	0	0	0	0	0	0	0	0.0
168.5-191.0	0	0	0	0	0	0	0	0	0	0	0	0	0	0	0	0	0.0
146.0-168.5	0	0	1	0	0	0	0	0	0	0	0	0	0	0	0	1	0.0
123.5-146.0	0	0	0	0	0	0	0	0	0	0	0	0	0	0	0	0	0.0
101.0-123.5	0	1	0	1	1	0	0	0	0	0	0	0	0	0	0	3	1.0
78.5-101.0	1	5	5	13	35	74	62	12	3	4	0	0	0	0	0	214	86.0
56.0- 78.5	0	1	3	4	8	11	1	1	0	0	0	0	0	0	0	29	11.0
33.5- 56.0	0	0	0	0	0	0	0	0	0	0	0	0	0	0	0	0	0.0
11.0- 33.5	0	0	0	0	0	1	0	0	0	0	0	0	0	0	0	1	0.0
348.5- 11.0	0	0	0	0	0	0	0	0	0	0	0	0	0	0	0	0	0.0

Table 1. Bivariate distribution of wind direction versus wind speed data (three hourly) for Unalakleet, Alaska in January, 1966. Winds above 14 ms⁻¹ are considered gale class.

D I R E C T I O N (Vg)	D I R E C T I O N (Us)															(obs. 248)		
	0.0	11.0	33.5	56.0	78.5	101.0	123.5	146.0	168.5	191.0	213.5	236.0	258.5	281.0	303.5	326.0	TOTAL	PER
326.0-348.5	0	0	0	1	5	0	0	0	0	0	0	0	0	0	0	0	6	2.0
303.5-326.0	0	0	0	0	2	0	0	0	0	0	0	0	0	0	0	0	2	0.0
281.0-303.5	0	0	0	1	2	1	0	0	0	0	0	0	0	0	0	0	4	1.0
258.5-281.0	0	0	0	1	4	0	0	0	0	0	0	0	0	0	0	0	5	2.0
236.0-258.5	0	0	0	1	1	0	0	0	0	0	0	0	0	0	0	0	2	0.0
213.5-236.0	0	0	0	0	3	0	0	0	0	0	0	0	0	0	0	0	3	1.0
191.0-213.5	0	0	0	0	3	0	0	0	0	0	0	0	0	0	0	0	3	1.0
168.5-191.0	0	0	0	0	4	0	0	0	0	0	0	0	0	0	0	0	4	1.0
146.0-168.5	0	0	0	0	19	0	0	0	0	0	0	0	0	0	0	0	19	7.0
123.5-146.0	0	0	0	6	59	0	0	1	0	0	0	0	0	0	0	0	66	26.0
101.0-123.5	0	1	0	9	72	2	0	0	0	0	0	0	0	0	0	0	84	33.0
78.5-101.0	0	0	0	4	27	0	0	0	0	0	0	0	0	0	0	0	31	12.0
56.0-78.5	0	0	0	3	4	0	0	0	0	0	0	0	0	0	0	0	7	2.0
33.5-56.0	0	0	0	0	3	0	0	0	0	0	0	0	0	0	0	0	3	1.0
11.0-33.5	0	0	0	2	4	0	0	0	0	0	0	0	0	0	0	0	6	2.0
348.5-11.0	0	0	0	1	2	0	0	0	0	0	0	0	0	0	0	0	3	1.0

Table 2. Bivariate distribution of calculated geostrophic winds (Vg) versus Unalakleet simultaneous surface winds (Us) for January, 1966. Horizontal directions represent the same sectors as the vertical except that 0 is the middle of the 348.5°-11.0° sector instead of the minimum direction value.

channeling. The extent of these winter effects in other years (1964-1968) can be seen in January bivariate distribution tables (Appendix A) for Unalakleet and Nome. Table 3 is a bivariate distribution of wind direction versus speed at Unalakleet for July, 1967. This Unalakleet wind distribution is similar to those shown in Brower et al. (1977) in the summer months. The summer mesoscale effects on the surface wind are due to the thermal contrast at the coast, the decrease in atmospheric stability with land warming, and mountain valley combined orographic-thermal phenomena. The distribution shows the typical increase in onshore winds over that of the winter months and also a decrease in frequency of easterly winds. Table 4, however, shows that 24% of the recorded surface SW to NW winds at Unalakleet occur simultaneous to geostrophic winds from 56° to 168° . Again, this "turning" of the geostrophic wind at the surface is CW rather than CCW and often greater than 45° . The extent of these summer effects in other years (1964-1968) can be seen in July bivariate distribution tables (Appendix A) for Unalakleet and Nome. As in winter, the surface wind histograms do not show the true large scale wind distribution which would be the major factor in surface pollutant and ice floe movement in the Sound proper.

Figure 9 shows a percentage directional distribution of the winds for Vg, Nome (N) and Unalakleet (U) in January (average of the years 1964-1968). The Vg distribution has a SE peak and a wide peak in W to NW winds. Again, the great dominance of the easterly winds at Unalakleet can be seen. As explained above, the combination of synoptic wind direction, channeling of winds and pure cold air drainage down a main river valley act to produce this unimodal distribution at Unalakleet. The directional distribution for Nome has two "bumps". The winds from the east are mainly large scale (synoptic), but those from the north are mesoscale in origin again caused by cold air

D I R E C T I O N

	S P E E D (ms^{-1})															(obs. 248)	
	0-2	2-4	4-6	6-8	8-10	10-12	12-14	14-16	16-18	18-20	20-22	22-24	24-26	26-28	28-30	TOTAL	PER
325.0-348.5	0	1	3	3	0	0	0	0	0	0	0	0	0	0	0	7	2.0
303.5-326.0	0	4	7	2	0	0	0	0	0	0	0	0	0	0	0	13	5.0
281.0-303.5	1	5	6	1	0	0	0	0	0	0	0	0	0	0	0	13	5.0
258.5-281.0	0	8	22	10	2	8	1	1	0	0	0	0	0	0	0	52	20.0
236.0-258.5	1	6	16	12	7	8	2	0	0	0	0	0	0	0	0	52	20.0
213.5-236.0	1	4	4	10	14	0	1	0	0	0	0	0	0	0	0	34	13.0
191.0-213.5	0	2	2	5	1	0	0	0	0	0	0	0	0	0	0	10	4.0
168.5-191.0	1	5	4	2	2	0	0	0	0	0	0	0	0	0	0	14	5.0
146.0-168.5	1	2	1	0	0	0	0	0	0	0	0	0	0	0	0	4	1.0
123.5-146.0	0	4	2	2	1	0	0	0	0	0	0	0	0	0	0	9	3.0
101.0-123.5	1	9	3	0	0	0	0	0	0	0	0	0	0	0	0	13	5.0
78.5-101.0	1	9	6	1	0	0	0	0	0	0	0	0	0	0	0	17	6.0
56.0-78.5	0	1	1	0	0	0	0	0	0	0	0	0	0	0	0	2	0.0
33.5-56.0	0	0	1	0	0	0	0	0	0	0	0	0	0	0	0	1	0.0
11.0-33.5	0	0	0	0	0	0	0	0	0	0	0	0	0	0	0	0	0.0
348.5-11.0	5	2	0	0	0	0	0	0	0	0	0	0	0	0	0	7	2.0

Table 3. Bivariate distribution of wind direction versus wind speed data (three hourly) for Unalakleet, Alaska in July, 1967. Winds above 14 ms^{-1} are considered gale class.

D I R E C T I O N (Vg)	D I R E C T I O N (Us)																TOTAL	PER
	0.0	11.0	33.5	56.0	78.5	101.0	123.5	146.0	168.5	191.0	213.5	236.0	258.5	281.0	303.5	326.0		
326.0-348.5	0	0	0	0	1	0	0	0	0	0	0	0	0	0	0	0	1	0.0
303.5-326.0	0	0	0	0	0	0	0	0	0	0	0	0	0	0	0	0	0	0.0
281.0-303.5	0	0	0	0	1	2	0	0	1	1	5	3	6	3	1	0	23	9.0
258.5-281.0	3	0	0	0	0	0	0	1	1	2	4	5	5	0	0	0	21	8.0
236.0-258.5	0	0	0	0	0	0	1	0	1	2	9	16	4	0	0	0	33	13.0
213.5-236.0	0	0	0	0	0	1	3	0	1	2	2	6	7	0	0	0	22	8.0
191.0-213.5	0	0	0	0	0	1	1	1	1	2	2	3	6	1	0	0	18	7.0
168.5-191.0	1	0	0	0	0	2	2	0	2	1	6	8	4	1	0	0	27	10.0
146.0-168.5	1	0	0	0	1	1	1	0	5	0	3	2	2	2	0	1	19	7.0
123.5-146.0	1	0	0	2	6	5	0	1	2	0	2	2	3	1	1	2	28	11.0
101.0-123.5	1	0	1	0	6	1	0	0	0	0	1	2	5	1	4	1	23	9.0
78.5-101.0	0	0	0	0	1	0	0	0	0	0	0	3	6	2	4	0	16	6.0
56.0-78.5	0	0	0	0	0	0	0	0	0	0	0	1	3	1	2	2	9	3.0
33.5-56.0	0	0	0	0	0	0	0	0	0	0	0	0	0	0	0	0	0	0.0
11.0-33.5	0	0	0	0	1	0	0	0	0	0	0	0	1	1	0	0	3	1.0
348.5-11.0	0	0	0	0	0	0	1	1	0	0	0	1	0	0	1	1	5	2.0

Table 4. Bivariate distribution of calculated geostrophic winds (Vg) versus Unalakleet simultaneous surface winds (Us) for July, 1967. Horizontal directions represent the same sectors as the vertical except that 0 is the middle of the 348.5°-11.0° sector instead of the minimum direction value.

drainage down its main river valley (runs north and south), channeling, and corner effects (Dickey, 1961). These corner effects will redirect winds and will produce simultaneous wind speeds that are supergeostrophic or almost zero depending on the large scale wind direction and orographic obstacle orientation. The monthly percentage occurrence of two types of corner effects (Fig. 10) can be seen at Nome and Unalakleet. These were measured zero winds (Nome [NB], Unalakleet [UB]) and supergeostrophic winds (Nome [NSG], Unalakleet [USG] for cases where V_g was greater than 6 ms^{-1}). The months with the Norton Sound completely ice covered and greatest atmospheric stability show the greatest occurrence of corner effects. The monthly percentage (Fig. 11) of cold air drainage (CAD) winds at Nome (NCAD) and Unalakleet (UCAD) is highest in the winter months when the sound is ice covered. However, the summer mountain-valley wind system will produce a high percentage of CAD during its night time cycle (see below). Pure CAD winds were observed during V_g speeds below 5 ms^{-1} . The highest CAD wind speeds measured were 14.5 ms^{-1} and 16 ms^{-1} at Nome and Unalakleet respectively in the winter. These were higher than the maximum CAD winds associated with summer mountain valley winds because daylight hours were minimal and no thermal contrast existed at the coast to cause a flow reversal.

Figure 12 shows the average percentage directional distribution of winds for V_g , Nome (N) and Unalakleet (U) in July (years 1964-1968). V_g has a broad SW to W peak. Unalakleet has a small east peak and a broad peak in the SW to W sectors. Nome has a peak in the North, South and SW-W sectors. There is no striking dominance of direction as seen in Fig. 9. The east peak in the Unalakleet and north peak in the Nome distributions are mainly due to CAD from their respective mountain valley systems (see Fig. 13). The maximum CAD winds in the summer reached 11.3 ms^{-1} and 10.8 ms^{-1} at Nome and

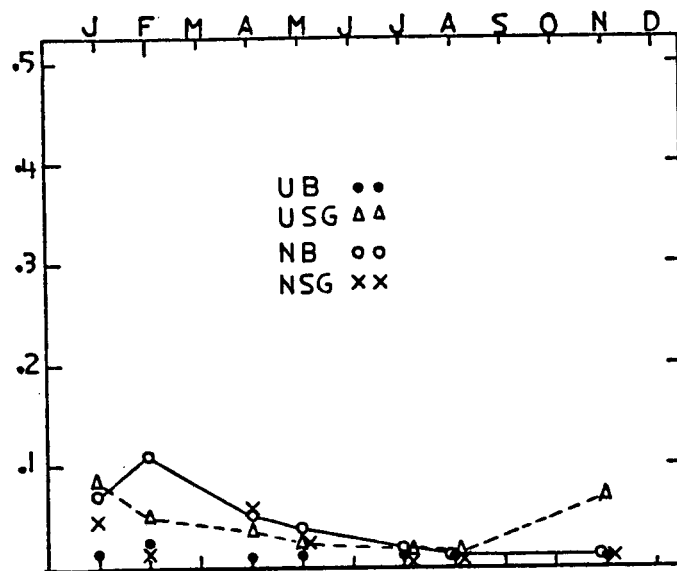


Fig. 10. The average percentage of occurrence for two types of corner effects at Unalakleet (U) and Nome (N). Seven months are shown for the 1964 to 1968 time period. The zero wind speed cases are designated B and the supergeostrophic wind cases are designated SG.

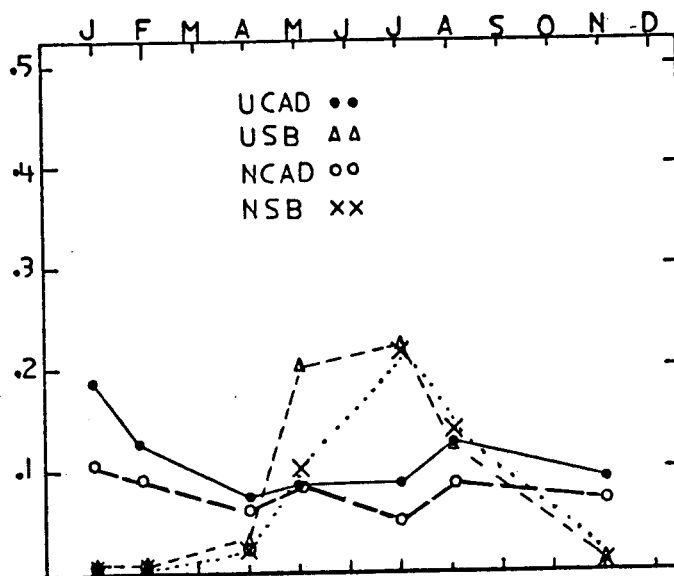


Fig. 11. The average occurrence percentage of cold air drainage (CAD), winds and sea breeze (SB) winds at Nome (N) and Unalakleet (U). Seven months are shown for the 1964 to 1968 time period.

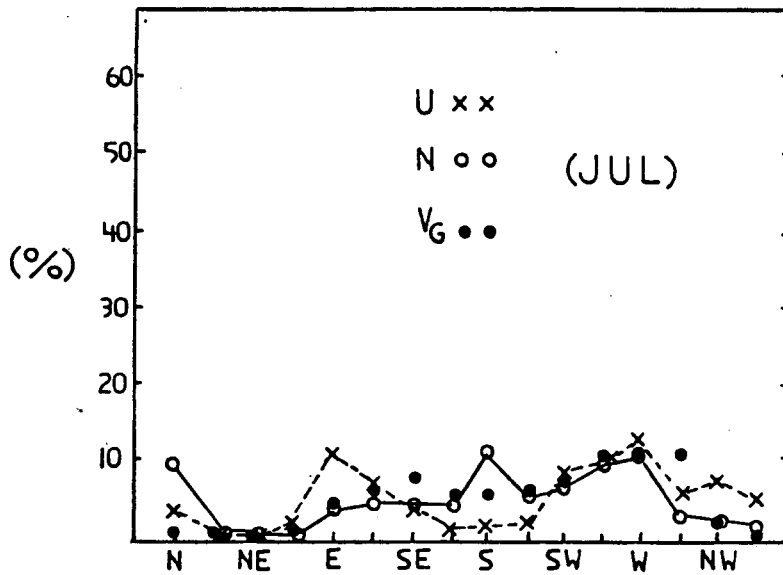


Fig. 12. The average directional distribution (%) for Nome (N), Unalakleet (U) and the calculated geostrophic (Vg) winds in July (1964-1968).

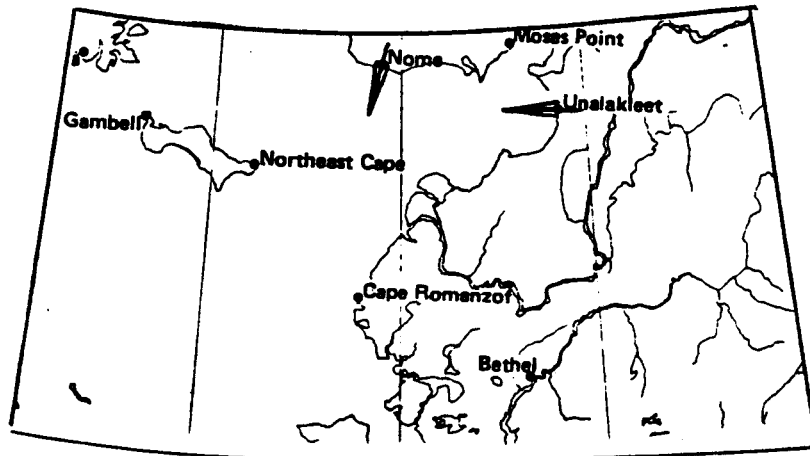


Fig. 13. Major directions of offshore winds due to cold air drainage at Nome and Unalakleet.

Unalakleet respectively. The south peak in the Nome data is due to sea breeze influence, but for Unalakleet both the surface distribution and the Vg distribution have west peaks. However, using a simple speed test, the sea breeze influence at Unalakleet can be discerned if coastline orientation is remembered. When Vg is less than 5 ms^{-1} the afternoon winds at Nome are usually from the south while the winds at Unalakleet are from the west. Figure 14 is an idealized case of this which leads to the conclusion that sea breeze winds will come from the NW at the Yukon Delta (lowest arrow) a region that will produce limited mitigating orographic effects. Figure 11 (above) also shows the monthly percentage of sea breeze effects at Nome (NSB) and Unalakleet (USB). The open water months are the obvious periods of high sea breeze incidence which can occur as early as May. The highest sea breeze winds measured (1964-1968) during low speed synoptic wind cases were 10.8 ms^{-1} at both Nome and Unalakleet. This casts doubt on the 15 ms^{-1} sea breeze speeds in Norton Sound observed by Robin Muench (SAI, personal communication) and reported in Zimmerman (1982). The synoptic winds were probably onshore at the time and the observers assumed that they were sea breezes.

Figure 15 shows the average percentage of the combined mesoscale effects due to mountain valley wind systems, sea breeze wind systems, corner effects and pure cold air drainage at Nome and Unalakleet (1964-1968) in seven study months. Nome and Unalakleet usually experience mesoscale dominated winds more than 20% of the time with Unalakleet reaching 30% in the winter and summer. Again these effects will hide the real wind stress directions in the sound proper and near the Yukon Delta. The offshore distance of influence for sea breeze (Kozo, 1982) and CAD winds (Reynolds, 1980) in the Arctic open water season is at least 20 km. The sea breeze produces onshore flow while CAD winds produce offshore flow. The above evidence is further proof that

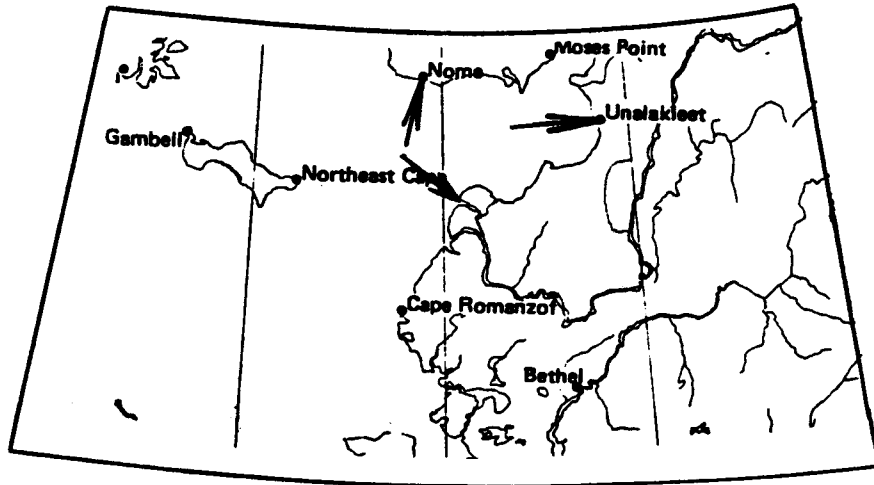


Fig. 14. Major directions of onshore winds due to sea breeze influence at Nome and Unalakleet. The probable direction of these winds at the Yukon Delta is shown at the lowest arrow.

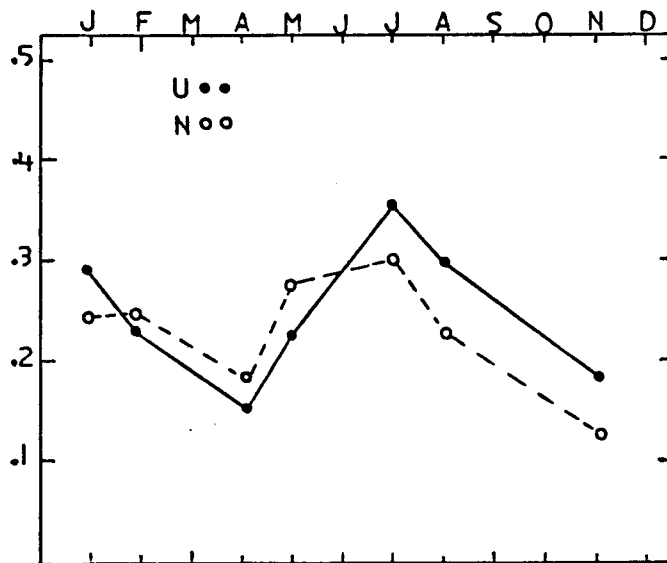


Fig. 15. The total amount of monthly mesoscale influence provided by mountain valley winds, sea breezes, corner effects and pure cold air drainage combined for Nome and Unalakleet (1964-1968).

time series data of winds from Nome should not be used in oil spill trajectory models without extensive modification.

c. Analysis of surface wind time series

Semi-log plots of January 1964 (Fig. 16a) and July 1964 (Fig. 16b) rotary spectra from time series data at Unalakleet, Northeast Cape and Nome are shown with 95% confidence limits (C) and bandwidth (B) indicated. The vertical axes are in units of spectral density (m^2s^{-2} per cycle $[3\text{h}]^{-1}$) with the horizontal axes in frequency units of cycles day^{-1} . Figure 16a (January, 1964) does not have significant peaks at mesoscale frequencies and shows dominance by low frequency synoptic wind systems for all three station locations. Figure 16b (July, 1964) is characteristic of most of the summer spectral plots for the five-year data set. Rotary spectra plots for the transition months of May, 1968 (Fig. 17a) and November, 1968 (Fig. 17b) are also shown. May, the first open water month in the Sound (Fig. 6) has curves with the same characteristics as those of July (Fig. 16b) for all three stations. The -1 and $+1$ cycle day^{-1} peaks are not as pronounced since the May land temperatures (Fig. 4) are not as high. November, the first ice covered month (Fig. 7) after summer, has curves with no significant mesoscale peaks at any of the three stations. This was also characteristic of the January curves (Fig. 16a) and shows the effects of total ice cover and lack of daylight. The spectral plots for January-July and May-November in the years 1964-1968 can be seen in Appendix B.

There are several important features to notice in the open water spectral plots (Fig. 16b and 17a). The first is the general absence of significant peaks in the Northeast cape curve (dashed line). The second is the significant peak on the negative frequency side of the spectrum at -1

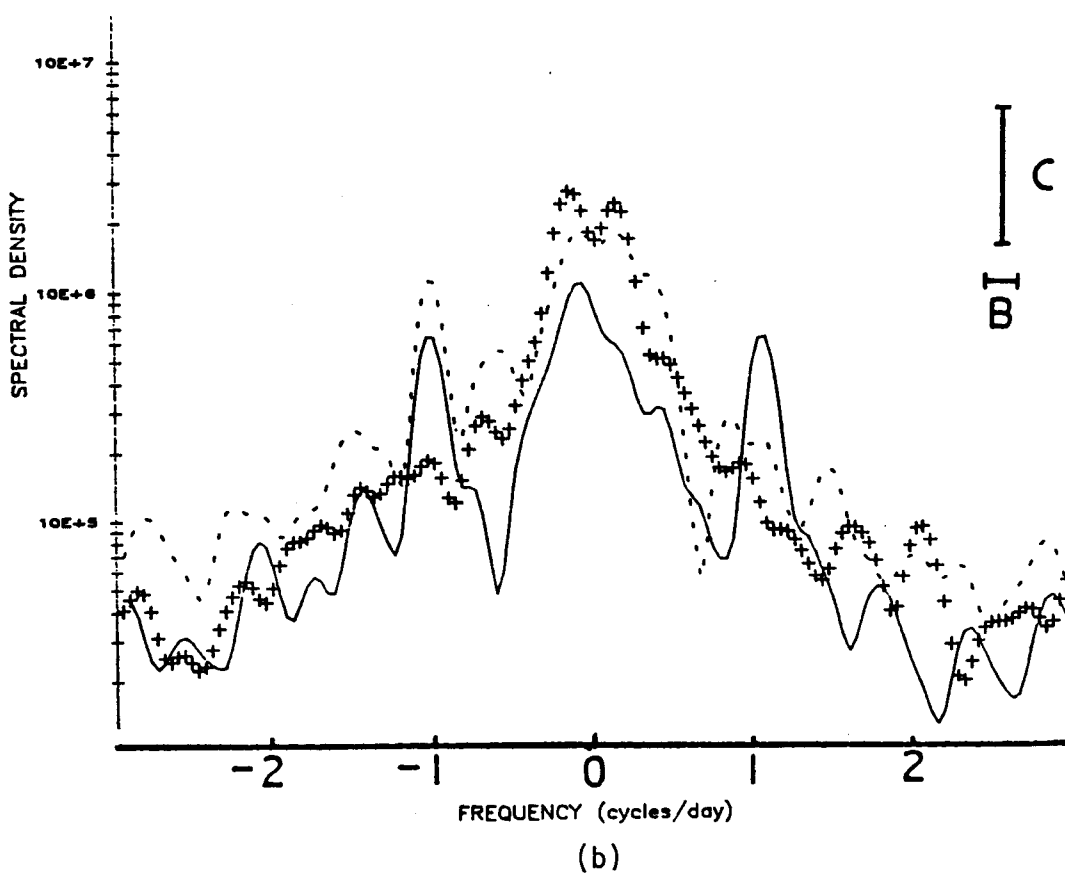
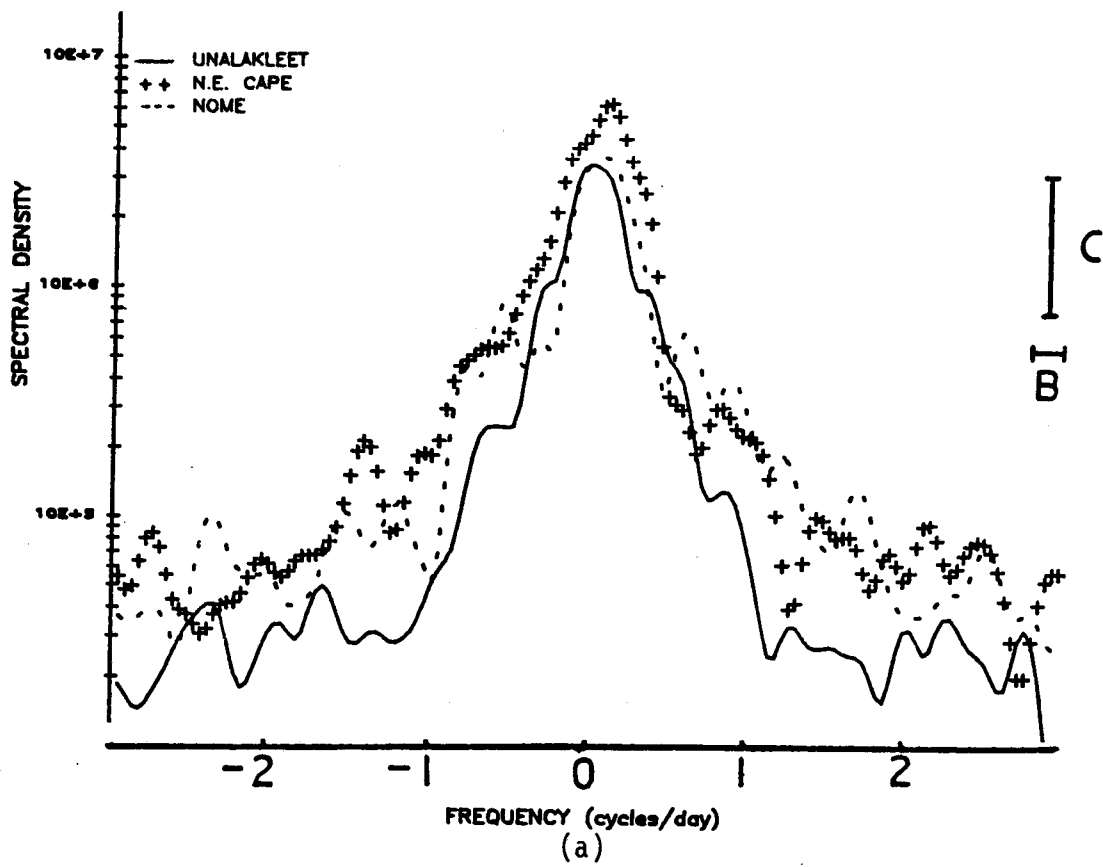


Fig. 16. Time series rotary spectra of surface wind velocity data from Unalakleet, Northeast Cape, and Nome for (a) January, 1964 and (b) November, 1968.

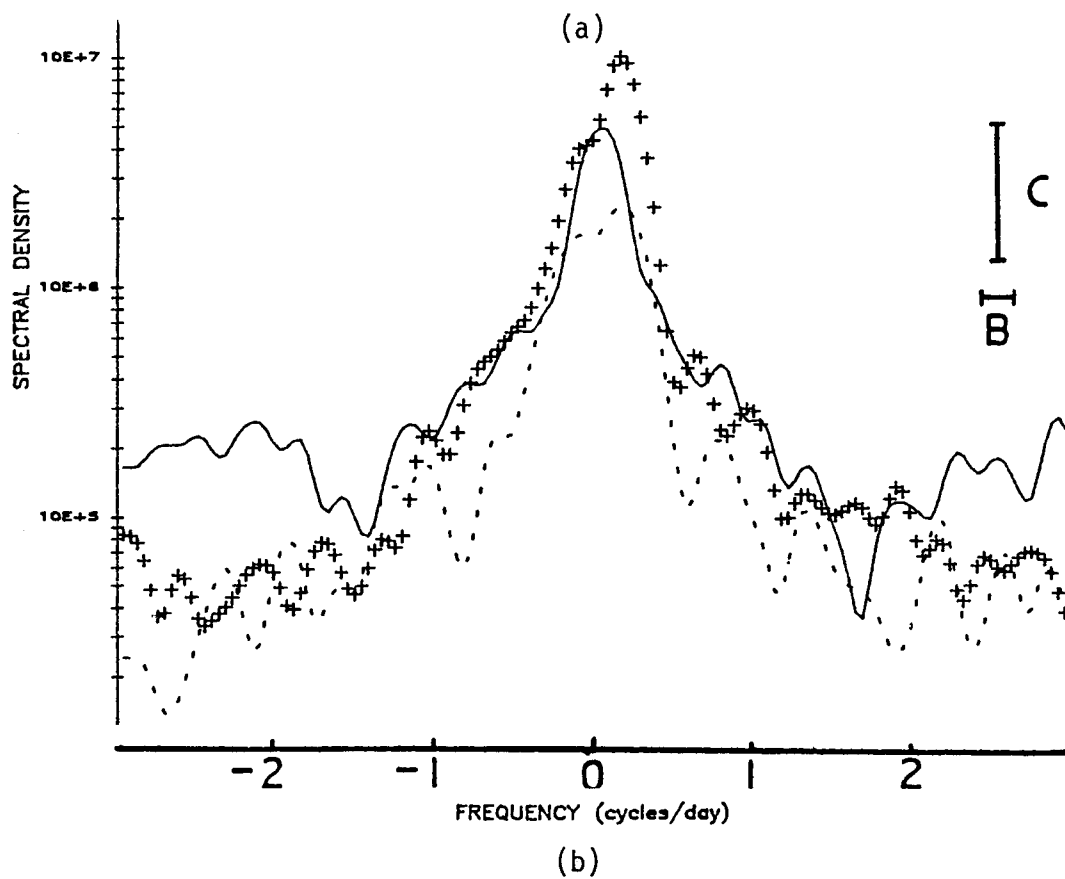
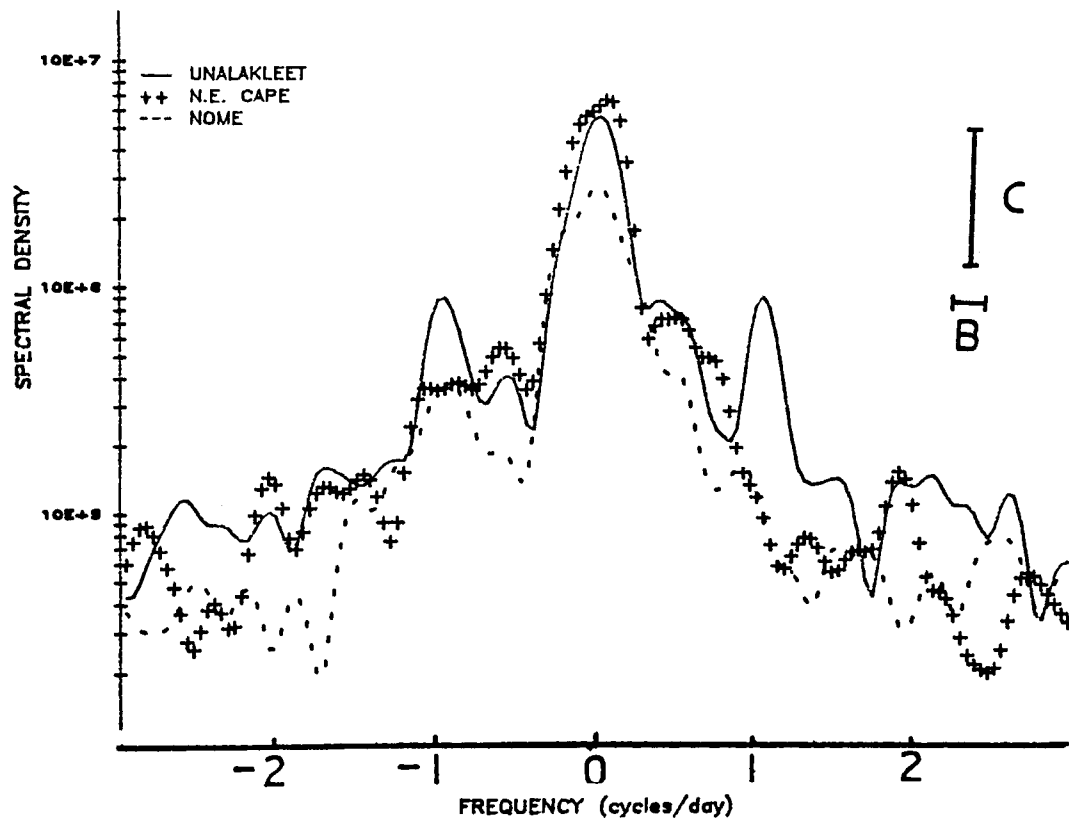


Fig. 17. Time series rotary spectra of surface wind velocity data from Unalakleet, Northeast Cape, and Nome for (a) May, 1968 and (b) November 1968.

cycle day⁻¹ for both Unalakleet (solid line) and Nome (dashed line). The third is the significant peak on the positive frequency side at +1 cycle day⁻¹ for both Unalakleet (solid line) and Nome (dashed line). The fourth is that the variance (energy) represented in the negative and positive diurnal peaks (mesoscale) is close to that of the central synoptic peak (July in particular).

The absence of peaks in the Northeast Cape curve indicates that the data station had no dominant coastal orientation to set up ideal sea breeze type winds. The Northeast Cape curve in other years is not usually this "clean", however. The negative frequency peaks at -1 cycle day⁻¹ for Unalakleet and Nome are characteristic of Arctic sea breeze effects on surface wind data (Kozo, 1982). Figure 18 is a monthly plot of coherence (five year data set average) between winds at Nome and Unalakleet for -1 day periods (sea breeze period). The dashed line represents the coherence at the 1% limit for 10 degrees of freedom which characterize the monthly data sets. The two stations are strongly linked by sea breeze effects during the warmest open water months of July and August. The chances are 1 in 100 that these stations are related by accident at this one day period. Remember, however, that the sea breeze wind direction at Unalakleet will be ideally 90° from the sea breeze direction at Nome (Fig. 14).

The significant positive frequency peaks (CCW wind vector rotation) seen in the rotary spectra from Figs. 16b and 17a have not appeared on previous data analyses of other Alaskan Arctic coastal sites (Kozo, 1984) and they do not appear on Northeast Cape spectra either.

The Nome and Unalakleet data sites have river valleys which are perfect for mountain valley wind systems that are generated by combined orographic and thermal mesoscale conditions. Figures 19 (a-h) illustrate (Fairbridge,

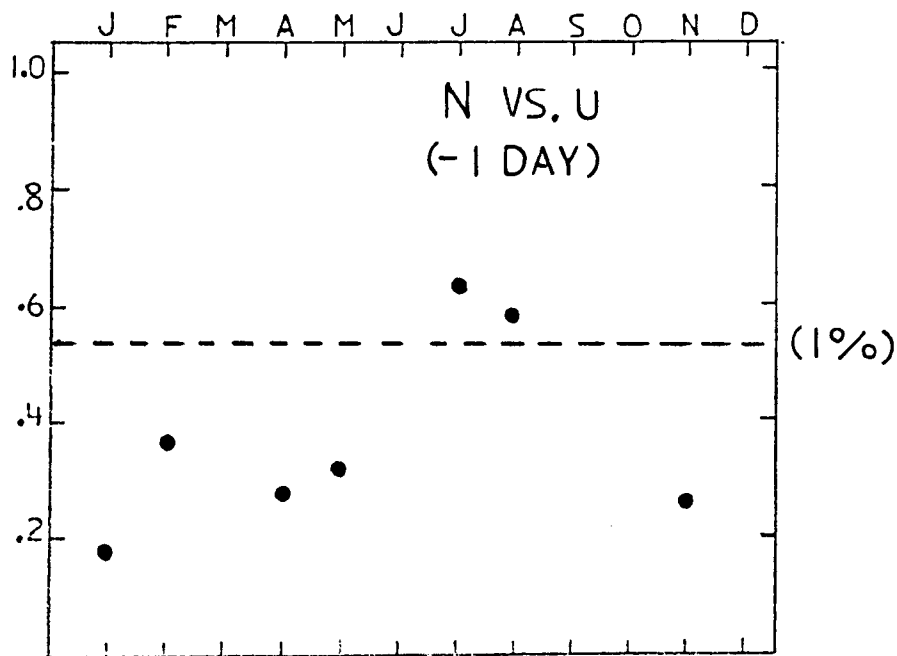


Fig. 18. The average monthly coherence (1964-1968) between sea breeze winds at Nome and Unalakleet. These winds have a one day period on the CW (-) side of spectral plots such as seen in Figs. 16 and 17. The dashed line represents the 1% coherence limit for 10 degrees of freedom.

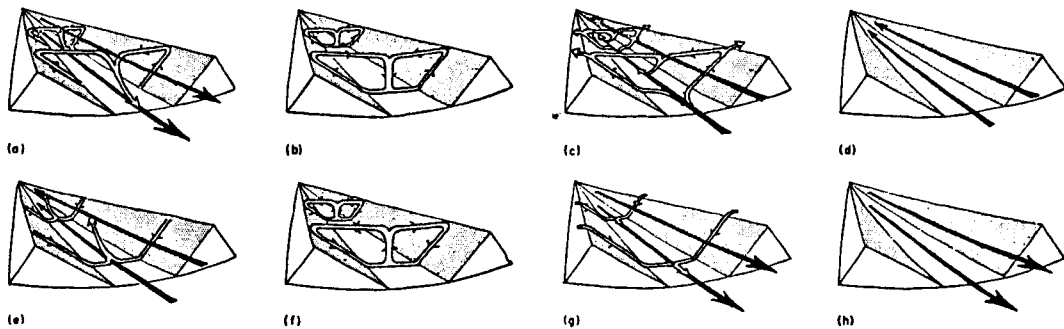


Fig. 19. The normal diurnal variation of air currents in a valley (Fairbridge, 1967). (a-h): a. sunrise--onset of upslope winds (white arrows) and the continuation of mountain drainage winds (black arrows); b. forenoon--transition from down mountain to up valley winds; c. early afternoon--the fully developed valley wind with diminishing slope winds; d. late afternoon--the valley wind; e. evening--the beginning of downslope winds and a diminishing valley wind; f. early night--the transition from valley to mountain winds showing well-developed downslope winds; g. middle of the night--continuing downslope winds and fully developed mountain winds; h. late night to morning--downslope winds ceasing with full mountain winds.

1967) the normal diurnal variation of air currents in a valley. Figure 19a shows the sunrise with the onset of upslope winds (white arrows) and the continuation of mountain drainage winds (black arrows). Figure 19b shows the forenoon transition from down mountain to up valley winds, Fig. 19c shows the early afternoon fully developed valley wind with diminishing slope winds. Figure 19d is in the late afternoon with only a valley wind. Figure 19e is in the evening with the beginning of downslope winds and a diminishing valley wind. Figure 19f is the early night and is the transition from valley to mountain winds showing well-developed downslope winds. Figure 19g is the middle of the night with continuing downslope winds and fully developed mountain winds. Figure 19h is the late night to morning with downslope winds ceasing and full mountain winds. This sequence illustrates that a measuring site on the plains area would experience CCW rotation with time as the spectra indicate and is similar to rotation of tidal currents in an embayment. This phenomenon can produce mesoscale offshore winds in an Arctic coastal zone at least 20 km seaward where only onshore mesoscale winds were thought to exist. In effect this valley drainage wind acts as a false summer land breeze in sections of an Arctic coastline having river valley wind systems with the proper geometry. This mountain valley wind system acts to augment the onshore afternoon seabreeze in the Arctic and to reverse the flow at night to offshore under favorable synoptic conditions.

The amount of variance contained in the mesoscale frequencies in the rotary spectral plots for the open water months again points to the inadequacies of Nome land station data to drive oil spill trajectory models in offshore areas.

6. Summary and conclusions

The use of several analytical "tools" on surface meteorological time series of pressure, temperature, wind speed and wind direction from Nome, Northeast Cape and Unalakleet has led to important results for the Norton Sound. A profound influence of mesoscale effects was discovered both of orographic and thermal causes. These effects only play a part in actual transport of pollutants or ice floes in a narrow zone within 20 km of the coastline. However, they mask the "real" wind direction in the Sound proper which is often different from the wind directions and speeds recorded at coastal sites. The extent of this difference is ample evidence that Nome and Unalakleet winds should not be used as input for oil spill trajectory models unless in the very nearshore.

Combined mesoscale effects in the Sound's warmest open water months averaged 33% for Unalakleet and 26% for Nome. In the coldest ice covered months, mesoscale effects (mainly orographic) averaged 25% at both Nome and Unalakleet. The approximate summer large scale wind field as determined by pressure data from the above three stations indicates a general westerly flow which coupled with the sea breeze effect would bring out-of-Sound pollutants toward the Yukon Delta.

Rotary spectral analysis has pinpointed a summer wind system due to river valleys running perpendicular to coastlines and cutting through mountain ranges at Nome and Unalakleet. This mountain valley system produces winds that augment shoreward blowing sea breezes in the afternoons, but create "false" offshore blowing land breezes in the evening. The Arctic coastal areas were thought to be void of land breezes since the land stayed warmer than the water in the summer (Kozo, 1982).

This study has quantified the amount of mesoscale influence in the Sound with further breakdowns into orographic and thermal causes. The necessary preliminary determination of the large scale wind field gives a good approximation of the winds that would affect the Yukon Delta. The percentage of thermally induced mesoscale effects seen in the summer Yukon Delta region will be similar to the Sound proper. Future studies in the Delta should no longer concentrate on the frequency of sea breeze occurrence but on the offshore extent instead. This offshore extent may be greater than 20 km for several reasons. The convex shape of the coastline can act to focus the onshore winds creating a convergence and uplift over land. This will tend to increase the "drawing" power of the onshore winds. The land elevations are low in the delta area which precludes mountain valley systems and other orographic effects that might cause opposing offshore flows. The land surface itself with a large extent of mud flats may heat up faster and to a greater extent than areas with more common tundra grass type surfaces.

7. Acknowledgement

This study was funded by the Minerals Management Service, U. S. Department of the Interior, through inter-agency agreement with the National Oceanic and Atmospheric Administration, U. S. Department of Commerce, as part of the Outer Continental Shelf Environmental Assessment Program.

REFERENCES

- Brower, W. A., H. F. Diaz, A. S. Prechtel, H. W. Searby and J. L. Wise, 1977: Climatic atlas of the Outer Continental Shelf Waters and Coastal Regions of Alaska, NOAA, NCC, EDS, Asheville, North Carolina, 1-409.
- Dickey, W. W., 1961: A study of a topographic effect on wind in the arctic. J. Meteor., 18, 790-803.
- Fairbridge, R. W., 1967: Mountain and Valley Winds, Encyclopedia of Atmospheric Sciences and Astrogeology (ed. by R. W. Fairbridge), Reinhold Publishing Corp., New York, 662-666.
- Gonella, J., 1972: A rotary-component method for analyzing meteorological and oceanographic vector time series. Deep-Sea Res., 19, 833-846.
- Halpern, D., 1979: Surface wind measurements and low-level cloud motion vectors near the Intertropical Convergence Zone in the Central Pacific Ocean from November 1977 to March 1978, Mon. Wea. Rev. 107, 1525-1534.
- Kozo, T. L., 1984: Mesoscale wind phenomena along the Alaska Beaufort Sea Coast, in The Alaska Beaufort Sea: Ecosystems and Environment (ed. by P. W. Barnes, D. M. Schell and E. Reimnitz). Academic Press, New York, pp. 23-45.
- _____, 1982: An observational study of sea breezes along the Alaska Beaufort Sea Coast: Part I. J. App. Meteor., 12, 891-905.
- _____, 1980: Mountain barrier baroclinity effects on surface winds along the Alaskan Arctic Coast. Geophysical Research Letters, 7, 377-380.
- Krumbein, W. D., 1959: Trend surface analysis of contour-type maps with irregular control point spacing. J. Geophys. Res. 64, 823-834.

- McPherson, P. D. 1970. A numerical study of the effect of a coastal irregularity on the sea breeze. J. App. Meteor., 9, 767-777.
- O'Brien, J. J., and R. D. Pillsbury, 1974: Rotary wind spectra in a sea breeze regime. J. Appl. Meteor., 13, 820-825.
- Panofsky, H. A. and G. W. Brier, 1968: Some applications of statistics to meteorology, Pennsylvania State University Press, University Park, Pennsylvania, 155-158.
- Reynolds, R. M., 1980: On the Dynamics of Cold Offshore Flow, Second Conference on Coastal Meteorology, Los Angeles, California, American Meteorological Society, Boston, Massachusetts, 181-184.
- Thomas, D. R. and R. S. Pritchard, 1981: Norton Sound and Bering Sea Ice Motion: 1981. Flow Research Report #209, Kent, Washington, 37 p.
- Zimmerman, S. T., 1982: The Norton Sound environment and possible consequences of planned oil and gas development, in Proceedings of a Synthesis Meeting, Anchorage, Alaska, October 28-30, 1980, BLM, NOAA, 55 p.

APPENDIX A

BIVARIATE DISTRIBUTIONS FOR NOME AND UNALAKLEET



D I R E C T I O N

	S P E E D (ms ⁻¹)															(obs. 248)	
	0-2	2-4	4-6	6-8	8-10	10-12	12-14	14-16	16-18	18-20	20-22	22-24	24-26	26-28	28-30	TOTAL	PER
326.0-348.5	0	2	3	0	0	0	0	0	0	0	0	0	0	0	0	5	2.0
303.5-326.0	1	0	0	0	0	0	0	0	0	0	0	0	0	0	0	1	0.0
281.0-303.5	0	0	0	0	0	0	0	0	0	0	0	0	0	0	0	0	0.0
258.5-281.0	1	2	2	1	0	0	0	0	0	0	0	0	0	0	0	6	2.0
236.0-258.5	0	3	4	1	0	0	0	0	0	0	0	0	0	0	0	8	3.0
213.5-236.0	0	0	1	0	0	0	0	0	0	0	0	0	0	0	0	1	0.0
191.0-213.5	0	1	0	0	0	0	0	0	0	0	0	0	0	0	0	1	0.0
168.5-191.0	0	0	0	0	0	0	0	0	0	0	0	0	0	0	0	0	0.0
146.0-168.5	1	0	0	0	0	0	0	0	0	0	0	0	0	0	0	1	0.0
123.5-146.0	4	3	0	0	0	0	0	0	0	0	0	0	0	0	0	7	2.0
101.0-123.5	4	13	6	3	3	1	0	0	0	0	0	0	0	0	0	30	12.0
78.5-101.0	4	16	26	25	41	37	9	0	0	0	0	0	0	0	0	158	63.0
56.0-78.5	2	2	3	1	0	0	0	0	0	0	0	0	0	0	0	8	3.0
33.5-56.0	0	0	0	0	0	0	0	0	0	0	0	0	0	0	0	0	0.0
11.0-33.5	0	2	0	0	0	0	0	0	0	0	0	0	0	0	0	2	0.0
348.5-11.0	19	1	0	0	0	0	0	0	0	0	0	0	0	0	0	20	8.0

Table AU-1. Bivariate distribution of wind direction versus wind speed data (three hourly) for Unalakleet, in January, 1964. Winds above 14 ms⁻¹ are considered gale class.

DIRECTION

	S P E E D (ms^{-1})															(obs. 248)	
	0-2	2-4	4-6	6-8	8-10	10-12	12-14	14-16	16-18	18-20	20-22	22-24	24-26	26-28	28-30	TOTAL	PER
326.0-348.5	1	3	0	0	0	0	0	0	0	0	0	0	0	0	0	4	1.0
303.5-326.0	1	3	1	0	0	0	0	0	0	0	0	0	0	0	0	5	2.0
281.0-303.5	1	1	1	2	2	0	0	0	0	0	0	0	0	0	0	7	2.0
258.5-281.0	0	2	3	1	0	0	0	0	0	0	0	0	0	0	0	6	2.0
236.0-258.5	0	0	0	0	0	0	0	0	0	0	0	0	0	0	0	0	0.0
213.5-236.0	0	1	0	0	0	0	0	0	0	0	0	0	0	0	0	1	0.0
191.0-213.5	0	1	0	0	0	0	0	0	0	0	0	0	0	0	0	1	0.0
168.5-191.0	0	0	0	0	0	0	0	0	0	0	0	0	0	0	0	0	0.0
146.0-168.5	0	1	0	0	0	0	0	0	0	0	0	0	0	0	0	1	0.0
123.5-146.0	0	0	0	0	0	0	0	0	0	0	0	0	0	0	0	0	0.0
101.0-123.5	1	3	1	0	0	0	0	0	0	0	0	0	0	0	0	5	2.0
78.5-101.0	1	4	13	17	11	14	7	3	0	0	0	0	0	0	0	70	28.0
56.0-78.5	0	8	7	8	4	2	2	2	0	0	0	0	0	0	0	33	13.0
33.5-56.0	0	4	1	4	3	3	4	0	0	0	0	0	0	0	0	19	7.0
11.0-33.5	0	9	5	7	4	2	0	0	0	0	0	0	0	0	0	27	10.0
348.5-11.0	46	11	7	4	1	0	0	0	0	0	0	0	0	0	0	69	27.0

Table AN-1. Bivariate distribution of wind direction versus wind speed data (three hourly) for Nome, in January, 1964. Winds above 14 ms^{-1} are considered gale class.

DIRECTION (Vg)	S P E E D (ms ⁻¹)															(Obs. 248)		
	0.0	11.0	33.5	56.0	78.5	101.0	123.5	146.0	168.5	191.0	213.5	236.0	258.5	281.0	303.5	326.0	TOTAL	PER
326.0-348.5	1	0	0	0	1	0	1	0	0	0	0	0	0	0	0	1	4	1.0
303.5-326.0	5	1	0	2	5	0	2	0	0	0	0	0	1	0	0	0	16	6.0
281.0-303.5	1	0	0	1	25	9	3	1	0	0	0	1	3	0	0	0	44	17.0
258.5-281.0	3	0	0	0	28	10	0	0	0	0	0	4	1	0	1	0	47	18.0
236.0-258.5	0	0	0	1	7	4	0	0	0	0	1	0	0	0	0	0	13	5.0
213.5-236.0	1	0	0	1	10	3	0	0	0	0	0	0	0	0	0	0	15	6.0
191.0-213.5	2	0	0	0	6	0	1	0	0	0	0	1	0	0	0	0	10	4.0
168.5-191.0	1	0	0	0	18	1	0	0	0	0	0	0	0	0	0	0	20	8.0
146.0-168.5	0	0	0	0	31	1	0	0	0	1	0	1	1	0	0	0	35	14.0
123.5-146.0	2	0	0	3	23	2	0	0	0	0	0	1	0	0	0	0	31	12.0
101.0-123.5	0	0	0	0	4	0	0	0	0	0	0	0	0	0	0	0	4	1.0
78.5-101.0	4	0	0	0	0	0	0	0	0	0	0	0	0	0	0	1	5	2.0
56.0-78.5	0	0	0	0	0	0	0	0	0	0	0	0	0	0	0	1	1	0.0
33.5-56.0	0	0	0	0	0	0	0	0	0	0	0	0	0	0	0	1	1	0.0
11.0-33.5	0	0	0	0	0	0	0	0	0	0	0	0	0	0	0	1	1	0.0
348.5-11.0	0	1	0	0	0	0	0	0	0	0	0	0	0	0	0	0	1	0.0

Table AU-2. Bivariate distribution of calculated geostrophic winds (Vg) versus Unalakleet simultaneous surface winds (Us) for January, 1964. Horizontal directions represent the same sectors as the vertical except that 0 is the middle of the 348.5°-11.0° sector instead of the minimum direction value.

DIRECTION (Vg)

	DIRECTION (Us)															(obs. 248)		
	0.0	11.0	33.5	56.0	78.5	101.0	123.5	146.0	168.5	191.0	213.5	236.0	258.5	281.0	303.5	326.0	TOTAL	PER
326.0-348.5	3	0	0	1	0	0	0	0	0	0	0	0	0	0	0	0	4	1.0
303.5-326.0	8	6	0	0	1	0	0	0	0	0	0	0	0	1	0	0	16	6.0
281.0-303.5	16	11	2	1	1	1	0	1	0	0	0	0	3	2	3	3	44	17.0
258.5-281.0	21	5	5	3	4	1	0	0	0	1	1	0	0	4	1	1	47	18.0
236.0-258.5	3	2	2	0	4	0	0	0	0	0	0	0	2	0	0	0	13	5.0
213.5-236.0	3	0	6	3	2	0	0	0	0	0	0	0	0	0	1	0	15	6.0
191.0-213.5	1	0	1	1	6	0	0	0	0	0	0	0	1	0	0	0	10	4.0
168.5-191.0	1	0	1	6	12	0	0	0	0	0	0	0	0	0	0	0	20	8.0
146.0-168.5	1	1	2	10	19	2	0	0	0	0	0	0	0	0	0	0	35	14.0
123.5-146.0	3	1	0	6	20	1	0	0	0	0	0	0	0	0	0	0	31	12.0
101.0-123.5	0	1	0	2	1	0	0	0	0	0	0	0	0	0	0	0	4	1.0
78.5-101.0	5	0	0	0	0	0	0	0	0	0	0	0	0	0	0	0	5	2.0
56.0-78.5	1	0	0	0	0	0	0	0	0	0	0	0	0	0	0	0	1	0.0
33.5-56.0	1	0	0	0	0	0	0	0	0	0	0	0	0	0	0	0	1	0.0
11.0-33.5	1	0	0	0	0	0	0	0	0	0	0	0	0	0	0	0	1	0.0
348.5-11.0	1	0	0	0	0	0	0	0	0	0	0	0	0	0	0	0	1	0.0

Table AN-2. Bivariate distribution of calculated geostrophic winds (Vg) versus Nome simultaneous surface winds (Ns) for January, 1964. Horizontal directions represent the same sectors as the vertical except that 0 is the middle of the 348.5°-11.0° sector instead of the minimum direction value.

DIRECTION	S P E E D (ms ⁻¹)															(obs. 248)	
	0-2	2-4	4-6	6-8	8-10	10-12	12-14	14-16	16-18	18-20	20-22	22-24	24-26	26-28	28-30	TOTAL	PER
325.0-348.5	1	11	15	3	0	0	0	0	0	0	0	0	0	0	0	30	12.0
303.5-326.0	3	10	9	2	1	0	0	0	0	0	0	0	0	0	0	25	10.0
281.0-303.5	2	12	3	2	0	0	0	0	0	0	0	0	0	0	0	19	7.0
258.5-281.0	9	14	11	3	0	0	0	0	0	0	0	0	0	0	0	37	14.0
236.0-258.5	2	9	9	0	0	0	0	0	0	0	0	0	0	0	0	20	8.0
213.5-236.0	2	5	7	0	0	0	0	0	0	0	0	0	0	0	0	14	5.0
191.0-213.5	0	2	0	0	0	0	0	0	0	0	0	0	0	0	0	2	0.0
168.5-191.0	0	1	0	0	0	0	0	0	0	0	0	0	0	0	0	1	0.0
146.0-168.5	0	1	0	0	0	0	0	0	0	0	0	0	0	0	0	1	0.0
123.5-146.0	5	4	2	1	0	0	0	0	0	0	0	0	0	0	0	12	4.0
101.0-123.5	7	12	3	0	0	0	0	0	0	0	0	0	0	0	0	22	8.0
78.5-101.0	5	12	7	1	0	0	0	0	0	0	0	0	0	0	0	25	10.0
56.0-78.5	1	1	0	1	0	0	0	0	0	0	0	0	0	0	0	3	1.0
33.5-56.0	0	0	0	0	0	0	0	0	0	0	0	0	0	0	0	0	0.0
11.0-33.5	1	2	0	0	0	0	0	0	0	0	0	0	0	0	0	3	1.0
348.5-11.0	24	5	2	3	0	0	0	0	0	0	0	0	0	0	0	34	13.0

Table AU-3. Bivariate distribution of wind direction versus wind speed data (three hourly) for Unalakleet, in July, 1964. Winds above 14 ms⁻¹ are considered gale class.

DIRECTION	S P E E D (ms ⁻¹)															(obs. 248)	
	0-2	2-4	4-6	6-8	8-10	10-12	12-14	14-16	16-18	18-20	20-22	22-24	24-26	26-28	28-30	TOTAL	PER
326.0-348.5	2	3	4	3	0	0	0	0	0	0	0	0	0	0	0	12	4.0
303.5-326.0	3	6	1	3	0	0	0	0	0	0	0	0	0	0	0	13	5.0
281.0-303.5	0	5	5	2	0	0	0	0	0	0	0	0	0	0	0	12	4.0
258.5-281.0	0	7	11	7	3	4	0	0	0	0	0	0	0	0	0	32	12.0
236.0-258.5	2	5	10	5	1	0	0	0	0	0	0	0	0	0	0	23	9.3
213.5-236.0	1	10	9	0	0	0	0	0	0	0	0	0	0	0	0	20	8.0
191.0-213.5	0	3	6	0	0	0	0	0	0	0	0	0	0	0	0	9	3.0
168.5-191.0	4	20	10	1	0	0	0	0	0	0	0	0	0	0	0	35	14.2
146.0-168.5	0	3	5	0	0	0	0	0	0	0	0	0	0	0	0	8	3.0
123.5-146.0	1	2	3	1	0	0	0	0	0	0	0	0	0	0	0	7	2.3
101.0-123.5	0	0	2	3	0	1	0	0	0	0	0	0	0	0	0	6	2.0
78.5-101.0	0	1	2	2	4	1	0	0	0	0	0	0	0	0	0	11	4.0
56.0-78.5	0	2	2	1	0	0	0	0	0	0	0	0	0	0	0	3	1.0
33.5-56.0	1	2	2	5	1	0	0	0	0	0	0	0	0	0	0	11	4.0
11.0-33.5	1	1	0	4	0	0	0	0	0	0	0	0	0	0	0	6	2.0
348.5-11.0	22	5	6	4	2	1	0	0	0	0	0	0	0	0	0	40	16.0

Table AN-3. Bivariate distribution of wind direction versus wind speed data (three hourly) for Nome, in July, 1964. Winds above 14 ms⁻¹ are considered gale class.

D I R E C T I O N (Vg)	D I R E C T I O N (Us)															(obs. 248)		
	0.0	11.0	33.5	56.0	78.5	101.0	123.5	146.0	168.5	191.0	213.5	236.0	258.5	281.0	303.5	326.0	TOTAL	PER
326.0-348.5	0	0	0	0	0	0	0	0	0	0	0	0	0	0	1	1	0.0	
303.5-326.0	5	0	0	0	0	1	0	0	0	0	1	0	0	0	1	5	13	5.0
281.0-303.5	12	2	0	1	1	3	1	0	1	0	8	3	7	4	10	12	65	26.0
258.5-281.0	2	0	0	0	5	2	2	0	0	0	2	8	16	8	3	1	49	19.0
236.0-258.5	3	0	0	1	3	9	4	1	0	1	0	5	3	2	5	2	39	15.0
213.5-236.0	4	1	0	0	6	4	2	0	0	1	0	1	6	1	2	3	31	12.0
191.0-213.5	5	0	0	0	2	3	1	0	0	0	2	3	3	1	1	2	23	9.0
168.5-191.0	2	0	0	1	5	0	1	0	0	0	1	0	1	2	2	0	15	6.0
146.0-168.5	0	0	0	0	0	0	1	0	0	0	0	0	0	1	0	2	4	1.0
123.5-146.0	0	0	0	0	2	0	0	0	0	0	0	0	1	0	0	0	3	1.0
101.0-123.5	0	0	0	0	1	0	0	0	0	0	0	0	0	0	0	2	3	1.0
78.5-101.0	1	0	0	0	0	0	0	0	0	0	0	0	0	0	0	0	1	0.0
56.0-78.5	0	0	0	0	0	0	0	0	0	0	0	0	0	0	0	0	0	0.0
33.5-56.0	0	0	0	0	0	0	0	0	0	0	0	0	0	0	1	0	1	0.0
11.0-33.5	0	0	0	0	0	0	0	0	0	0	0	0	0	0	0	0	0	0.0
348.5-11.0	0	0	0	0	0	0	0	0	0	0	0	0	0	0	0	0	0	0.0

Table AU-4. Bivariate distribution of calculated geostrophic winds (Vg) versus Unalakleet simultaneous surface winds (Us) for July, 1964. Horizontal directions represent the same sectors as the vertical except that 0 is the middle of the 348.5°-11.0° sector instead of the minimum direction value.

D I R E C T I O N (Vg)	D I R E C T I O N (Us)															(obs. 248)		
	0.0	11.0	33.5	56.0	78.5	101.0	123.5	146.0	168.5	191.0	213.5	236.0	258.5	281.0	303.5	326.0	TOTAL	PER
	326.0-348.5	0	0	0	0	0	0	0	0	0	0	0	0	0	1	0	0	1
303.5-326.0	6	0	0	0	0	0	0	0	0	0	0	1	2	1	0	3	13	5.0
281.0-303.5	14	5	6	1	1	1	0	1	6	2	1	6	8	3	5	5	65	26.0
258.5-281.0	8	0	0	0	0	1	0	1	5	0	5	6	13	4	5	1	49	19.0
236.0-258.5	7	1	0	0	1	0	1	0	3	3	4	6	7	2	2	2	39	15.0
213.5-236.0	3	0	3	0	3	2	2	2	5	2	6	1	0	1	1	0	31	12.0
191.0-213.5	1	0	0	1	3	1	1	3	9	0	2	0	2	0	0	0	23	9.0
168.5-191.0	0	0	2	0	3	1	2	0	4	1	1	1	0	0	0	0	15	5.0
146.0-168.5	0	0	0	0	0	0	1	1	2	0	0	0	0	0	0	0	4	1.0
123.5-146.0	0	0	0	1	0	0	0	0	0	0	0	1	0	0	0	1	3	1.0
101.0-123.5	1	0	0	0	0	0	0	0	1	1	0	0	0	0	0	0	3	1.0
78.5-101.0	0	0	0	0	0	0	0	0	0	0	0	1	0	0	0	0	1	0.0
56.0-78.5	0	0	0	0	0	0	0	0	0	0	0	0	0	0	0	0	0	0.0
33.5-56.0	0	0	0	0	0	0	0	0	0	0	1	0	0	0	0	0	1	0.0
11.0-33.5	0	0	0	0	0	0	0	0	0	0	0	0	0	0	0	0	0	0.0
348.5-11.0	0	0	0	0	0	0	0	0	0	0	0	0	0	0	0	0	0	0.0

Table AN-4. Bivariate distribution of calculated geostrophic winds (Vg) versus Nome simultaneous surface winds (Ns) for July, 1964. Horizontal directions represent the same sectors as the vertical except that 0 is the middle of the 348.5°-11.0° sector instead of the minimum direction value.

DIRECTION	S P E E D (ms^{-1})															(obs. 248)	
	0-2	2-4	4-6	6-8	8-10	10-12	12-14	14-16	16-18	18-20	20-22	22-24	24-26	26-28	28-30	TOTAL	PER
325.0-348.5	1	0	1	0	0	0	0	0	0	0	0	0	0	0	0	2	0.8
303.5-326.0	0	3	1	0	0	0	0	0	0	0	0	0	0	0	0	4	1.6
281.0-303.5	1	1	1	0	0	0	0	0	0	0	0	0	0	0	0	3	1.0
258.5-281.0	1	5	0	0	0	0	0	0	0	0	0	0	0	0	0	6	2.0
236.0-258.5	1	0	2	0	0	0	0	0	0	0	0	0	0	0	0	3	1.0
213.5-236.0	0	2	4	1	0	0	0	0	0	0	0	0	0	0	0	7	2.0
191.0-213.5	0	1	0	0	0	0	0	0	0	0	0	0	0	0	0	1	0.8
168.5-191.0	1	0	0	0	0	0	0	0	0	0	0	0	0	0	0	1	0.8
146.0-168.5	1	0	0	0	0	0	0	0	0	0	0	0	0	0	0	1	0.8
123.5-146.0	3	0	2	0	0	0	0	0	0	0	0	0	0	0	0	5	2.0
101.0-123.5	6	7	6	4	3	3	3	0	0	0	0	0	0	0	0	32	12.0
78.5-101.0	8	12	12	21	33	34	11	6	0	0	0	0	0	0	0	137	55.0
56.0-78.5	2	12	2	0	1	0	0	0	0	0	0	0	0	0	0	17	6.0
33.5-56.0	2	4	2	0	0	0	0	0	0	0	0	0	0	0	0	8	3.0
11.0-33.5	1	0	2	0	0	0	0	0	0	0	0	0	0	0	0	3	1.0
348.5-11.0	8	7	3	0	0	0	0	0	0	0	0	0	0	0	0	18	7.0

Table AU-5. Bivariate distribution of wind direction versus wind speed data (three hourly) for Unalakleet, in January, 1965. Winds above 14 ms^{-1} are considered gale class.

DIRECTION

	S P E E D (ms^{-1})															(obs. 248)	
	0-2	2-4	4-6	6-8	8-10	10-12	12-14	14-16	16-18	18-20	20-22	22-24	24-26	26-28	28-30	TOTAL	PER
326.0-348.5	6	7	3	3	1	0	1	0	0	0	0	0	0	0	0	21	8.0
303.5-326.0	2	3	2	2	0	1	0	0	0	0	1	0	0	0	0	11	4.0
281.0-303.5	0	3	3	2	1	0	0	0	0	0	0	0	0	0	0	9	3.0
258.5-281.0	1	0	1	0	0	0	0	0	0	0	0	0	0	0	0	2	0.0
236.0-258.5	0	0	1	0	0	0	0	0	0	0	0	0	0	0	0	1	0.0
213.5-236.0	0	0	0	0	0	0	0	0	0	0	0	0	0	0	0	0	0.0
191.0-213.5	0	0	0	0	0	0	0	0	0	0	0	0	0	0	0	0	0.0
168.5-191.0	0	0	0	0	1	0	0	0	0	0	0	0	0	0	0	1	0.0
146.0-168.5	0	0	0	0	0	0	0	0	0	0	0	0	0	0	0	0	0.0
123.5-146.0	1	1	0	1	0	0	0	0	0	0	0	0	0	0	0	3	1.0
101.0-123.5	1	4	1	1	3	2	0	1	0	0	0	0	0	0	0	13	5.0
78.5-101.0	3	6	9	7	8	14	4	4	2	0	0	0	0	0	0	57	22.0
56.0-78.5	3	7	5	2	4	5	1	2	0	0	0	0	0	0	0	27	10.0
33.5-56.0	2	2	4	6	8	4	1	1	2	0	0	0	0	0	0	30	12.0
11.0-33.5	1	6	3	3	4	3	0	0	0	0	0	0	0	0	0	20	8.0
346.5-11.0	16	20	4	10	3	0	0	0	0	0	0	0	0	0	0	53	21.0

Table AN-5. Bivariate distribution of wind direction versus wind speed data (three hourly) for Nome, in January, 1965. Winds above 14 ms^{-1} are considered gale class.

DIRECTION (Vg)	DIRECTION (Us)															(obs. 248)		
	0.0	11.0	33.5	56.0	78.5	101.0	123.5	146.0	168.5	191.0	213.5	236.0	258.5	281.0	303.5	326.0	TOTAL	PER
326.0-348.5	2	0	3	2	3	1	0	0	1	0	1	0	0	0	0	0	13	5.0
303.5-326.0	9	3	2	4	7	8	1	0	0	1	3	2	3	1	1	2	47	18.0
281.0-303.5	6	0	0	1	16	4	0	0	0	0	2	0	1	0	2	0	32	12.0
258.5-281.0	1	0	0	0	12	2	0	0	0	0	0	0	0	0	0	0	15	5.0
236.0-258.5	0	0	0	0	6	3	0	0	0	0	0	0	0	0	0	0	9	3.0
213.5-236.0	0	0	0	0	1	1	0	0	0	0	0	0	0	0	0	0	2	2.0
191.0-213.5	0	0	0	0	2	2	0	0	0	0	0	0	0	0	0	0	4	1.0
168.5-191.0	0	0	0	0	4	0	0	0	0	0	0	0	0	0	0	0	4	1.0
146.0-168.5	0	0	0	0	5	1	1	0	0	0	0	0	0	0	0	0	7	2.0
123.5-146.0	0	0	0	0	24	2	0	0	0	0	0	0	0	0	0	0	26	10.0
101.0-123.5	0	0	0	0	22	0	0	0	0	0	0	0	1	1	0	0	24	9.0
78.5-101.0	0	0	0	0	10	0	0	0	0	0	0	1	1	1	1	0	14	5.0
56.0-78.5	0	0	1	0	6	1	0	0	0	0	1	0	0	0	0	0	11	4.0
33.5-56.0	0	0	0	2	9	3	0	0	0	0	0	0	0	0	0	0	15	6.0
11.0-33.5	0	0	2	4	3	2	3	0	0	0	0	0	0	0	0	0	14	5.0
348.5-11.0	0	0	0	4	5	2	0	0	0	0	0	0	0	0	0	0	11	4.0

Table AU-6. Bivariate distribution of calculated geostrophic winds (Vg) versus Unalakleet simultaneous surface winds (Us) for January, 1965. Horizontal directions represent the same sectors as the vertical except that 0 is the middle of the 348.5°-11.0° sector instead of the minimum direction value.

	D I R E C T I O N (Us)															TOTAL	PER	
	0.0	11.0	33.5	56.0	78.5	101.0	123.5	146.0	168.5	191.0	213.5	236.0	258.5	281.0	303.5			326.0
326.0-348.5	3	1	2	1	0	1	0	0	0	0	0	0	0	1	1	3	13	5.0
303.5-326.0	23	2	2	1	3	1	0	0	0	0	0	0	1	6	2	6	47	18.0
281.0-303.5	10	4	0	2	1	2	0	0	0	0	0	0	0	2	5	6	32	12.0
258.5-281.0	1	1	4	4	3	1	1	0	0	0	0	0	0	0	0	0	15	6.0
236.0-258.5	1	1	3	1	3	0	0	0	0	0	0	0	0	0	0	0	9	3.0
213.5-236.0	0	0	0	0	1	1	0	0	0	0	0	0	0	0	0	0	2	0.0
191.0-213.5	0	1	0	1	2	0	0	0	0	0	0	0	0	0	0	0	4	1.0
168.5-191.0	0	0	0	0	2	2	0	0	0	0	0	0	0	0	0	0	4	1.0
146.0-168.5	0	1	0	1	4	1	0	0	0	0	0	0	0	0	0	0	7	2.0
123.5-146.0	0	0	0	1	22	2	1	0	0	0	0	0	0	0	0	0	26	10.0
101.0-123.5	1	0	2	6	11	2	0	0	1	0	0	1	0	0	0	0	24	9.0
78.5-101.0	4	1	3	0	3	0	1	0	0	0	0	0	0	0	1	1	14	5.0
56.0-78.5	1	1	3	4	0	0	0	0	0	0	0	0	1	0	0	1	11	4.0
33.5-56.0	4	2	5	3	1	0	0	0	0	0	0	0	0	0	0	0	15	5.0
11.0-33.5	2	2	3	1	1	0	0	0	0	0	0	0	0	0	2	3	14	5.0
348.5-11.0	3	3	3	1	0	0	0	0	0	0	0	0	0	0	0	1	11	4.0

Table AN-6. Bivariate distribution of calculated geostrophic winds (Vg) versus Nome simultaneous surface winds (Ns) for January, 1965. Horizontal directions represent the same sectors as the vertical except that 0 is the middle of the 348.5°-11.0° sector instead of the minimum direction value.

D I R E C T I O N

	S P E E D (ms^{-1})															(obs. 248)	
	0-2	2-4	4-6	6-8	8-10	10-12	12-14	14-16	16-18	18-20	20-22	22-24	24-26	26-28	28-30	TOTAL	PER
326.2-349.5	0	5	4	1	0	0	0	0	0	0	0	0	0	0	0	10	4.0
303.5-326.0	0	6	14	0	1	1	0	0	0	0	0	0	0	0	0	22	8.0
281.0-303.5	1	12	9	1	1	0	0	0	0	0	0	0	0	0	0	24	9.0
258.5-281.0	4	15	14	2	1	3	0	0	0	0	0	0	0	0	0	39	15.0
236.0-258.5	4	6	3	10	5	2	0	0	0	0	0	0	0	0	0	30	12.0
213.5-236.0	1	8	8	4	3	0	0	0	0	0	0	0	0	0	0	24	9.0
191.0-213.5	2	4	5	3	0	0	0	0	0	0	0	0	0	0	0	14	5.0
168.5-191.0	1	4	2	3	0	0	0	0	0	0	0	0	0	0	0	10	4.0
146.0-168.5	2	5	4	3	0	0	0	0	0	0	0	0	0	0	0	14	5.0
123.5-146.0	4	5	5	0	0	0	1	0	0	0	0	0	0	0	0	15	6.0
101.0-123.5	0	7	6	2	0	0	0	0	0	0	0	0	0	0	0	15	6.0
78.5-101.0	0	5	10	4	1	0	0	0	0	0	0	0	0	0	0	20	8.0
56.0-78.5	1	0	1	3	0	0	0	0	0	0	0	0	0	0	0	5	2.0
33.5-56.0	0	0	1	0	0	0	0	0	0	0	0	0	0	0	0	1	0.0
11.0-33.5	0	0	0	0	0	0	0	0	0	0	0	0	0	0	0	0	0.0
348.5-11.0	4	1	0	0	0	0	0	0	0	0	0	0	0	0	0	5	2.0

Table AU-7. Bivariate distribution of wind direction versus wind speed data (three hourly) for Unalakleet, in July, 1965. Winds above 14 ms^{-1} are considered gale class.

D I R E C T I O N

	S P E E D (ms^{-1})															(obs. 248)	
	0-2	2-4	4-6	6-8	8-10	10-12	12-14	14-16	16-18	18-20	20-22	22-24	24-26	26-28	28-30	TOTAL	PER
326.0-348.5	1	4	1	0	0	0	0	0	0	0	0	0	0	0	0	6	2.0
303.5-326.0	0	5	1	4	0	2	0	1	0	0	0	0	0	0	0	13	5.0
281.0-303.5	2	2	3	4	0	0	0	0	0	0	0	0	0	0	0	11	4.0
258.5-281.0	0	6	7	11	11	4	0	0	0	0	0	0	0	0	0	39	15.0
236.0-258.5	1	6	12	10	1	4	0	0	0	0	0	0	0	0	0	34	13.0
213.5-236.0	0	5	7	2	0	0	0	0	0	0	0	0	0	0	0	14	5.0
191.0-213.5	0	2	6	4	0	0	0	0	0	0	0	0	0	0	0	12	4.0
168.5-191.0	3	8	8	11	3	0	0	0	0	2	0	0	0	0	0	33	13.0
146.0-168.5	1	4	2	2	4	0	0	0	0	0	0	0	0	0	0	13	5.0
123.5-146.0	0	0	8	8	2	5	0	1	0	0	0	0	0	0	0	24	9.0
101.0-123.5	0	1	2	6	3	1	2	1	0	0	0	0	0	0	0	16	6.0
78.5-101.0	0	1	2	5	0	0	0	0	0	0	0	0	0	0	0	8	3.0
55.0-78.5	0	0	0	0	0	0	0	0	0	0	0	0	0	0	0	0	0.0
33.5-55.0	0	0	0	0	0	0	0	0	0	0	0	0	0	0	0	1	0.0
11.0-33.5	0	0	0	0	0	0	0	0	0	0	0	0	0	0	0	0	0.0
249.5-11.0	19	3	0	1	1	0	0	0	0	0	0	0	0	0	0	24	9.0

Table AN-7. Bivariate distribution of wind direction versus wind speed data (three hourly) for Nome, in July, 1965. Winds above 14 ms^{-1} are considered gale class.

D I R E C T I O N (Us)

(obs. 248)

D I R E C T I O N (Vg)	D I R E C T I O N (Us)																PER	
	0.0	11.0	33.5	56.0	78.5	101.0	123.5	146.0	168.5	191.0	213.5	236.0	258.5	281.0	303.5	326.0		
326.0-348.5	0	0	0	0	0	0	0	0	0	1	0	0	0	0	1	0	2	0.0
303.5-326.0	0	0	0	0	0	1	2	0	0	0	1	1	2	1	1	1	10	4.0
281.0-303.5	1	0	0	0	0	0	1	0	1	5	5	2	7	4	5	3	34	13.0
258.5-281.0	2	0	0	0	0	2	2	0	2	1	7	7	11	7	7	3	51	20.0
236.0-258.5	0	0	0	0	2	2	2	4	0	2	4	4	5	1	4	0	30	12.0
213.5-236.0	0	0	0	0	4	0	1	0	0	2	1	11	3	4	0	1	27	10.0
191.0-213.5	0	0	0	0	5	1	2	3	0	0	1	2	3	3	1	1	22	8.0
168.5-191.0	0	0	0	0	2	4	0	3	4	1	2	1	3	3	0	0	23	9.0
146.0-168.5	0	0	0	0	3	3	3	2	2	2	2	2	0	0	0	1	20	8.0
123.5-146.0	0	0	0	3	4	0	1	2	1	0	1	0	2	0	1	0	15	6.0
101.0-123.5	0	0	0	0	0	0	1	0	0	0	0	0	1	0	1	0	3	1.0
78.5-101.0	1	0	1	1	0	0	0	0	0	0	0	0	1	1	1	0	6	2.0
56.0-78.5	0	0	0	1	0	0	0	0	0	0	0	0	0	0	0	0	1	0.0
33.5-56.0	0	0	0	0	0	1	0	0	0	0	0	0	0	0	0	0	1	0.0
11.0-33.5	0	0	0	0	0	0	0	0	0	0	0	0	1	0	0	0	1	0.0
348.5-11.0	1	0	0	0	0	1	0	0	0	0	0	0	0	0	0	0	2	0.0

Table AU-8. Bivariate distribution of calculated geostrophic winds (Vg) versus Unalakleet simultaneous surface winds (Us) for July, 1965. Horizontal directions represent the same sectors as the vertical except that 0 is the middle of the 348.5°-11.0° sector instead of the minimum direction value.

D I R E C T I O N (Vg)	D I R E C T I O N (Us)															(obs. 248)		
	0.0	11.0	33.5	56.0	78.5	101.0	123.5	146.0	168.5	191.0	213.5	236.0	258.5	281.0	303.5	326.0	TOTAL	PER
326.0-348.5	1	0	0	0	0	0	0	0	0	0	0	1	0	0	0	0	2	0.0
303.5-326.0	0	0	0	0	0	0	0	0	0	0	0	2	2	1	4	1	10	4.0
281.0-303.5	3	0	0	0	0	0	0	0	0	1	0	6	13	5	4	2	34	13.0
258.5-281.0	8	0	0	0	1	0	0	1	2	0	1	13	19	2	3	1	51	20.0
236.0-258.5	2	0	0	0	0	3	0	1	7	4	6	3	2	0	1	1	30	12.0
213.5-236.0	1	0	0	0	1	1	2	2	9	5	2	3	1	0	0	0	27	10.0
191.0-213.5	2	0	0	0	2	1	6	1	3	1	2	2	1	0	1	0	22	8.0
168.5-191.0	0	0	0	0	2	5	5	3	4	0	1	2	0	1	0	0	23	9.0
146.0-168.5	0	0	1	0	0	4	8	2	2	1	2	0	0	0	0	0	20	8.0
123.5-146.0	2	0	0	0	2	1	3	1	5	0	0	0	1	0	0	0	15	6.0
101.0-123.5	0	0	0	0	0	1	0	0	1	0	0	1	0	0	0	0	3	1.0
78.5-101.0	2	0	0	0	0	0	0	2	0	0	0	1	0	0	0	1	6	2.0
56.0- 78.5	0	0	0	0	0	0	0	0	0	0	0	0	0	1	0	0	1	0.0
33.5- 56.0	1	0	0	0	0	0	0	0	0	0	0	0	0	0	0	0	1	0.0
11.0- 33.5	0	0	0	0	0	0	0	0	0	0	0	0	0	1	0	0	1	0.0
348.5- 11.0	2	0	0	0	0	0	0	0	0	0	0	0	0	0	0	0	2	3.0

Table AN-8. Bivariate distribution of calculated geostrophic winds (Vg) versus Nome simultaneous surface winds (Ns) for July, 1965. Horizontal directions represent the same sectors as the vertical except that 0 is the middle of the 348.5°-11.0° sector instead of the minimum direction value.

DIRECTION	S P E E D (ms ⁻¹)															(obs. 248)	
	0-2	2-4	4-6	6-8	8-10	10-12	12-14	14-16	16-18	18-20	20-22	22-24	24-26	26-28	28-30	TOTAL	PER
326.0-348.5	0	0	0	0	0	0	0	0	0	0	0	0	0	0	0	0	0.0
303.5-326.0	0	0	0	0	0	0	0	0	0	0	0	0	0	0	0	0	0.0
281.0-303.5	0	0	0	0	0	0	0	0	0	0	0	0	0	0	0	0	0.0
258.5-281.0	0	0	0	0	0	0	0	0	0	0	0	0	0	0	0	0	0.0
236.0-258.5	0	0	0	0	0	0	0	0	0	0	0	0	0	0	0	0	0.0
213.5-236.0	0	0	0	0	0	0	0	0	0	0	0	0	0	0	0	0	0.0
191.0-213.5	0	0	0	0	0	0	0	0	0	0	0	0	0	0	0	0	0.0
168.5-191.0	0	0	0	0	0	0	0	0	0	0	0	0	0	0	0	0	0.0
146.0-168.5	0	0	1	0	0	0	0	0	0	0	0	0	0	0	0	1	0.0
123.5-146.0	0	0	0	0	0	0	0	0	0	0	0	0	0	0	0	0	0.0
101.0-123.5	0	1	0	1	1	0	0	0	0	0	0	0	0	0	0	3	1.0
78.5-101.0	1	5	5	13	35	74	62	12	3	4	0	0	0	0	0	214	86.0
56.0-78.5	0	1	3	4	8	11	1	1	0	0	0	0	0	0	0	29	11.0
33.5-56.0	0	0	0	0	0	0	0	0	0	0	0	0	0	0	0	0	0.0
11.0-33.5	0	0	0	0	0	1	0	0	0	0	0	0	0	0	0	1	0.0
348.5-11.0	0	0	0	0	0	0	0	0	0	0	0	0	0	0	0	0	0.0

Table AU-9. Bivariate distribution of wind direction versus wind speed data (three hourly) for Unalakleet, in January, 1966. Winds above 14 ms⁻¹ are considered gale class.

D I R E C T I O N

	S P E E D (ms ⁻¹)															(obs. 248)	
	0- 2	2- 4	4- 6	6- 8	8-10	10-12	12-14	14-16	16-18	18-20	20-22	22-24	24-26	26-28	28-30	TOTAL	PER
326.0-348.5	0	1	0	0	0	0	0	0	0	0	0	0	0	0	0	1	0.0
303.5-326.0	0	2	1	0	0	0	0	0	0	0	0	0	0	0	0	3	1.0
281.0-303.5	1	3	0	0	0	0	0	0	0	0	0	0	0	0	0	4	1.0
258.5-281.0	1	0	0	0	0	0	0	0	0	0	0	0	0	0	0	1	0.0
236.0-258.5	1	0	0	0	0	0	0	0	0	0	0	0	0	0	0	1	0.0
213.5-236.0	0	0	0	0	0	0	0	0	0	0	0	0	0	0	0	0	0.0
191.0-213.5	0	0	0	0	0	0	0	0	0	0	0	0	0	0	0	0	0.0
168.5-191.0	1	3	0	0	0	0	0	0	0	0	0	0	0	0	0	4	1.0
146.0-168.5	0	2	0	0	0	0	0	0	0	0	0	0	0	0	0	2	0.0
123.5-146.0	0	0	1	0	0	0	0	0	0	0	0	0	0	0	0	1	0.0
101.0-123.5	0	2	0	0	0	0	0	0	0	0	0	0	0	0	0	2	0.0
78.5-101.0	0	7	7	6	10	13	5	21	1	0	0	0	0	0	0	70	28.0
56.0- 78.5	2	12	6	4	5	8	16	0	0	0	0	0	0	0	0	53	21.0
33.5- 56.0	0	2	4	5	4	3	3	1	0	0	0	0	0	0	0	22	8.0
11.0- 33.5	1	1	3	5	2	3	5	0	0	0	0	0	0	0	0	20	8.0
348.5- 11.0	54	3	3	2	1	0	1	0	0	0	0	0	0	0	0	64	25.0

Table AN-9. Bivariate distribution of wind direction versus wind speed data (three hourly)
for Nome, in January, 1966. Winds above 14 ms⁻¹ are considered gale class.

D I R E C T I O N (Us)

(obs. 248)

D I R E C T I O N (Vg)	D I R E C T I O N (Us)															TOTAL	PER	
	0.0	11.0	33.5	56.0	78.5	101.0	123.5	146.0	168.5	191.0	213.5	236.0	258.5	281.0	303.5			326.0
326.0-348.5	0	0	0	1	5	0	0	0	0	0	0	0	0	0	0	0	6	2.0
303.5-326.0	0	0	0	0	2	0	0	0	0	0	0	0	0	0	0	0	2	0.0
281.0-303.5	0	0	0	1	2	1	0	0	0	0	0	0	0	0	0	0	4	1.0
258.5-281.0	0	0	0	1	4	0	0	0	0	0	0	0	0	0	0	0	5	2.0
236.0-258.5	0	0	0	1	1	0	0	0	0	0	0	0	0	0	0	0	2	0.0
213.5-236.0	0	0	0	0	3	0	0	0	0	0	0	0	0	0	0	0	3	1.0
191.0-213.5	0	0	0	0	3	0	0	0	0	0	0	0	0	0	0	0	3	1.0
168.5-191.0	0	0	0	0	4	0	0	0	0	0	0	0	0	0	0	0	4	1.0
146.0-168.5	0	0	0	0	19	0	0	0	0	0	0	0	0	0	0	0	19	7.0
123.5-146.0	0	0	0	6	59	0	0	1	0	0	0	0	0	0	0	0	66	26.0
101.0-123.5	0	1	0	9	72	2	0	0	0	0	0	0	0	0	0	0	84	33.0
78.5-101.0	0	0	0	4	27	0	0	0	0	0	0	0	0	0	0	0	31	12.0
56.0-78.5	0	0	0	3	4	0	0	0	0	0	0	0	0	0	0	0	7	2.0
33.5-56.0	0	0	0	0	3	0	0	0	0	0	0	0	0	0	0	0	3	1.0
11.0-33.5	0	0	0	2	4	0	0	0	0	0	0	0	0	0	0	0	6	2.0
348.5-11.0	0	0	0	1	2	0	0	0	0	0	0	0	0	0	0	0	3	1.0

Table AU-10. Bivariate distribution of calculated geostrophic winds (Vg) versus Unalakleet simultaneous surface winds (Us) for January, 1966. Horizontal directions represent the same sectors as the vertical except that 0 is the middle of the 348.5°-11.0° sector instead of the minimum direction value.

D I R E C T I O N (Vg)	D I R E C T I O N (Us)															(obs. 248)		
	0.0	11.0	33.5	56.0	78.5	101.0	123.5	146.0	168.5	191.0	213.5	236.0	258.5	281.0	303.5	326.0	TOTAL	PER
326.0-348.5	5	0	0	1	0	0	0	0	0	0	0	0	0	0	0	0	6	2.0
303.5-326.0	0	0	0	1	0	0	0	0	0	0	0	0	0	0	0	1	2	0.0
281.0-303.5	2	1	0	1	0	0	0	0	0	0	0	0	0	0	0	0	4	1.0
258.5-281.0	1	0	1	2	1	0	0	0	0	0	0	0	0	0	0	0	5	2.0
236.0-258.5	0	0	0	2	0	0	0	0	0	0	0	0	0	0	0	0	2	0.0
213.5-236.0	1	0	0	2	0	0	0	0	0	0	0	0	0	0	0	0	3	1.0
191.0-213.5	1	0	1	1	0	0	0	0	0	0	0	0	0	0	0	0	3	1.0
168.5-191.0	1	1	0	0	2	0	0	0	0	0	0	0	0	0	0	0	4	1.0
146.0-168.5	2	1	1	5	7	1	1	1	0	0	0	0	0	0	0	0	19	7.0
123.5-146.0	8	5	4	10	36	1	0	0	2	0	0	0	0	0	0	0	66	26.0
101.0-123.5	24	6	11	21	19	0	0	0	1	0	0	1	0	1	0	0	84	33.0
78.5-101.0	10	3	3	5	5	0	0	0	1	0	0	0	1	2	1	0	31	12.0
56.0-78.5	3	1	1	1	0	0	0	0	0	0	0	0	0	1	0	0	7	2.0
33.5-56.0	1	1	0	1	0	0	0	0	0	0	0	0	0	0	0	0	3	1.0
11.0-33.5	5	1	0	0	0	0	0	0	0	0	0	0	0	0	0	0	6	2.0
348.5-11.0	0	0	0	0	0	0	0	1	0	0	0	0	0	0	2	0	3	1.0

Table AN-10. Bivariate distribution of calculated geostrophic winds (Vg) versus Nome simultaneous surface winds (Ns) for January, 1966. Horizontal directions represent the same sectors as the vertical except that 0 is the middle of the 348.5°-11.0° sector instead of the minimum direction value.

D I R E C T I O N

	S P E E D (ms^{-1})															(obs. 248)	
	0-2	2-4	4-6	6-8	8-10	10-12	12-14	14-16	16-18	18-20	20-22	22-24	24-26	26-28	28-30	TOTAL	PER
326.0-348.5	0	2	6	2	1	0	0	0	0	0	0	0	0	0	0	11	4.0
303.5-326.0	2	3	6	3	1	0	0	0	0	0	0	0	0	0	0	15	6.0
281.0-303.5	0	6	5	2	0	0	0	0	0	0	0	0	0	0	0	13	5.0
258.5-281.0	0	12	6	0	0	0	0	0	0	0	0	0	0	0	0	18	7.0
236.0-258.5	0	12	10	3	8	0	0	0	0	0	0	0	0	0	0	33	13.0
213.5-236.0	0	4	8	1	4	4	0	0	0	0	0	0	0	0	0	21	8.0
191.0-213.5	1	2	1	0	5	2	0	0	0	0	0	0	0	0	0	11	4.0
168.5-191.0	1	3	5	4	1	0	0	0	0	0	0	0	0	0	0	14	5.0
146.0-168.5	0	3	4	1	2	0	0	0	0	0	0	0	0	0	0	10	4.0
123.5-146.0	0	7	7	4	0	0	0	0	0	0	0	0	0	0	0	18	7.0
101.0-123.5	1	6	14	3	2	0	0	0	0	0	0	0	0	0	0	26	10.0
78.5-101.0	0	6	17	10	6	1	0	0	0	0	0	0	0	0	0	40	16.0
56.0-78.5	0	4	4	3	2	0	0	0	0	0	0	0	0	0	0	13	5.0
33.5-56.0	1	0	0	0	0	0	0	0	0	0	0	0	0	0	0	1	0.0
11.0-33.5	0	1	0	0	0	0	0	0	0	0	0	0	0	0	0	1	0.0
348.5-11.0	1	1	1	0	0	0	0	0	0	0	0	0	0	0	0	3	1.0

Table AU-11. Bivariate distribution of wind direction versus wind speed data (three hourly) for Unalakleet, in July, 1966. Winds above 14 ms^{-1} are considered gale class.

DIRECTION	S P E E D (ms ⁻¹)															(obs. 248)	
	0-2	2-4	4-6	6-8	8-10	10-12	12-14	14-16	16-18	18-20	20-22	22-24	24-26	26-28	28-30	TOTAL	PER
326.0-348.5	0	1	0	0	0	0	0	0	0	0	0	0	0	0	0	1	0.0
303.5-326.0	0	6	0	0	0	0	0	0	0	0	0	0	0	0	0	6	2.0
281.0-303.5	1	7	1	2	0	0	0	0	0	0	0	0	0	0	0	11	4.0
258.5-281.0	2	9	8	4	1	0	0	0	0	0	0	0	0	0	0	24	9.0
236.0-258.5	1	5	17	3	3	0	0	0	0	0	0	0	0	0	0	29	11.0
213.5-236.0	1	11	6	1	0	0	0	0	0	0	0	0	0	0	0	19	7.0
191.0-213.5	1	5	5	1	0	3	1	0	0	0	0	0	0	0	0	16	6.0
168.5-191.0	2	11	3	2	3	3	1	0	0	0	0	0	0	0	0	25	10.0
146.0-168.5	2	4	9	3	0	0	0	0	0	0	0	0	0	0	0	18	7.0
123.5-146.0	0	5	9	7	2	0	0	0	0	0	0	0	0	0	0	23	9.0
101.0-123.5	0	7	4	6	8	2	0	0	0	0	0	0	0	0	0	27	10.0
78.5-101.0	1	1	6	5	1	0	0	0	0	0	0	0	0	0	0	14	5.0
56.0-78.5	0	1	3	1	1	0	0	0	0	0	0	0	0	0	0	6	2.0
33.5-56.0	0	4	0	2	0	0	0	0	0	0	0	0	0	0	0	6	2.0
11.0-33.5	1	3	2	3	0	0	0	0	0	0	0	0	0	0	0	9	3.0
348.5-11.0	5	5	0	2	2	0	0	0	0	0	0	0	0	0	0	14	5.0

Table AN-11. Bivariate distribution of wind direction versus wind speed data (three hourly) for Nome, in July, 1966. Winds above 14 ms⁻¹ are considered gale class.

D I R E C T I O N (Us)

(obs. 248)

D I R E C T I O N (Vg)	D I R E C T I O N (Us)																TOTAL	PER
	0.0	11.0	33.5	56.0	78.5	101.0	123.5	146.0	168.5	191.0	213.5	236.0	258.5	281.0	303.5	326.0		
335.0-348.5	0	0	0	1	1	0	0	0	0	0	0	0	0	0	1	2	5	2.0
303.5-326.0	0	0	0	0	2	0	0	0	0	0	0	1	0	0	0	0	3	1.0
281.0-303.5	0	0	0	1	1	1	0	0	0	0	0	1	0	0	1	0	5	2.0
258.5-281.0	0	0	0	0	1	1	0	0	3	0	3	2	2	2	3	2	19	7.0
236.0-258.5	0	0	0	1	5	7	2	1	2	5	7	8	2	4	1	0	45	18.0
213.5-236.0	1	0	0	1	3	2	0	1	1	1	5	5	1	2	0	0	23	9.0
191.0-213.5	1	0	1	0	5	5	3	4	4	4	1	3	2	1	1	0	35	14.0
168.5-191.0	0	0	0	3	3	1	0	2	2	0	2	2	3	0	1	0	27	10.0
146.0-168.5	0	0	0	0	4	3	4	2	1	1	2	4	4	2	2	0	29	11.0
123.5-146.0	0	0	0	1	9	2	0	0	0	0	0	5	1	2	0	2	22	8.0
101.0-123.5	0	1	0	4	4	2	1	0	0	0	1	1	2	0	4	2	22	8.0
78.5-101.0	1	0	0	1	1	1	0	0	0	0	0	0	1	0	0	2	7	2.0
56.0-78.5	0	0	0	0	0	1	0	0	0	0	0	0	0	0	0	0	1	0.0
33.5-56.0	0	0	0	0	0	0	0	0	0	0	0	1	0	0	1	1	3	1.0
11.0-33.5	0	0	0	0	0	0	0	0	1	0	0	0	0	0	0	0	1	0.0
348.5-11.0	0	0	0	0	1	0	0	0	0	0	0	0	0	0	0	0	1	0.0

Table AU-12. Bivariate distribution of calculated geostrophic winds (Vg) versus Unalakleet simultaneous surface winds (Us) for July, 1966. Horizontal directions represent the same sectors as the vertical except that 0 is the middle of the 348.5°-11.0° sector instead of the minimum direction value.

D I R E C T I O N (Vg)	D I R E C T I O N (Us)																TOTAL	PER
	0.0	11.0	33.5	56.0	78.5	101.0	123.5	146.0	168.5	191.0	213.5	236.0	258.5	281.0	303.5	326.0		
326.0-348.5	1	1	0	0	0	0	0	0	2	0	0	1	0	0	0	0	5	2.0
303.5-326.0	2	0	0	0	0	0	0	0	0	0	0	0	1	0	0	0	3	1.0
281.0-303.5	2	0	0	0	0	0	0	0	0	0	1	0	0	2	0	0	5	2.0
258.5-281.0	1	1	0	0	0	2	1	0	2	0	2	5	3	2	0	0	19	7.0
236.0-258.5	3	0	0	1	1	3	1	1	4	2	5	8	12	4	0	0	45	18.0
213.5-236.0	0	1	0	0	2	1	0	2	3	3	3	4	3	1	0	0	23	9.0
191.0-213.5	3	2	0	1	2	5	2	2	8	4	1	1	2	0	2	0	35	14.0
168.5-191.0	0	0	0	2	1	5	9	4	2	2	1	1	0	0	0	0	27	10.3
146.0-168.5	0	0	0	0	2	5	4	5	2	2	3	3	1	2	0	0	29	11.0
123.5-146.0	1	0	1	0	5	4	2	3	1	1	2	2	0	0	0	0	22	8.0
101.0-123.5	0	4	2	2	0	2	4	1	0	2	1	1	0	0	2	1	22	8.0
78.5-101.0	0	0	3	0	1	0	0	0	1	0	0	0	1	0	1	0	7	2.0
56.0-78.5	0	0	0	0	0	0	0	0	0	0	0	0	0	0	1	0	1	0.0
33.5-56.0	0	0	0	0	0	0	0	0	0	0	0	2	1	0	0	0	3	1.0
11.0-33.5	1	0	0	0	0	0	0	0	0	0	0	0	0	0	0	0	1	0.0
348.5-11.0	0	0	0	0	0	0	0	0	0	0	0	1	0	0	0	0	1	0.0

Table AN-12. Bivariate distribution of calculated geostrophic winds (Vg) versus Nome simultaneous surface winds (Ns) for July, 1966. Horizontal directions represent the same sectors as the vertical except that 0 is the middle of the 348.5°-11.0° sector instead of the minimum direction value.

D I R E C T I O N

	S P E E D (ms ⁻¹)															(obs. 248)	
	0-2	2-4	4-6	6-8	8-10	10-12	12-14	14-16	16-18	18-20	20-22	22-24	24-26	26-28	28-30	TOTAL	PER
326.0-348.5	0	1	6	1	0	0	0	0	0	0	0	0	0	0	0	8	3.0
303.5-326.0	0	2	0	0	0	0	0	0	0	0	0	0	0	0	0	2	0.2
281.0-303.5	0	0	1	0	0	0	0	0	0	0	0	0	0	0	0	1	0.2
258.5-281.0	0	0	0	2	2	0	0	0	0	0	0	0	0	0	0	4	1.0
236.0-258.5	1	1	3	5	1	2	0	0	0	0	0	0	0	0	0	13	5.0
213.5-236.0	0	0	4	2	5	3	1	1	0	0	0	0	0	0	0	16	6.0
191.0-213.5	0	0	0	3	0	1	0	0	0	0	0	0	0	0	0	4	1.2
168.5-191.0	0	0	1	2	0	0	0	0	0	0	0	0	0	0	0	3	1.0
146.0-168.5	0	0	3	0	0	0	0	0	0	0	0	0	0	0	0	3	1.0
123.5-146.0	0	1	0	2	0	0	0	0	0	0	0	0	0	0	0	3	1.0
101.0-123.5	1	10	8	10	6	0	2	0	0	0	0	0	0	0	0	37	14.0
78.5-101.0	1	6	15	18	29	31	21	3	4	4	4	0	0	0	0	136	54.2
56.0-78.5	0	0	3	0	1	1	0	0	0	0	0	0	0	0	0	5	2.0
33.5-56.0	0	0	1	0	1	1	0	0	0	0	0	0	0	0	0	3	1.0
11.0-33.5	0	1	0	0	0	0	0	0	0	0	0	0	0	0	0	1	0.0
348.5-11.0	1	2	4	2	0	0	0	0	0	0	0	0	0	0	0	9	3.0

Table AU-13. Bivariate distribution of wind direction versus wind speed data (three hourly) for Unalakleet, in January, 1967. Winds above 14 ms⁻¹ are considered gale class.

D I R E C T I O N

	S P E E D (ms ⁻¹)															(obs. 248)	
	0-2	2-4	4-6	6-8	8-10	10-12	12-14	14-16	16-18	18-20	20-22	22-24	24-26	26-28	28-30	TOTAL	PER
326.0-348.5	0	2	5	1	2	0	0	0	0	0	0	0	0	0	0	10	4.0
303.5-326.0	1	2	2	1	1	1	0	0	0	0	0	0	0	0	0	8	3.0
281.0-303.5	2	1	3	1	0	0	0	0	0	0	0	0	0	0	0	7	2.0
258.5-281.0	0	4	2	3	0	0	0	0	0	0	0	0	0	0	0	9	3.0
236.0-258.5	1	1	1	0	0	0	0	0	0	0	0	0	0	0	0	3	1.0
213.5-236.0	1	0	0	1	1	0	0	0	0	0	0	0	0	0	0	3	1.0
191.0-213.5	0	0	2	1	5	0	0	0	0	0	0	0	0	0	0	8	3.0
168.5-191.0	0	0	1	3	0	1	0	0	0	0	0	0	0	0	0	5	2.0
146.0-168.5	0	0	2	2	3	2	0	0	0	0	0	0	0	0	0	9	3.0
123.5-146.0	0	1	2	1	1	0	0	0	0	0	0	0	0	0	0	5	2.0
101.0-123.5	2	4	4	1	3	0	0	0	0	0	0	0	0	0	0	14	5.0
78.5-101.0	0	7	10	15	6	6	10	1	2	1	0	1	1	0	0	60	24.0
56.0-78.5	1	2	12	9	4	2	0	0	0	0	0	0	0	0	0	30	12.0
33.5-56.0	0	3	5	4	2	4	0	0	0	0	0	0	0	0	0	18	7.0
11.0-33.5	0	7	2	0	1	2	2	0	0	0	0	0	0	0	0	14	5.0
348.5-11.0	35	7	2	0	0	1	0	0	0	0	0	0	0	0	0	45	18.0

Table AN-13. Bivariate distribution of wind direction versus wind speed data (three hourly) for Nome, in January, 1967. Winds above 14 ms⁻¹ are considered gale class.

D I R E C T I O N (Vg)

	D I R E C T I O N (Us)															(obs. 248)		
	0.0	11.0	33.5	56.0	78.5	101.0	123.5	146.0	168.5	191.0	213.5	236.0	258.5	281.0	303.5	326.0	TOTAL	PER
326.0-348.5	0	0	0	0	1	1	0	0	0	0	0	1	0	0	0	0	3	1.0
303.5-326.0	3	0	0	0	3	1	0	0	0	1	0	0	0	0	1	4	13	5.0
281.0-303.5	1	0	0	0	3	1	0	0	0	2	2	0	1	0	0	2	12	4.0
258.5-281.0	0	0	0	0	3	2	0	0	0	0	5	3	0	1	0	0	14	5.0
236.0-258.5	0	0	0	0	3	4	1	0	0	0	1	2	0	0	0	0	11	4.0
213.5-236.0	0	0	0	0	5	2	0	0	1	0	0	1	0	0	0	0	9	3.0
191.0-213.5	0	0	0	0	4	3	1	0	0	0	3	1	0	0	0	0	12	4.0
168.5-191.0	0	0	1	0	12	3	1	0	1	0	2	0	0	0	0	0	20	8.0
146.0-168.5	1	0	1	0	16	0	0	0	1	1	1	0	0	0	0	0	21	8.0
123.5-146.0	0	0	0	1	40	4	0	3	0	0	2	4	1	0	0	0	55	22.0
101.0-123.5	0	0	0	0	23	3	0	0	0	0	0	1	1	0	0	0	28	11.0
78.5-101.0	1	0	1	3	11	5	0	0	0	0	0	0	1	0	0	1	23	9.0
56.0-78.5	2	0	0	1	4	4	0	0	0	0	0	0	0	0	1	0	12	4.0
33.5-56.0	0	0	0	0	4	1	0	0	0	0	0	0	0	0	0	0	5	2.0
11.0-33.5	0	0	0	0	3	2	0	0	0	0	0	0	0	0	0	1	6	2.0
348.5-11.0	1	1	0	0	1	1	0	0	0	0	0	0	0	0	0	0	4	1.0

Table AU-14. Bivariate distribution of calculated geostrophic winds (Vg) versus Unalakleet simultaneous surface winds (Us) for January, 1967. Horizontal directions represent the same sectors as the vertical except that 0 is the middle of the 348.5°-11.0° sector instead of the minimum direction value.

D I R E C T I O N (Vg)	D I R E C T I O N (Us)															(obs. 248)		
	0.0	11.0	33.5	56.0	78.5	101.0	123.5	146.0	168.5	191.0	213.5	236.0	258.5	281.0	303.5	326.0	TOTAL	PER
326.0-348.5	0	0	0	0	0	0	0	0	0	0	1	0	2	0	0	0	3	1.0
303.5-326.0	6	2	0	1	0	0	0	0	0	0	0	0	0	2	1	1	13	5.0
281.0-303.5	4	2	0	0	0	0	0	0	0	0	0	0	0	0	2	4	12	4.0
258.5-281.0	4	1	0	0	0	0	0	0	0	0	0	0	2	2	1	4	14	5.0
236.0-258.5	3	0	0	1	0	0	0	0	0	0	2	2	2	0	1	0	11	4.0
213.5-236.0	3	0	0	0	2	0	0	0	0	2	0	0	1	1	0	0	9	3.0
191.0-213.5	1	0	0	0	1	3	0	1	3	2	0	1	0	0	0	0	12	4.0
168.5-191.0	1	0	0	2	5	0	2	6	0	3	0	0	0	0	1	0	20	8.0
146.0-168.5	0	0	1	4	12	2	1	0	0	1	0	0	0	0	0	0	21	8.0
123.5-146.0	3	0	3	6	30	7	2	2	2	0	0	0	0	0	0	0	55	22.0
101.0-123.5	3	0	2	14	7	2	0	0	0	0	0	0	0	0	0	0	28	11.0
78.5-101.0	5	4	7	2	2	0	0	0	0	0	0	0	0	1	1	1	23	9.0
56.0-78.5	6	1	1	0	1	0	0	0	0	0	0	0	2	0	1	0	12	4.0
33.5-56.0	1	3	1	0	0	0	0	0	0	0	0	0	0	0	0	0	5	2.0
11.0-33.5	3	1	2	0	0	0	0	0	0	0	0	0	0	0	0	0	6	2.0
348.5-11.0	2	0	1	0	0	0	0	0	0	0	0	0	0	1	0	0	4	1.0

Table AN-14. Bivariate distribution of calculated geostrophic winds (Vg) versus Nome simultaneous surface winds (Ns) for January, 1967. Horizontal directions represent the same sectors as the vertical except that 0 is the middle of the 348.5°-11.0° sector instead of the minimum direction value.

D I R E C T I O N

	S P E E D (ms ⁻¹)															(obs. 248)	
	0-2	2-4	4-6	6-8	8-10	10-12	12-14	14-16	16-18	18-20	20-22	22-24	24-26	26-28	28-30	TOTAL	PER
325.0-348.5	0	1	3	3	0	0	0	0	0	0	0	0	0	0	0	7	2.0
303.5-326.0	0	4	7	2	0	0	0	0	0	0	0	0	0	0	0	13	5.0
281.0-303.5	1	5	6	1	0	0	0	0	0	0	0	0	0	0	0	13	5.0
258.5-281.0	0	8	22	10	2	8	1	1	0	0	0	0	0	0	0	52	20.0
236.0-258.5	1	6	16	12	7	8	2	0	0	0	0	0	0	0	0	52	20.0
213.5-236.0	1	4	4	10	14	0	1	0	0	0	0	0	0	0	0	34	13.0
191.0-213.5	0	2	2	5	1	0	0	0	0	0	0	0	0	0	0	10	4.0
168.5-191.0	1	5	4	2	2	0	0	0	0	0	0	0	0	0	0	14	5.0
146.0-168.5	1	2	1	0	0	0	0	0	0	0	0	0	0	0	0	4	1.0
123.5-146.0	0	4	2	2	1	0	0	0	0	0	0	0	0	0	0	9	3.0
101.0-123.5	1	9	3	0	0	0	0	0	0	0	0	0	0	0	0	13	5.0
78.5-101.0	1	9	6	1	0	0	0	0	0	0	0	0	0	0	0	17	6.0
56.0-78.5	0	1	1	0	0	0	0	0	0	0	0	0	0	0	0	2	0.0
33.5-56.0	0	0	1	0	0	0	0	0	0	0	0	0	0	0	0	1	0.0
11.0-33.5	0	0	0	0	0	0	0	0	0	0	0	0	0	0	0	0	0.0
348.5-11.0	5	2	0	0	0	0	0	0	0	0	0	0	0	0	0	7	2.0

Table AU-15. Bivariate distribution of wind direction versus wind speed data (three hourly) for Unalakleet, in July, 1967. Winds above 14 ms⁻¹ are considered gale class.

DIRECTION

	S P E E D (ms ⁻¹)															(obs. 248)	
	0- 2	2-4	4- 6	6- 8	8-10	10-12	12-14	14-16	16-18	18-20	20-22	22-24	24-26	26-28	28-30	TOTAL	PER
326.0-348.5	2	2	3	0	0	0	0	0	0	0	0	0	0	0	0	7	2.0
303.5-326.0	2	8	0	0	0	0	0	0	0	0	0	0	0	0	0	10	4.0
281.0-303.5	1	4	2	6	0	0	0	0	0	0	0	0	0	0	0	13	5.0
258.5-281.0	1	1	15	9	2	3	0	0	0	0	0	0	0	0	0	31	12.0
236.0-258.5	0	9	15	9	1	0	0	0	0	0	0	0	0	0	0	34	13.0
213.5-236.0	1	13	17	5	0	0	0	0	0	0	0	0	0	0	0	36	14.0
191.0-213.5	0	12	14	4	1	0	0	0	0	0	0	0	0	0	0	31	12.0
168.5-191.0	0	13	8	4	0	0	0	0	0	0	0	0	0	0	0	25	10.0
146.0-168.5	1	6	5	1	1	0	0	0	0	0	0	0	0	0	0	14	5.0
123.5-146.0	0	4	5	1	0	0	0	0	0	0	0	0	0	0	0	10	4.0
101.0-123.5	1	4	1	1	0	0	0	0	0	0	0	0	0	0	0	7	2.0
78.5-101.0	0	3	2	0	0	1	0	0	0	0	0	0	0	0	0	6	2.0
56.0- 78.5	0	1	2	0	0	0	0	0	0	0	0	0	0	0	0	3	1.0
33.5- 56.0	0	3	1	1	0	0	0	0	0	0	0	0	0	0	0	5	2.0
11.0- 33.5	0	0	0	0	0	0	0	0	0	0	0	0	0	0	0	0	0.0
348.5- 11.0	10	2	3	1	0	0	0	0	0	0	0	0	0	0	0	16	6.0

Table AN-15. Bivariate distribution of wind direction versus wind speed data (three hourly) for Nome, in July, 1967. Winds above 14 ms⁻¹ are considered gale class.

D I R E C T I O N (Vg)	D I R E C T I O N (Us)															TOTAL	PER	
	0.0	11.0	33.5	56.0	78.5	101.0	123.5	146.0	168.5	191.0	213.5	236.0	258.5	281.0	303.5			326.0
326.0-348.5	0	0	0	0	1	0	0	0	0	0	0	0	0	0	0	0	1	0.0
303.5-326.0	0	0	0	0	0	0	0	0	0	0	0	0	0	0	0	0	0	0.0
281.0-303.5	0	0	0	0	1	2	0	0	1	1	5	3	6	3	1	0	23	9.0
258.5-281.0	3	0	0	0	0	0	0	1	1	2	4	5	5	0	0	0	21	8.0
236.0-258.5	0	0	0	0	0	0	1	0	1	2	9	16	4	0	0	0	33	13.0
213.5-236.0	0	0	0	0	0	1	3	0	1	2	2	6	7	0	0	0	22	8.0
191.0-213.5	0	0	0	0	0	1	1	1	1	2	2	3	6	1	0	0	18	7.0
168.5-191.0	1	0	0	0	0	2	2	0	2	1	6	8	4	1	0	0	27	10.0
146.0-168.5	1	0	0	0	1	1	1	0	5	0	3	2	2	2	0	1	19	7.0
123.5-146.0	1	0	0	2	6	5	0	1	2	0	2	2	3	1	1	2	28	11.0
101.0-123.5	1	0	1	0	6	1	0	0	0	0	1	2	5	1	4	1	23	9.0
78.5-101.0	0	0	0	0	1	0	0	0	0	0	0	3	6	2	4	0	16	6.0
56.0-78.5	0	0	0	0	0	0	0	0	0	0	0	1	3	1	2	2	9	3.0
33.5-56.0	0	0	0	0	0	0	0	0	0	0	0	0	0	0	0	0	0	0.0
11.0-33.5	0	0	0	0	1	0	0	0	0	0	0	0	1	1	0	0	3	1.0
348.5-11.0	0	0	0	0	0	0	1	1	0	0	0	1	0	0	1	1	5	2.0

Table AU-16. Bivariate distribution of calculated geostrophic winds (Vg) versus Unalakleet simultaneous surface winds (Us) for July, 1967. Horizontal directions represent the same sectors as the vertical except that 0 is the middle of the 348.5°-11.0° sector instead of the minimum direction value.

DIRECTION (Vg)	DIRECTION (Us)															TOTAL	PER	
	0.0	11.0	33.5	56.0	78.5	101.0	123.5	146.0	168.5	191.0	213.5	236.0	258.5	281.0	303.5			326.0
326.0-348.5	0	0	1	0	0	0	0	0	0	0	0	0	0	0	0	0	1	0.0
303.5-326.0	0	0	0	0	0	0	0	0	0	0	0	0	0	0	0	0	0	0.0
281.0-303.5	4	0	0	0	0	0	0	0	0	0	1	2	7	4	2	3	23	9.0
258.5-281.0	4	0	0	0	1	0	0	0	3	0	1	4	3	3	1	1	21	8.0
236.0-258.5	1	0	1	0	0	0	0	2	2	5	7	5	6	3	1	0	33	13.0
213.5-236.0	0	0	0	0	1	0	0	1	4	3	5	3	5	0	0	0	22	8.0
191.0-213.5	0	0	0	0	0	1	2	1	1	2	8	2	1	0	0	0	18	7.0
168.5-191.0	0	0	0	0	0	1	1	2	7	10	2	2	1	1	0	0	27	10.0
146.0-168.5	0	0	0	1	2	2	0	4	2	4	1	3	0	0	0	0	19	7.0
123.5-146.0	2	0	1	0	2	2	3	3	5	2	4	1	1	0	1	1	28	11.0
101.0-123.5	3	0	0	0	0	0	3	1	1	3	3	6	0	0	1	2	23	9.0
78.5-101.0	1	0	0	0	0	0	0	0	0	2	3	3	3	1	3	0	16	6.0
56.0-78.5	0	0	0	0	0	1	1	0	0	0	1	3	3	0	0	0	9	3.0
33.5-56.0	0	0	0	0	0	0	0	0	0	0	0	0	0	0	0	0	0	0.0
11.0-33.5	0	0	0	1	0	0	0	0	0	0	0	0	1	1	0	0	3	1.0
348.5-11.0	1	0	2	1	0	0	0	0	0	0	0	0	0	0	1	0	5	2.0

Table AN-16. Bivariate distribution of calculated geostrophic winds (Vg) versus Nome simultaneous surface winds (Ns) for July, 1967. Horizontal directions represent the same sectors as the vertical except that 0 is the middle of the 348.5°-11.0° sector instead of the minimum direction value.

DIRECTION

	S P E E D (ms ⁻¹)															(obs. 248)	
	0-2	2-4	4-6	6-8	8-10	10-12	12-14	14-16	16-18	18-20	20-22	22-24	24-26	26-28	28-30	TOTAL	PER
326.0-348.5	0	3	1	4	0	0	0	0	0	0	0	0	0	0	0	8	3.0
303.5-326.0	0	2	1	0	0	0	0	0	0	0	0	0	0	0	0	3	1.0
281.0-303.5	0	2	0	2	0	0	0	0	0	0	0	0	0	0	0	4	1.0
258.5-281.0	0	3	0	0	3	0	0	0	0	0	0	0	0	0	0	6	2.0
236.0-258.5	0	2	4	1	3	4	1	0	0	0	0	0	0	0	0	15	6.0
213.5-236.0	1	1	2	6	5	4	2	0	0	0	0	0	0	0	0	21	8.0
191.0-213.5	0	0	0	2	0	2	0	1	0	0	0	0	0	0	0	5	2.0
168.5-191.0	0	0	2	0	0	1	1	0	0	0	0	0	0	0	0	4	1.0
146.0-168.5	0	1	1	2	1	1	0	0	0	0	0	0	0	0	0	6	2.0
123.5-146.0	2	3	6	5	0	0	0	0	0	0	0	0	0	0	0	16	6.0
101.0-123.5	1	22	17	2	3	3	1	0	0	0	0	0	0	0	0	49	19.0
78.5-101.0	2	13	12	10	13	11	7	5	2	2	0	0	0	0	0	77	31.0
56.0-78.5	1	4	0	3	2	0	0	0	0	0	0	0	0	0	0	10	4.0
33.5-56.0	2	4	1	1	0	0	0	0	0	0	0	0	0	0	0	8	3.0
11.0-33.5	2	2	2	0	0	0	0	0	0	0	0	0	0	0	0	6	2.0
348.5-11.0	2	4	3	0	0	0	0	1	0	0	0	0	0	0	0	10	4.0

Table AU-17. Bivariate distribution of wind direction versus wind speed data (three hourly) for Unalakleet, in January, 1968. Winds above 14 ms⁻¹ are considered gale class.

(obs. 248)

S P E E D (ms⁻¹)

	0-2	2-4	4-6	6-8	8-10	10-12	12-14	14-16	16-18	18-20	20-22	22-24	24-26	26-28	28-30	TOTAL	PER
326.0-348.5	1	5	0	0	0	0	0	0	0	0	0	0	0	0	0	7	2.0
303.5-326.0	5	4	0	0	0	0	0	0	0	0	0	0	0	0	0	9	3.0
281.0-303.5	0	5	2	0	0	0	0	0	0	0	0	0	0	0	0	0	3.0
258.5-281.0	3	3	4	0	0	0	0	0	0	0	0	0	0	0	0	10	4.0
236.0-258.5	0	1	0	0	0	0	0	0	0	0	0	0	0	0	0	1	0.0
213.5-236.0	1	4	7	0	0	0	0	0	0	0	0	0	0	0	0	12	4.0
191.0-213.5	0	3	2	1	0	0	0	0	0	0	0	0	0	0	0	6	2.0
168.5-191.0	1	3	0	1	0	0	0	0	0	0	0	0	0	0	0	13	5.0
146.0-168.5	1	3	3	4	2	0	0	0	0	0	0	0	0	0	0	13	5.0
123.5-146.0	3	2	3	2	1	0	0	0	0	0	0	0	0	0	0	11	4.0
101.0-123.5	4	3	1	2	0	0	0	0	0	0	0	0	0	0	0	10	4.0
76.5-101.0	1	24	19	5	0	0	0	0	0	0	0	0	0	0	0	49	19.0
55.0-76.5	1	13	2	1	0	0	0	0	0	0	0	0	0	0	0	17	6.0
33.5-55.0	4	5	3	0	0	0	0	0	0	0	0	0	0	0	0	12	4.0
11.0-33.5	4	4	1	0	0	0	0	0	0	0	0	0	0	0	0	9	3.0
345.5-11.0	53	6	2	0	0	0	0	0	0	0	0	0	0	0	0	61	24.0

D I R E C T I O N

Table AN-17. Bivariate distribution of wind direction versus wind speed data (three hourly) for Nome, in January, 1968. Winds above 14 ms⁻¹ are considered gale class.

D I R E C T I O N (Vg)	D I R E C T I O N (Us)															TOTAL	PER	
	0.0	11.0	33.5	56.0	78.5	101.0	123.5	146.0	168.5	191.0	213.5	236.0	258.5	281.0	303.5			326.0
326.0-348.5	0	1	0	0	2	0	0	0	0	0	0	0	0	0	1	12	4.0	
303.5-326.0	1	2	2	0	3	12	3	0	0	0	0	0	0	1	2	1	27	10.0
281.0-303.5	1	0	1	0	2	2	1	0	0	0	0	2	2	0	0	1	12	4.0
258.5-281.0	0	0	1	0	0	2	1	0	0	0	3	3	0	0	0	0	10	4.0
236.0-258.5	0	0	0	0	0	0	0	0	0	1	0	0	0	0	0	0	1	0.0
213.5-236.0	0	0	1	0	1	2	2	0	0	2	4	1	1	0	0	0	14	5.0
191.0-213.5	0	0	0	0	3	2	0	0	1	1	1	0	0	0	0	0	8	3.0
168.5-191.0	0	0	0	0	6	1	2	1	0	0	1	2	0	0	0	0	13	5.0
146.0-168.5	0	0	0	1	3	3	3	4	0	2	4	2	0	0	0	0	22	8.0
123.5-146.0	1	1	0	1	12	4	0	0	0	0	4	2	0	0	0	0	25	10.0
101.0-123.5	1	0	1	5	31	4	0	0	3	0	1	1	2	1	0	1	51	20.0
78.5-101.0	1	0	0	0	7	3	0	0	0	0	1	1	0	0	1	0	14	5.0
56.0-78.5	1	0	0	0	4	1	1	0	0	0	1	1	0	1	0	2	12	4.0
33.5-56.0	1	1	2	0	2	1	0	1	0	0	0	0	0	1	0	1	10	4.0
11.0-33.5	2	0	0	1	1	1	2	0	0	0	0	0	1	0	0	1	9	3.0
348.5-11.0	1	1	0	2	0	3	1	0	0	0	0	0	0	0	0	0	6	3.0

Table AU-18. Bivariate distribution of calculated geostrophic winds (Vg) versus Unalakleet simultaneous surface winds (Us) for January, 1968. Horizontal directions represent the same sectors as the vertical except that 0 is the middle of the 348.5°-11.0° sector instead of the minimum direction value.

DIRECTION (Vg)

	DIRECTION (Us)															(obs. 248)		
	0.0	11.0	33.5	56.0	78.5	101.0	123.5	146.0	168.5	191.0	213.5	236.0	258.5	281.0	303.5	326.0	TOTAL	PER
326.0-348.5	5	0	0	0	2	1	0	0	0	0	0	0	0	1	1	2	12	4.0
303.5-326.0	8	3	5	3	1	0	1	1	0	0	0	0	0	1	2	2	27	10.0
281.0-303.5	4	0	0	0	1	1	0	0	0	0	0	0	2	1	3	0	12	4.0
258.5-281.0	1	0	0	0	1	0	0	0	0	0	0	0	5	3	0	0	10	4.0
236.0-258.5	0	0	0	0	0	0	0	0	0	0	0	1	0	0	0	0	1	0.0
213.5-236.0	2	0	0	0	0	0	1	2	0	2	6	0	1	0	0	0	14	5.0
191.0-213.5	0	0	0	0	1	0	1	1	3	0	2	0	0	0	0	0	8	3.0
168.5-191.0	0	1	0	0	2	1	2	3	1	3	0	0	0	0	0	0	13	5.0
146.0-168.5	0	0	0	0	4	1	3	4	7	1	1	0	1	0	0	0	22	8.0
123.5-146.0	1	0	0	3	12	2	1	2	2	0	1	0	1	0	0	0	25	10.0
101.0-123.5	8	3	3	7	25	2	1	0	0	0	1	0	0	1	0	0	51	22.0
78.5-101.0	13	1	0	0	0	0	0	0	0	0	0	0	0	0	0	0	14	5.0
56.0-78.5	7	0	1	1	0	0	0	0	0	0	0	0	0	0	2	1	12	4.0
33.5-56.0	5	0	2	1	0	0	2	0	0	0	0	0	0	0	0	2	10	4.0
11.0-33.5	4	1	1	1	0	0	0	0	0	0	0	0	0	1	1	0	9	3.0
348.5-11.0	3	0	0	1	0	2	1	0	0	2	1	0	0	0	0	0	8	3.0

Table AN-18. Bivariate distribution of calculated geostrophic winds (Vg) versus Nome simultaneous surface winds (Ns) for January, 1968. Horizontal directions represent the same sectors as the vertical except that 0 is the middle of the 348.5°-11.0° sector instead of the minimum direction value.

D I R E C T I O N

	S P E E D (ms ⁻¹)															(obs. 248)	
	0-2	2-4	4-6	6-8	8-10	10-12	12-14	14-16	16-18	18-20	20-22	22-24	24-26	26-28	28-30	TOTAL	PER
326.0-348.5	0	0	1	3	1	0	0	0	0	0	0	0	0	0	0	5	2.0
303.5-326.0	0	2	7	6	3	1	0	0	0	0	0	0	0	0	0	19	7.0
281.0-303.5	0	6	3	2	1	0	0	0	0	0	0	0	0	0	0	12	4.0
258.5-281.0	2	13	11	2	1	0	0	0	0	0	0	0	0	0	0	29	11.0
236.0-258.5	0	10	10	7	2	0	0	0	0	0	0	0	0	0	0	29	11.0
213.5-236.0	1	8	11	4	2	0	0	0	0	0	0	0	0	0	0	26	10.0
191.0-213.5	0	4	5	4	2	0	0	0	0	0	0	0	0	0	0	15	6.0
168.5-191.0	0	1	3	3	0	0	0	0	0	0	0	0	0	0	0	7	2.0
146.0-168.5	0	3	3	2	0	0	0	0	0	0	0	0	0	0	0	8	3.0
123.5-146.0	0	3	0	1	1	0	0	0	0	0	0	0	0	0	0	5	2.0
101.0-123.5	2	7	6	1	0	2	0	0	0	0	0	0	0	0	0	18	7.0
78.5-101.0	3	20	13	4	3	1	0	0	0	0	0	0	0	0	0	44	17.0
56.0-78.5	1	6	4	3	0	0	0	0	0	0	0	0	0	0	0	14	5.0
33.5-56.0	1	3	1	1	1	0	0	0	0	0	0	0	0	0	0	7	2.0
11.0-33.5	0	0	1	0	0	0	0	0	0	0	0	0	0	0	0	1	0.2
348.5-11.0	7	2	0	0	0	0	0	0	0	0	0	0	0	0	0	9	3.0

Table AU-19. Bivariate distribution of wind direction versus wind speed data (three hourly) for Unalakleet, in July, 1968. Winds above 14 ms⁻¹ are considered gale class.

	S P E E D (ms ⁻¹)															(obs. 248)	
	0- 2	2- 4	4- 6	6- 8	8-10	10-12	12-14	14-16	16-18	18-20	20-22	22-24	24-26	26-28	28-30	TOTAL	PER
326.0-348.5	4	7	3	0	0	0	0	0	0	0	0	0	0	0	0	14	5.0
303.5-326.0	3	3	1	0	0	0	0	0	0	0	0	0	0	0	0	7	2.0
281.0-303.5	0	3	2	1	0	0	0	0	0	0	0	0	0	0	0	6	2.0
258.5-281.0	2	3	9	6	2	0	0	0	0	0	0	0	0	0	0	22	8.0
236.0-258.5	1	7	10	0	0	0	0	0	0	0	0	0	0	0	0	18	7.0
213.5-236.0	0	4	3	0	0	0	0	0	0	0	0	0	0	0	0	7	2.0
191.0-213.5	1	6	1	0	0	0	0	0	0	0	0	0	0	0	0	8	3.0
168.5-191.0	1	11	16	8	3	0	0	0	0	0	0	0	0	0	0	39	15.0
146.0-168.5	2	6	16	5	3	0	0	0	0	0	0	0	0	0	0	32	12.0
123.5-146.0	1	2	7	4	1	1	0	0	0	0	0	0	0	0	0	16	6.0
101.0-123.5	1	10	1	2	1	0	0	0	0	0	0	0	0	0	0	15	6.0
78.5-101.0	0	13	5	1	0	1	0	0	0	0	0	0	0	0	0	20	8.0
56.0- 78.5	1	0	0	3	1	0	0	0	0	0	0	0	0	0	0	5	2.0
33.5- 56.0	0	3	2	3	0	0	0	0	0	0	0	0	0	0	0	8	3.0
11.0- 33.5	1	4	0	0	0	0	0	0	0	0	0	0	0	0	0	5	2.0
348.5- 11.0	16	8	2	0	0	0	0	0	0	0	0	0	0	0	0	26	10.0

Table AN-19. Bivariate distribution of wind direction versus wind speed data (three hourly) for Nome, in July, 1968. Winds above 14 ms⁻¹ are considered gale class.

D I R E C T I O N (Vg)

	D I R E C T I O N (Us)															(obs. 248)		
	0.0	11.0	33.5	56.0	78.5	101.0	123.5	146.0	168.5	191.0	213.5	236.0	258.5	281.0	303.5	326.0	TOTAL	PER
326.0-348.5	0	1	0	1	0	0	0	0	0	0	0	0	1	0	0	0	3	1.0
303.5-326.0	0	0	0	1	1	0	0	0	0	0	0	1	1	1	0	0	5	2.0
281.0-303.5	2	0	0	0	4	1	0	0	1	2	3	4	6	2	1	0	26	10.0
258.5-281.0	1	0	0	0	3	0	0	0	0	1	0	0	1	2	1	0	25	10.0
236.0-258.5	0	0	0	0	1	0	0	0	1	1	1	4	4	1	0	0	13	5.0
213.5-236.0	0	0	0	0	1	0	0	0	0	0	2	3	2	1	0	0	9	3.0
191.0-213.5	1	0	1	0	0	0	0	1	0	1	1	0	0	0	0	0	5	2.0
168.5-191.0	0	0	0	0	2	1	1	1	0	0	1	0	1	0	0	0	7	2.0
146.0-168.5	1	0	2	1	4	3	1	0	1	2	2	1	1	1	0	0	20	8.0
123.5-146.0	2	0	0	6	7	0	2	4	1	2	0	2	3	0	1	0	26	15.0
101.0-123.5	2	0	4	1	7	3	0	1	2	1	1	1	2	2	9	1	37	14.0
78.5-101.0	0	0	0	2	7	2	1	1	1	2	4	3	6	2	6	2	39	15.0
56.0-78.5	0	0	0	2	2	0	0	0	0	1	2	2	1	0	1	2	13	5.0
33.5-56.0	0	0	0	0	1	0	0	0	0	1	0	0	0	0	0	0	2	0.0
11.0-33.5	0	0	0	0	0	0	0	0	0	1	0	0	0	0	0	0	1	0.0
348.5-11.0	0	0	0	0	4	0	0	0	0	0	1	0	0	0	0	0	5	2.0

Table AU-20. Bivariate distribution of calculated geostrophic winds (Vg) versus Unalakleet simultaneous surface winds (Us) for July, 1968. Horizontal directions represent the same sectors as the vertical except that 0 is the middle of the 348.5°-11.0° sector instead of the minimum direction value.

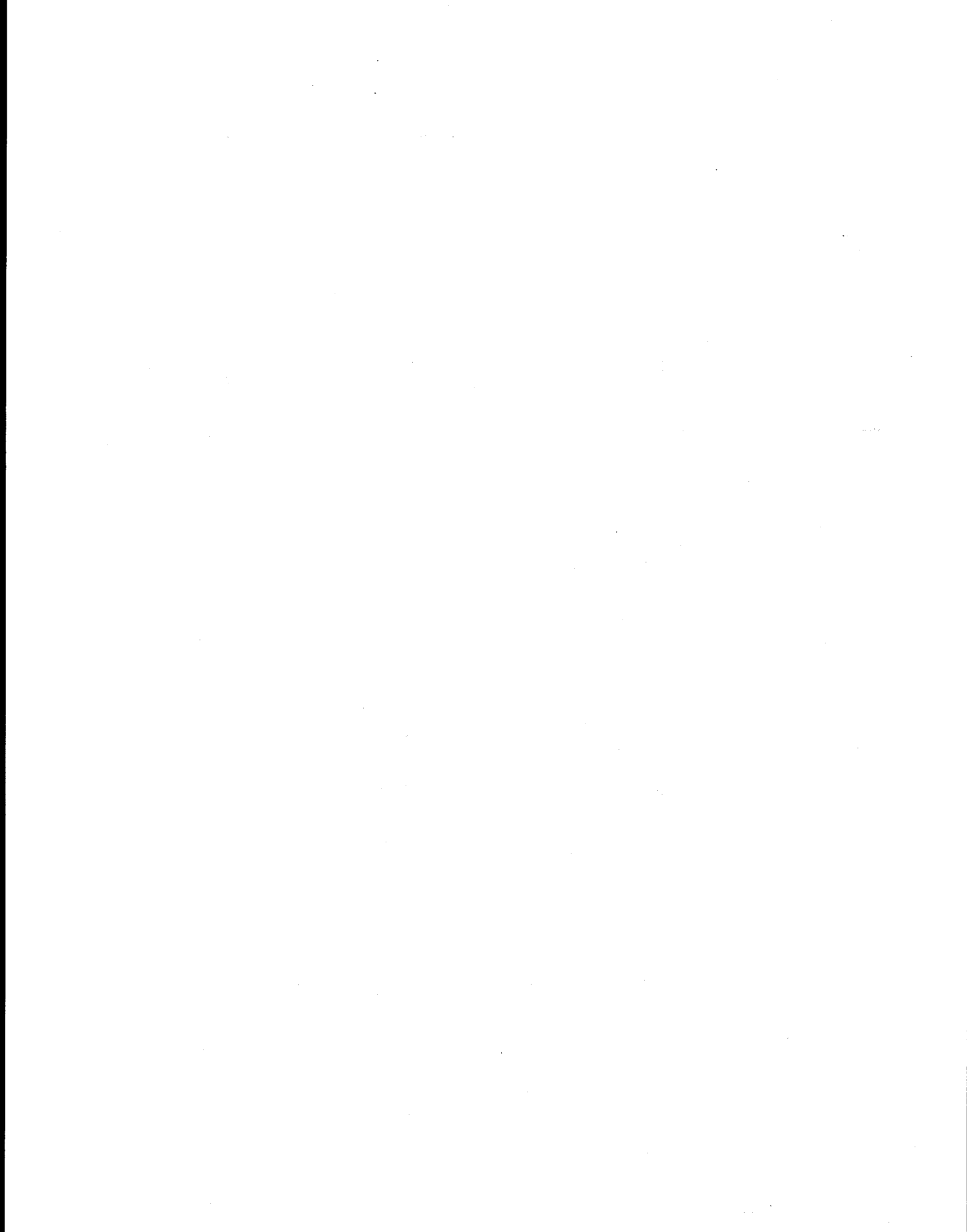
D I R E C T I O N (Vg)

	D I R E C T I O N (Us)															(obs. 248)		
	0.0	11.0	33.5	56.0	78.5	101.0	123.5	146.0	168.5	191.0	213.5	236.0	258.5	281.0	303.5	326.0	TOTAL	PER
326.0-348.5	0	0	2	0	0	0	0	0	0	0	0	0	1	0	0	0	3	1.0
303.5-326.0	1	0	2	1	0	0	0	0	0	0	0	0	0	0	0	1	5	2.0
281.0-303.5	6	0	2	1	1	1	0	3	1	1	0	0	5	1	1	3	26	10.0
258.5-281.0	4	0	0	0	1	0	0	0	2	2	0	5	4	0	3	4	25	10.0
236.0-258.5	0	0	0	0	0	0	1	1	2	1	0	1	5	2	0	0	13	5.0
213.5-236.0	0	0	0	0	2	0	0	1	1	0	0	4	0	0	1	0	9	3.0
191.0-213.5	0	0	1	0	1	2	0	1	0	0	0	0	0	0	0	0	5	2.0
168.5-191.0	0	0	0	0	1	0	0	1	3	0	1	1	0	0	0	0	7	2.0
146.0-168.5	1	0	0	0	4	0	2	6	4	0	2	1	0	0	0	0	20	8.0
123.5-146.0	2	0	0	1	2	3	7	12	8	1	0	0	0	2	0	0	38	15.0
101.0-123.5	2	2	0	0	5	5	5	3	11	0	0	1	2	0	1	0	37	14.0
78.5-101.0	5	3	1	0	2	4	1	3	6	2	2	3	3	0	1	3	39	15.0
56.0-78.5	3	0	0	0	0	0	0	1	1	1	2	1	1	0	0	3	13	5.0
33.5-56.0	1	0	0	0	0	0	0	0	0	0	0	0	1	0	0	0	2	0.0
11.0-33.5	0	0	0	0	0	0	0	0	0	0	0	1	0	0	0	0	1	0.0
348.5-11.0	1	0	0	2	1	0	0	0	0	0	0	0	0	1	0	0	5	2.0

Table AN-20. Bivariate distribution of calculated geostrophic winds (Vg) versus Nome simultaneous surface winds (Ns) for July, 1968. Horizontal directions represent the same sectors as the vertical except that 0 is the middle of the 348.5°-11.0° sector instead of the minimum direction value.

APPENDIX B

Rotary Spectra From Northeast Cape, Unalakleet and Nome



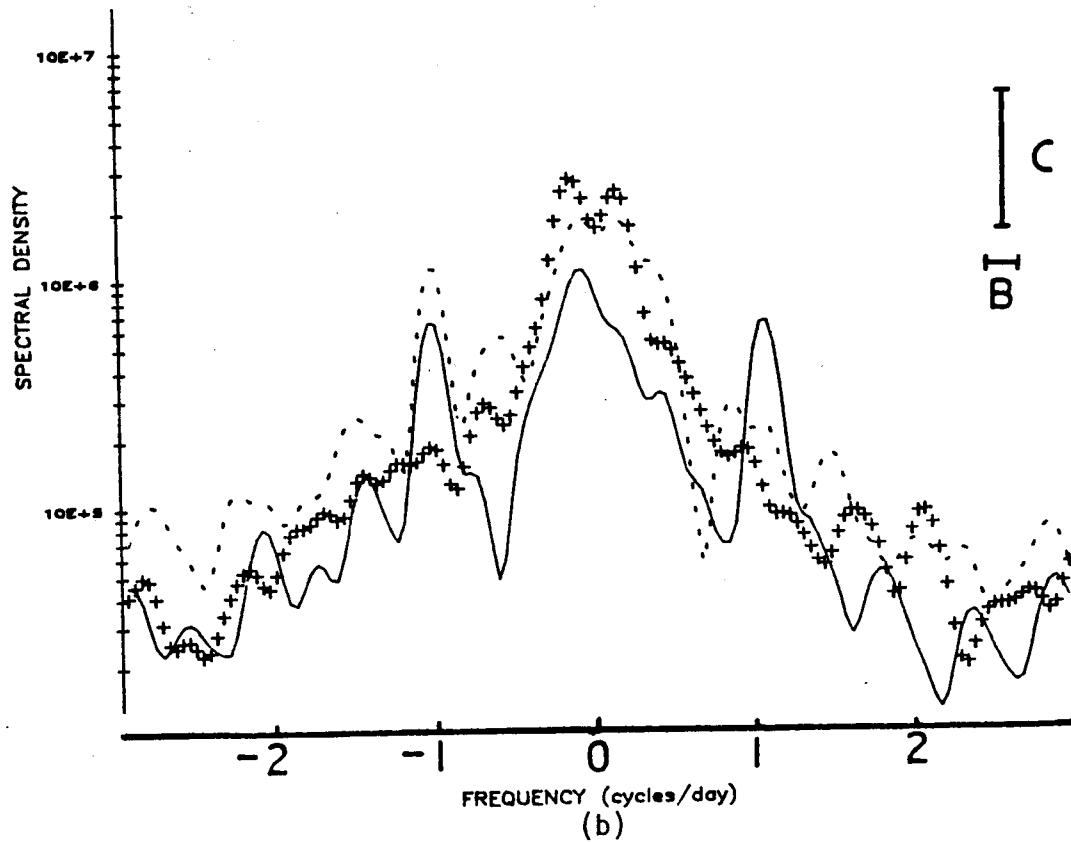
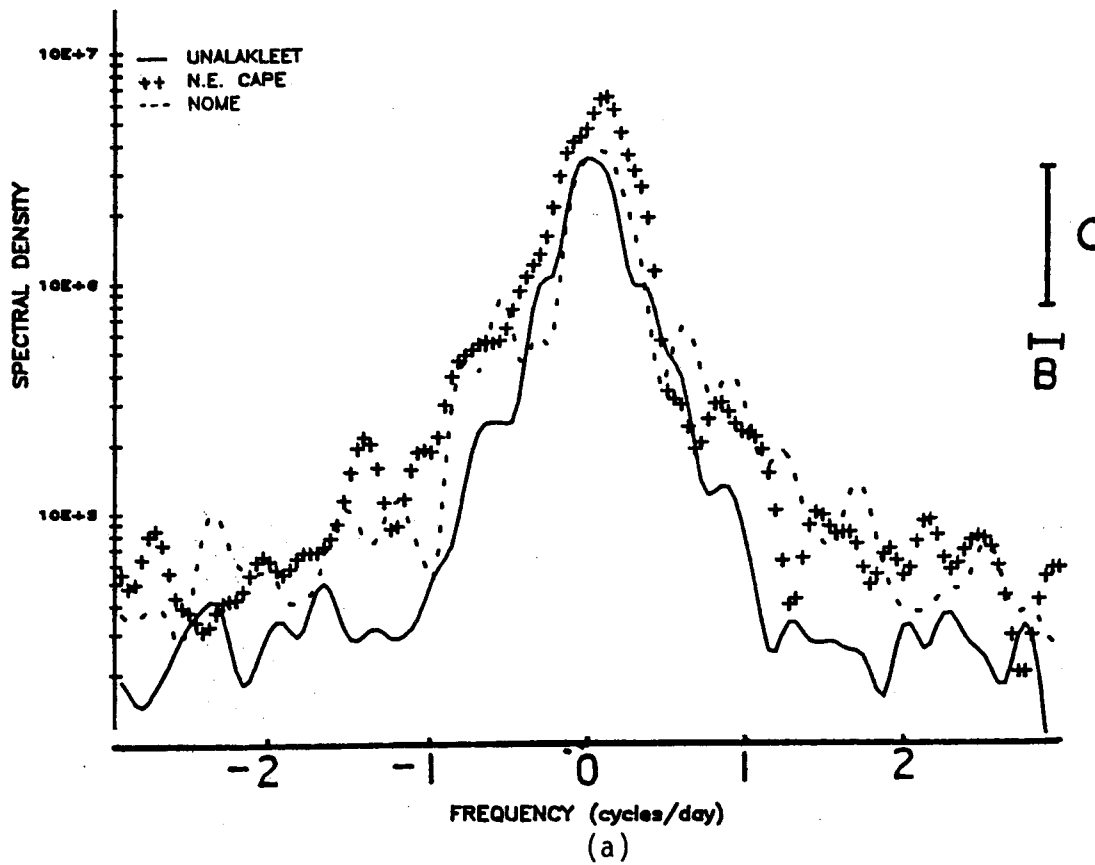
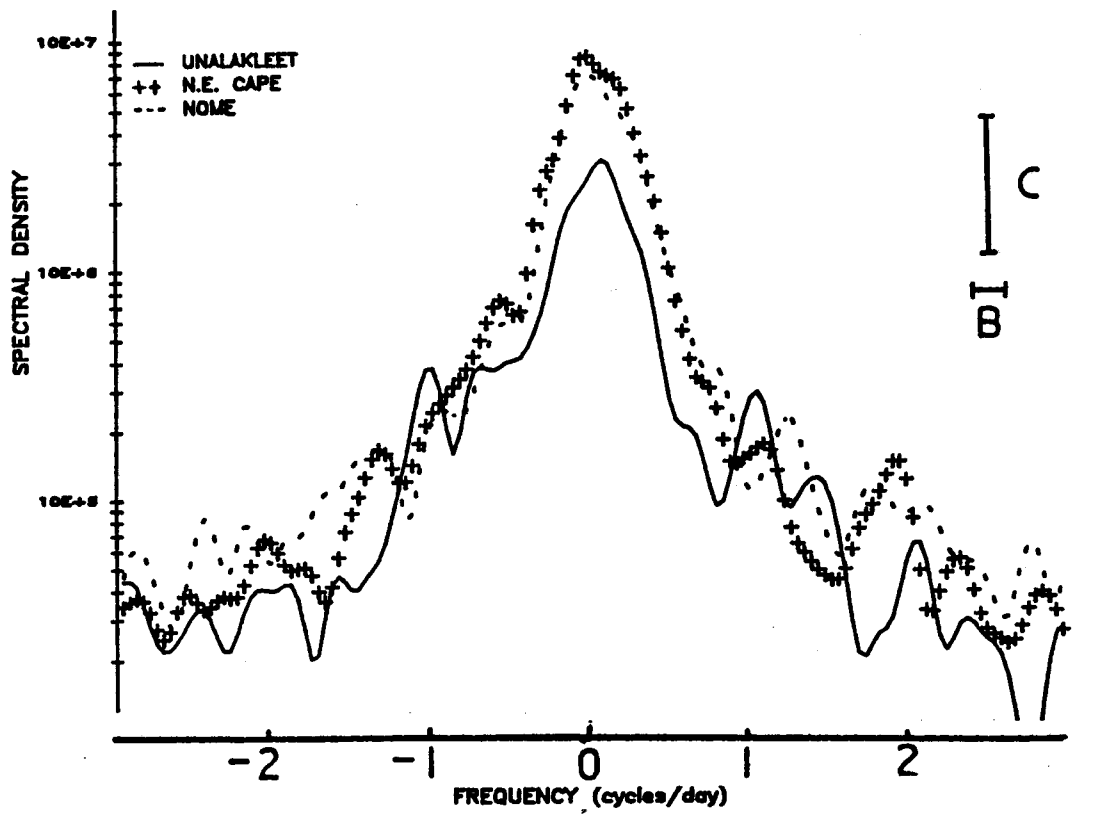
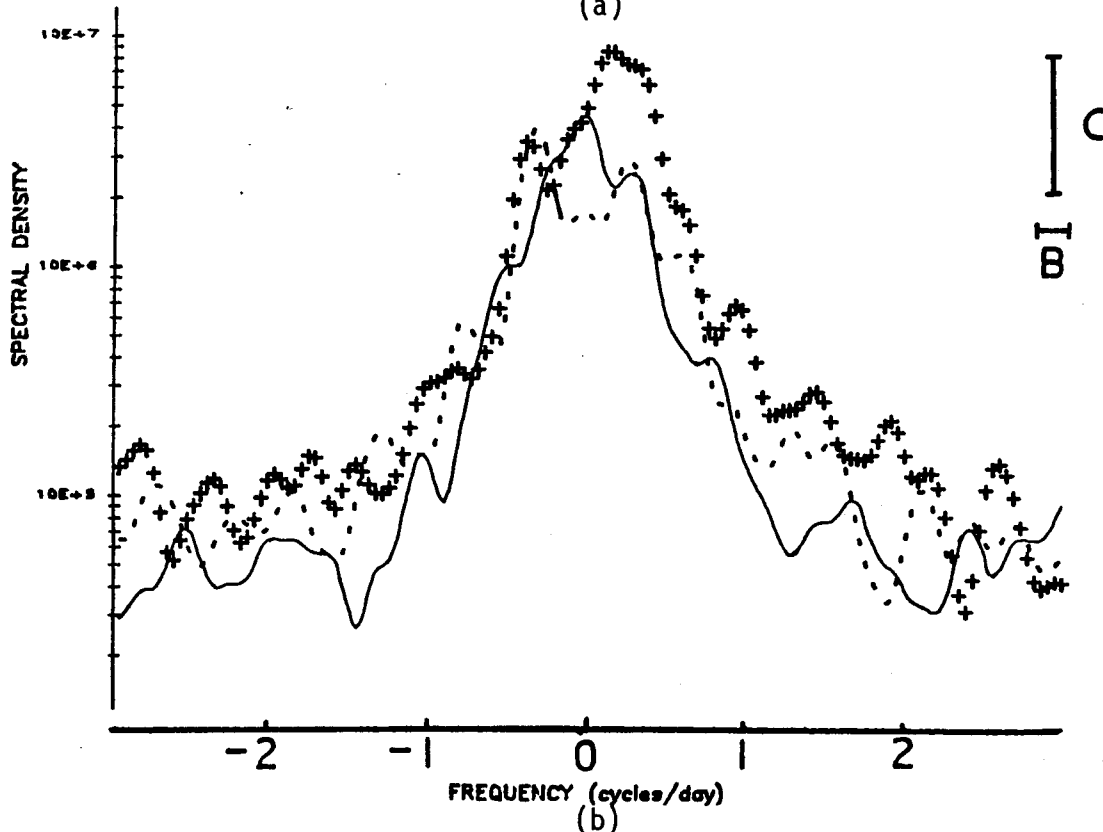


Fig. B1. Time series rotary spectra of surface wind velocity data from Unalakleet, Northeast Cape and Nome for (a) January 1964 and (b) July 1964. The 95% confidence limits (C) and bandwidth (B) are shown.

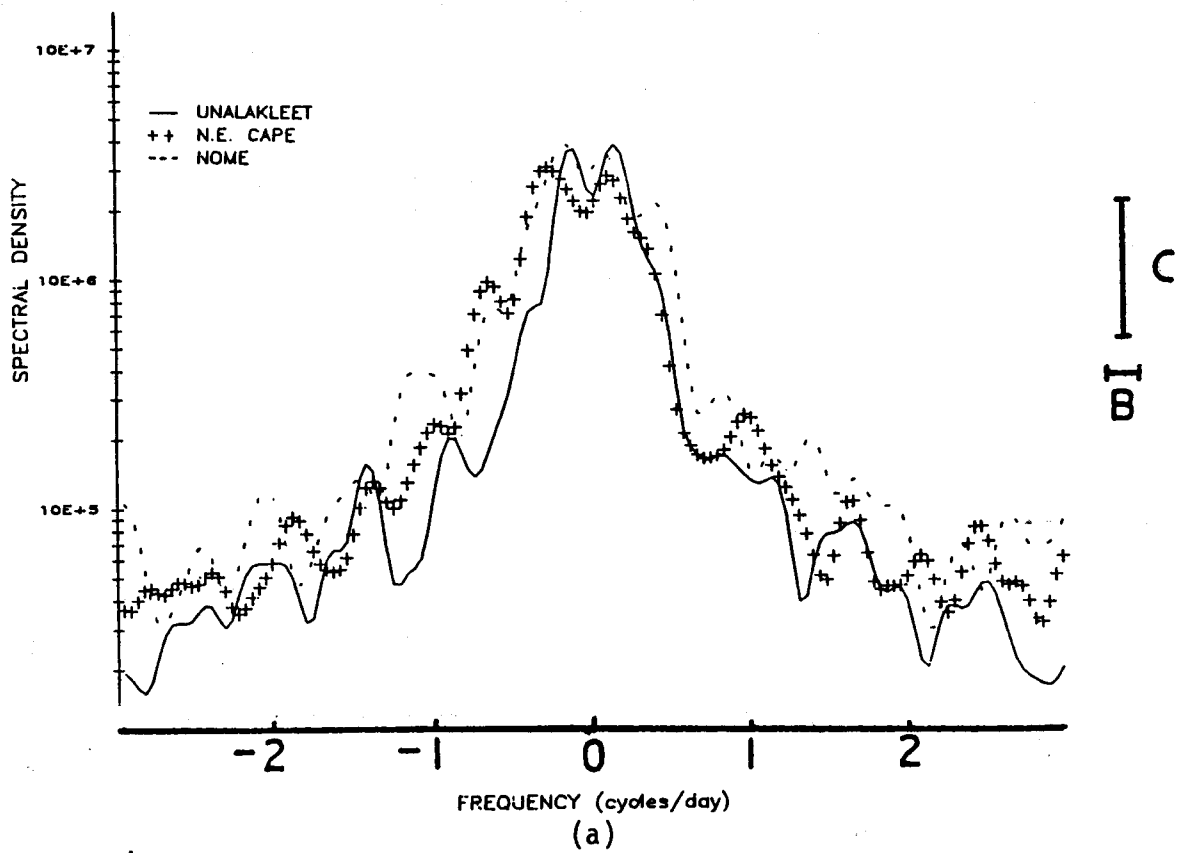


(a)

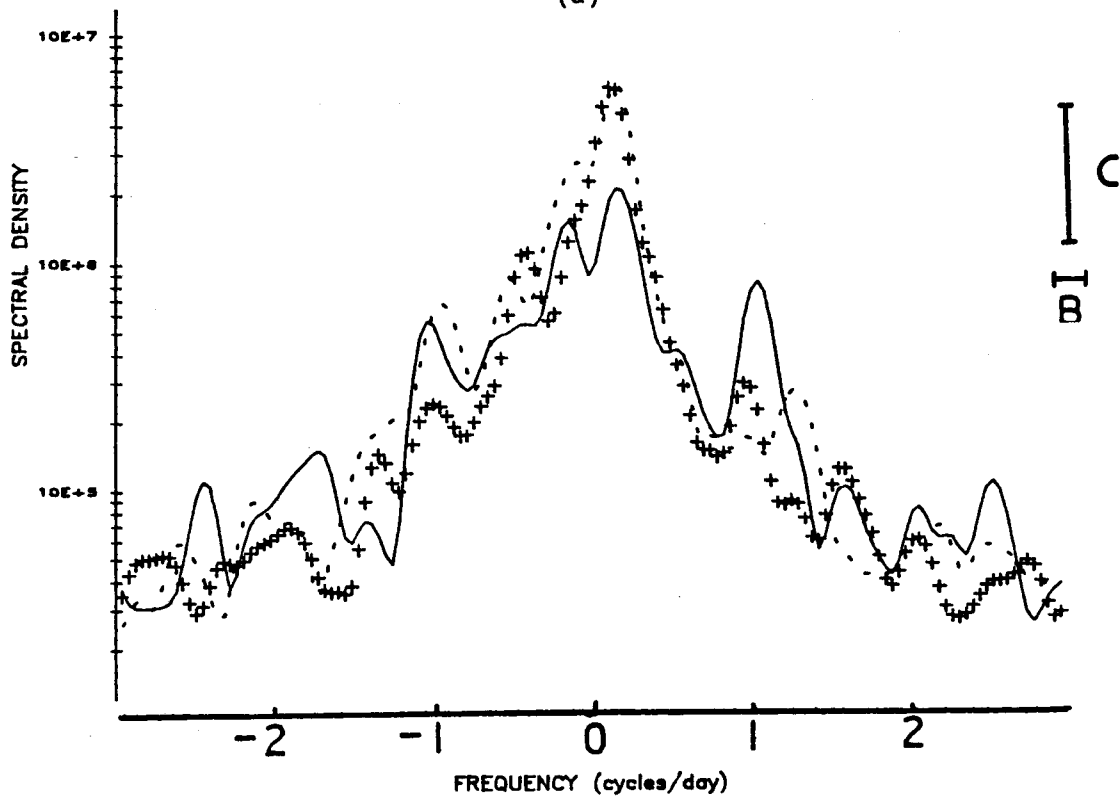


(b)

Fig. B2. Time series rotary spectra of surface wind velocity data from Unalakleet, Northeast Cape, and Nome for (a) May 1964 and (b) November 1964. The 95% confidence limits (C) and bandwidth (B) are shown.



(a)



(b)

Fig. B3. Time series rotary spectra of surface wind velocity data from Unalakleet, Northeast Cape and Nome for (a) January 1965 and (b) July 1965. The 95% confidence limits (C) and bandwidth (B) are shown.

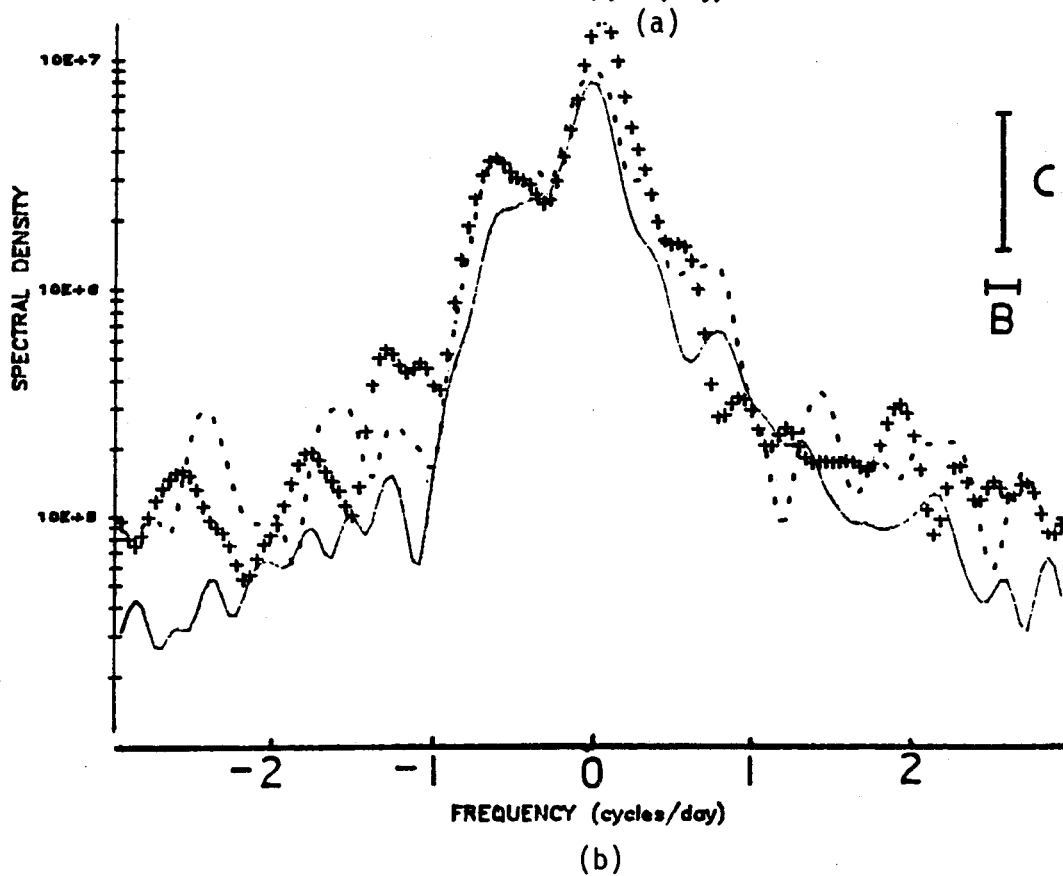
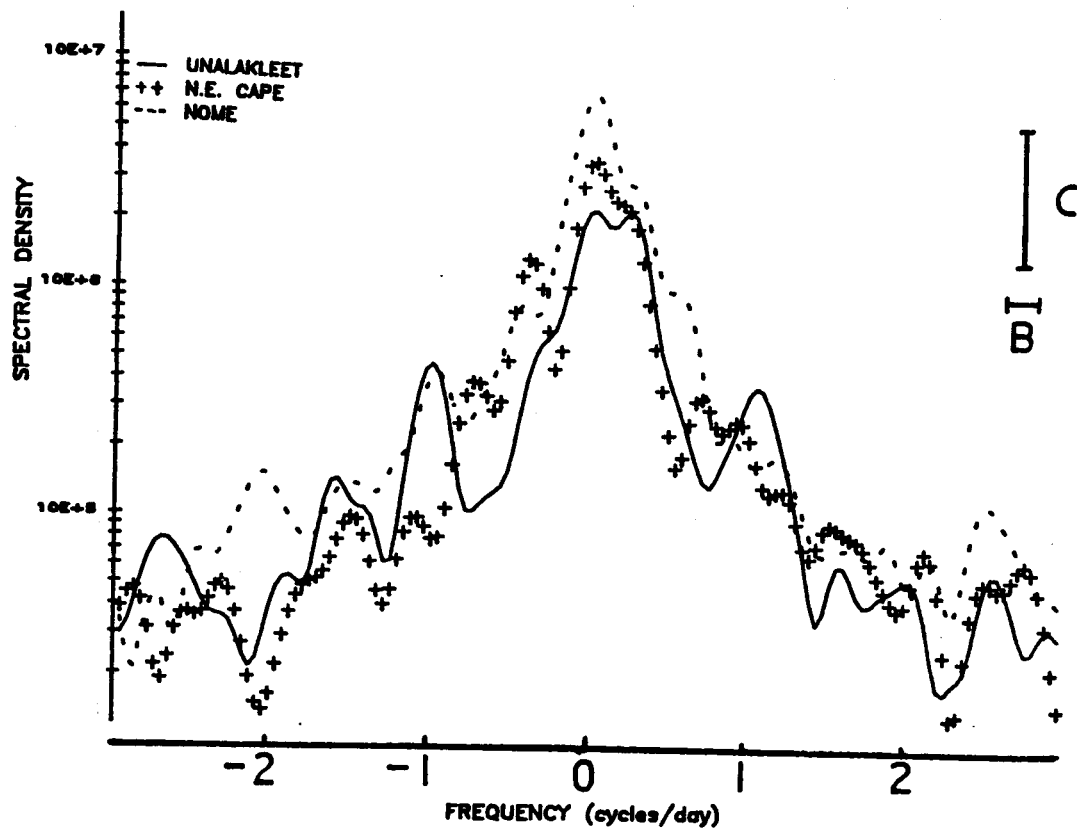


Fig. B4. Time series rotary spectra of surface wind velocity data from Unalakleet, Northeast Cape, and Nome for (a) May 1965 and (b) November 1965. The 95% confidence limits (C) and bandwidth (B) are shown.

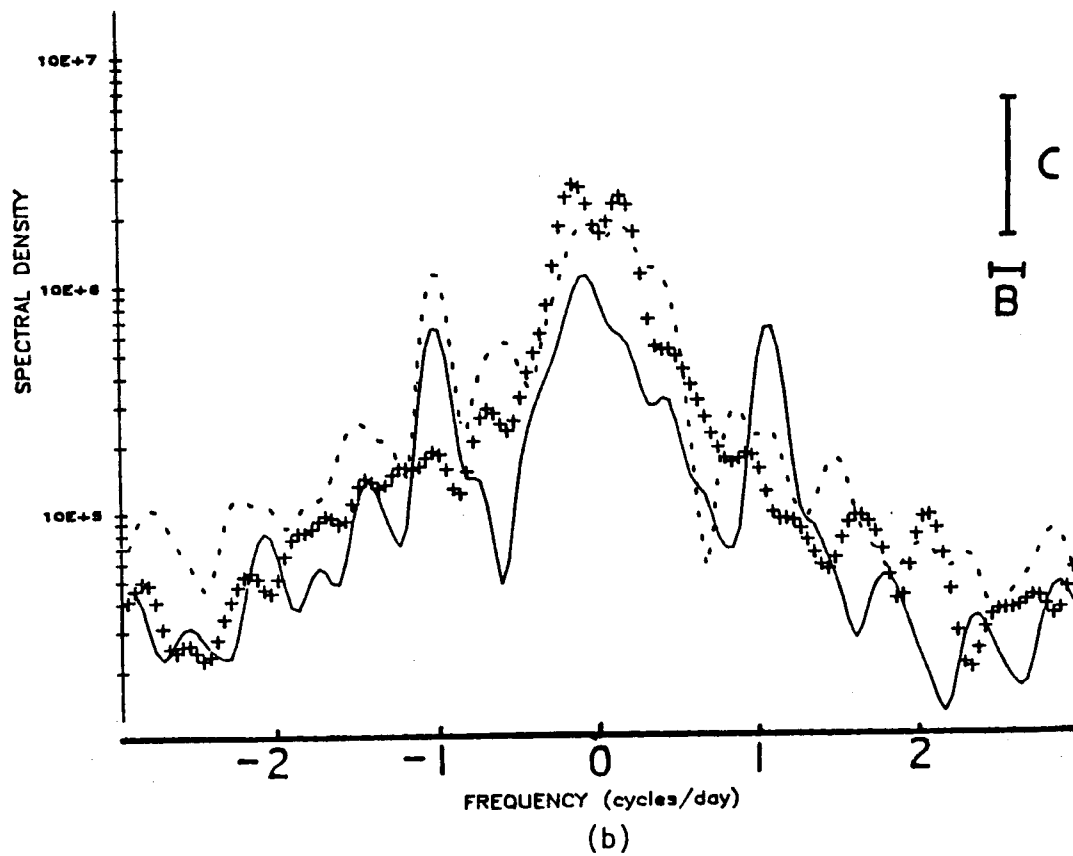
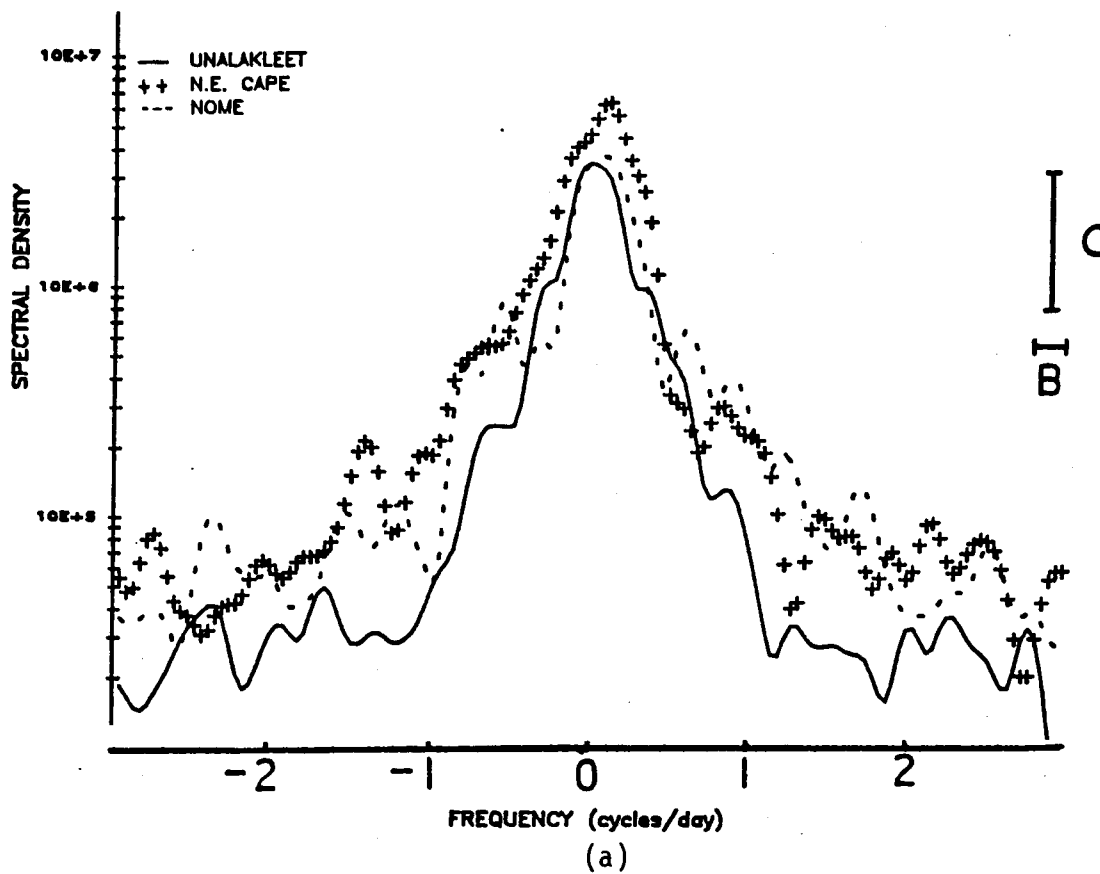


Fig. B5. Time series rotary spectra of surface wind velocity data from Unalakleet, Northeast Cape and Nome for (a) January 1966 and (b) July 1966. The 95% confidence limits (C) and bandwidth (B) are shown.

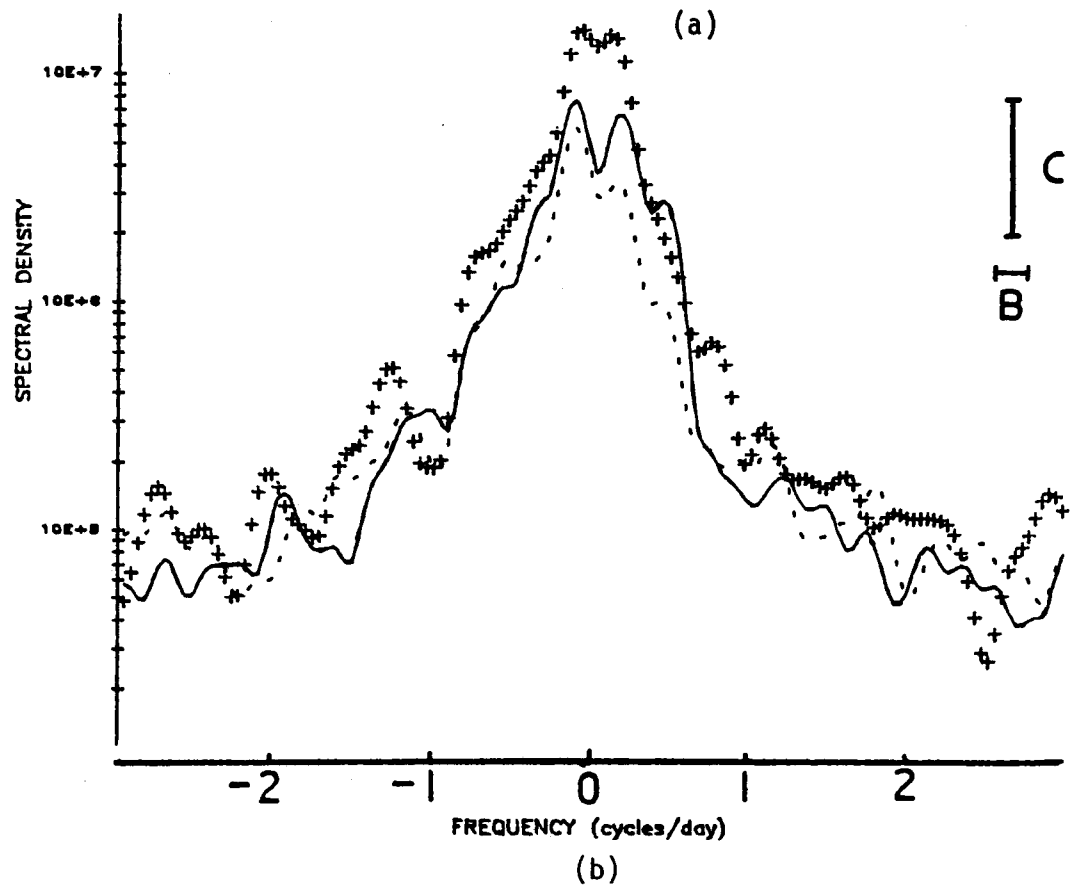
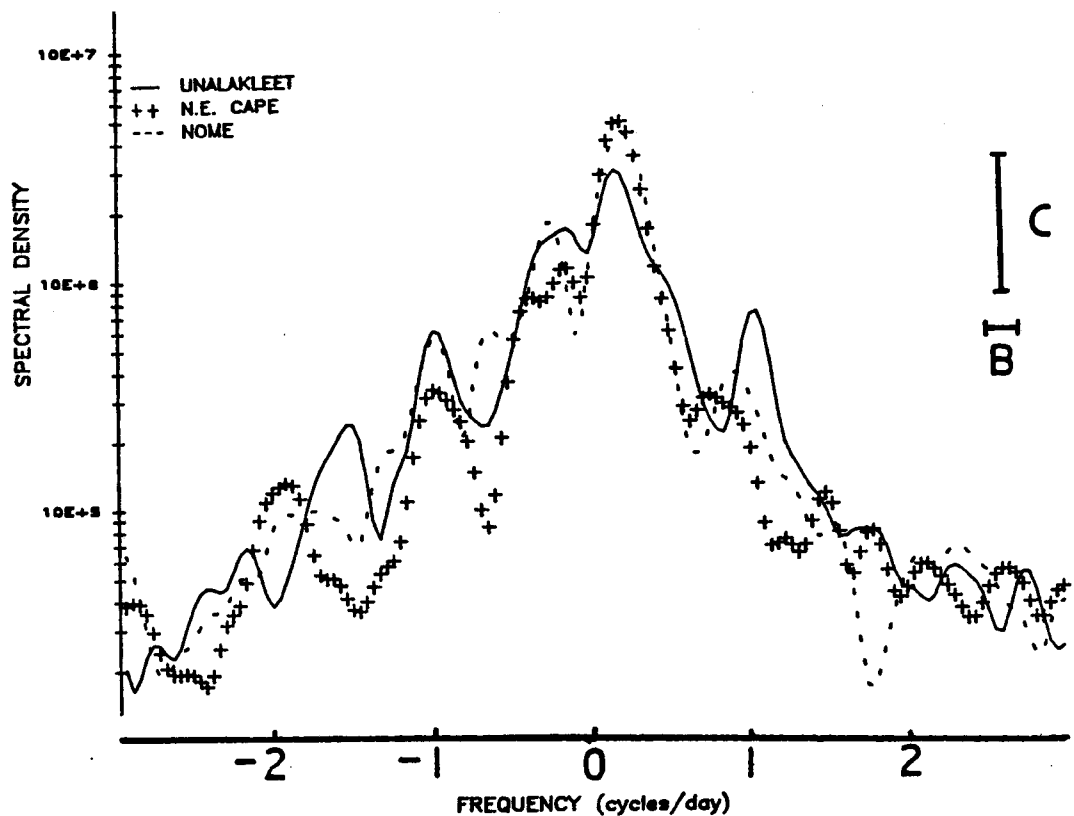


Fig. B6. Time series rotary spectra of surface wind velocity data from Unalakleet, Northeast Cape, and Nome for (a) May 1966 and (b) November 1966. The 95% confidence limits (C) and bandwidth (B) are shown.

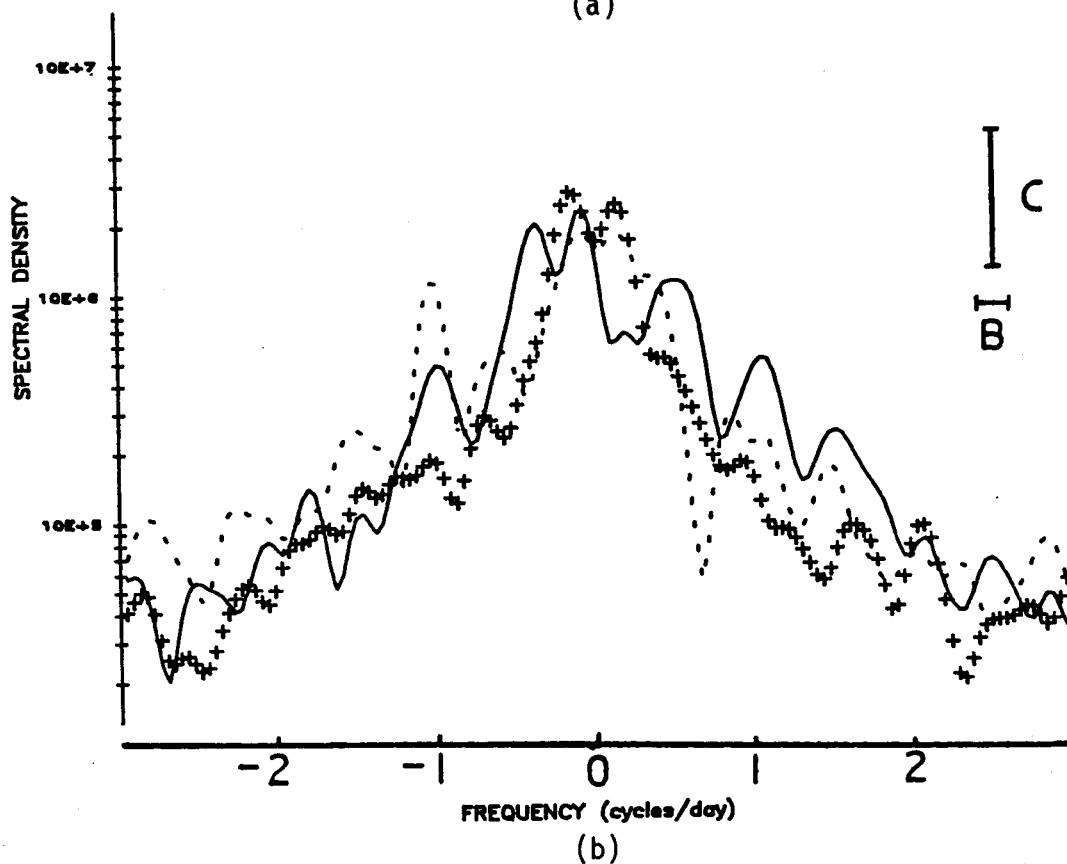
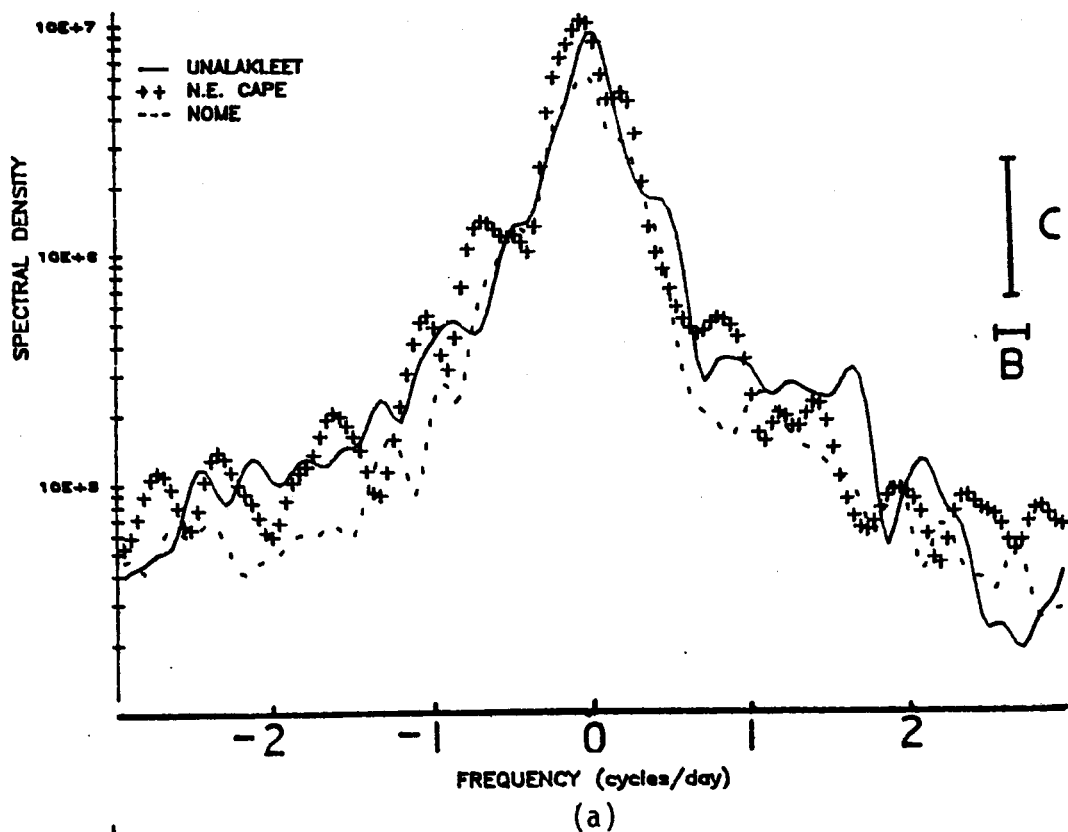


Fig. B7. Time series rotary spectra of surface wind velocity data from Unalakleet, Northeast Cape and Nome for (a) January 1967 and (b) July 1967. The 95% confidence limits (C) and bandwidth (B) are shown.

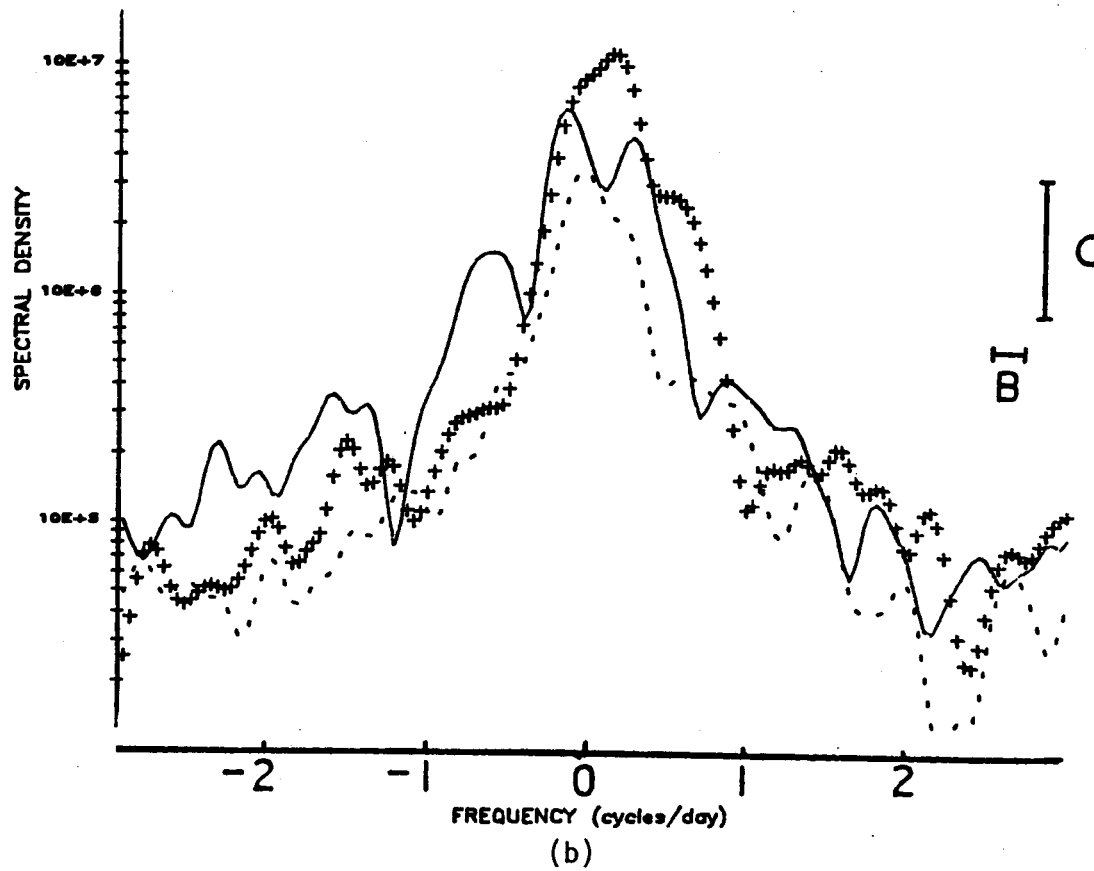
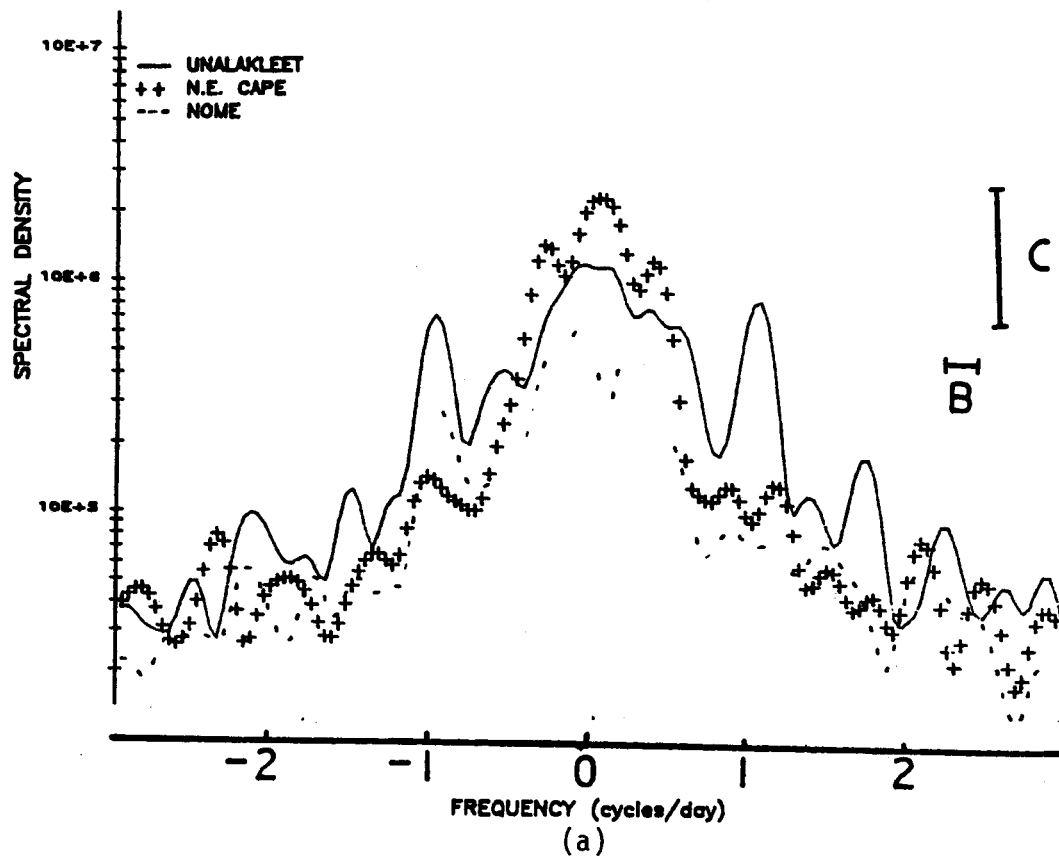
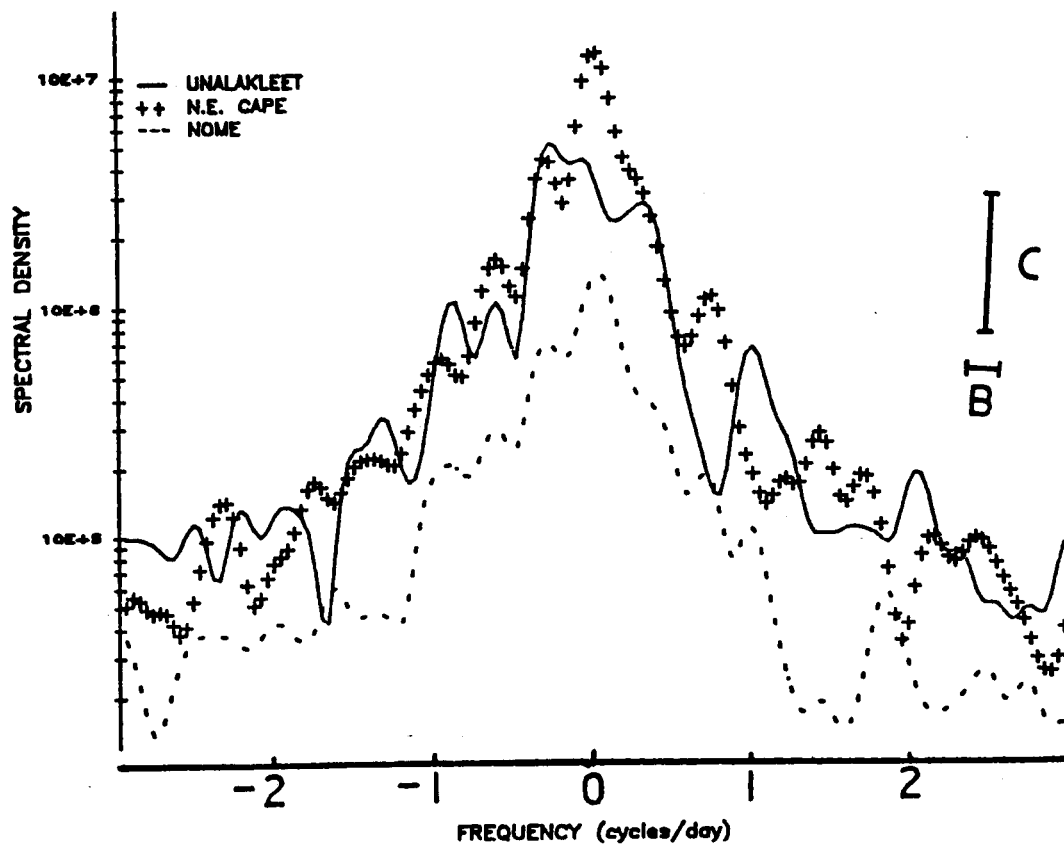
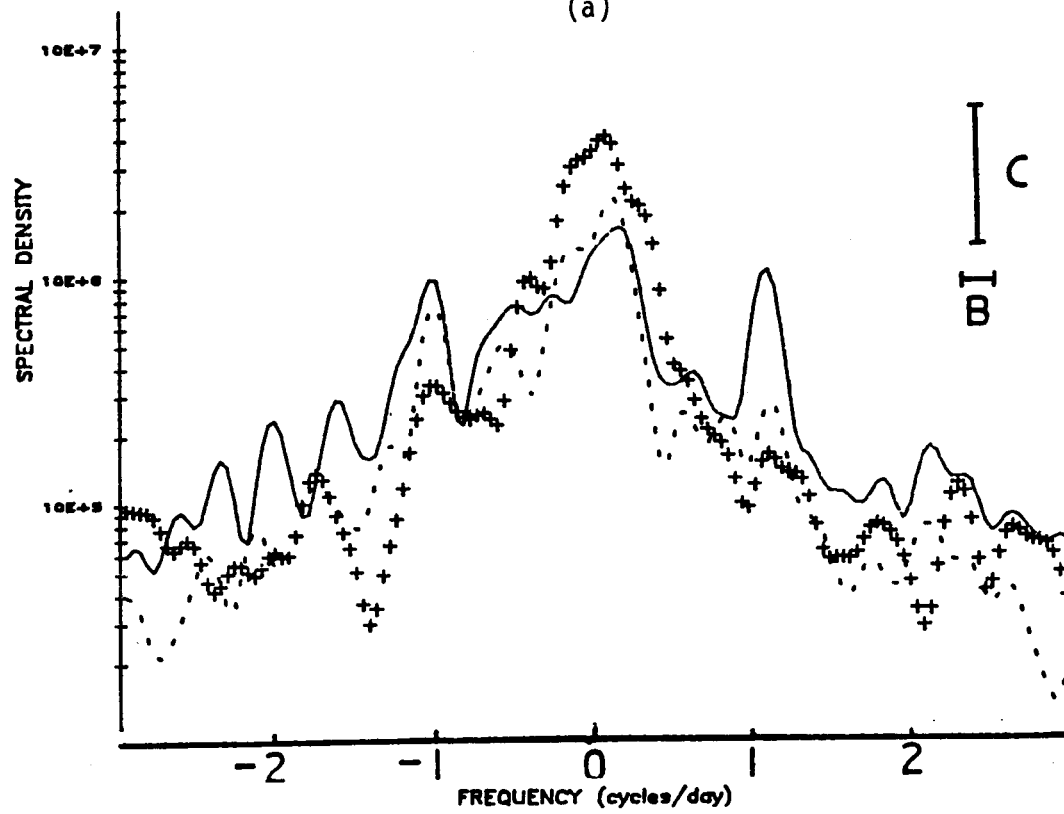


Fig. B8. Time series rotary spectra of surface wind velocity data from Unalakleet, Northeast Cape, and Nome for (a) May 1967 and (b) November 1967. The 95% confidence limits (C) and bandwidth (B) are shown.

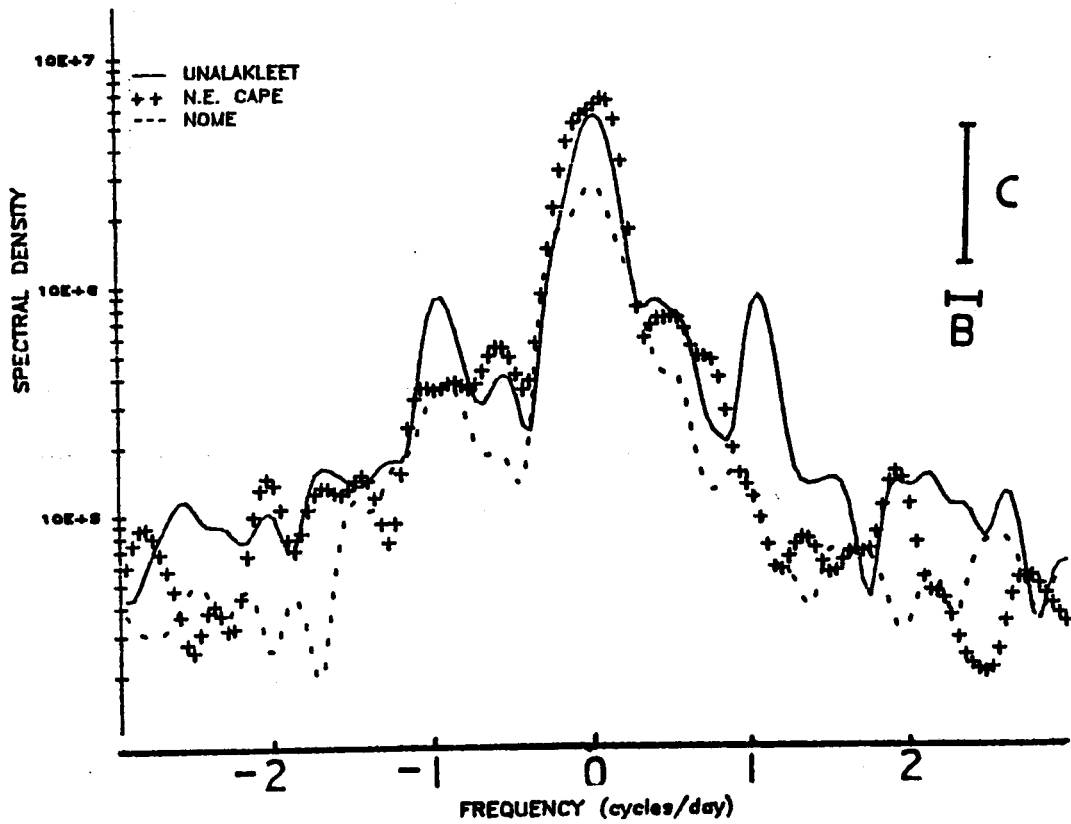


(a)

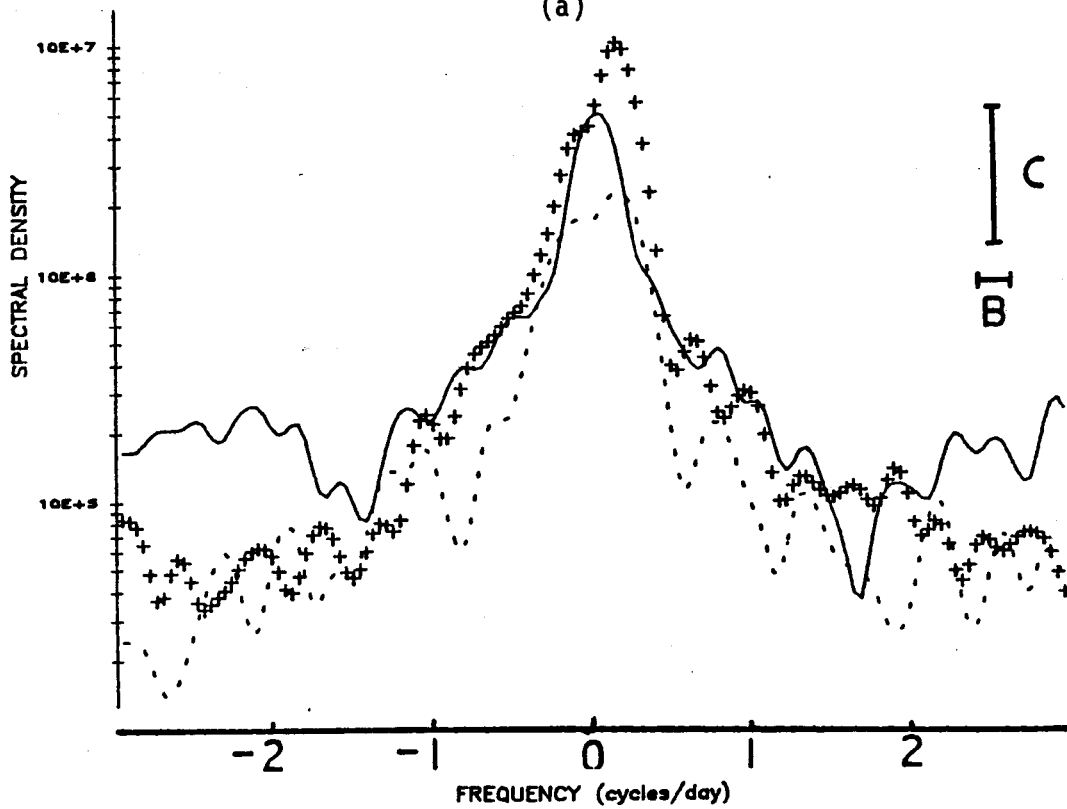


(b)

Fig. B9. Time series rotary spectra of surface wind velocity data from Unalakleet, Northeast Cape and Nome for (a) January 1968 and (b) July 1968. The 95% confidence limits (C) and bandwidth (B) are shown.



(a)



(b)

Fig. B10. Time series rotary spectra of surface wind velocity data from Unalakleet, Northeast Cape, and Nome for (a) May 1968 and (b) November 1968. The 95% confidence limits (C) and bandwidth (B) are shown.

SHORT TERM PREDICTION (NOWCASTING) OF NET DAILY SEA
ICE MOVEMENT IN THE BERING STRAIT WITH A
MESOSCALE METEOROLOGICAL NETWORK

by

Thomas L. Kozo, Ph.D.

VANTUNA Research Group

Occidental College

Final Report
Outer Continental Shelf Environmental Assessment Program
Research Unit 519

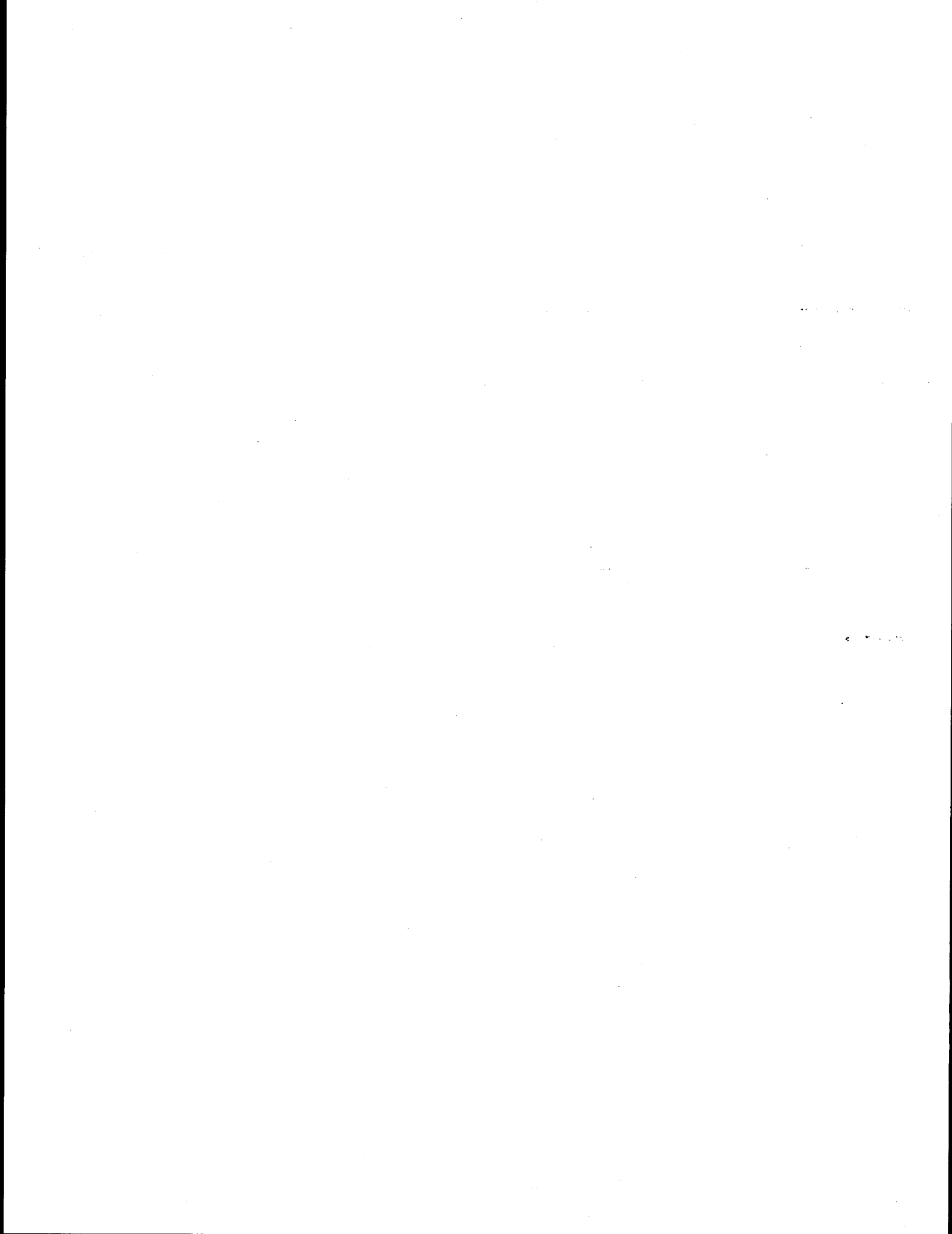
1984

103



TABLE OF CONTENTS

LIST OF FIGURES.....	
LIST OF TABLES.....	
ABSTRACT.....	
1. INTRODUCTION.....	
2. STUDY AREA.....	
3. DATA	
a. Surface Atmospheric Pressure and Temperature.....	
b. Geostrophic Wind Data.....	
c. Satellite Imagery.....	
4. RESULTS WITH DISCUSSION	
a. Sea Ice Injections.....	
b. Advantages of the Mesoscale Atmospheric Pressure Network..	
c. Implications for Oceanic Transport Mechanisms.....	
d. Constructing the Sea Ice Movement Prediction Nomogram.....	
e. Using the Nomogram.....	
f. Testing the Nomogram Technique.....	
(1) NOAA Satellite Imagery.....	
(2) Buoy Drift Data (Description from Reynolds and 1984).....	
g. Discovery of Solid Double Sea Ice Arches.....	
5. SUMMARY AND CONCLUSIONS	
a. Sea Ice Movement Modes.....	
b. Sea Ice Immobilization Modes.....	
c. Driving Force Behind the North Flowing Current in the Strait.....	
d. Recommendation for Future Work.....	
6. REFERENCES.....	



LIST OF FIGURES

- Fig. 1 The surface pressure station network P-U-N covering the Bering Strait region. P is Bukhta Provideniya, U is Uelen (both in Siberia) and N is Nome, Alaska. The Diomedede Islands (D) are in the center of the Strait, Cape Schmidt (S) is below Wrangel Island, and Cape Wales (W) and Cape Dezhneva (X) are on the tips of the Seward and Chukchi Peninsulas respectively. Mountain axes are shaded for emphasis.....
- Fig. 2. The atmospheric pressure field (top) determined by pattern recognition techniques (Hufford 1984) that is associated with southward ice movement below the Strait and westward movement (bottom) of ice out of Norton Sound (Stringer and Hufford, 1982). Arrows on isobars (top) indicate wind direction in the Strait area.....
- Fig. 3. The "relaxed" atmospheric pressure field (top) determined by pattern recognition techniques (Hufford, 1984) that results in northward ice movement into the Strait and eastward movement (bottom) of ice into Norton Sound (Stringer and Hufford, 1982).....
- Fig. 4. An example of the lack of detail on an NMC surface isobaric analysis (dashed lines in mb). The mesoscale network (Provideniya [P], Uelen [U], and Nome [N]) shows a V_G (see arrow) of 12.4 ms^{-1} from 248° . The surface wind speeds at designated station locations are $\sim 5 \text{ ms}^{-1}$ for each perpendicular flag, $\sim 2.5 \text{ ms}^{-1}$ for slant flags (i.e. Kotzebue [K]) and ~ 0 for a circle (i.e. P). Other stations

shown are Point Lay (L) and Cape Schmidt (S). The sea ice in the Strait area moved 15 km to the north.....

Fig. 5. An example of the advantages of the network P-U-N analysis over both pattern recognition and NMC surface isobaric analysis (dashed lines in mb). Despite an apparent "relaxation", the 1200 GMT network analysis shows a V_G (see arrow) of 11.0 ms^{-1} from 75° . The station and flag designations are as in Fig. 4. The sea ice in the Strait area moved 6 km to the south.....

Fig. 6. An example of the effects of orography on the surface wind directions despite a well defined isobaric pattern (dashed lines in mb). The P-U-N network analysis shows V_G (see arrow) of 23 ms^{-1} from 56.8° . The station and flag designations are as in Fig. 4. The Nome (N) and Kotzebue (K) winds would give no clue that the sea ice in the Strait moved 50 km to the south during this day..

Fig. 7. A section of an NMC surface pressure analysis that indicates weak surface winds and no apparent reasons for sea level in the Bering to be higher than that of the Chukchi. The net sea ice movement calculated with P-U-N data was 18 km to the north for a V_G (see arrow) of 2.6 ms^{-1} from 58.7°

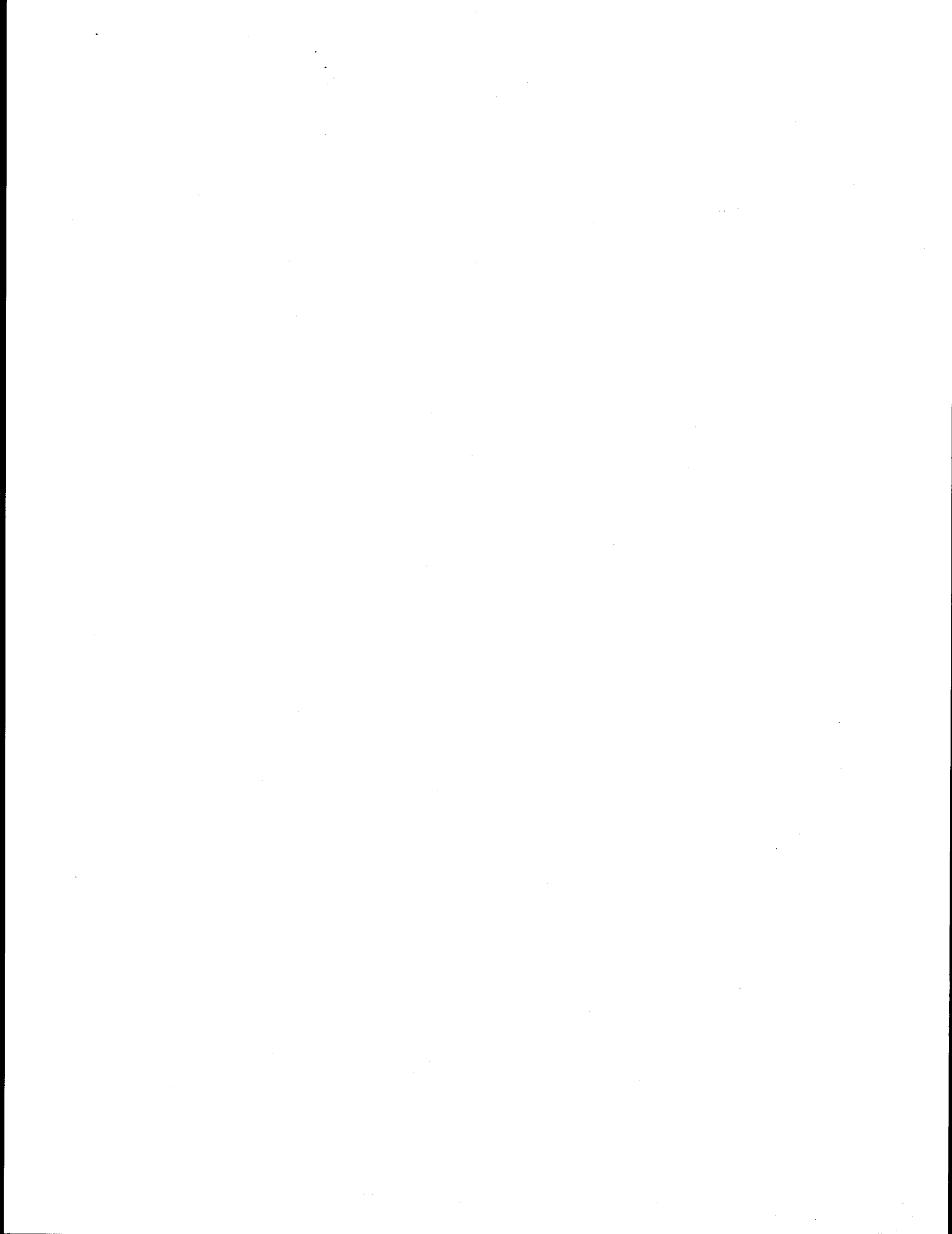
Fig. 8. The Bering Strait sea ice movement prediction nomogram with Greek and Latin letters representing sample MAPN computed \bar{V}_G 's used in its construction (see Table 2). The Strait axis is 40° from the north and has ice movement arrows meeting in the Force Balance Zone. The center solid circle is the $\leq 3 \text{ ms}^{-1}$ wind speed zone and it represents direction uncertainties $>15^\circ$

Fig. 9. Ice displacement (top) compared to MAPN V_G 's for 6-28 April 1982 plotted with corresponding day numbers on the sea ice movement prediction nomogram (bottom). The number positions represent wind velocity vectors whose V_{40} components define the daily predicted ice movement zone. X is a sample V_G calculated from surface pressure data in Fig. 6. Drawing a perpendicular line from X to the Strait axis results in a $V_{40} = 22 \text{ ms}^{-1}$. This is the Ice Into Bering $> 20 \text{ km (day)}^{-1}$ Zone.....

Fig. 10. A satellite photograph taken May 5, 1980 showing the characteristic solid double ice arch in the Bering Strait using the tip of the Chukchi Peninsula (D), the Diomed Islands and the Seward Peninsula (W) tip as anchor points. There is a large expanse of open water (OW) south of the Strait, south of the Chukchi Peninsula and in Norton Sound.....

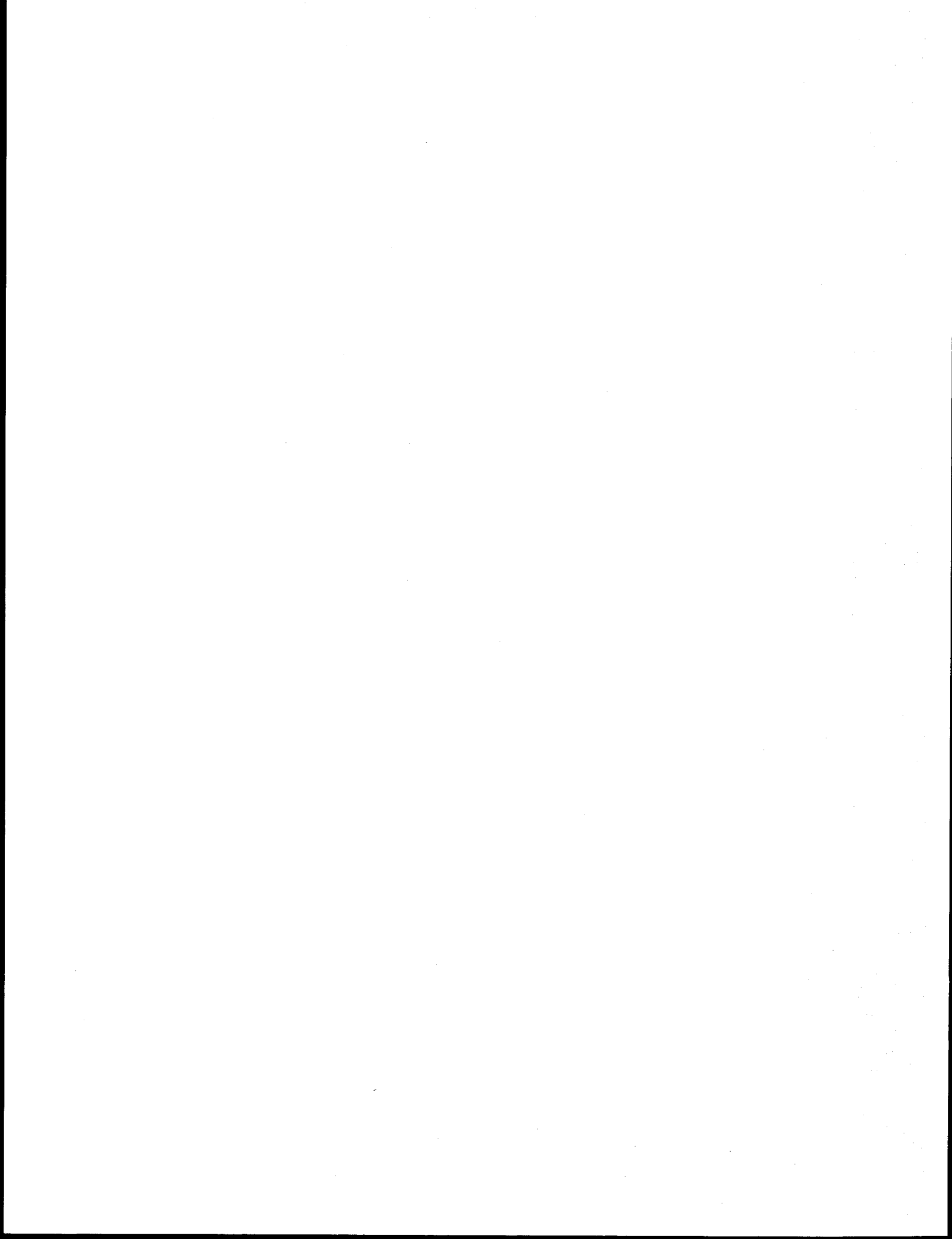
Fig. 11. Samples of MAPN V_G 's from designated double arch periods April 14-May 10, 1980, February 26-March 8, 1984, and March 22-April 21, 1984 plotted on the nomogram. There are several cases (enclosed by dashed oval) with $V_{40} \geq 17 \text{ ms}^{-1}$ indicating a predicted ice movement into the Bering Sea of greater than 20 km(day)^{-1}

Fig. 12. An enlargement of the Strait area taken from the Fig. 10 photograph. The dashed curves show the actual sea ice arches to avoid confusion with land boundaries. The dark area is open water. The inset (top) is a sketch of an idealized free arch showing the span width (2λ) and the angle (θ) between the horizontal and tangent to the free surface.....



LIST OF TABLES

- Table 1. Examples of past sea ice movements events through the Bering Strait documented by satellite imagery.....
- Table 2. Selected sea ice movement events for the Bering Strait plotted in Fig. 8.....
- Table 3. Net buoy displacements (x) versus nomogram predictions (NP)...



ABSTRACT

The weather stations at Uelen (Siberia), Bukhta Provideniya (Siberia) and Nome (Alaska) surround the Bering Strait. Surface atmospheric pressure data from this mesoscale triangular station network can be used to calculate hypothetical geostrophic wind velocities in the area of the Strait axis. Net 24 h Strait ice movement has been derived from daily visible and infrared NOAA satellite imagery for the months of November through May from 1974 to 1984. These historical ice motion data and network velocity data have recently been matched to form an empirical 12 h advance forecast (nowcast) prediction scheme for sea ice movement that has all-weather capabilities. In addition, study results have identified three modes of ice movement and two modes of ice immobilization.

The first movement mode is southward requiring a network geostrophic wind of at least 12 ms^{-1} from the northeast and results in transport of ice from the Chukchi Sea to the Bering Sea. The second mode is northward ice movement from the Bering to the Chukchi Sea during weak northerly or southerly winds, driven mainly by a pre-existing north flowing ocean current. The third and least common mode is northward ice movement under the combined influence of a geostrophic wind from the southwest and the north flowing ocean current.

The first immobilization mode is an apparent balance between the wind stress from the north and water stress from the south, plus internal ice stresses resulting in 0 net movement but existing for time periods generally less than one week. The second and least common immobilization mode was discovered during cases where the model erroneously predicted large ice

movement southward through the Strait. Instead, satellite imagery showed large double solid sea ice arches had formed in the Strait. One arch reached from the Chukchi Peninsula (Cape Dezhneva) to the Diomed Islands and one reached from the Diomed Islands to the Seward Peninsula (Cape Wales). These arches remained intact under 26 ms^{-1} geostrophic winds from the northeast and resulted in 0 net ice movement through the Strait for up to four weeks.

1. Introduction

The prospect of oil development in the northern Bering Sea has led to recent studies of northward and southward sea ice movement through the Bering Strait (Fig. 1). This movement in the months from November to May can be quite extensive and be intimately connected to destructive interactions with sea ice in the St. Lawrence Island (Shapiro and Burns, 1975a; Sodhi, 1977) and Norton Sound vicinities (Stringer and Hufford, 1982). One example of these interactions can be seen in Fig. 2 (bottom) where southward ice movement below the Strait is related to westward movement of ice out of the Sound (Stringer and Hufford, 1982). Figure 2 (top) shows the atmospheric pressure field determined by pattern recognition techniques (Hufford and Scheidt, 1984), most often associated with this interaction. Another example can be seen in Fig. 3 (bottom) where northward ice movement into the Bering Strait and eastward ice movement into the Sound occur simultaneously (Stringer and Hufford, 1982). Fig. 3 (top) again shows the atmospheric pressure pattern most often associated with this phenomenon (Hufford and Scheidt, 1984). Note that this last case is a type of relaxation with wind forcing at a minimum.

Sequential Landsat (NASA) and DAPP (U.S. Air Force) imagery was used as early as March 1973 to construct displacement vectors for ice floes moving through the Bering Strait (Shapiro and Burns, 1975b). They showed an apparent relationship between southward ice movement and northerly winds at Cape Wales on the western tip of the Seward Peninsula (Fig. 1). This movement occurred despite average yearly northward water transport (Coachman et al., 1975). Ray and Dupre (1981) also noted that the National Weather

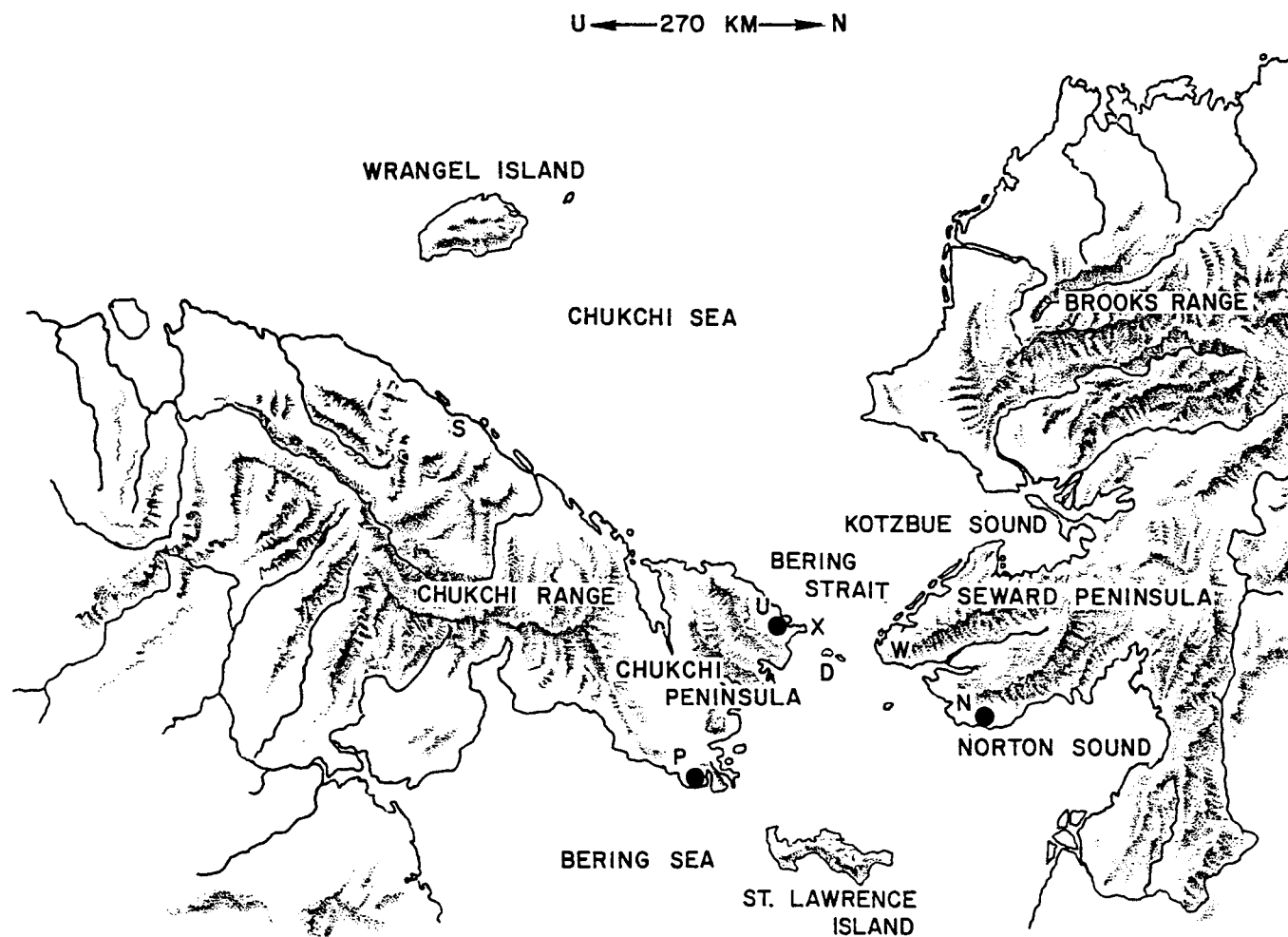


Fig. 1 The surface pressure station network P-U-N covering the Bering Strait region. P is Bukhta Provideniya, U is Uelen (both in Siberia) and N is Nome, Alaska. The Diomedede Islands (D) are in the center of the Strait, Cape Schmidt (S) is below Wrangel Island, and Cape Wales (W) and Cape Dezhneva (X) are on the tips of the Seward and Chukchi Peninsulas respectively. Mountain axes are shaded for emphasis.

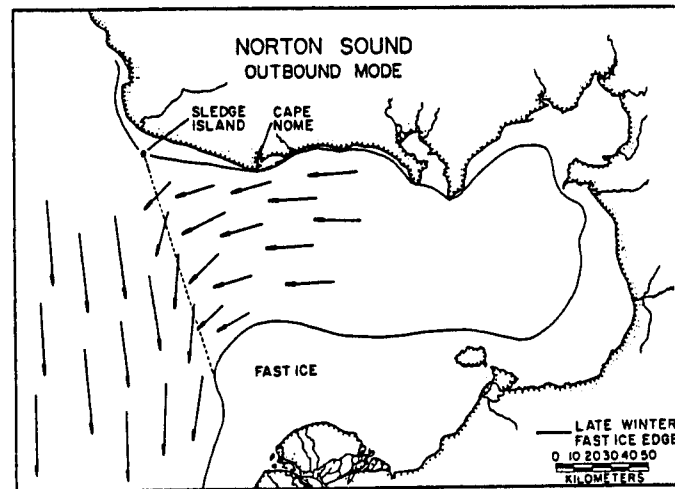
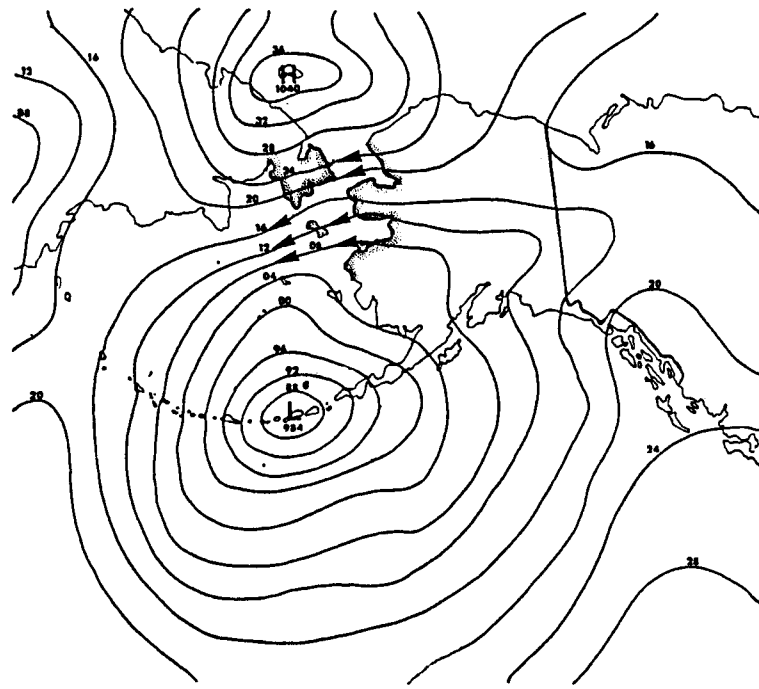


Fig. 2. The atmospheric pressure field (top) determined by pattern recognition techniques (Hufford 1984) that is associated with southward ice movement below the Strait and westward movement (bottom) of ice out of Norton Sound (Stringer and Hufford, 1982). Arrows on isobars (top) indicate wind direction in the Strait area.

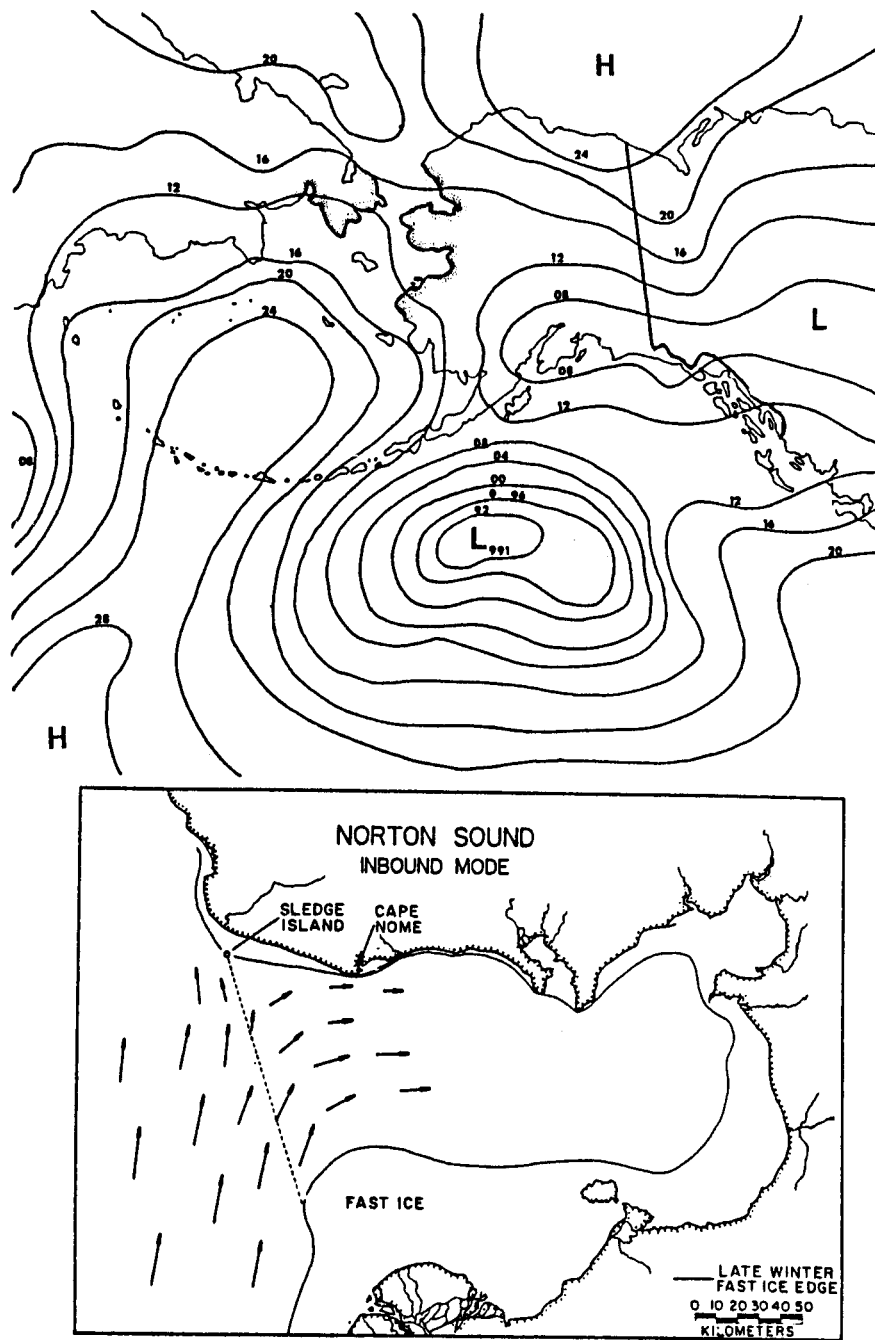


Fig. 3. The "relaxed" atmospheric pressure field (top) determined by pattern recognition techniques (Hufford, 1984) that results in northward ice movement into the Strait and eastward movement (bottom) of ice into Norton Sound (Stringer and Hufford, 1982).

Service surface synoptic charts apparently explained alternating southward and northward sea ice movement in the Bering Strait region deduced from February 1976 sequential Landsat imagery. Large-scale sea ice fracture resulting in southward flow through the Bering Strait (ice breakout) has been studied (Reimer et al., 1979). They modeled the Strait as a two-dimensional chute and computed the necessary load required to fracture and push ice. An atmospheric pressure difference from Cape Schmidt (Siberia) to Nome Alaska, (see Fig. 1) exceeding 20 mb was related to ice breakout events in the winters of 1975 and 1976. This was an interesting study, but the geostrophic wind which can be related to the direction of stress application is perpendicular to the pressure gradient, not parallel. It will be shown below, on examination of a greater data sample, that a whole suite of wind directions often produced by pressure differences less than 20 mb from Cape Schmidt to Nome can shove ice south through the Strait.

The tools for short range, less than 24 h prediction (nowcasting [Browning, 1982]) of sea ice movement through the Bering Strait existed, but two preliminary tasks were still to be performed. First, an appropriate atmospheric pressure network encompassing the Bering Strait with at least three World Meteorological Organization (WMO) reporting stations had to be found for computation of geostrophic wind velocities. Second, long records of continuous north and south sea ice motion had to be compiled from available satellite imagery to determine precursor characteristics. The three network stations found were Uelen (U, Siberia), Provideniya (P, Siberia) and Nome (N, Alaska) (Fig. 1). The continuous records of sea ice motion were computed from 11 years of daily visible and infrared NOAA 3-8 satellite photographs. Table 1 is a listing of some Strait sea ice movement events documented from these photographs.

TABLE 1

EXAMPLES OF PAST SEA ICE MOVEMENT EVENTS THROUGH THE BERING STRAIT
 Documented by Satellite Imagery

Courtesy of Dr. Bill Stringer, University of Alaska, Geophysical Institute

Year	Month	South Days	North Days
1974	April	8-12	
1976	February	5-12, 22-25	26-28
	April	17-20	
	Nov.-Dec.	29-2	
	December	10-11	3-9
1977	February	10-12	
	March	1-2, 25-26	
	April	2-3, 9-12	
1978	March	4-7, 27-28	21-25
	April	7-9	
1979	February	26-27	16-24
	April	9-11	
1980	February	20-22	1-3 (March)
	April	6-7, 18	
	December	7-13, 24-25, 30-31	19-21
1981	February	13, 16-19	4
	December	5-7	13
1982	March	14-15, 19-20	2-4
	April	12-13, 27	18-21
1983	January	1-4, 7-8, 16-19	18-15
	February	17-22	
	March	9-15, 22-24, 16-30	
	April	4-6	

2. Study Area

The Bering Strait's oceanic cross section is roughly 85 km x 50 m and its annual average transport is ~ 1 Sv to the north, attributed to higher sea level in the Bering Sea than in the Arctic Ocean (Coachman and Aagaard, 1981). This relatively small annual northward transport would be five times greater if not for wind induced flow reversals to the south occurring two to three times per month and lasting six to 12 days (Kovacs and Sodhi, 1981). Daily mean transport can reach 3.1 Sv (Coachman and Aagaard, 1981) to the north which implies currents up to 70 cms^{-1} , given the above cross sectional area. Current velocities of this magnitude are indications that oceanic flow driven north or south tend to be funneled (see Fig. 1) and accelerated on entering the Strait (Coachman *et al.*, 1975).

The same funneling applies to arctic winds in the Strait which tend to flow around rather than over topography (Kozo, 1984). The Chukchi Peninsula has small mountain range axes setting north to east while the Seward Peninsula has small mountain range axes setting north to west (Fig. 1). The elevations are at least equal to 600 m which Dickey (1961) has shown are sufficient to redirect and accelerate air flow during winter conditions.

During the course of this study, it became apparent that ice moved north and south through the Strait as if on a conveyor belt (Kozo and Tucker, 1974) for a suite of computed wind velocity vectors. Therefore, relating ice movement thresholds to a wind velocity component parallel to an assumed strait axis orientation would simplify development of a prediction nomogram. However, determining the precise axis orientation for ice transit thresholds was not easy. In addition to water and wind stresses, the ice movement

threshold values would be affected by interplay of internal ice stresses, land boundary effects and fast (immobile shore-attached) ice zone boundary effects. Even the fixed land boundaries (Fig. 1) present a problem. The Chukchi Peninsula coastlines above and below the Strait are oriented 135° and 45° from the north, respectively. The Seward Peninsula coastlines above and below the Strait are oriented 55° and 145° from the north, respectively. The perpendicular to the line of minimal distance (Cape Dezhneva to Cape Wales, Fig. 1) across the Strait is 31° from the north. Evidently there were several choices of axis orientation. For the purposes of this paper, the internal ice stresses and fast ice edge effects were neglected and the Strait axis orientation was chosen to be 40° from the north. This angle represents a perpendicular to the line from Cape Schmidt to Nome (Fig. 1). In this way, comparisons can be made with earlier work by Reimer *et al.* (1979) where a positive pressure difference (20 mb) between Cape Schmidt and Nome was related to ice breakout into the Bering Sea.

3. Data

a. Surface atmospheric pressure and temperature

Barometric pressure data, reduced to sea level, and temperature data are taken simultaneously from a three station weather network and used to compute a hypothetical geostrophic wind for the Bering Strait. The three stations are part of the global weather network and transmit real-time data to the National Meteorological Center (NMC). They are Uelen ($66^\circ 10'N$, $169^\circ 50'W$), Bukhta Provideniya ($64^\circ 26'N$, $173^\circ 14'W$), and Nome ($64^\circ 30'N$, $165^\circ 24'W$) (see Fig. 1). The accuracies of these pressure and temperature data from Nome, a first order weather station, are better than ± 0.25 mb and $\pm 1^\circ C$, respectively.

The two Russian stations are assumed to be within these limits also.

b. Geostrophic wind data

These data were computed from the pressure and temperature data provided by the three above weather stations. The atmospheric flow was assumed to be in geostrophic balance (1):

$$f(k \times V) + \frac{\nabla p}{\rho} = 0 \quad (1)$$

The first term is the Coriolis force, and the second is the pressure gradient force. f is the Coriolis parameter ($1.321 \times 10^{-4} \text{ sec}^{-1}$ at 65°N), k is the vertical unit vector, V is the velocity vector, ∇p is the gradient of the atmospheric pressure, and ρ is the air density. Using the above station grid (triangle in Fig. 1) and noting that pressure can be represented as a function of latitude (y) and longitude (x) on a plane surface, the following set of equations:

$$\begin{aligned} P_N(x,y) &= ax_N + by_N + c \\ P_U(x,y) &= ax_U + by_U + c \\ P_P(x,y) &= ax_P + by_P + c \end{aligned} \quad (2)$$

are generated, where the subscripts N, U, and P denote Nome, Uelen and Provideniya, respectively. Pressure (P) data is broadcast by each station and relative positions of each station are known on an x,y grid. Cramer's rule can be applied to (2) to solve for unknowns a , b and c . Since $\partial P/\partial x = a$ and $\partial P/\partial y = b$, the pressure gradient (∇P) can be computed. The geostrophic velocity can now be calculated from (1) since f is known and ρ for dry air can be estimated from station temperatures.

Station errors of $\pm 1^\circ\text{C}$ (see above) in temperature can cause errors of .34% in the velocity magnitude since they affect ρ estimates. Station errors in pressure of $\pm .25$ mb can cause maximum speed errors ± 1.4 ms^{-1} and direction errors greater than $\pm 15^\circ$ for wind speeds below 3 ms^{-1} . Therefore, at wind speed ≤ 3 ms^{-1} , wind directions should not be considered significant.

The main objective of this study was to create a nomogram for predicting ice movement in the Bering Strait from computed geostrophic wind velocities. The "true" geostrophic winds, therefore, are not as important as geostrophic wind values derived from consistent data sources that comprise the triangular network surrounding the Strait. Successful use of mesoscale network computed geostrophic winds and their increased resolution and predictive capabilities over synoptic networks in the Arctic has been documented by Kozo (1980, 1984).

c. Satellite imagery

The imagery used in this study came primarily from visible and infrared NOAA 3-8 VHRR (very high resolution radiometer) satellite photographs. The infrared imagery was utilized primarily during the months of December, January and February when daylight was minimal. In order to minimize errors due to the earth's curvature, the scale was taken from the closest land mass. The net ice motion in a 24 h period was measured directly by tracking identifiable floes or indirectly by measuring the change in open water extent south or north of the Diomed Islands (Fig. 1). A minimum of two consecutive days of imagery is necessary to document a displacement. The error for a typical two-day sequence is estimated at ± 5 km. However, for sequences greater than two days, the error reduces significantly.

From November 1974 to May 1984, close to 40% of the total observation days during the ice-covered months (November through May) have been obscured due to cloud related undercast. Therefore, the nomogram produced from these empirical observations has not included a large percentage of the total possible ice movement data. However, the product and technique outlined below based on the remaining 60% of the data, if representative, will be an all-weather, undercast independent, predictive tool.

4. Results with Discussion

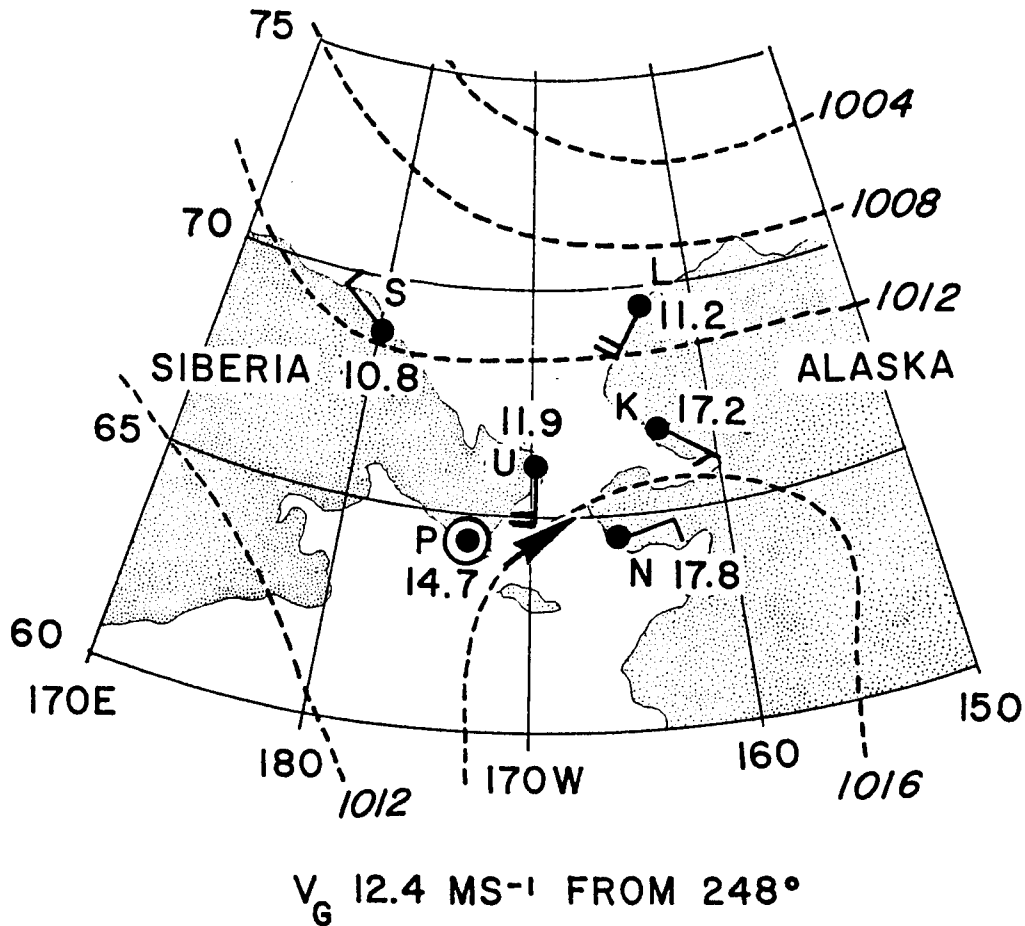
a. Sea ice injections

The available satellite imagery (1974 to 1984) has shown many episodes of extensive south and north sea ice movement analogous to ice injections through the Strait typically lasting five to seven days. There have been 39 cases of southward injections into the Bering Sea and 19 cases of northward injections into the Chukchi Sea where the total ice input approximately equaled the areal extent of St. Lawrence Island (Fig. 1, SLI). Of the 39 southward cases, 17 had an input more than twice the area of SLI. For the 18 northward cases, only seven occurred with an input of double SLI's area.

b. Advantages of the mesoscale atmospheric pressure network

Fig. 4 shows the advantage of a mesoscale atmospheric pressure network (MAPN) for predicting ice movement through the Bering Strait over that of the NMC surface pressure analysis. The NMC surface isobaric analysis for 21 April 1982, 1200 Greenwich Mean Time (GMT) gives no indication of a strong southwesterly wind. In addition, the surface wind directions at Uelen (U),

21 APRIL 1982 (1200 GMT)



V_G 12.4 MS⁻¹ FROM 248°

ICE MOVED 15 KM N

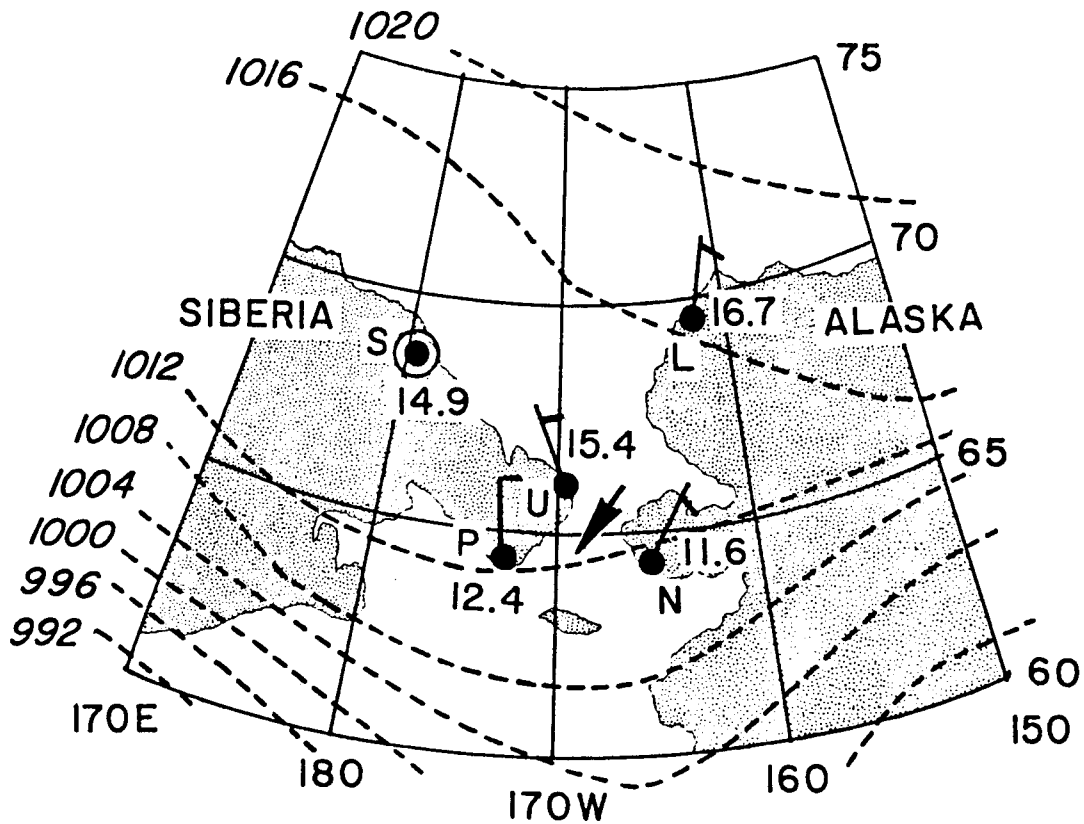
Fig. 4. An example of the lack of detail on an NMC surface isobaric analysis (dashed lines in mb). The mesoscale network (Provideniya [P], Uelen [U], and Nome [N]) shows a V_G (see arrow) of 12.4 ms⁻¹ from 248°. The surface wind speeds at designated station locations are ~ 5 ms⁻¹ for each perpendicular flag, ~ 2.5 ms⁻¹ for slant flags (i.e. Kotzebue [K]) and ~ 0 for a circle (i.e. P). Other stations shown are Point Lay (L) and Cape Schmidt (S). The sea ice in the Strait area moved 15 km to the north.

Provideniya (P), and Nome (N) are all different (Fig. 4). However, the surface wind velocity ($\sim 10 \text{ ms}^{-1}$ from 180°) at Uelen may offer a clue to the eventual ice push direction. Satellite imagery indicated that ice in the Strait moved 15 km north (± 5 km) for this day. The MAPN calculated geostrophic wind (V_G) was 12.4 ms^{-1} from 248° which fits the observed net motion.

Fig. 5 is a case demonstrating the advantage of the MAPN over both pattern recognition and NMC synoptic analysis. A type of relaxation mode has existed for four days (as in Fig. 3, top) which denotes probable northward ice movement. However, the MAPN calculated geostrophic wind velocity indicates that the "brakes" are being applied to northward sea ice movement. The 1200 GMT, 25 March 1978 V_G was 11.0 ms^{-1} from 75° and the average V_G for the next 12 h period was 12.4 ms^{-1} from 68.4° . The net ice movement for 25 March was 6 km south (± 5 km). The surface winds surrounding the Strait (Fig. 5) appear to be less than 5 ms^{-1} , but their northerly direction may also be a clue to the direction of wind push.

The effects of orography are striking, even with a well defined surface pressure pattern as demonstrated on April 5, 1983 (Fig. 6). The "dog's breakfast" of surface wind directions at P, U and N are evidence that previous attempts to correlate these local winds with ice movement or ocean current direction in their vicinity met with limited success (Coachman et al., 1975 and Reimer et al., 1979). The MAPN calculated V_G was 23 ms^{-1} from 56.8° , again agreeing with the satellite determined large net ice movement of 50 km (± 5 km) south in one day.

25 MARCH 1978 (1200 GMT)

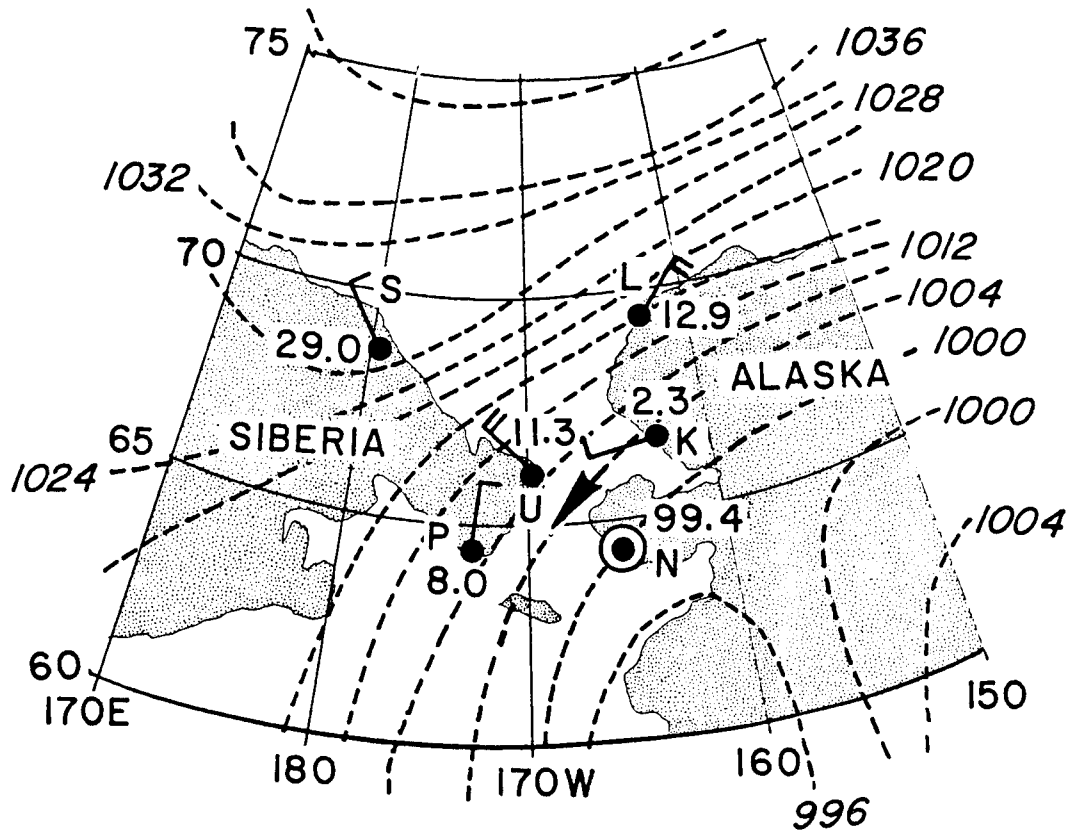


$V_G \parallel \text{MS}^{-1}$ FROM 75°

ICE MOVED 6 KM S

Fig. 5. An example of the advantages of the network P-U-N analysis over both pattern recognition and NMC surface isobaric analysis (dashed lines in mb). Despite an apparent "relaxation", the 1200 GMT network analysis shows a V_G (see arrow) of 11.0 ms^{-1} from 75° . The station and flag designations are as in Fig. 4. The sea ice in the Strait area moved 6 km to the south.

5 APRIL 1983 (1200 GMT)



V_G 23 MS⁻¹ FROM 56.8°

ICE MOVED 50 KM S

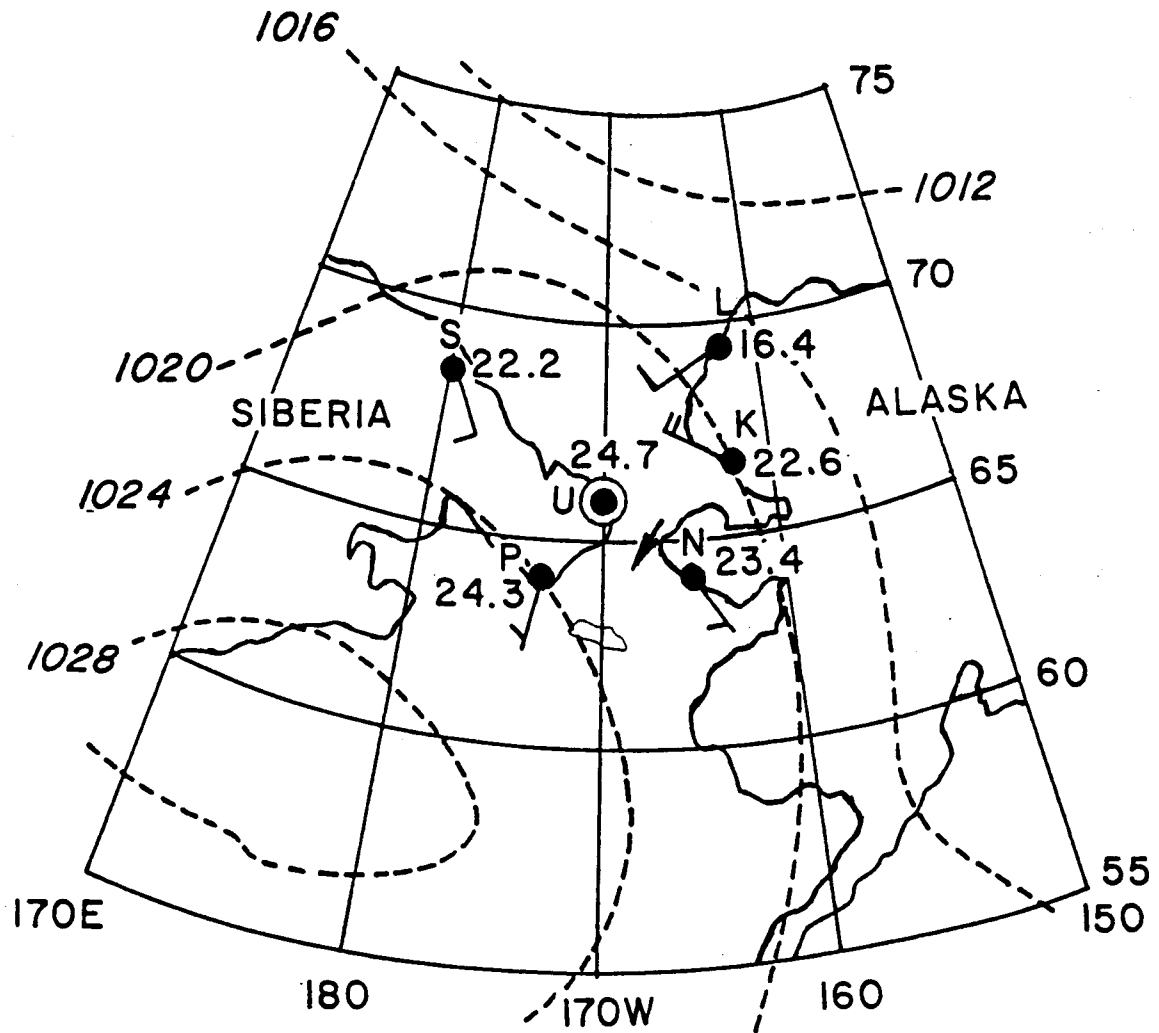
Fig. 6. An example of the effects of orography on the surface wind directions despite a well defined isobaric pattern (dashed lines in mb). The P-U-N network analysis shows V_G (see arrow) of 23 ms⁻¹ from 56.8°. The Nome (N) and Kotzebue (K) winds would give no clue that the sea ice in the Strait moved 50 km to the south during this day.

c. Implications for oceanic transport mechanisms

During the course of this nowcasting study, several minor discoveries were made. One of them provides evidence that previous conclusions concerning the persistent northward oceanic transport through the Strait may have to be reexamined. Coachman and Aagaard (1981) have stated that the basic driving force for this transport is a yet unexplained higher mean sea level in the Bering Sea than in the Arctic Ocean. They also state that short (several day) increases in northward flow volume have two causes. The first is a compensatory acceleration of flow following a wind induced southward transport event. After the driving wind subsides, ocean transport continues south for a short time raising the water level in the St. Lawrence Island-Norton Sound area (Fig. 1), resulting in an enhanced sea level slope down to the north. This creates a large increase in transport to the north with a one day time lag. The second cause was the development of a strong low-pressure center (counterclockwise rotation) in the western Bering Sea, south and west of the Strait with isobars oriented north-south through the Strait. In this case, southwesterly winds push water onto the relatively shallow northern Bering Sea shelf, again enhancing sea level slope down to the north.

It must be noted that current data were not measured coincident with the time period discussed below, however net sea ice movement was measured. This movement, in cases of weak synoptic winds, will indicate surface current velocities. The 00 GMT, 11 May 1984 NMC synoptic chart (Fig. 7) shows a weak high to the southwest of the Strait promoting slight off-shelf water movement in the Bering Sea. In addition, the atmospheric pressure field shows a 12 mb decrease in sea level pressure from the southwestern Bering to the

11 MAY 1984 (00 GMT)



V_G 2.6 MS⁻¹ FROM 58.7°

(LOW WIND CONDITIONS)

Fig. 7. A section of an NMC surface pressure analysis that indicates weak surface winds and no apparent reasons for sea level in the Bering to be higher than that of the Chukchi. The net sea ice movement calculated with P-U-N data was 18 km to the north for a V_G (see arrow) of 2.6 ms⁻¹ from 58.7°.

northeastern Chukchi Sea. Both effects would tend to make the sea level in the Bering lower than in the Arctic Ocean, promoting southward current flow since it is opposite to the condition mentioned by Coachman and Aagaard (1981). This synoptic condition persisted on May 11 and was imbedded in a period from May 4 to May 15, 1984 of relatively weak synoptic winds. The net sea ice movement on May 11 was 18 km (± 5 km) north and followed a day of almost no motion. This event was evidence that northward current flow occurs without southwesterly wind forcing or a sea level slope down to the north. The same event also showed that accelerated flow can occur without a sea level imbalance caused by a previous northerly wind. The MAPN calculated V_G (Fig. 7) was a low 2.6 ms^{-1} from 58.7° (see errors for speeds $< 3 \text{ ms}^{-1}$ in Section 3b). The synoptic charts for the entire day showed no winds strong or persistent enough to produce the recorded ice movement. This event took place under relaxed conditions similar to those depicted in Fig. 3 which were found by pattern recognition techniques to be representative of northward ice movement.

There is ample evidence that all the mechanisms listed above (Coachman and Aagaard, 1981) are sufficient conditions for northward oceanic transport, however, this example shows that they are not necessary conditions for this type of transport. The recent ocean modeling work of Liu and Leendertse (1982) has shown a net residual circulation in the Strait area due to only the tides and density field (baroclinic mode) with current amplitudes of $\sim 10 \text{ cms}^{-1}$. Their current characteristics match the data of Drury *et al.* (1981). Based on this new modeling effort, weather map analysis such as Fig. 7 and net ice motion data, a northward flowing current driven only by tidal residuals and the ocean density distribution must exist in the Strait without the need for additional wind push or sea level differences.

d. Constructing the sea ice movement prediction nomogram

Sea ice satellite images from November 1974 to May 1984 have been examined and compared to simultaneous MAPN computed V_G 's to produce an empirical 12-hour advance forecast (nowcast) nomogram. Table 2 gives the dates and mode categories for some of the sea ice movement events used in constructing the nomogram (Fig. 8). The Greek and Latin letters from Table 2 are positioned in Fig. 8 to represent a MAPN computed V_G (direction and speed as independent variables). The directions indicated are those from which the wind is blowing. The small center circle (Fig. 8) represents V_G 's with speeds less than 3 ms^{-1} . Due to the errors mentioned in Section 3 and the minimal effects on ice motion at these low wind speeds, V_G 's within this circle should be considered as ~ 0 winds. V_{40} (see Table 1 for sign) represents the V_G component parallel to the assumed Strait axis, 40° from north. This axis is indicated by ice movement direction arrows (Fig. 8) that meet in the Force Balance Zone, one of five zones defined by wind speed ranges along the V_{40} axis. These zones and the nomogram technique have characterized three modes of ice motion and two modes of ice immobilization in the Strait. Four predictable modes will be described below in conjunction with Fig. 8 and Table 2. The fifth mode, though not predictable, was a discovery of this procedure and will be discussed in Section 4g below.

Mode 1 covers two zones and represents wind-forced sea ice movement into the Bering Sea which initially at least must offset a northward flowing ocean current. To get measurable ice movement into the Bering, V_{40} must exceed 11.5 ms^{-1} (Fig. 8, Table 2). The ICE INTO BERING ZONE has $11.5 \text{ ms}^{-1} < V_{40} \leq 16.5 \text{ ms}^{-1}$ and produces net ice movement of $< 20 \text{ km (day)}^{-1}$. The ICE INTO BERING $> 20 \text{ km (day)}^{-1}$ (ZONE) has $V_{40} > 16.5 \text{ ms}^{-1}$. The latter zone

TABLE 2
 SELECTED SEA ICE MOVEMENT EVENTS FOR THE BERING STRAIT
 PLOTTED IN FIG. 8.

-
- A. Referring to Fig. 8, $V_{40} \equiv V_G$ speed component to Strait axis 40° from north.
- | | |
|--------------------------------|-------|
| $> 310^\circ$ or $< 130^\circ$ | > 0 |
|--------------------------------|-------|
- B. If V_G direction
- | | |
|--------------------------------|--------------|
| $= 310^\circ$ or $= 130^\circ$ | $V_{40} = 0$ |
| $130^\circ < V_G < 310^\circ$ | < 0 |
- C. No estimates of turning angle (directional difference between V_G and V surface) were made since orographic effects such as channeling and blockage were very apparent and no concomitant long term data base exists.

Mode 1. Into Bering Sea (wind-forced)

- a. $> 20 \text{ km (day)}^{-1}$ ($V_{40} > 16.5 \text{ ms}^{-1}$)

Events: Y(14,15 Apr 82), Z(14,15 Mar 82)
 γ (13 May 78, λ (18 May 77), Δ (11 Feb 84)
 ϕ (6,7 Mar 78), Ψ (27 Dec 76)**

** Ψ also represents the average value needed to reverse the ocean current, at 10 m off the bottom in the Bering Strait, from north to south for all three cases in Dec 76 (Coachman and Aagaard, 1981) during total ice cover

- b. $< 20 \text{ km (day)}^{-1}$, ($11.5 \text{ ms}^{-1} < V_{40} \leq 16.5 \text{ ms}^{-1}$)

Events: U(18 Feb 84), X(19 Feb 83), N(12 May 81)
 V(22 Feb 76), W(19 Feb 76), M(11 May 81)

TABLE 2. (continued)

Mode 2. Into Chukchi Sea (ocean current forced, wind influence minor)

- a. $> 20 \text{ km (day)}^{-1}$, $(-7.5 \text{ ms}^{-1} < V_{40} \leq 0 \text{ ms}^{-1})^{***}$, weak winds in current direction

***If V_{surface} is $\sim 60\%$ of V_{40} , then $(7.5 \text{ ms}^{-1} \times .6) = 4.5 \text{ ms}^{-1}$
or WMO equivalent of a gentle breeze

Events: A(10,11 Feb 79), B(16,17 Feb 79), C(1,2 Feb 76)
D(27,28 Feb 76), E(20,21 Mar 78), F(2,3 Mar 82)

- b. $< 20 \text{ km (day)}^{-1}$, $(0 \text{ ms}^{-1} < V_{40} \leq 7.5 \text{ ms}^{-1})$, weak winds oppose current direction

Events: K(9 Apr 82), R(27 Apr 82), T(3 May 84)
Q(24 Feb 79), I(23 Jan 82)

Mode 3. Into Chukchi Sea (ocean current and wind influence as major forces)

- a. $> 20 \text{ km (day)}^{-1}$, $(V_{40} \leq -7.5 \text{ ms}^{-1})$

Events: G(8 Apr 82), Θ (6 Feb 82), Π (4 Feb 82)
 ω (24 Feb 82)

- b. no cases $< 20 \text{ km (day)}^{-1}$ for $V_{40} \leq -7.5 \text{ ms}^{-1}$

Mode 4. First immobilization mode (no movement through Strait)

- a. $(7.5 \text{ ms}^{-1} < V_{40} \leq 11.5 \text{ ms}^{-1})$, wind and water stresses in balance

Events: J(23,24 Mar 82), S(2 May 77), H(30 Mar 82)
L(20,21 Apr 81), O(11 Apr 78), P(2 Apr 78)

FORCE BALANCE \equiv J,S,H,L,O,P

CURRENT REVERSALS \equiv Ψ (ICE COVER)

20 KM/DAY INTO CHUKCHI \equiv A-G, θ , ω , π

20 KM/DAY INTO BERING \equiv Y,Z, γ , λ , Δ , ϕ , Ψ

INTO CHUKCHI \equiv K,R,T,Q,I

INTO BERING \equiv U,X,N,M,V,W

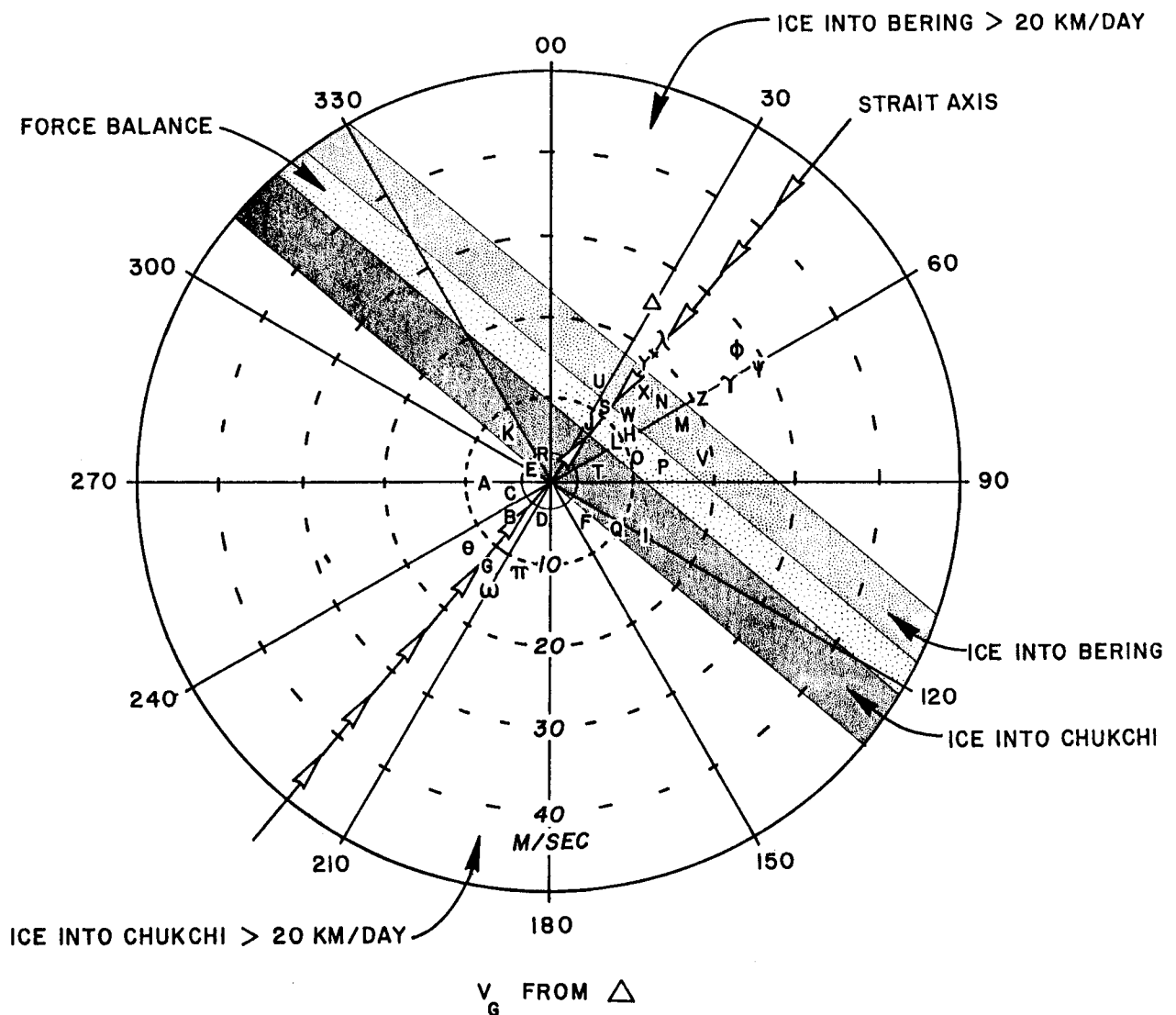


Fig. 8. The Bering Strait sea ice movement prediction nomogram with Greek and Latin letters representing sample MAPN computed \bar{V}_G 's used in its construction (see Table 2). The Strait axis is 40° from the north and has ice movement arrows meeting in the Force Balance Zone. The center solid circle is the $\leq 3 \text{ ms}^{-1}$ wind speed zone and it represents direction uncertainties $>15^\circ$.

conditions, if persisting for five days, would represent a total sea ice injection into the Bering Sea approximately equal to double the area of St. Lawrence Island (Fig. 1).

Included in these zone conditions were three cases (December 11, 20, and 27, 1976) during total ice cover when the ocean current at 10 m from the bottom switched from north to south in the Bering Strait (Coachman and Aagaard, 1981). Ψ (Fig. 8) represent the average MAPN computed V_G during these three cases (29 ms^{-1} from 61°). The 27 December 1976 event was the only one with clear satellite imagery. It showed net southward ice movement through the Strait of 25 km.

Mode 2 (Table 2) includes two zones of northward sea ice movement into the Chukchi Sea and represents an ocean current dominated mode with only minor wind influence. The ICE INTO CHUKCHI $> 20 \text{ km}(\text{day})^{-1}$ ZONE (Fig. 8), for $-7.5 \text{ ms}^{-1} < V_{40} \leq 0 \text{ ms}^{-1}$, exists due to a pre-existing northward flowing ocean current. This current (see Section 4c) appears to be a combination of residual contributions from the Bering Sea tide and density fields (Liu and Leendertse, 1982) and a semi-permanent downward sea level slope from the Bering toward the Chukchi (Coachman and Aagaard, 1981). This also corresponds to the relaxed wind field case (Fig. 3, top) of Hufford and Scheidt (1984) that results in northward ice motion adjacent to Norton Sound (Fig. 3, bottom). Sea ice injections into the Chukchi Sea equal to double the area of St. Lawrence Island (Fig. 1) will occur in five days. The ICE INTO CHUKCHI ZONE (Fig. 8) with $0 \text{ ms}^{-1} < V_{40} \leq 7.5 \text{ ms}^{-1}$ has a weak wind regime that opposes the northward flowing ocean current reducing the net sea ice movement to $< 20 \text{ km}(\text{day})^{-1}$.

Mode 3 does not occur as frequently as the previous two. It (Table 2) includes only one zone of northward sea ice movement into the Chukchi Sea

(Fig. 8) and represents a mode under the combined influence of both the wind and ocean current. Mode 3 is always within the ICE INTO CHUKCHI > 20 km(day)⁻¹ ZONE (Fig. 8) since the wind and water stress are in the same direction. However, Mode 3 has sometimes produced less net movement than the ~ 0 wind push cases in Mode 2. The Mode 2 case represents a localized Strait area ocean current push on the sea ice canopy from below. The Mode 3 case is a combination of the localized ocean current push and a large area wind stress pushing the entire sea ice canopy in the northern Bering Sea. This indicates that opposing internal and boundary stresses within the ice may play a larger role in the Mode 3 case.

Mode 4 is one of 0 net ice movement, usually lasting less than one week, and it includes the Force Balance Zone with $7.5 \text{ ms}^{-1} < V_{40} \leq 11.5 \text{ ms}^{-1}$. The primary force balance in the Strait area is between the wind stress pushing ice south and the water stress pushing ice north. Again, internal ice stresses and shore-fast ice boundary effects must play a role, but they are beyond the scope of this study. A check on the relative magnitudes of the opposing surface wind stress (τ_a) and water stress (τ_w) can be made as follows using values typical of the Strait conditions:

$$\tau_a = \rho_a C_a (u_a \cdot r_a)^2 \quad (3)$$

$$\tau_w = \rho_w C_w U_w^2 \quad (4)$$

where

- $\rho_a \equiv$ density of dry air at $-20^\circ\text{C} \sim 1.4 \text{ kgm}^{-3}$
- $C_a \equiv$ 10 m drag coefficient for air/water in the Bering Sea area $\sim 3 \times 10^{-3}$ (Walter et al., 1984)
- $U_a \equiv$ average wind speed in the Force Balance Zone $\sim 10 \text{ ms}^{-1}$
- $r_a \equiv$ ratio of surface wind speed (10 m) to the calculated geostrophic wind $\sim .6 \text{ ms}^{-1}$ (Albright, 1980) for Arctic

conditions. Note: Albright used a high resolution surface pressure grid and multiyear data base to derive his r_a .

$$\rho_w \equiv \text{density of water at } 0^\circ\text{C} \sim 1 \times 10^3 \text{ kgm}^{-3}$$

$$C_w \equiv 2 \text{ m drag coefficient for ice/water in the Bering Sea area} \\ \sim 16 \times 10^{-3} \text{ (Pease and Overland, 1984)}$$

$$u_w \equiv \text{typical current speed due to residual contributions from} \\ \text{the tide and density distribution in the Bering Strait} \\ \text{area} \sim .1 \text{ ms}^{-1} \text{ (Liu and Leendertse, 1982)}$$

comparing (3) and (4) after inserting the above values:

$$\tau_a \equiv 1.4 \times 3 \times 10^{-3} \times (10 \times .6)^2 = .15 \text{ N}_m^{-2}$$

$$\tau_w \equiv 1 \times 10^3 \times 16 \times 10^{-3} (.1)^2 = .16 \text{ N}_m^{-2}$$

These values are quite comparable for the opposing stresses and add credibility to the nomogram design.

e. Using the nomogram

The users of this nomogram would follow a simple procedure provided that they have access to weather data transmissions similar to that of NMC. Simultaneous surface pressure and temperature data from Uelen, Provideniya, and Nome (Fig. 1) for 00 and 1200 GMT should be available to the user less than three hours after recording at the respective stations. These data (P_N , P_U , P_P) can be input into the system of equations (2) in Section 3b to solve for ∇p . Air density (ρ) can be approximated using an average temperature from the three stations and the equation of state for dry air, $\rho = P(RT)^{-1}$. P is the standard sea level atmospheric pressure (1013.3 mb), R is the gas constant and T is the absolute temperature. The solution for ∇p , ρ and ultimately V (V_G in our case) can be obtained from (1) using any programmable hand calculator. The V_G for 00 and 1200 GMT are combined to obtain an

average velocity (\bar{V}_G). Once \bar{V}_G is known, the two necessary independent variables, speed (radius vector) and direction (vectorial angle), can be plotted on polar coordinate graph paper (for best resolution) with the nomograms five wind speed zones and V_{40} axis superimposed. For example, using data from Fig. 6, $P_N = 999.4$ mb, $P_P = 1008.0$ mb, $P_U = 1011.3$ mb, and an average temperature of -5°C (not shown in Fig. 6), $V_G = 23 \text{ ms}^{-1}$ from 56.8° . Plotting this value on Fig. 9 (X, bottom) and finding the V_{40} component by drawing a perpendicular from the V_{40} axis to X shows that the nomogram predicts net ice movement $> 20 \text{ km (day)}^{-1}$ to the south. The actual net ice movement was 50 km south.

f. Testing the nomogram technique

(1) NOAA satellite imagery

Fig. 9 (bottom) represents the nomogram base chart as constructed from data in Fig. 8. In this case, a time period having 23 consecutive days (April 6-28, 1982) free of major undercast was chosen to test the accuracy of the MAPN and nomogram predictions. The numbers 6-28 are April dates and represent the positions of the 00 and 1200 GMT mean V_G 's on those days. If the wind direction changes by more than 90° in 12 h, and/or the change would reverse the direction of ice motion, no prediction would be made. If any of the three network stations failed to report at either the 000 or 1200 GMT time periods, then the closest available simultaneous time period was used for the average V_G . Fig. 9 (top) shows the net sea ice direction and movement in km for the corresponding days. Remembering that the error bounds on the imagery were ± 5 km and the V_G 's were $\pm 1.4 \text{ ms}^{-1}$, the nomogram technique failed in only three cases.

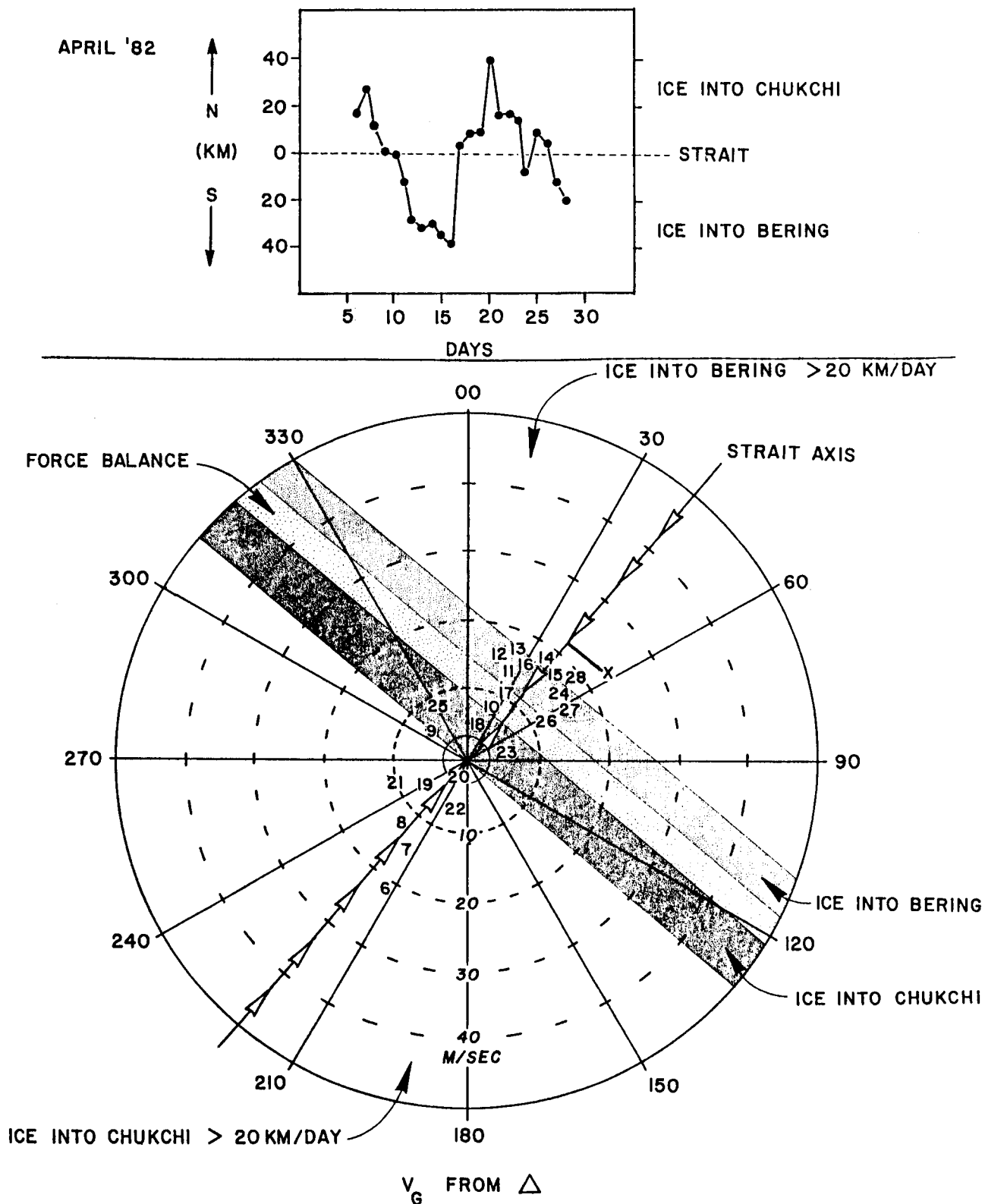


Fig. 9. Ice displacement (top) compared to MAPN V_G 's for 6-28 April 1982 plotted with corresponding day numbers on the sea ice movement prediction nomogram (bottom). The number positions represent wind velocity vectors whose V_{40} components define the daily predicted ice movement zone. X is a sample V_G calculated from surface pressure data in Fig. 6. Drawing a perpendicular line from X to the Strait axis results in a $V_{40} = 22 \text{ ms}^{-1}$. This is the Ice Into Bering $> 20 \text{ km (day)}^{-1}$ Zone.

The first case was April 8, 1982 where > 20 km of northward movement was predicted but only 8 km measured. Possibly the unusually long string of previous days (17) with both recorded and predicted (by techniques from this study) northward sea ice movement resulted in minimal space for new ice advected into the Chukchi Sea.

The second case was April 12, 1982 where a V_G of 13.6 ms^{-1} from 22.5° produced 31 km of actual ice movement to the south instead of < 20 km south predicted by the nomogram. Here the wind direction was 180° from the last major northward push (April 8, 1982) and only the second day of consistent V_G 's from the northeast. There was evidently ample room for sea ice advection south through the Strait from the Chukchi Sea without need for additional deformation. It must be noted that these observed tendencies for diminished sea ice motion after 17 consecutive day of northward push (case 1) and enhanced sea ice motion after 180° wind direction reversals (case 2) agree with the observations of Agerton and Kreider (1979). Their results for the Beaufort Sea have shown that the conditions for major sea ice movement are a wind speed threshold of 13 ms^{-1} and alternation of stress application direction by 180° .

The third case on April 19, 1982 had 10 km of net northward sea ice movement shown on the satellite imagery. The nomogram predicted movement >20 km to the north. There is no explanation for this discrepancy, however, the motion on the next day (April 20, 1982) was unusually large to the north, indicating that some compensating mechanism may be at work.

In summary, there were three bad predictions out of 23 or 87% correct. None of the "bad" predictions were off on the direction of ice movement, only the magnitude. The nomogram can be overlaid on polar coordinate graph paper and MAPN computed V_G 's plotted very simply. The perpendicular to the V_{40} axis should give the predicted net sea ice movement.

(2) Buoy drift data (description from Reynolds and Pease, 1984)

Data buoys implanted on ice floes in the winter of 1982 were tracked by satellite through use of a position transponder called an ARGOS Data Acquisition Platform (ADAP), Model 901. These were made by Polar Research Laboratories in Santa Barbara, California. ARGOS is a cooperative project between Centre National d'Etudes Spatiales (CNES) of France, the U.S. National Aeronautics and Space Administration (NASA) and the National Oceanic and Atmospheric Administration (NOAA). The ARGOS receiving system is carried by NOAA polar orbiting satellites. Each ADAP platform position is received 8-12 times per day with an accuracy of 200 m in longitude and 100 m latitude. Table 3 presents the nomogram predictions versus various net buoy drift distances (Reynolds and Pease, 1984). The buoy locations chosen were between 1° south and $.5^{\circ}$ north of the Strait, because the MAPN grid is essentially south of the Strait proper (Fig. 1). The net movement of individual buoys on various ice floes is from a smaller data base and is not exactly the same as net ice movement taken from satellite photographs. However, future projects, using the high resolution all-weather capabilities of the buoys, might provide data for fine-tuning the nomogram technique. At least one buoy and sometimes three were in the Strait area at various times from 3 February to 3 April 1982. In Table 3, net buoy displacement (X) to the north (N) or south (S) can be compared to the nomogram predictions (NP) for the given MAPN computed average velocities (V_G). There was agreement in 33 out of 40 days for 82.5% correct predictions. One case, February 12, 1982, had V_G change from 256° , 13 ms^{-1} to 74° , 18 ms^{-1} in 12 hours which is a condition not included in the nomogram construction. On February 17, 18, and 27 and March 22 and 26, the predictions were off on net distance but not direction. The March 29 and 30 dates each had buoy movement (X) of 8 km north while the

TABLE 3

NET BUOY DISPLACEMENTS (X) VERSUS NOMOGRAM PREDICTIONS (NP)

Date (82)	Buoy #	X (km, N or S)	\bar{V}_G (direction)[(°from], speed [ms^{-1}])	NP(km)	Agreement
3 Feb	2324	39N	139, 11	> 20N	yes
4 Feb	2324	39N	195, 11	> 20N	yes
5 Feb	2324	12N	112, 17 (sea ice moved westward also)	< 20N	yes
6 Feb	2320,2323, 2324	44N (Ave.)	226, 16	> 20N	yes
7 Feb	2320,2323 2324	72N (Ave.)	213, 16	> 20N	yes
8 Feb	2320,2323	66N (Ave.)	231, 9	> 20N	yes
9 Feb	2325	16N	320, 4	< 20N	yes
10 Feb	2325	10N	057, 7	< 20N	yes
11 Feb	2325	22N	011, 3 *(in 3 ms^{-1} zone consider ~ 0)	> 20N	yes*
12 Feb	2325	36N	(256, 13 to 74, 18 in 12 hrs)	no prediction	-
13 Feb	2325	10S	075, 16	< 20S	yes
14 Feb	2325	65S	021, 17	> 20S	yes
15 Feb	2323,2325	74S (Ave.)	017, 17	> 20S	yes
16 Feb	2320,2324	77S (Ave.)	025, 18	> 20S	yes
17 Feb	2320,2324	45S (Ave.)	037, 13	< 20S	no
18 Feb	2324	44S	024, 13	< 20S	no
24 Feb	2320,2324	45N	205, 14	> 20N	yes
25 Feb	2320,2324	27N (Ave.)	195, 8	> 20N	yes
26 Feb	2320,2324	76N (Ave.)	193, 10	> 20N	yes
27 Feb	2324	12N	251, 6	> 20N	no

TABLE 3. (continued)

Date (82)	Buoy #	X (km, N or S)	\bar{V}_G (direction) [(° from], speed [ms^{-1}])	NP(km)	Agreement
5 Mar	2325	36N	152, 11	> 20N	yes
6 Mar	2325	45N	125, 18	> 20N	yes
7 Mar	2325	45N	140, 15	> 20N	yes
8 Mar	2325	78N	137, 24	> 20N	yes
9 Mar	2325	65N	168, 13	> 20N	yes
19 Mar	2325	24S	057, 23	> 20S	yes
20 Mar	2325	51S	053, 29	> 20S	yes
21 Mar	2325	36S	062, 23	> 20S	yes
22 Mar	2325	8S	045, 21 *(P increased ~ 8 mb in 12 hrs at all 3 stations)	> 20S	no*
23 Mar	2325	5N	339, 4 *(sea ice moved eastward also)	< 20N	yes*
24 Mar	2325	~3N	002, 8 *(mainly east motion)	force balance	yes*
25 Mar	2325	~3N	039, 8 *(some east motion)	force balance	yes*
26 Mar	2325	11N	135, 10 *(close to error bounds of MAPN)	> 20N	no*
27 Mar	2325	23N	133, 13	> 20N	yes
28 Mar	2325	22N	123, 5	> 20N	yes
29 Mar	2325	8N	049, 10 *(P increased ~ 5 mb in 12 hrs at all stations)	force balance	no*
30 Mar	2325	8N	036, 9	force balance	no
31 Mar	2325	~2N	062, 6	< 20N	yes
1 Apr	2325	7N	008, 6	< 20N	yes
2 Apr	2325	47N	163, 9	> 20N	yes
3 April	2325	36N	216, 16	> 20N	yes

nomogram predicted (NP) a force balance or 0 motion. The March 26 date showed X equal to 11 km north while NP was > 20 km north. In this last case, errors in the MAPN (Section 3) could have made the prediction incorrect.

The above mentioned cases on March 22 and 29, 1982 were probably not in geostrophic balance (1). Both showed the pressure field changing rapidly during the 00 to 1200 GMT time period at stations in the MAPN. Therefore, an additional wind velocity component proportional to the barometric tendencies directed from high to low tendency isopleths (isallobars) existed. The mathematical expression (5) for the wind component due to a changing pressure distribution, isallobaric component (V_I), was derived in Brunt (1941):

$$V_I = \frac{-\nabla \dot{\rho}}{f^2 \rho} \quad (5)$$

where all terms are defined as in (1) and ($\dot{\cdot}$) represents the partial derivative with respect to time. Using (5) the March 22, 1982, MAPN V_G (see Table 3) would have neglected an opposing V_I of $\sim 2 \text{ ms}^{-1}$ from 145° . The March 29, 1982 MAPN V_G (see Table 3) would have an opposing V_I of $\sim 1.5 \text{ ms}^{-1}$ from 227° .

The same days also had maps showing isobars with the radius of curvature less than 300 km (see Kozo 1982). This type of wind flow, called gradient flow, requires that centrifugal force be added to the terms in (1) for a force balance. The March 22 and 29 dates were instances of cyclonic flow making V_G an overestimate of the true free stream wind velocity (V_T). The expression (6) for V_T is (Holton, 1973):

$$\frac{V_T^2}{R} + fV_T - fV_G = 0 \quad (6)$$

where $R \equiv$ radius of curvature of the isobars. Using (6), the March 22 V_T is 15.9 ms^{-1} from 45° which if used in the nomogram would give a correct prediction of < 20 km S (see Table 2). The March 19 V_T is 8.5 ms^{-1} from 049°

which combined with V_I above gives a correct prediction of < 20 km N within the MAPN error bounds.

The present MAPN does not account for isallobaric effects or gradient flow since a simple procedure for prediction was examined first. These extra refinements can be built into the wind velocity calculation and on application to the nomogram will increase the accuracy $\sim 5\%$.

g. Discovery of solid double sea ice arches

The double sea ice arch represents the longer duration second mode of ice immobilization mentioned in Section 4d. This mode is rare in the Bering Strait since only five cases have been seen on inspection of 11 years of sea ice satellite data. A satellite photograph (Fig. 10) taken May 5, 1980 shows the characteristic solid double ice arch in the Strait using the tip of the Chukchi Peninsula (Cape Dezhneva), the Diomed Islands and the Seward Peninsula tip (Cape Wales) as anchor points. Norton Sound is totally free of ice (see Fig. 2 for possible mechanism of ice removal) except for shore-fast sea ice on the southern side. Also, there is a large expanse of open water south of the Bering Strait arches and south of St. Lawrence Island. Since the image was taken 21 days after the arches formed, it appears that it was not cold enough for new ice formation and the presence of arches prevented resupply by old ice advection south into the Bering. These arches are not the arched fractures seen in sea ice during failure modes (Sodhi, 1977; Reimer *et al.*, 1979), but evidently represent strong impediments to sea ice movement to the south. As evidence of the lack of fractures in the ice canopy during the solid arch phase, the above (April 14 to May 10, 1980) period represented a halt in Bowhead whale migration through the Strait (Hufford, 1984; National Weather Service, Anchorage, pers. comm.).

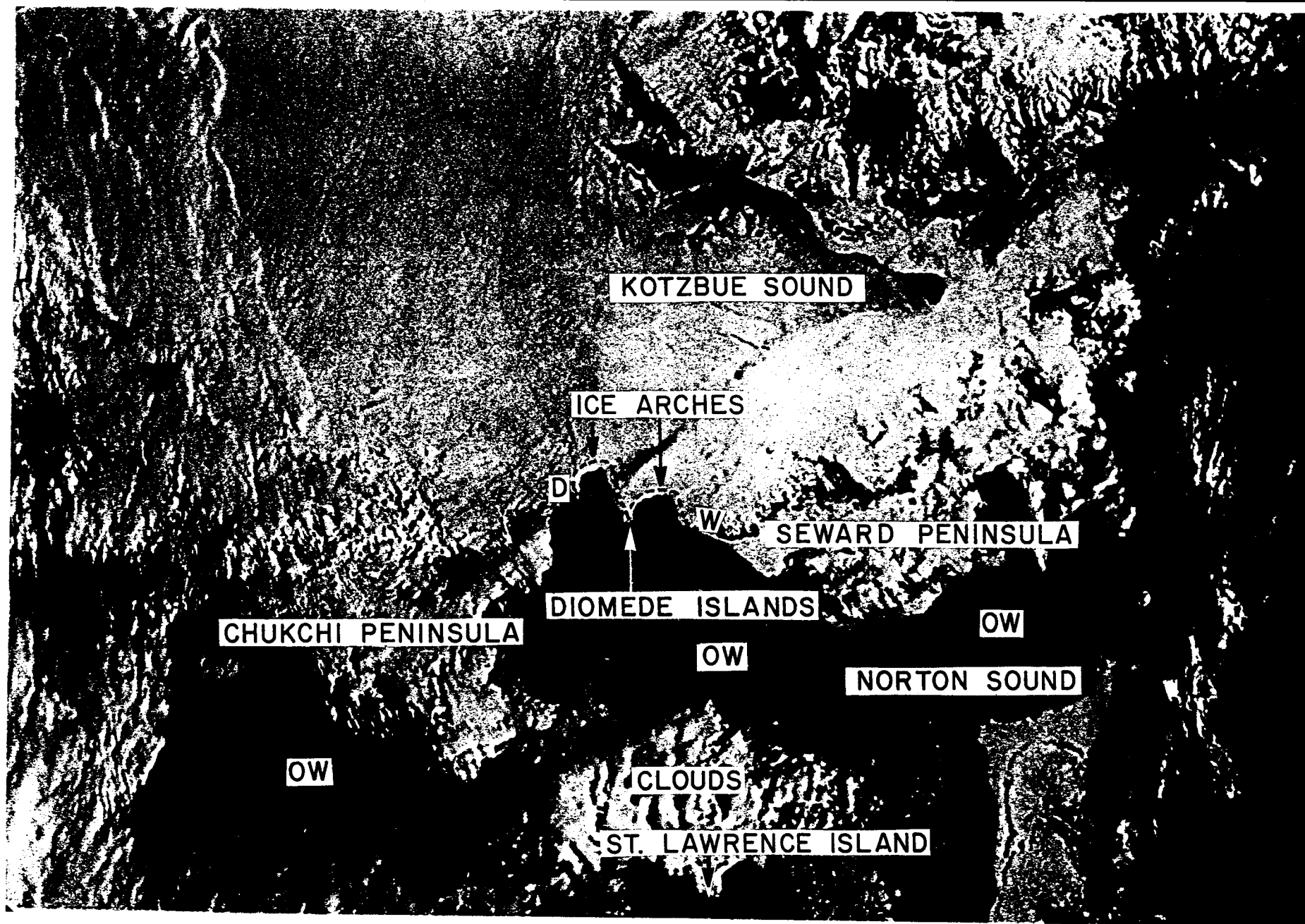


Fig. 10. A photograph made from a satellite image taken May 5, 1980 showing the characteristic solid double ice arch in the Bering Strait using the tip of the Chukchi Peninsula (D), the Diomedede Islands and the Seward Peninsula (W) tip as anchor points. There is a large expanse of open water (OW) south of the Strait, south of the Chukchi Peninsula and in Norton Sound.

The double arches were discovered indirectly through failure of the nomogram prediction system. In all double arch cases, the nomogram with \bar{V}_G from the MAPN predicted $> 20 \text{ km (day)}^{-1}$ of net ice movement into the Bering for at least 50% of the arch period. In addition, the $> 20 \text{ mb}$ pressure difference ice breakout criterion (Reimer et al., 1979) from Cape Schmidt to Nome (Fig. 1, Section 1) was exceeded at some time during all the double arch periods. This criterion represents a V_{40} of 13.5 ms^{-1} for an air density of 1.4 kg m^{-3} which would produce a $< 20 \text{ km (day)}^{-1}$ sea ice movement south through the Strait according to the nomogram. Fig. 11 shows sample MAPN V_G 's from designated periods such as April 14-May 10, 1980, February 26-March 8, 1984, and March 22-April 21, 1984 plotted on the nomogram. There were several cases with $V_{40} \sim 26 \text{ ms}^{-1}$ and no ice movement at all through the Strait, though movement could be seen above and below.

The theory predicting the limiting spans for arching of granular material flowing through a chute (Gardner, 1962; Richmond and Gardner 1962) as adapted by Sodhi (1977) will be used to show the reason for double arch existence despite the strong MAPN winds seen in Fig. 11. It seems possible that the double arches are a natural phenomenon resulting from a persistent period of strong wind velocities which most certainly would destroy a single arch across the entire Strait. Fig. 12 is a blow-up of the Strait area from Fig. 10 with the Chukchi and Seward Peninsulas and the Diomed Islands again shown as anchor points for the sea ice. The dashed curves differentiate the sea ice arches from the coastal boundaries and the dark areas are open water. The strength of a single arch can be estimated by comparing the arches in Fig. 12 to the inset drawing. The span width (2λ) of the arch from the Diomed Islands to Seward Peninsula is 41 km and from the Chukchi Peninsula to the Diomedes is 37 km. The width of the Diomed Island blockage zone (see

V_G FROM Δ FOR 0 MOVEMENT CASES WITH DOUBLE ARCHES

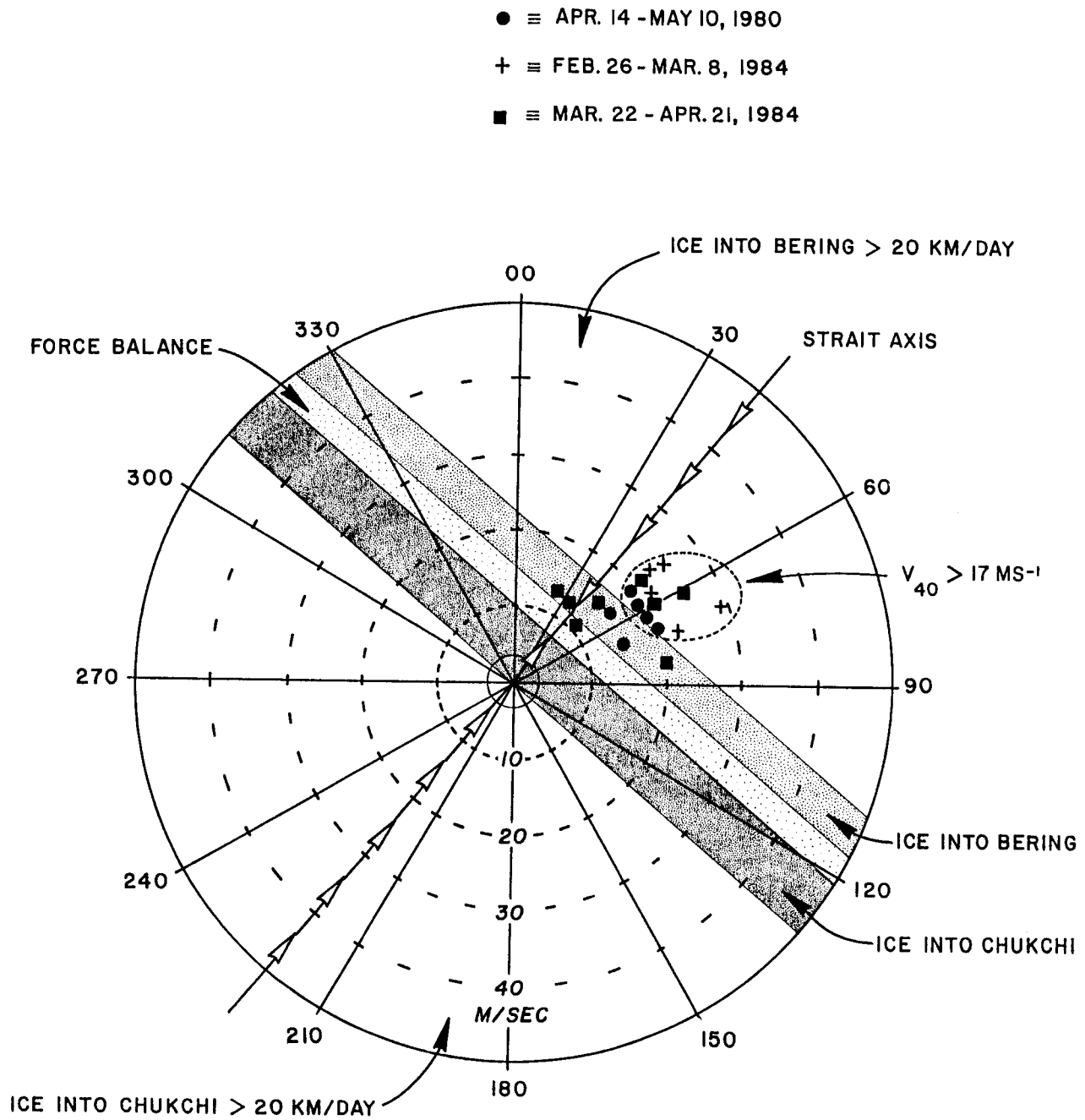


Fig. 11. Samples of MAPN V_G 's from designated double arch periods April 14-May 10, 1980, February 26-March 8, 1984, and March 22-April 21, 1984 plotted on the nomogram. There are several cases (enclosed by dashed oval) with $V_{40} \geq 17 \text{ ms}^{-1}$ indicating a predicted ice movement into the Bering Sea of greater than $20 \text{ km}(\text{day})^{-1}$.

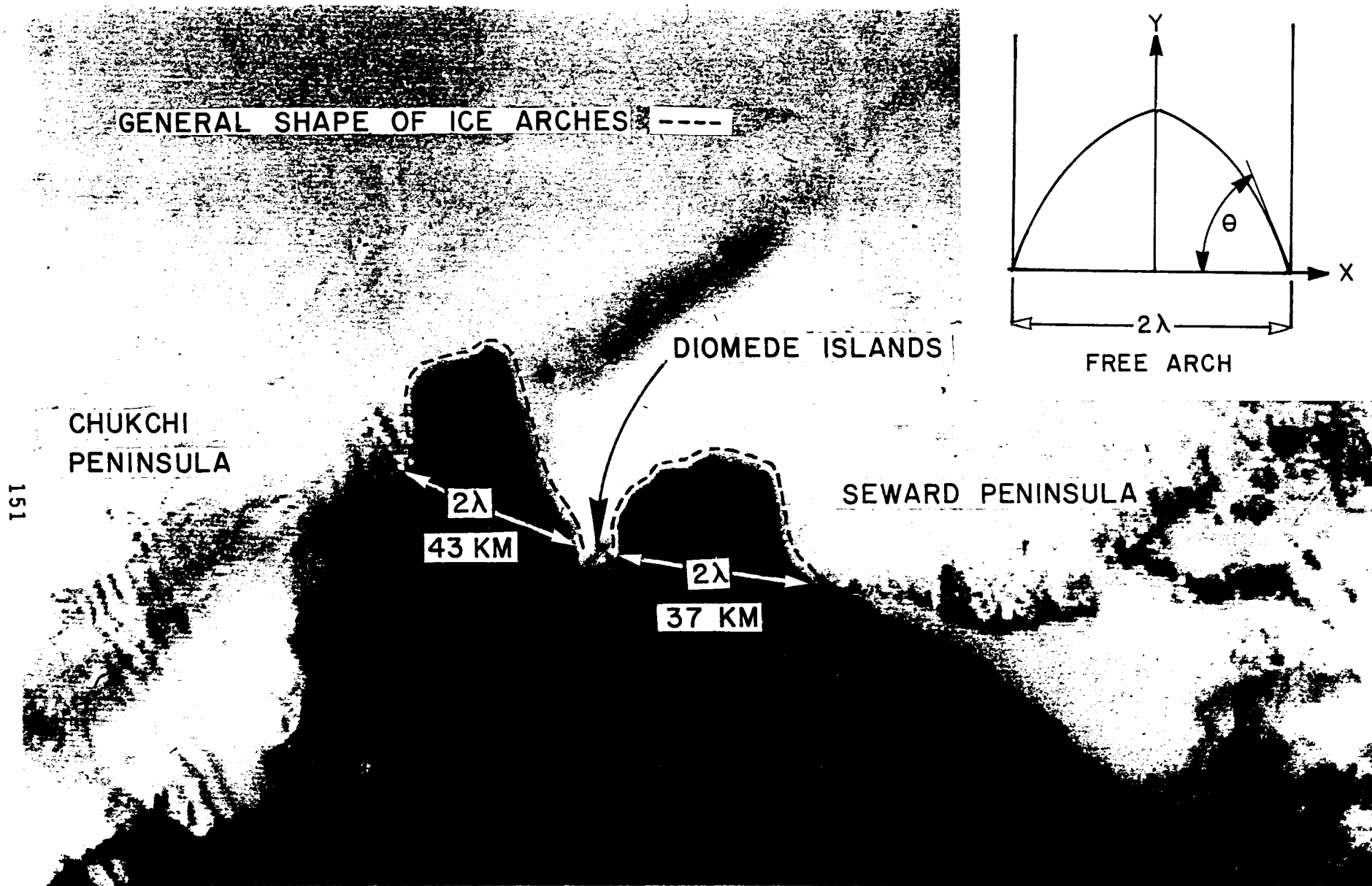


Fig. 12. An enlargement of the Strait area taken from the Fig. 10 photograph. The dashed curves show the actual sea ice arches to avoid confusion with land boundaries. The dark area is open water. The inset (top) is a sketch of an idealized free arch showing the span width (2λ) and the angle (θ) between the horizontal and tangent to the free surface.

Shapiro and Burns, 1975a) is 7 km. θ can be read with a compass from Fig. 12. The eastern arch (Diomed Islands-Seward Peninsula) has a $\theta \sim 80^\circ$ while the western arch (Diomed Islands-Chukchi Peninsula) is more irregular with an average θ of $\sim 80^\circ$ also. From (7)

$$\theta = \pi/4 + \phi/2 \quad (7)$$

where

$\phi \equiv$ angle of internal friction

$\theta \equiv$ angle between the horizontal and tangent to the arch profile

ϕ is estimated as 70° for both arches. Next (8) is used to solve for τ as defined by (9).

$$\lambda = \frac{c}{\tau} (1 + \sin \phi) \quad (8)$$

$$\tau = \rho CV^2 \quad (9)$$

Here:

$\lambda \equiv$ half span width (m)

$c \equiv$ cohesive strength (Nm^{-1})

$\tau \equiv$ net stress per unit area (Nm^{-2})

(wind and water stress combined)

$\rho \equiv$ mass density of medium (kg m^{-3})

$C \equiv$ drag coefficient (unitless)

$V \equiv$ wind velocity (ms^{-1})

Cohesive strength (c) for Amundsen Channel (Beaufort Sea, June) sea ice in a solid arch was estimated from (8) and (9) at failure to be 1993 nm^{-1} (Sodhi, 1977). The net stress (τ) applied to this arch (0 water stress assumed) was calculated using a typical 10 m air-ice drag coefficient of 1×10^{-3} for C and local winds for V . Recent Bering Sea work by Walter et al.

(1984) shows the drag coefficient to be 3×10^{-3} or three times the Sodhi (1977) estimate. Using this newer value for C would give $c = 5979 \text{ Nm}^{-1}$ as the cohesive strength of sea ice at failure. Given this c, taking $\phi = 70^\circ$, and $\lambda \sim 20 \times 10^3 \text{ m}$ (double arches) and substituting into (8), $\tau \text{ (net)} = .58 \text{ Nm}^{-2}$.

Remembering that water stress generally opposes wind stress from the north, τ_w is defined by (3) in Section 4d and estimated to be $-.16 \text{ Nm}^2$. The net stress τ , as seen in (10), will allow calculation of air stress τ_a (defined by [4], Section 4d).

$$\tau = \tau_a + \tau_w \quad (10)$$

Therefore $\tau_a = (.58) - (-.16) = .74 \text{ Nm}^{-2}$.

Hence from (3)

$$U_a^2 = \frac{\tau_a}{\rho_a C_a r_a^2} = \frac{.74}{1.3 \times 3 \times 10^{-3} \times (.6)^2}$$

or $U_a = 23 \text{ ms}^{-1} = V_{40}$ on nomogram axis.

This geostrophic wind corresponds to a surface wind of 13.8 ms^{-1} . Surface winds of this magnitude from November through May occur less than 10% of the time (Brower et al., 1977) at Tin City (near Cape Wales, Fig. 1) which is close to the Strait. The estimated V_{40} value of 23 ms^{-1} is similar to the maximum V_{40} seen on Fig. 11 which is approximately 26 ms^{-1} . The cohesive strength estimate used here could have been slightly larger since no evidence of arch breakup during these winds existed. The actual way that the arches are finally destroyed is a relaxation of the northerly winds and a switch to pure water stress or wind and water stress combined from the south. It should be noted that using the half span length for a single arch across the entire Strait ($\sim 42.5 \text{ km}$) in (8) with all other parameters the same yields $\tau = .27$

Insertion into (10) gives a $V_{40} = 17.5 \text{ ms}^{-1}$ which would be exceeded by 50% of the values shown in Fig. 11, thereby leading to arch failure.

5. Summary and conclusions

The combination of MAPN calculated V_G 's and the polar coordinate nomogram provides an all weather sea ice movement nowcasting capability for the Bering Strait with an average accuracy of 85%. The MAPN improvement over NMC surface pressure analyses and pattern recognition techniques has been demonstrated. This study, though meteorologically oriented, also has shed further light on both sea ice and oceanographic phenomena. The ocean currents, in particular, in the Strait area are crucial to the prediction scheme.

a. Sea ice movement modes

Three modes of ice movement were found. The first is a southward movement into the Bering Sea requiring a $V_{40} \geq 12 \text{ ms}^{-1}$. The second mode is movement into the Chukchi Sea during weak synoptic winds, driven by a north flowing ocean current made up of tidal and baroclinic residuals. The third mode is northward ice movement under the combined influence of winds from the southwest and a pre-existing north flowing ocean current.

b. Sea ice immobilization modes

There were two modes of ice immobilization found in the Strait. The first mode is an apparent balance between wind stress from the north and a water stress provided by a current from the south. Internal ice stresses and fast-ice boundary orientation must play a role, but they are not covered in

this study. The 0 net movement is short term, usually lasting less than one week. The second mode was discovered only five times in 11 years. In each case, the polar coordinate nomogram predicted large ice movement south through the Strait when, in fact, there was none. Double solid sea ice arches made possible by the Diomed Islands anchoring the middle column of the arches were seen as the culprits. A theoretical calculation of the strength of single arches across the entire Bering Strait showed fracturing at the MAPN generated V_G 's. However, the same calculation on double arches showed the ability to withstand the V_G 's ($V_{40} \sim 26 \text{ ms}^{-1}$) generated during the arch periods. This longer period immobilization mode (up to three weeks) can hinder spring whale migration into the Chukchi and aid in opening up the region below the Strait as well as Norton Sound.

c. Driving force behind the north flowing current in the Strait

The general higher sea level in the Bering over that of the Arctic Ocean and the compensatory circulations caused by local sea level differences after northeasterly winds can create northward flowing ocean currents through the Bering Strait without apparent local wind pushing. However, through the course of this study, several northward ice flow movement events were seen without apparent wind forcing or large scale atmospheric pressure fields conducive to raising the sea level in the Bering over that of the Arctic Ocean (Chukchi). Also, northward ice movement continued three days beyond relaxation of strong northeasterly winds, precluding compensatory circulations due to local sea level differences. Work by investigators mentioned above, plus evidence presented, points to residual northward transport from the tide and ocean density fields.

d. Recommendations for future work

The MAPN-nomogram technique can be improved in several respects if a need arises. Bad prediction can often be traced to two major cases where a geostrophic balance does not exist. One case is under accelerating conditions when pressure is changing rapidly requiring an isallobaric component of the wind. Another case is when strong curvature of the isobars exists (radius of curvature less than 300 km), implying that a gradient wind balance is needed. The nomogram itself can be finer tuned if more data of the type collected by Reynolds and Pease (1984) can be matched to satellite information. This data might prove very useful to determine further differences in northward ice movement driven by a wind and current push versus movement driven by a current alone. The MAPN accuracy can be improved by a cooperative visitation program involving the Russian sites in the network. A barometric standard could be used to calibrate all three sites to arrive at more precise V_p values from which V_G is calculated.

Acknowledgments. The investigator would like to credit the extensive work by Dr. William J. Stringer and Ms. Lenora J. Wattum of the Geophysical Institute at the University of Alaska, without whose efforts this report would not be possible. This project was funded by the Minerals Management Service, U. S. Department of the Interior, through interagency agreement with the National Oceanic and Atmospheric Administration, U. S. Department of Commerce, as part of the Outer Continental Shelf Environmental Assessment Program.

REFERENCES

- Agerton, D. J. and J. R. Kreider, 1979: Correlation of storms and major ice movements in the nearshore Alaska Beaufort Sea. Fifth International Conference on Port and Ocean Engineering under Arctic Conditions. Norwegian Institute of Technology, 1,177-189.
- Albright, M., 1980: Geostrophic wind calculations for AIDJEX, in A Symposium on Sea Ice Processes and Models. Proc. International Commission on Snow and Ice/Arctic Ice Dynamics Joint Experiment (ed. by Robert S. Pritchard), University of Washington Press, Seattle, 402-409.
- Brower, W. A., H. F. Diaz, A. S. Prechtel, H. W. Searby and J. L. Wise, 1977: Climatic Atlas of the Outer Continental Shelf Waters and Coastal Regions of Alaska. NOAA, NCC, EDS, Asheville, 409 pp.
- Browning, K. A., 1982: Preface in Nowcasting (ed. by K. A. Browning). Academic Press, New York, IX-XI.
- Brunt, D., 1941: Physical and Dynamical Meteorology. Cambridge University Press, London, 428 pp.
- Coachman, L. K. and K. Aagaard, 1981: Reevaluation of water transports in the vicinity of Bering Strait, Chapter 7 in The Eastern Bering Sea Shelf: Oceanography and Resources (ed. by D. W. Hood and J. A. Calder), University of Washington Press, Seattle, 95-110.
- Coachman, L. K., K. Aagaard and R. B. Tripp, 1975: Bering Strait: The Regional Physical Oceanography. University of Washington Press, Seattle and London, 172 pp.
- Dickey, W. W., 1961: A study of a topographic effect on wind in the arctic. J. Meteor., 18, 790-803.

- Drury, W. H., C. Ramsdell, J. B. French, Jr., 1981: Ecological studies in the Bering Strait region. Environmental assessment of the Alaska Continental shelf. NOAA/OCSEAP Final Rpt. Bio. Studies, 11,175-487.
- Gardner, G. C., 1962: Limiting conditions for flow of a cohesive granular material down an inclined plane (chute) or between parallel inclined walls (bin or channel). Chem. Eng. Sci., 17,107-1086.
- Holton, J. R., 1972: An Introduction to Dynamic Meteorology. Academic Press, New York, 319 pp.
- Hufford, G. and R. Scheidt, 1984: Interaction of Norton Sound Ice and Weather, Abs. in 1984 Arctic Science Conference (35th Alaskan Conference), Oct. 2-5, 1984, Anchorage, Alaska, sponsored by Amer. Ass. for Adv. of Sci.-Arctic Div., Amer. Met. Soc. and Arctic Inst. of North America, 109 pp.
- Kovacs, A. and D. S. Sodhi, 1981: Sea ice piling at Fairway Rock, Bering Strait, Alaska: Observations and theoretical analyses. Proc. Sixth Int. Conf. on Port and Ocean Eng. under Arctic Cond. POAC-81, Quebec, Canada, 2,985-999.
- Kozo, T. L., 1984: Mesoscale wind phenomena along the Alaska Beaufort Sea Coast, in The Alaska Beaufort Sea: Ecosystems and Environment (ed. by P. W. Barnes, D. M. Schell and E. Reimnitz). Academic Press, New York, pp. 23-45.
- , 1982: An observational study of sea breezes along the Alaska Beaufort Sea Coast: Part I. J. App. Meteor., 12, 891-905.
- , 1980: Mountain barrier baroclinity effects on surface winds along the Alaskan Arctic Coast. Geophysical Research Letters, 7,377-380.
- and W. B. Tucker, 1974: Sea ice bottomside features in the Denmark Strait. J. Geophys. Res., 79, 4505-4511.

- Liu, S. K. and J. J. Leenderste, 1984: Modeling the Alaskan coastal waters, in Three-dimensional Shelf Models (ed. by N. Heaps), Amer. Geophys Union, Washington, D. C., in press.
- Pease, C. H. and J. E. Overland, 1984: An atmospherically driven sea-ice drift model for the Bering Sea. Ann. Glaciol., 5, 111-113.
- Ray, V. M. and W. R. Dupre, 1981: The ice-dominated regimen of Norton Sound and adjacent areas of the Bering Sea. Chapter 16 in The Eastern Bering Sea Shelf: Oceanography and Resources (ed. by D. W. Hood and J. A. Calder). University of Washington Press, Seattle, pp. 263-178.
- Reimer, R. W., R. S. Pritchard and M. D. Coon, 1979: Beaufort and Chukchi Sea ice motion: Part 2. Onset of large scale Chukchi Sea ice breakout, Flow Res. Rpt. No. 133, Kent, Washington, 92 pp.
- Reynolds, M. and C. H. Pease, 1984: Drift characteristics of the northeastern Bering sea ice during 1982. NOAA Tech. Memo. ERL-PMEL-55, Seattle, Washington, 135 pp.
- Richmond, O. and G. C. Gardner, 1962: Limiting spans for arching of bulk material in vertical channels. Chem. Eng. Sci., 17, 1071-1078.
- Shapiro, L. H. and J. J. Burns, 1975a: Major late-winter features of ice in Northern Bering and Chukchi Seas as determined from satellite imagery. Geophysical Inst. Rpt. No UAG R-236, Sea Grant Rpt. No. 75-8, University of Alaska, Fairbanks, 14 pp.
- Shapiro, L. H. and J. J. Burns, 1975b: Satellite observations of sea ice movement in the Bering Strait region. In Climate of the Arctic, University of Alaska, Fairbanks, pp. 379-386.
- Sodhi, D. S., 1977: Ice arching and the drift of pack ice through restricted channels. Cold Regions Research and Engineering Laboratory, CRREL Rpt. 77-18, Hanover, New Hampshire, 11 pp.

Stringer, W. J. and G. L. Hufford, 1982: Interaction of Bering Sea and Norton Sound pack ice. Arctic and Alpine Res., 14,149-156.

Walter, B. A., J. E. Overland and R. O. Gilmer, 1984: Air-ice drag coefficients for first-year sea ice derived from aircraft measurements.

J. Geophys. Res., 89, 6525-6531.

WAVE HINDCAST STATISTICS FOR THE HOPE BASIN, NORTH CHUKCHI
AND SOUTH CHUKCHI AREAS

by

Thomas L. Kozo, Ph.D.

VANTUNA Research Group

Occidental College

Final Report
Outer Continental Shelf Environmental Assessment Program
Research Unit 519

1984

161

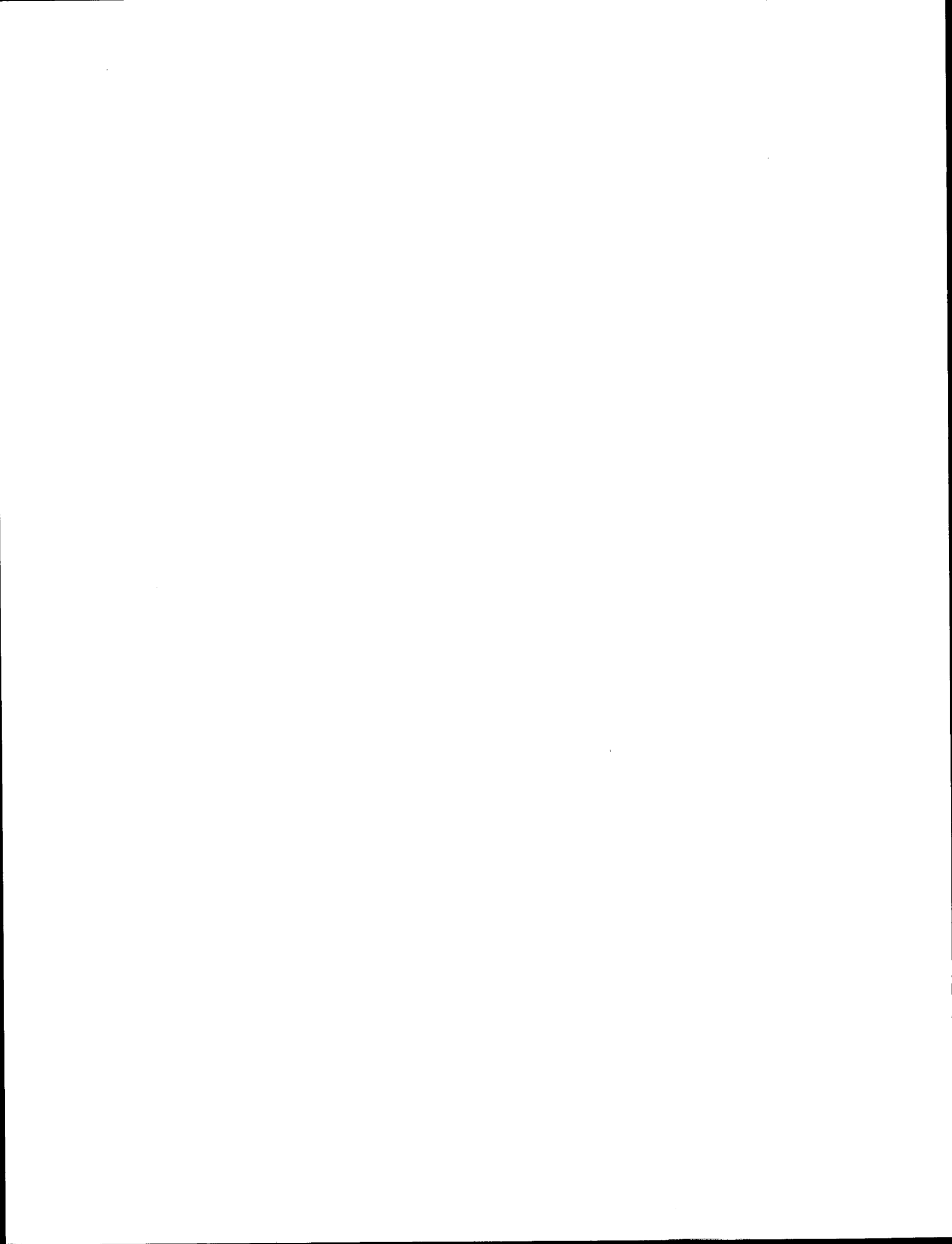
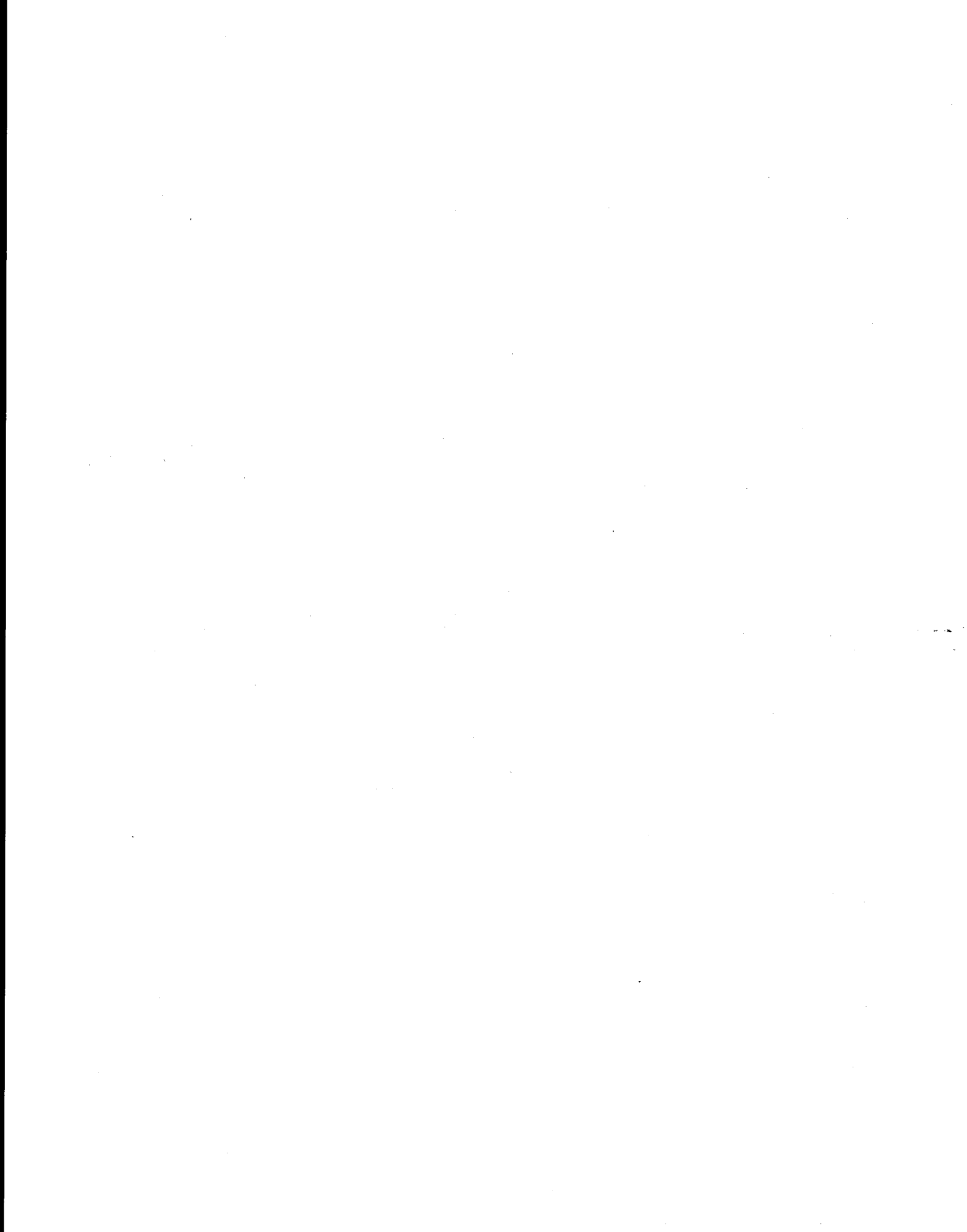


TABLE OF CONTENTS

LIST OF FIGURES.....	
LIST OF TABLES.....	
INTRODUCTION.....	
DEEP WATER WAVE HINDCAST THEORY.....	
WAVE BREAKING CRITERIA.....	
WAVE RUN-UP.....	
RESULTS AND CONCLUSIONS.....	
DEEP WATER WAVE STATISTICS.....	
Region C.....	
Region B.....	
Region A.....	
Five percent highest waves.....	
WAVE BREAKING STATISTICS.....	
Coastline 1.....	
Coastline 2.....	
Coastline 3.....	
Coastline 4.....	
Coastline 5.....	
SUMMARY.....	
FURTHER STUDY.....	
ACKNOWLEDGEMENTS.....	
REFERENCES.....	
FIGURES.....	
TABLES.....	



LIST OF FIGURES

- Figure 1. The three study regions A, B, and C (solid lines) and five coastlines (dashed lines) chosen for respective wave hindcast and breaking wave height analyses.....
- Figure 2a. The minimum sea ice extent (maximum fetch condition) in May (Stringer, 1984; Brower et al, 1977) relative to Regions A-C.....
- Figure 2b. There is typically no open water in Regions A-C in May for mean sea ice extent.....
- Figure 3a. The minimum sea ice extent (maximum fetch condition) in June (Stringer, 1984; Brower et al, 1977) relative to Regions A-C.....
- Figure 3b. The mean sea ice extent (average fetch condition) in June (Stringer, 1984; Brower et al, 1977) relative to Regions A-C.....
- Figure 4a. The minimum sea ice extent (maximum fetch condition) in July (Stringer, 1984; Brower et al, 1977) relative to Regions A-C.....
- Figure 4b. The mean sea ice extent (average fetch condition) in July (Stringer, 1984; Brower et al, 1977) relative to Regions A-C.....
- Figure 5a. The minimum sea ice extent (maximum fetch condition) in August (Stringer, 1984; Brower et al, 1977) relative to Regions A-C.....
- Figure 5b. The mean sea ice extent (average fetch condition) in August (Stringer, 1984; Brower et al, 1977) relative to Regions A-C.....
- Figure 6a. The minimum sea ice extent (maximum fetch condition) in September (Stringer, 1984; Brower et al, 1977) relative to Regions A-C.....
- Figure 6b. The mean sea ice extent (average fetch condition) in September (Stringer, 1984; Brower et al, 1977) relative to Regions A-C.....
- Figure 7a. The minimum sea ice extent (maximum fetch condition) in October (Stringer, 1984; Brower et al, 1977) relative to Regions A-C.....

Figure 7b. The mean sea ice extent (average fetch condition) in October (Stringer, 1984; Brower et al, 1977) relative to Regions A-C....

Figure 8a. The minimum sea ice extent (maximum fetch condition) in November (Stringer, 1984; Brower et al, 1977) relative to Regions A-C.....

Figure 8b. The mean sea ice extent (average fetch condition) in November (Stringer, 1984; Brower et al, 1977) relative to Regions A-C....

LIST OF TABLES

- Table 1a. The predicted frequency of significant wave heights (H_s) in meters for waves from eight specified directions in May. These data were derived from wind velocity histograms (Brower et al., 1977) compiled at stations near Region C for maximum fetch conditions.....
- Table 1b. The predicted frequency of peak wave periods (T_p) in seconds for waves coming from eight specified directions in May. These data were derived from wind velocity measurements (Brower et al., 1977) compiled at stations near Region C for maximum fetch conditions.....
- Table 2a. The predicted frequency of significant wave heights (H_s) in meters for waves from eight specified directions in June. These data were derived from wind velocity histograms (Brower et al., 1977) compiled at stations near Region C for maximum fetch conditions.....
- Table 2b. The predicted frequency of peak wave periods (T_p) in seconds for waves coming from eight specified directions in June. These data were derived from wind velocity measurements (Brower et al., 1977) compiled at stations near Region C for maximum fetch conditions.....
- Table 3a. The predicted frequency of significant wave heights (H_s) in meters for waves from eight specified directions in July. These data were derived from wind velocity histograms (Brower et al., 1977) compiled at stations near Region C for maximum fetch conditions.....
- Table 3b. The predicted frequency of peak wave periods (T_p) in seconds for waves coming from eight specified directions in July. These data were derived from wind velocity measurements (Brower et al., 1977) compiled at stations near Region C for maximum fetch conditions.....
- Table 4a. The predicted frequency of significant wave heights (H_s) in meters for waves from eight specified directions in August. These data were derived from wind velocity histograms (Brower et al., 1977) compiled at stations near Region C for maximum fetch conditions.....
- Table 4b. The predicted frequency of peak wave periods (T_p) in seconds for waves coming from eight specified directions in August. These data were derived from wind velocity measurements (Brower et al., 1977) compiled at stations near Region C for maximum fetch conditions.....

- Table 5a. The predicted frequency of significant wave heights (H_s) in meters for waves from eight specified directions in September. These data were derived from wind velocity histograms (Brower et al., 1977) compiled at stations near Region C for maximum fetch conditions.....
- Table 5b. The predicted frequency of peak wave periods (T_p) in seconds for waves coming from eight specified directions in September. These data were derived from wind velocity measurements (Brower et al., 1977) compiled at stations near Region C for maximum fetch conditions.....
- Table 6a. The predicted frequency of significant wave heights (H_s) in meters for waves from eight specified directions in October. These data were derived from wind velocity histograms (Brower et al., 1977) compiled at stations near Region C for maximum fetch conditions.....
- Table 6b. The predicted frequency of peak wave periods (T_p) in seconds for waves coming from eight specified directions in October. These data were derived from wind velocity measurements (Brower et al., 1977) compiled at stations near Region C for maximum fetch conditions.....
- Table 7a. The predicted frequency of significant wave heights (H_s) in meters for waves from eight specified directions in November. These data were derived from wind velocity histograms (Brower et al., 1977) compiled at stations near Region C for maximum fetch conditions.....
- Table 7b. The predicted frequency of peak wave periods (T_p) in seconds for waves coming from eight specified directions in November. These data were derived from wind velocity measurements (Brower et al., 1977) compiled at stations near Region C for maximum fetch conditions.....
- Table 8a. The predicted frequency of significant wave heights (H_s) in meters for waves from eight specified directions in June. These data were derived from wind velocity histograms (Brower et al., 1977) compiled at stations near Region C for mean fetch conditions.....
- Table 8b. The predicted frequency of peak wave periods (T_p) in seconds for waves coming from eight specified directions in June. These data were derived from wind velocity measurements (Brower et al., 1977) compiled at stations near Region C for mean fetch conditions.....
- Table 9a. The predicted frequency of significant wave heights (H_s) in meters for waves from eight specified directions in July. These data were derived from wind velocity histograms (Brower et al., 1977) compiled at stations near Region C for mean fetch conditions.....

- Table 9b. The predicted frequency of peak wave periods (T_p) in seconds for waves coming from eight specified directions in July. These data were derived from wind velocity measurements (Brower et al., 1977) compiled at stations near Region C for mean fetch conditions.....
- Table 10a. The predicted frequency of significant wave heights (H_s) in meters for waves from eight specified directions in August. These data were derived from wind velocity histograms (Brower et al., 1977) compiled at stations near Region C for mean fetch conditions.....
- Table 10b. The predicted frequency of peak wave periods (T_p) in seconds for waves coming from eight specified directions in August. These data were derived from wind velocity measurements (Brower et al., 1977) compiled at stations near Region C for mean fetch conditions.....
- Table 11a. The predicted frequency of significant wave heights (H_s) in meters for waves from eight specified directions in September. These data were derived from wind velocity histograms (Brower et al., 1977) compiled at stations near Region C for mean fetch conditions.....
- Table 11b. The predicted frequency of peak wave periods (T_p) in seconds for waves coming from eight specified directions in September. These data were derived from wind velocity measurements (Brower et al., 1977) compiled at stations near Region C for mean fetch conditions.....
- Table 12a. The predicted frequency of significant wave heights (H_s) in meters for waves from eight specified directions in October. These data were derived from wind velocity histograms (Brower et al., 1977) compiled at stations near Region C for mean fetch conditions.....
- Table 12b. The predicted frequency of peak wave periods (T_p) in seconds for waves coming from eight specified directions in October. These data were derived from wind velocity measurements (Brower et al., 1977) compiled at stations near Region C for mean fetch conditions.....
- Table 13a. The predicted frequency of significant wave heights (H_s) in meters for waves from eight specified directions in November. These data were derived from wind velocity histograms (Brower et al., 1977) compiled at stations near Region C for mean fetch conditions.....
- Table 13b. The predicted frequency of peak wave periods (T_p) in seconds for waves coming from eight specified directions in November. These data were derived from wind velocity measurements (Brower et al., 1977) compiled at stations near Region C for mean fetch conditions.....

- Table 14a. The predicted frequency of significant wave heights (Hs) in meters for waves from eight specified directions in June. These data were derived from wind velocity histograms (Brower et al., 1977) compiled at stations near Region B for maximum fetch conditions.....
- Table 14b. The predicted frequency of peak wave periods (Tp) in seconds for waves coming from eight specified directions in June. These data were derived from wind velocity measurements (Brower et al., 1977) compiled at stations near Region B for maximum fetch conditions.....
- Table 15a. The predicted frequency of significant wave heights (Hs) in meters for waves from eight specified directions in July. These data were derived from wind velocity histograms (Brower et al., 1977) compiled at stations near Region B for maximum fetch conditions.....
- Table 15b. The predicted frequency of peak wave periods (Tp) in seconds for waves coming from eight specified directions in July. These data were derived from wind velocity measurements (Brower et al., 1977) compiled at stations near Region B for maximum fetch conditions.....
- Table 16a. The predicted frequency of significant wave heights (Hs) in meters for waves from eight specified directions in August. These data were derived from wind velocity histograms (Brower et al., 1977) compiled at stations near Region B for maximum fetch conditions.....
- Table 16b. The predicted frequency of peak wave periods (Tp) in seconds for waves coming from eight specified directions in August. These data were derived from wind velocity measurements (Brower et al., 1977) compiled at stations near Region B for maximum fetch conditions.....
- Table 17a. The predicted frequency of significant wave heights (Hs) in meters for waves from eight specified directions in September. These data were derived from wind velocity histograms (Brower et al., 1977) compiled at stations near Region B for maximum fetch conditions.....
- Table 17b. The predicted frequency of peak wave periods (Tp) in seconds for waves coming from eight specified directions in September. These data were derived from wind velocity measurements (Brower et al., 1977) compiled at stations near Region B for maximum fetch conditions.....
- Table 18a. The predicted frequency of significant wave heights (Hs) in meters for waves from eight specified directions in October. These data were derived from wind velocity histograms (Brower et al., 1977) compiled at stations near Region B for maximum fetch conditions.....

- Table 18b. The predicted frequency of peak wave periods (Tp) in seconds for waves coming from eight specified directions in October. These data were derived from wind velocity measurements (Brower et al., 1977) compiled at stations near Region B for maximum fetch conditions.....
- Table 19a. The predicted frequency of significant wave heights (Hs) in meters for waves from eight specified directions in November. These data were derived from wind velocity histograms (Brower et al., 1977) compiled at stations near Region B for maximum fetch conditions.....
- Table 19b. The predicted frequency of peak wave periods (Tp) in seconds for waves coming from eight specified directions in November. These data were derived from wind velocity measurements (Brower et al., 1977) compiled at stations near Region B for maximum fetch conditions.....
- Table 20a. The predicted frequency of significant wave heights (Hs) in meters for waves from eight specified directions in July. These data were derived from wind velocity histograms (Brower et al., 1977) compiled at stations near Region B for mean fetch conditions.....
- Table 20b. The predicted frequency of peak wave periods (Tp) in seconds for waves coming from eight specified directions in July. These data were derived from wind velocity measurements (Brower et al., 1977) compiled at stations near Region B for mean fetch conditions.....
- Table 21a. The predicted frequency of significant wave heights (Hs) in meters for waves from eight specified directions in August. These data were derived from wind velocity histograms (Brower et al., 1977) compiled at stations near Region B for mean fetch conditions.....
- Table 21b. The predicted frequency of peak wave periods (Tp) in seconds for waves coming from eight specified directions in August. These data were derived from wind velocity measurements (Brower et al., 1977) compiled at stations near Region B for mean fetch conditions.....
- Table 22a. The predicted frequency of significant wave heights (Hs) in meters for waves from eight specified directions in September. These data were derived from wind velocity histograms (Brower et al., 1977) compiled at stations near Region B for mean fetch conditions.....
- Table 22b. The predicted frequency of peak wave periods (Tp) in seconds for waves coming from eight specified directions in September. These data were derived from wind velocity measurements (Brower et al., 1977) compiled at stations near Region B for mean fetch conditions.....

- Table 23a. The predicted frequency of significant wave heights (Hs) in meters for waves from eight specified directions in October. These data were derived from wind velocity histograms (Brower et al., 1977) compiled at stations near Region B for mean fetch conditions.....
- Table 23b. The predicted frequency of peak wave periods (Tp) in seconds for waves coming from eight specified directions in October. These data were derived from wind velocity measurements (Brower et al., 1977) compiled at stations near Region B for mean fetch conditions.....
- Table 24a. The predicted frequency of significant wave heights (Hs) in meters for waves from eight specified directions in July. These data were derived from wind velocity histograms (Brower et al., 1977) compiled at stations near Region A for maximum fetch conditions.....
- Table 24b. The predicted frequency of peak wave periods (Tp) in seconds for waves coming from eight specified directions in July. These data were derived from wind velocity measurements (Brower et al., 1977) compiled at stations near Region A for maximum fetch conditions.....
- Table 25a. The predicted frequency of significant wave heights (Hs) in meters for waves from eight specified directions in August. These data were derived from wind velocity histograms (Brower et al., 1977) compiled at stations near Region A for maximum fetch conditions.....
- Table 25b. The predicted frequency of peak wave periods (Tp) in seconds for waves coming from eight specified directions in August. These data were derived from wind velocity measurements (Brower et al., 1977) compiled at stations near Region A for maximum fetch conditions.....
- Table 26a. The predicted frequency of significant wave heights (Hs) in meters for waves from eight specified directions in September. These data were derived from wind velocity histograms (Brower et al., 1977) compiled at stations near Region A for maximum fetch conditions.....
- Table 26b. The predicted frequency of peak wave periods (Tp) in seconds for waves coming from eight specified directions in September. These data were derived from wind velocity measurements (Brower et al., 1977) compiled at stations near Region A for maximum fetch conditions.....
- Table 27a. The predicted frequency of significant wave heights (Hs) in meters for waves from eight specified directions in October. These data were derived from wind velocity histograms (Brower et al., 1977) compiled at stations near Region A for maximum fetch conditions.....

- Table 27b. The predicted frequency of peak wave periods (T_p) in seconds for waves coming from eight specified directions in October. These data were derived from wind velocity measurements (Brower et al., 1977) compiled at stations near Region A for maximum fetch conditions.....
- Table 28a. The predicted frequency of significant wave heights (H_s) in meters for waves from eight specified directions in November. These data were derived from wind velocity histograms (Brower et al., 1977) compiled at stations near Region A for maximum fetch conditions.....
- Table 28b. The predicted frequency of peak wave periods (T_p) in seconds for waves coming from eight specified directions in November. These data were derived from wind velocity measurements (Brower et al., 1977) compiled at stations near Region A for maximum fetch conditions.....
- Table 29a. The predicted frequency of significant wave heights (H_s) in meters for waves from eight specified directions in August. These data were derived from wind velocity histograms (Brower et al., 1977) compiled at stations near Region A for mean fetch conditions.....
- Table 29b. The predicted frequency of peak wave periods (T_p) in seconds for waves coming from eight specified directions in August. These data were derived from wind velocity measurements (Brower et al., 1977) compiled at stations near Region A for mean fetch conditions.....
- Table 30a. The predicted frequency of significant wave heights (H_s) in meters for waves from eight specified directions in September. These data were derived from wind velocity histograms (Brower et al., 1977) compiled at stations near Region A for mean fetch conditions.....
- Table 30b. The predicted frequency of peak wave periods (T_p) in seconds for waves coming from eight specified directions in September. These data were derived from wind velocity measurements (Brower et al., 1977) compiled at stations near Region A for mean fetch conditions.....
- Table 31a. The predicted frequency of significant wave heights (H_s) in meters for waves from eight specified directions in October. These data were derived from wind velocity histograms (Brower et al., 1977) compiled at stations near Region A for mean fetch conditions.....
- Table 31b. The predicted frequency of peak wave periods (T_p) in seconds for waves coming from eight specified directions in October. These data were derived from wind velocity measurements (Brower et al., 1977) compiled at stations near Region A for mean fetch conditions.....

- Table 32. The beach slope, appropriate region statistics (A, B, or C) and major wave directions contributing to the calculation of H, D and R.....
- Table 33a. Frequency table of breaking wave height (H), breaking water depth (D), and wave run-up (R) for coastline 1 in June under maximum fetch conditions.....
- Table 33b. Frequency table of breaking wave height (H), breaking water depth (D), and wave run-up (R) for coastline 1 in July under maximum fetch conditions.....
- Table 33c. Frequency table of breaking wave height (H), breaking water depth (D), and wave run-up (R) for coastline 1 in August under maximum fetch conditions.....
- Table 33d. Frequency table of breaking wave height (H), breaking water depth (D), and wave run-up (R) for coastline 1 in September under maximum fetch conditions.....
- Table 33e. Frequency table of breaking wave height (H), breaking water depth (D), and wave run-up (R) for coastline 1 in October under maximum fetch conditions.....
- Table 33f. Frequency table of breaking wave height (H), breaking water depth (D), and wave run-up (R) for coastline 1 in November under maximum fetch conditions.....
- Table 33g. Average of Tables 33(a-f) under maximum fetch conditions for Coastline 1.....
- Table 34a. Frequency table of breaking wave height (H), breaking water depth (D), and wave run-up (R) for coastline 1 in July under mean fetch conditions.....
- Table 34b. Frequency table of breaking wave height (H), breaking water depth (D), and wave run-up (R) for coastline 1 in August under mean fetch conditions.....
- Table 34c. Frequency table of breaking wave height (H), breaking water depth (D), and wave run-up (R) for coastline 1 in September under mean fetch conditions.....
- Table 34d. Frequency table of breaking wave height (H), breaking water depth (D), and wave run-up (R) for coastline 1 in October under mean fetch conditions.....
- Table 34e. Average of Tables 34(a-d) under mean fetch conditions for coastline 1.....
- Table 35a. Frequency table of breaking wave height (H), breaking water depth (D), and wave run-up (R) for coastline 2 in June under maximum fetch conditions.....

- Table 35b. Frequency table of breaking wave height (H), breaking water depth (D), and wave run-up (R) for coastline 2 in July under maximum fetch conditions.....
- Table 35c. Frequency table of breaking wave height (H), breaking water depth (D), and wave run-up (R) for coastline 2 in August under maximum fetch conditions.....
- Table 35d. Frequency table of breaking wave height (H), breaking water depth (D), and wave run-up (R) for coastline 2 in September under maximum fetch conditions.....
- Table 35e. Frequency table of breaking wave height (H), breaking water depth (D), and wave run-up (R) for coastline 2 in October under maximum fetch conditions.....
- Table 35f. Frequency table of breaking wave height (H), breaking water depth (D), and wave run-up (R) for coastline 2 in November under maximum fetch conditions.....
- Table 35g. Average of Tables 35(a-f) under maximum fetch conditions for coastline 2.....
- Table 36a. Frequency table of breaking wave height (H), breaking water depth (D), and wave run-up (R) for coastline 2 in July under mean fetch conditions.....
- Table 36b. Frequency table of breaking wave height (H), breaking water depth (D), and wave run-up (R) for coastline 2 in August under mean fetch conditions.....
- Table 36c. Frequency table of breaking wave height (H), breaking water depth (D), and wave run-up (R) for coastline 2 in September under mean fetch conditions.....
- Table 36d. Frequency table of breaking wave height (H), breaking water depth (D), and wave run-up (R) for coastline 2 in October under mean fetch conditions.....
- Table 36e. Average of Tables 36(a-d) under mean fetch conditions for coastline 2.....
- Table 37a. Frequency table of breaking wave height (H), breaking water depth (D), and wave run-up (R) for coastline 3 in June under maximum fetch conditions.....
- Table 37b. Frequency table of breaking wave height (H), breaking water depth (D), and wave run-up (R) for coastline 3 in July under maximum fetch conditions.....
- Table 37c. Frequency table of breaking wave height (H), breaking water depth (D), and wave run-up (R) for coastline 3 in August under maximum fetch conditions.....

- Table 37d. Frequency table of breaking wave height (H), breaking water depth (D), and wave run-up (R) for coastline 3 in September under maximum fetch conditions.....
- Table 37e. Frequency table of breaking wave height (H), breaking water depth (D), and wave run-up (R) for coastline 3 in October under maximum fetch conditions.....
- Table 37f. Frequency table of breaking wave height (H), breaking water depth (D), and wave run-up (R) for coastline 3 in November under maximum fetch conditions.....
- Table 37g. Average of Tables 37(a-f) under maximum fetch conditions for coastline 3.....
- Table 38a. Frequency table of breaking wave height (H), breaking water depth (D), and wave run-up (R) for coastline 3 in July under mean fetch conditions.....
- Table 38b. Frequency table of breaking wave height (H), breaking water depth (D), and wave run-up (R) for coastline 3 in August under mean fetch conditions.....
- Table 38c. Frequency table of breaking wave height (H), breaking water depth (D), and wave run-up (R) for coastline 3 in September under mean fetch conditions.....
- Table 38d. Frequency table of breaking wave height (H), breaking water depth (D), and wave run-up (R) for coastline 3 in October under mean fetch conditions.....
- Table 38e. Average of Table 38(a-d) under mean fetch conditions for coastline 3.....
- Table 39a. Frequency table of breaking wave height (H), breaking water depth (D), and wave run-up (R) for coastline 4 in June under maximum fetch conditions.....
- Table 39b. Frequency table of breaking wave height (H), breaking water depth (D), and wave run-up (R) for coastline 4 in July under maximum fetch conditions.....
- Table 39c. Frequency table of breaking wave height (H), breaking water depth (D), and wave run-up (R) for coastline 4 in August under maximum fetch conditions.....
- Table 39d. Frequency table of breaking wave height (H), breaking water depth (D), and wave run-up (R) for coastline 4 in September under maximum fetch conditions.....

- Table 39e. Frequency table of breaking wave height (H), breaking water depth (D), and wave run-up (R) for coastline 4 in October under maximum fetch conditions.....
- Table 39f. Frequency table of breaking wave height (H), breaking water depth (D), and wave run-up (R) for coastline 4 in November under maximum fetch conditions.....
- Table 39g. Average of Tables 39 (a-f) under maximum fetch conditions in coastline 4.....
- Table 40a. Frequency table of breaking wave height (H), breaking water depth (D), and wave run-up (R) for coastline 4 in July under mean fetch conditions.....
- Table 40b. Frequency table of breaking wave height (H), breaking water depth (D), and wave run-up (R) for coastline 4 in August under mean fetch conditions.....
- Table 40c. Frequency table of breaking wave height (H), breaking water depth (D), and wave run-up (R) for coastline 4 in September under mean fetch conditions.....
- Table 40d. Frequency table of breaking wave height (H), breaking water depth (D), and wave run-up (R) for coastline 4 in October under mean fetch conditions.....
- Table 40e. Average of Tables 40(a-d) under mean fetch conditions for coastline 4.....
- Table 41a. Frequency table of breaking wave height (H), breaking water depth (D), and wave run-up (R) for coastline 5 in June under maximum fetch conditions.....
- Table 41b. Frequency table of breaking wave height (H), breaking water depth (D), and wave run-up (R) for coastline 5 in July under maximum fetch conditions.....
- Table 41c. Frequency table of breaking wave height (H), breaking water depth (D), and wave run-up (R) for coastline 5 in August under maximum fetch conditions.....
- Table 41d. Frequency table of breaking wave height (H), breaking water depth (D), and wave run-up (R) for coastline 5 in September under maximum fetch conditions.....
- Table 41e. Frequency table of breaking wave height (H), breaking water depth (D), and wave run-up (R) for coastline 5 in October under maximum fetch conditions.....
- Table 41f. Frequency table of breaking wave height (H), breaking water depth (D), and wave run-up (R) for coastline 5 in November under maximum fetch conditions.....

- Table 41g. Average of Tables 41(a-f) under maximum fetch conditions for coastline 5.....
- Table 42a. Frequency table of breaking wave height (H), breaking water depth (D), and wave run-up (R) for coastline 5 in June under mean fetch conditions.....
- Table 42b. Frequency table of breaking wave height (H), breaking water depth (D), and wave run-up (R) for coastline 5 in July under mean fetch conditions.....
- Table 42c. Frequency table of breaking wave height (H), breaking water depth (D), and wave run-up (R) for coastline 5 in August under mean fetch conditions.....
- Table 42d. Frequency table of breaking wave height (H), breaking water depth (D), and wave run-up (R) for coastline 5 in September under mean fetch conditions.....
- Table 42e. Frequency table of breaking wave height (H), breaking water depth (D), and wave run-up (R) for coastline 5 in October under mean fetch conditions.....
- Table 42f. Average of Tables 42(a-e) under mean fetch conditions for coastline 5.....

INTRODUCTION

Wave predictions are necessary to determine the months and locations of highest risk for oil and gas development in the Chukchi Sea area. A wave hindcast scheme (Hasselmann, 1976) was used to characterize extreme wave conditions in Regions A, B and C (Fig. 1) for prescribed fetch distances. These fetch conditions were controlled by both ice cover and coastline orientation thereby becoming highly directionally dependent. Region C (Fig. 1) containing the Hope Basin and Kotzebue Sound has four primary coastline orientations (Wise et al., 1981). Region B has one, while A, existing in water depths greater than 25 meters, has none. Two ice cover positions were chosen utilizing data from Stringer (1984) and Brower et al. (1977). The first was the extreme minimum edge (50% areal coverage) which gives a maximum fetch. The second was the mean ice edge (50% areal coverage) which gives an average fetch.

Monthly wind statistics (Brower et al., 1977) from designated land stations bordering the Chukchi study regions and/or designated marine areas containing the Chukchi study areas were used as model wind field input. The output generated were deep water, significant wave height, period, and direction for the three regions (Fig. 1) plus breaking wave height, depth, and run-up for five coastline orientations (Fig. 1). The deep water wave heights and periods are based on the assumption of uniform steady wind conditions along each wind direction.

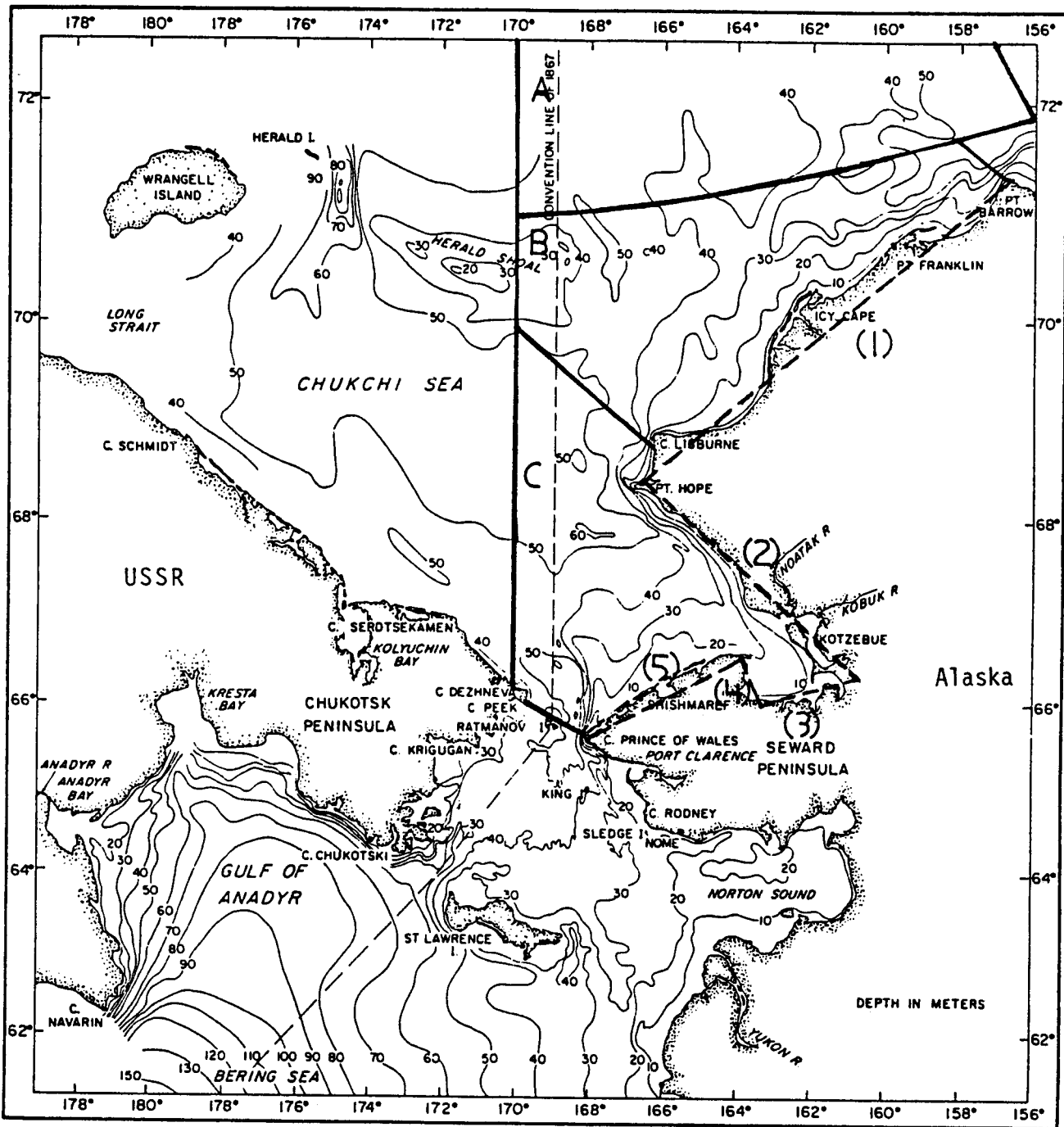


Figure 1. The three study regions A, B, and C (solid lines) and five coastlines (dashed lines) chosen for respective wave hindcast and breaking wave height analyses.

DEEP WATER WAVE HINDCAST THEORY

A parametric wind-wave model (Hasselmann, 1976) was adopted for the hindcast of the deep water wave. Hasselmann's one parameter model is based on the premise that the response of the wave field to the wind input can be described by two processes which occur at different rates:

- a. the rapid adjustment of the spectrum to a universal shape and an energy level such that the input by the wind in the dominant region of the spectrum is balanced by the nonlinear transfer and possibly dissipation and,
- b) the slower migration of the peak toward lower frequency due to the nonlinear energy transfer across the peak.

This concept has been verified by JONSWAP'S field results (Hasselmann et al., 1973) and also by laboratory results (Wu et al., 1979). The one parameter model is limited to growing seas and cannot be extended into the swell range. The governing equation is:

$$\frac{1}{f_0} \frac{\partial f_0}{\partial \tau} + P_0 \frac{\partial f_0}{\partial \eta} = -N_0 f_0^{7/3} + \frac{1}{u} \left(\frac{\partial u}{\partial \tau} + \frac{\partial u}{\partial \eta} \right)$$

Where

$$P_0 = 0.95$$

$$N_0 = 5.5 \times 10^{-4}$$

$$\frac{\partial}{\partial \tau} = \frac{u}{g} \frac{\partial}{\partial t}, \quad \frac{\partial}{\partial \eta} = \frac{u}{g} \vec{V}_m \cdot \vec{\nabla}, \quad |\vec{V}_m| = \frac{c c}{4 \pi f_m}$$

$$f_0 = U f_m / g, \quad c = 0.85 \text{ for } \cos^2 \theta \text{ spreading factor}$$

U is wind speed, g is gravitational acceleration,

f_m is peak wave frequency.

For a uniform wind field, the governing equation for predicting a local peak frequency can be simplified as:

$$\frac{\partial f_m}{\partial t} = -5.5 \times 10^{-4} \cdot \left(\frac{g}{U}\right)^{-4/3} \cdot f_m^{10/3}$$

The analytical solution of the above equation in terms of the normalized peak wave period, \hat{T}_p and normalized significant wave height, \hat{H}_s can be expressed as follows:

$$\begin{aligned} \hat{X} &\leq 3.5 \times 10^3 \\ \text{For } \hat{H}_s &= 1.53 \times 10^{-3} \hat{X}^{0.5} \\ \hat{T}_p &= 0.341 \hat{X}^{0.3} \end{aligned}$$

$$\begin{aligned} \text{otherwise } \hat{H}_s &= 0.283 \tanh(0.0125 \hat{X}^{0.42}), \\ \hat{T}_p &= 7.54 \tanh(0.077 \hat{X}^{0.25}), \end{aligned}$$

Where $\hat{X} = gX/U^2$, $\hat{H}_s = gH_s/U^2$, $\hat{T}_p = gT_p/U$. The results calculated by the above equations compare quite well with experimental observations made in other parts of the world over many years. For a given set of significant wave height (H_s), peak wave period (T_p), and wave direction (θ), a deep water directional wave spectrum $F(\omega, \theta)$ can be approximated. When a wave spectrum propagates through the shallow water region, it will be subject to the effects of shoaling and refraction. The transformed spectrum can be related to the initial wave spectrum (Battjes, 1974; Collins, 1972; Longuet-Higgins, 1957), as follows:

$$F(\omega, \theta) d\theta d\omega = \frac{k}{k_0} \frac{(C_g)_0}{C_g} F_0(\omega, \theta_0) \frac{d\theta}{d\theta_0} d\theta_0 d\omega$$

Where θ_0 denotes the initial conditions and $C_g = n\omega/k$ is the group velocity. Assume the directional spectrum $F_0(\omega, \theta_0)$ can be decomposed in such a form that the energy distributed in different frequencies, $E_0(\omega)$, are weighted by a directional spreading factor $\phi(\theta_0)$, i.e.:

$$F_0(\omega, \theta_0) = E_0(\omega)\phi(\theta_0).$$

Under the assumption of parallel bottom contours, Snell's Law, i.e.: $\sin \theta / \sin \theta_0 = k_0 / k$, can be applied to relate the refracted wave angle θ to simplify the calculation, i.e.:

$$d\theta = \frac{k_0 \cos \theta_0 d\theta_0}{(k^2 - k_0^2 \sin^2 \theta_0)^{1/2}}$$

Finally, the transformed wave spectrum can be written as follows:

$$F(\omega, \theta) d\theta d\omega = \frac{n_0 k^2 k_0 \cos \theta_0 \phi(\theta_0) E_0(\omega)}{n k_0^2 [k^2 - k_0^2 \sin^2 \theta_0]^{1/2}} d\theta_0 d\omega$$

This transformed wave spectrum is valid prior to wave breaking. After wave breaking, a different approach for the calculation of wave height in the surf zone is applied.

WAVE BREAKING CRITERIA

In the ocean, as a wave exceeds certain kinematical or dynamical limits, the wave will be broken and reformed. The visible white-capping phenomena is the result of wave breaking. It has been argued (Phillips, 1958; Kitaigorodskii et al., 1975; and Thornton, 1977) that in order to satisfy the kinematical dynamical constraints of wave breaking, the wave spectrum in the high frequency range where wave breaking occurs, must have a certain universal shape existing, which is known as the equilibrium range. One can employ dimensional analysis to derive a form for the equilibrium spectrum.

The equilibrium spectrum, $\psi(\omega)$ without the effect of current can be expressed as (Kitaigorodskii et al., 1975; Thornton, 1977, and Wu et al., 1980):

$$\psi(\omega) = \alpha k^{-2} (2n\omega)^{-1}$$

where α is Phillips' equilibrium constant, n is the ratio of group velocity to wave celerity, k is the wave number and ω is the angular frequency. The asymptotic forms of $\psi(\omega)$ in the deep and shallow water regions can be shown as:

$$\psi_D(\omega) = \alpha g^2 \omega^{-5}$$

and
$$\psi_S(\omega) = \frac{\alpha}{2} g h \omega^{-3}$$

respectively. The coefficient, $\alpha/2$ needs to be verified in the shallow water region.

As a wave field propagates toward the shallow water region, the process of wave dissipation, within the equilibrium range, is not sufficient to characterize the spilling, surging, or collapsing type of breakers which occur in shallow waters. Therefore, additional shallow water wave breaking criteria are needed. Based on a combination of the state-of-the-art knowledge of breaking height, breaking depth, deep water wave characteristics, and beach slope, the breaking criterion can be described by (Wu et al., 1980):

$$H < \gamma d$$

where $\gamma = H_b/d_b$ and H_b and d_b are breaking wave height and depth, respectively, which are functions of beach slope and incident wave characteristics. The breaking wave height is determined by the combination of Goda's (1970) index and LeMehaute and Koh's (1967) wave breaking condition, i.e.:

$$H_b = 0.74H_o \cdot S^{0.1} \cdot (H_o/L_o)^{-0.24} \cdot (\cos\theta_o)^{0.38} \cdot (\cos\theta_b)^{0.28}$$

and

$$\theta_b = (0.15 + 6.4 \cdot H_o \sqrt{\cos\theta_o}/L_o) \cdot \theta_o$$

for

$$0.002 < H_o \sqrt{\cos\theta_o}/L_o < 0.1 \quad \text{and} \quad 0.02 \leq S \leq 0.1$$

Where S is the beach slope, L_o is the deep water wave length and θ_b is the wave breaking angle.

The breaking water depth d_b is the summation of the still-water breaking depth, h_b and the maximum wave set-down, η_b at the breaking location. The still-water breaking depth h_b is (Weggel, 1972):

$$h_b = H_b / [b - (aH_b/gT_o^2)]$$

where

$$a = 1.36g(1 - e^{-19 \cdot S}) \quad \text{and} \quad b = 1.56/(1 + e^{-19.5 \cdot S})$$

The maximum wave set-down η_b at the wave breaking point can be estimated theoretically for a solitary wave. The theoretical form of η_b is:

$$\eta_b = -H_o^2 \sqrt{g} T_o \cos\theta_o / [64\pi(h_b + \eta_b)^{3/2}]$$

Finally, γ can be determined for a given set of initial wave conditions and beach slope. Then, the breaking condition can be established.

The combination of equilibrium spectrum check (which would limit the energy contained in the relatively high frequency range of a wave spectrum), and shallow water wave breaking conditions defines a very good breaking criterion, predicts a better breaking location, and provides a better simulation of surf zone processes.

WAVE RUN-UP

Wave run-up is defined as the maximum vertical water displacement on the face of the structure above the still-water surface during the wave attack. Since no sound theoretical background associated with the characteristics of breaking waves has been established, the state-of-the-art calculation of wave run-up is essentially based on experimental results. Since Hunt's equation always produces a reliable estimation of wave run-up for breaking wave cases, it was adopted for the basic analytical foundation. It is as follows:

$$\frac{R}{H} = 2.3 \cdot S \cdot (H/T)^{-\frac{1}{2}}$$

Where R is wave run-up, S is beach slope, H and T are wave height and period, respectively.

RESULTS AND CONCLUSIONS

DEEP WATER WAVE STATISTICS

Monthly frequency tables of significant wave height (H_s) and peak wave period (T_p) for both maximum (minimum ice edge) and mean (average ice edge) fetch have been compiled for Regions A, B and C. Results show that the values of H_s and T_p are consistently larger under maximum fetch conditions as expected.

The height of the 5% highest waves (H_5) is 1.73 H_s (Pierson et al., 1971). Tables of H_5 were prepared for this study, but it is much simpler to take a (H_s) table value and multiply by 1.73. H_5 frequency distributions can be approximated by taking the H_s tables and doubling the meter values across the top.

Region C

This is the farthest south of the three study regions and has the largest span of open water months (Kozo, 1985). The minimum ice edge position in the Chukchi Sea for May through November can be seen in Figs. 2a-8a. The mean Chukchi Sea ice edge position from June until November (shorter open water period) is shown in Figs. 3b-8b. Tables 1-7 and Tables 8-13 show H_s and T_p for maximum and mean fetch respectively. The months with the greatest amount of open water, July to October, show little difference between the corresponding maximum fetch data (Tables 3-6) and the mean fetch data (Tables 9-12) since Region C is so far from the ice edge.

The maximum H_s and T_p found for these open water months under both maximum and mean fetch conditions were 10 m and 14 s. These large waves can come from the south in July (Tables 3 and 9) and from the northeast and

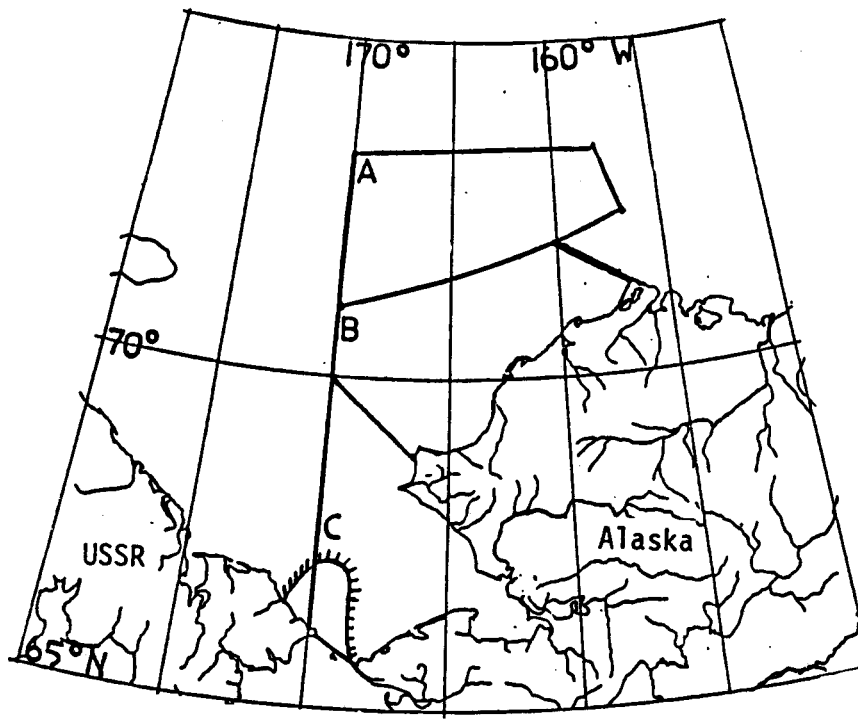


Figure 2a. The minimum sea ice extent (maximum fetch condition) in May (Stringer, 1984; Brower et al, 1977) relative to Regions A-C.

Figure 2b. There is typically no open water in Regions A-C in May for mean sea ice extent.

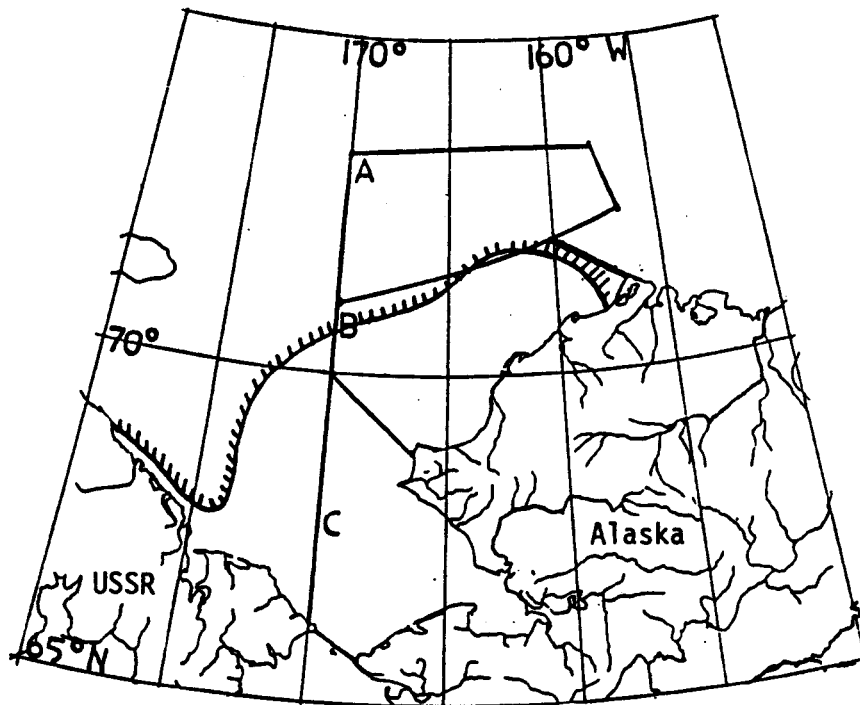


Figure 3a. The minimum sea ice extent (maximum fetch condition) in June (Stringer, 1984; Brower et al, 1977) relative to Regions A-C.

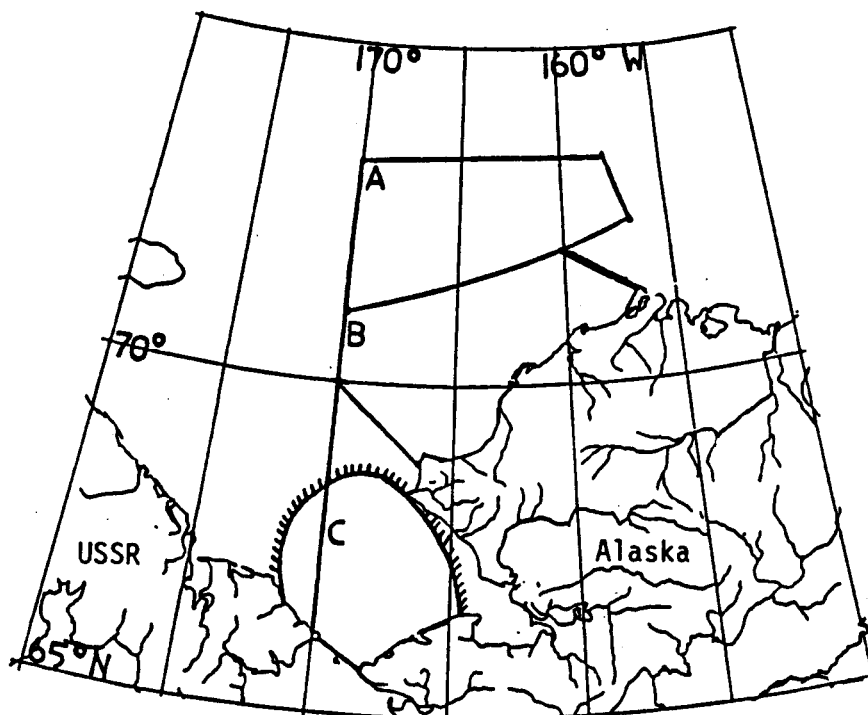


Figure 3b. The mean sea ice extent (average fetch condition) in June (Stringer, 1984; Brower et al, 1977) relative to Regions A-C.

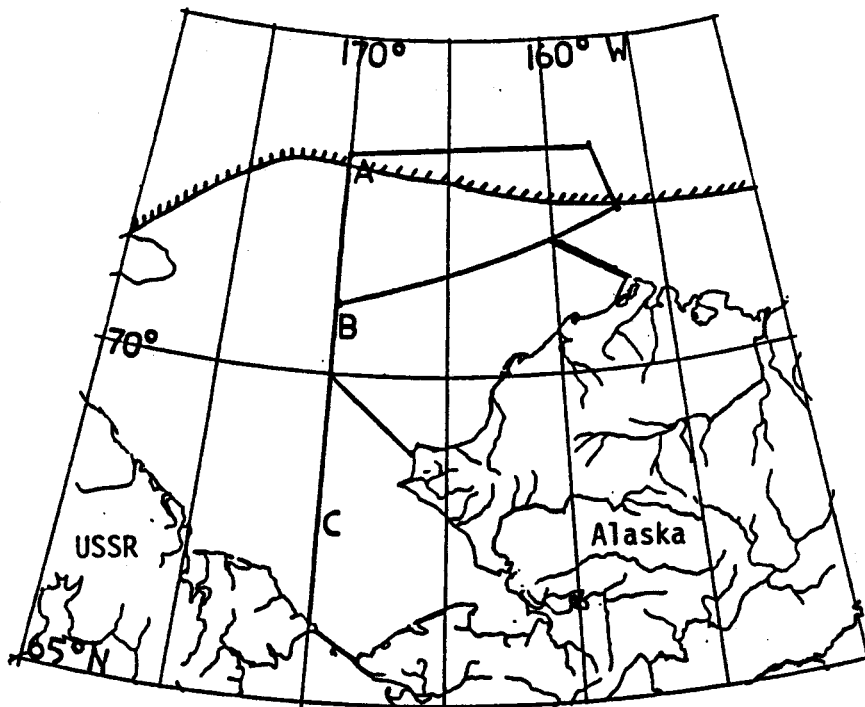


Figure 4a. The minimum sea ice extent (maximum fetch condition) in July (Stringer, 1984; Brower et al, 1977) relative to Regions A-C.

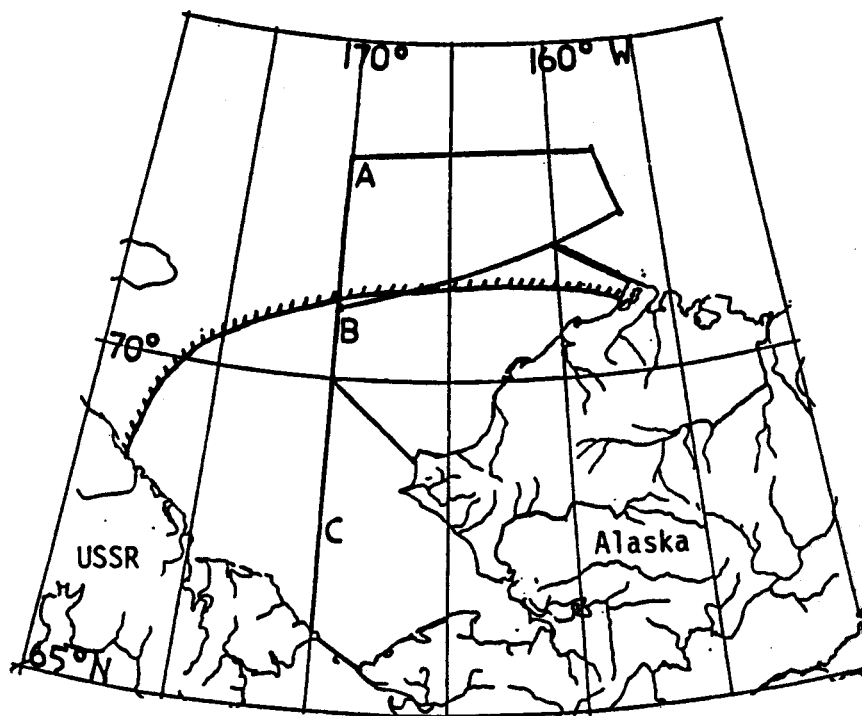


Figure 4b. The mean sea ice extent (average fetch condition) in July (Stringer, 1984; Brower et al, 1977) relative to Regions A-C.

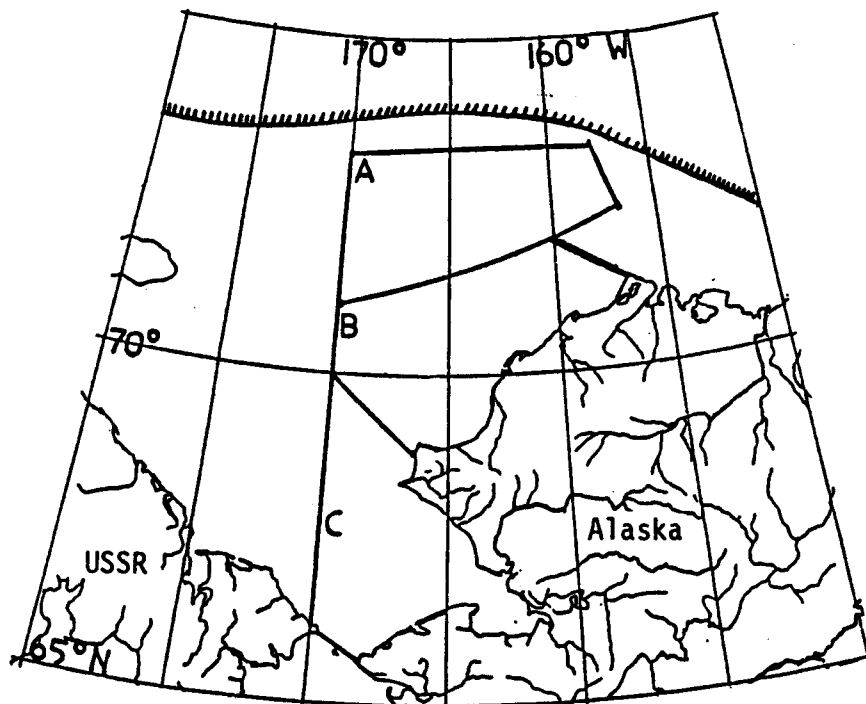


Figure 5a. The minimum sea ice extent (maximum fetch condition) in August (Stringer, 1984; Brower et al, 1977) relative to Regions A-C.

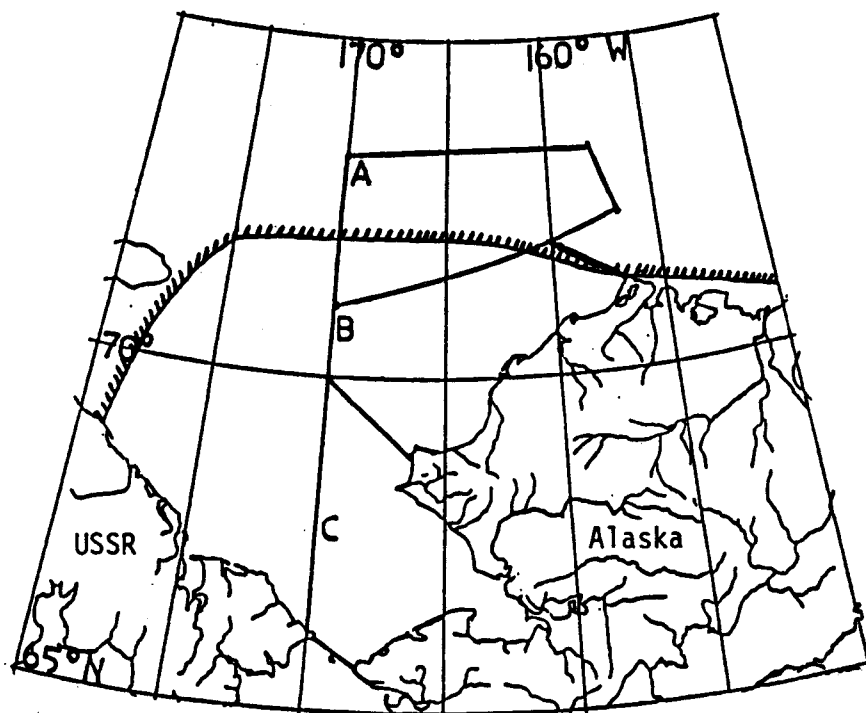


Figure 5b. The mean sea ice extent (average fetch condition) in August (Stringer, 1984; Brower et al, 1977) relative to Regions A-C.

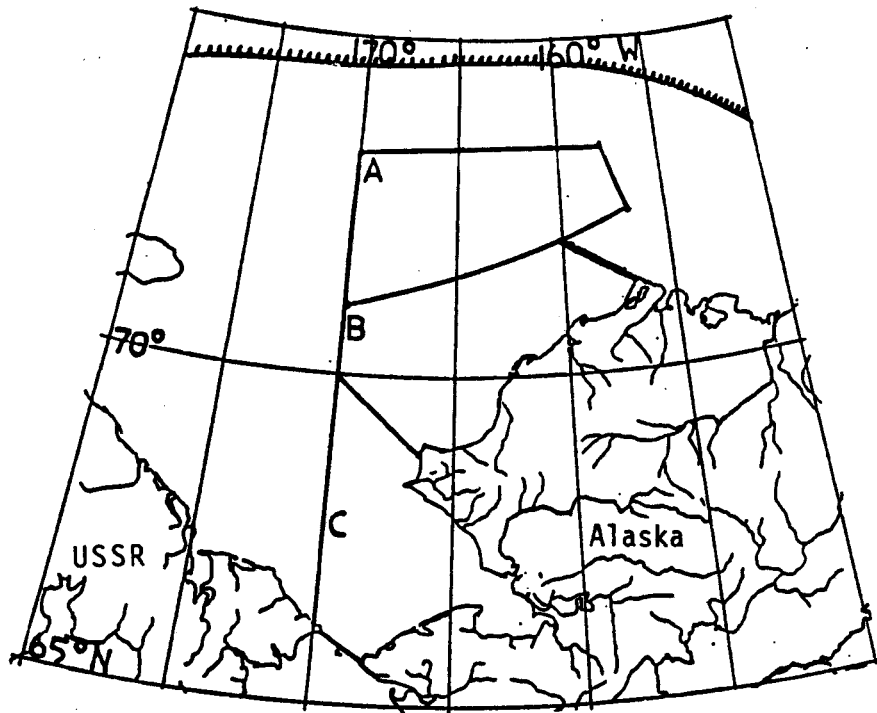


Figure 6a. The minimum sea ice extent (maximum fetch condition) in September (Stringer, 1984; Brower et al, 1977) relative to Regions A-C.

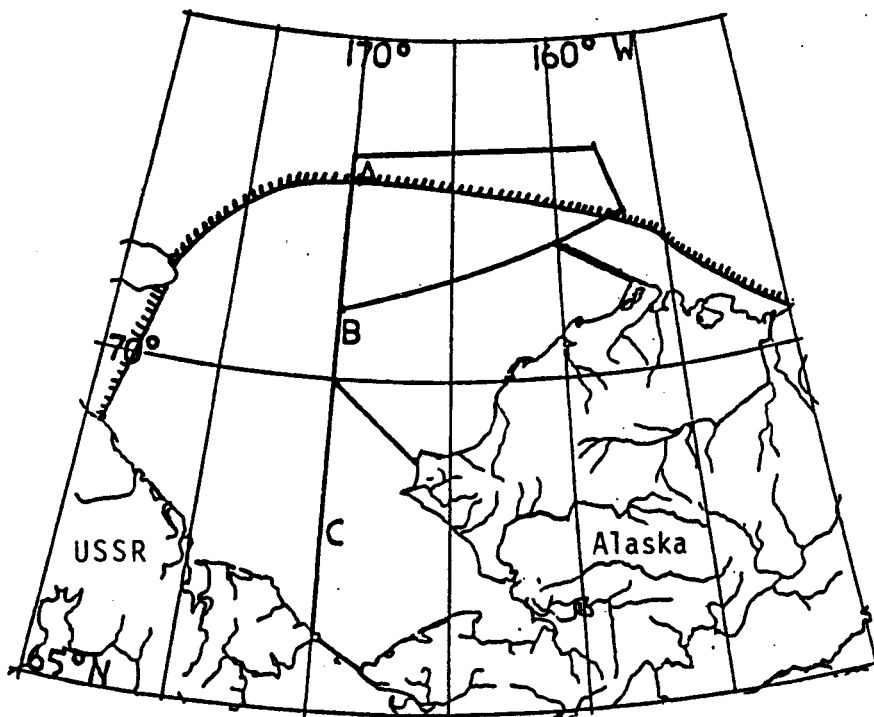


Figure 6b. The mean sea ice extent (average fetch condition) in September (Stringer, 1984; Brower et al, 1977) relative to Regions A-C.

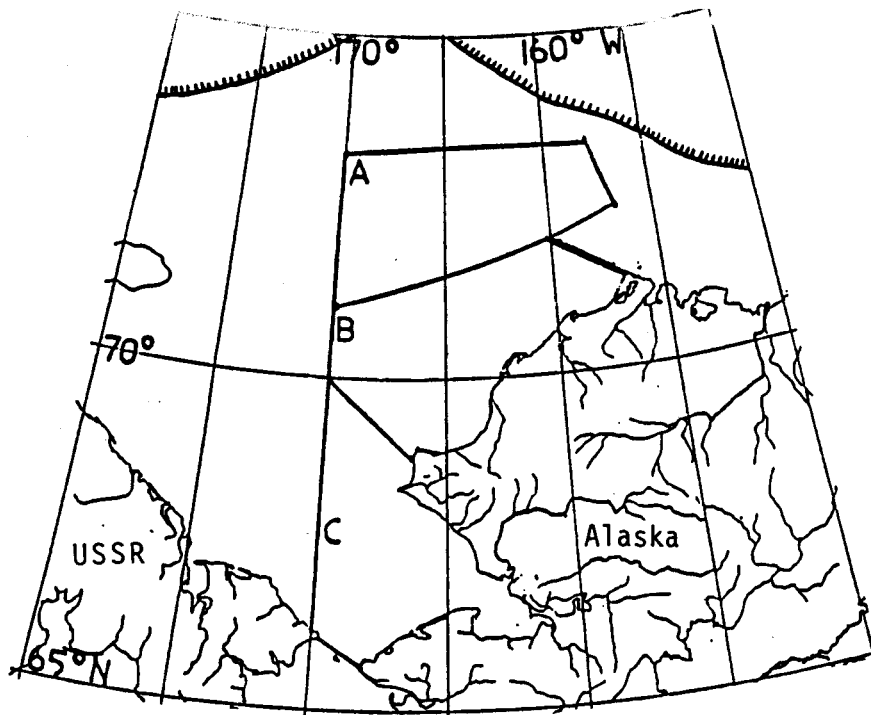


Figure 7a. The minimum sea ice extent (maximum fetch condition) in October (Stringer, 1984; Brower et al, 1977) relative to Regions A-C.

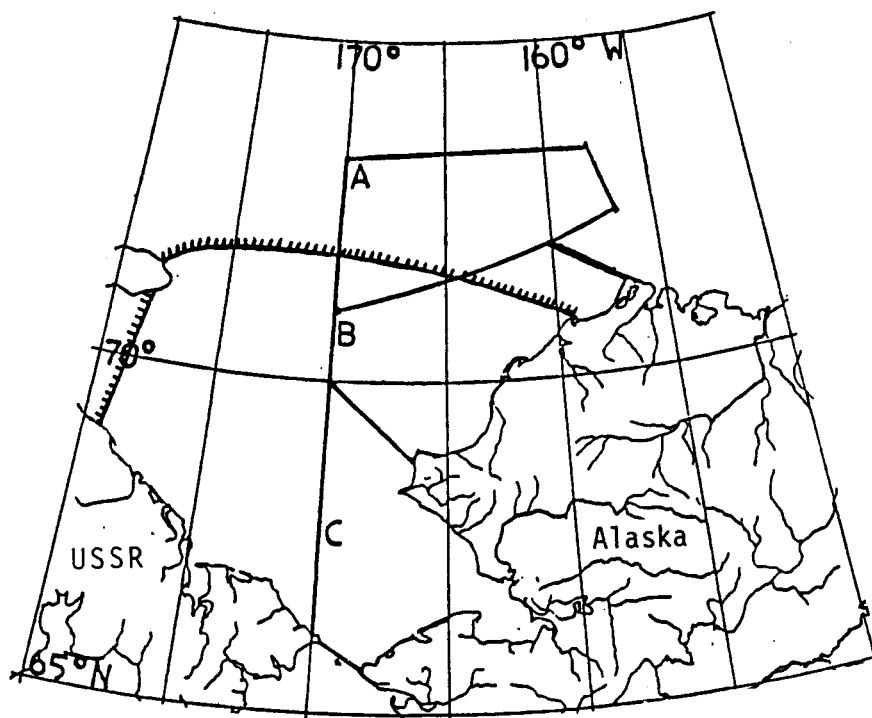


Figure 7b. The mean sea ice extent (average fetch condition) in October (Stringer, 1984; Brower et al, 1977) relative to Regions A-C.

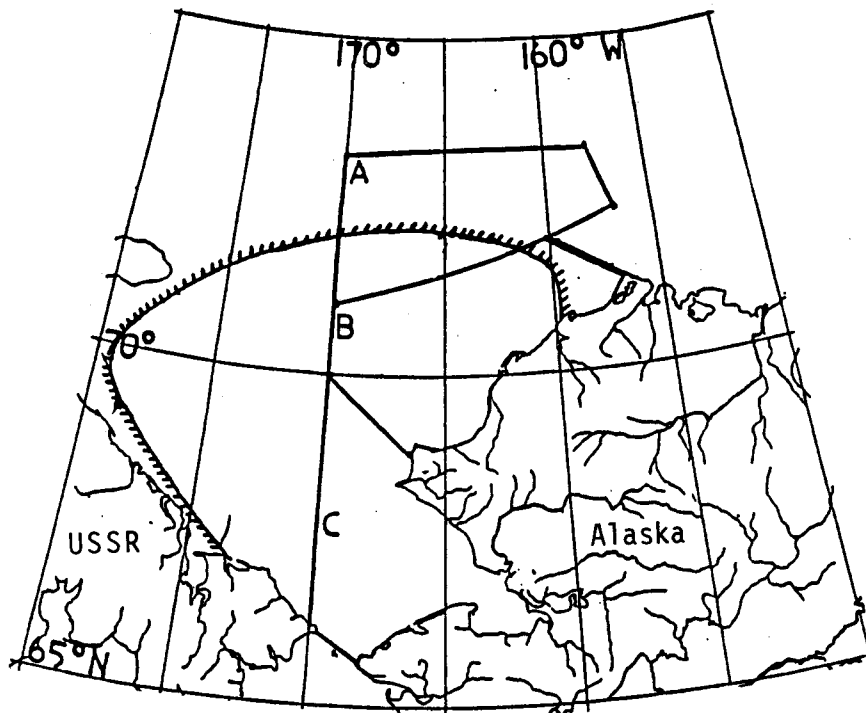


Figure 8a. The minimum sea ice extent (maximum fetch condition) in November (Stringer, 1984; Brower et al, 1977) relative to Regions A-C.

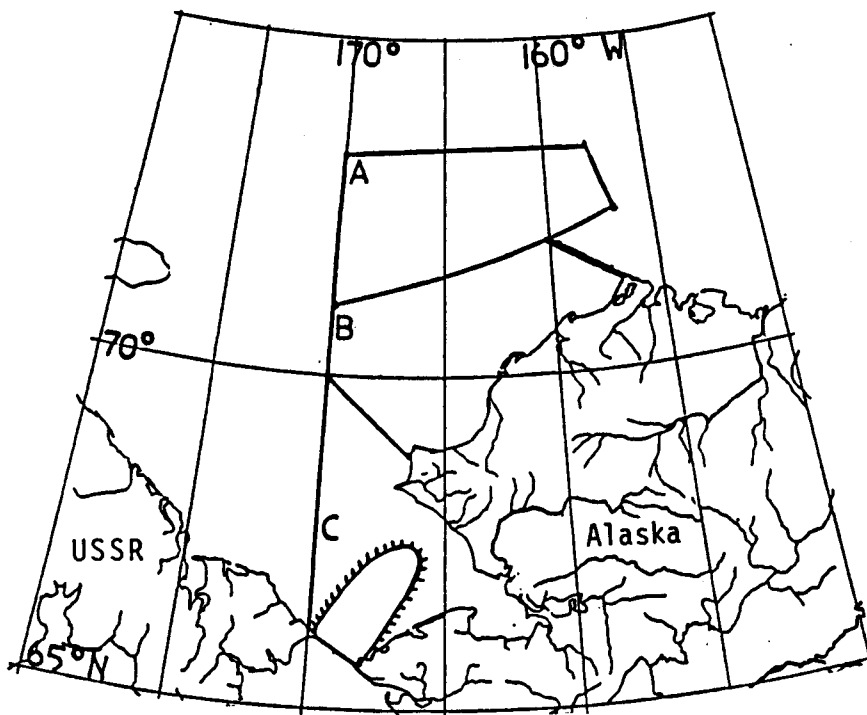


Figure 8b. The mean sea ice extent (average fetch condition) in November (Stringer, 1984; Brower et al, 1977) relative to Regions A-C.

H _s (m)	1	2	3	4	5	6	7	8	9	10	11	12	13	TOTAL %
N	21	11	5	+										37
NE	5	2	+											7
E	2	2	+											4
SE	+	+	+											1
S	8	6	4	3	2	0	0	1	1	+				25
SW	3	2	1	+										6
W	+	+	+	+										1
NW	4	3	+	+	+									7
CALM	12													12
TOTAL%	55	26	11	4	2	0	0	1	1	+				100

Table 1a. The predicted frequency of significant wave heights (H_s) in meters for waves from eight specified directions in May. These data were derived from wind velocity histograms (Brower et al., 1977) compiled at stations near Region C for maximum fetch conditions.

T _p (S)	2	4	6	8	10	12	14	16	TOTAL %
N	2	19	15	1					37
NE	1	4	2						7
E	+	2	2	+					4
SE	+	1	+	+					1
S	1	7	6	4	5	2			25
SW	1	2	2	2					7
W	+	+	+	+					+
NW	1	3	3	+	+				7
CALM	12								12
TOTAL%	18	38	30	7	5	2			100

Table 1b. The predicted frequency of peak wave periods (T_p) in seconds for waves coming from eight specified directions in May. These data were derived from wind velocity measurements (Brower et al., 1977) compiled at stations near Region C for maximum fetch conditions.

Hs (m)	1	2	3	4	5	6	7	8	9	10	11	12	13	TOTAL %
N	16	6	3	0	1	+								26
NE	8	1	+	0	+	+								10
E	5	1	+											6
SE	+	+	+	0	+	+	0	+	+					1
S	10	7	6	4	0	2	1	0	+	+				30
SW	4	2	1	1	+	0	+							8
W	+	0	0	0	0	+	+	+						+
NW	2	2	0	1	+	+								5
CALM	14													14
TOTAL%	59	19	10	6	2	3	1	+	+	+				100

Table 2a. The predicted frequency of significant wave heights (Hs) in meters for waves from eight specified directions in June. These data were derived from wind velocity histograms (Brower et al., 1977) compiled at stations near Region C for maximum fetch conditions.

Tp(S)	2	4	6	8	10	12	14	16	TOTAL %
N	3	13	6	3	1				26
NE	1	7	1	+	+				9
E	+	5	1	+					6
SE	+	+	+	+	+	+			1
S	2	8	7	6	6	1	+		30
SW	1	3	2	2	+	+			8
W	+	+	0	0	+				1
NW	+	2	2	1	+				5
CALM	14								14
TOTAL%	21	38	19	13	8	1	+		100

Table 2b. The predicted frequency of peak wave periods (Tp) in seconds for waves coming from eight specified directions in June. These data were derived from wind velocity measurements (Brower et al., 1977) compiled at stations near Region C for maximum fetch conditions.

H _s (m)	1	2	3	4	5	6	7	8	9	10	11	12	13	TOTAL %
N	4	0	1	+	+									5
NE	8	0	3	1	+									12
E	19	2	+	+	+	0	+							22
SE	6	1	+	0	+	+	0	+						8
S	4	4	3	0	2	1	1	0	+	+				15
SW	3	5	4	3	1	0	+	+	+					16
W	3	1	+	0	+	+								4
NW	5	0	1	+	+									6
CALM	12													12
TOTAL%	64	13	13	4	4	1	1	+	+	+				100

Table 3a. The predicted frequency of significant wave heights (H_s) in meters for waves from eight specified directions in July. These data were derived from wind velocity histograms (Brower et al., 1977) compiled at stations near Region C for maximum fetch conditions.

T _p (S)	2	4	6	8	10	12	14	16	TOTAL %
N	1	1	3	+	+				5
NE	1	3	7	1	+				12
E	3	16	2	+	+				22
SE	1	5	1	+	+	+			8
S	+	4	4	3	3	1	+		15
SW	+	3	5	7	1	+	+		16
W	+	3	1	+	+				4
NW	1	2	3	+	+				6
CALM	12								12
TOTAL%	19	37	26	12	5	1	+		100

Table 3b. The predicted frequency of peak wave periods (T_p) in seconds for waves coming from eight specified directions in July. These data were derived from wind velocity measurements (Brower et al., 1977) compiled at stations near Region C for maximum fetch conditions.

Hs (m)	1	2	3	4	5	6	7	8	9	10	11	12	13	TOTAL %
N	8	0	6	4	2	1	+							21
NE	5	0	3	2	1	0	1	+						12
E	4	2	1	1	+	+								8
SE	4	3	1	0	+	+								8
S	4	4	4	0	2	+	+							14
SW	5	2	1	1	+	0	+	+	+					10
W	4	2	1	0	1	+	+	+						9
NW	7	0	3	2	1	0	+	0	+					13
CALM	5													5
TOTAL%	46	13	20	10	8	2	1	+	+					100

Table 4a. The predicted frequency of significant wave heights (Hs) in meters for waves from eight specified directions in August. These data were derived from wind velocity histograms (Brower et al., 1977) compiled at stations near Region C for maximum fetch conditions.

Tp(S)	2	4	6	8	10	12	14	16	TOTAL %
N	1	3	10	4	2	1	+		21
NE	1	2	5	2	1	1	+		12
E	+	4	2	2	+	+			8
SE	1	3	4	+	+				8
S	+	4	4	4	2	+			14
SW	1	4	2	2	+	+	+		10
W	1	3	2	1	1	+	+		9
NW	1	3	6	2	1	+			13
CALM	5								5
TOTAL%	11	26	35	17	8	3	+		100

Table 4b. The predicted frequency of peak wave periods (Tp) in seconds for waves coming from eight specified directions in August. These data were derived from wind velocity measurements (Brower et al., 1977) compiled at stations near Region C for maximum fetch conditions.

H _s (m)	1	2	3	4	5	6	7	8	9	10	11	12	13	TOTAL %
N	5	0	5	4	3	0	1	0	1					19
NE	6	0	3	2	2	0	1	0	+	+				14
E	6	3	1	1	+									11
SE	5	2	2	+	+									9
S	5	2	3	0	1	+	0	+						11
SW	3	2	1	0	1	0	+	+	+	+				7
W	4	2	1	0	1	+	+							8
NW	6	0	5	3	2	0	1	0	1					18
CALM	3													3
TOTAL%	43	11	21	10	10	+	3	+	2	+				100

Table 5a. The predicted frequency of significant wave heights (H_s) in meters for waves from eight specified directions in September. These data were derived from wind velocity histograms (Brower et al., 1977) compiled at stations near Region C for maximum fetch conditions.

T _p (S)	2	4	6	8	10	12	14	16	TOTAL %
N	1	1	3	9	3	2			19
NE	1	2	6	2	2	1	+		14
E	1	5	3	1	1				11
SE	1	4	2	1	1	+	+		9
S	1	4	2	3	1	+			11
SW	+	3	2	1	1	+			7
W	1	3	2	1	1	+			8
NW	+	3	8	3	2	2			18
CALM	3								3
TOTAL%	9	25	28	21	12	5	+		100

Table 5b. The predicted frequency of peak wave periods (T_p) in seconds for waves coming from eight specified directions in September. These data were derived from wind velocity measurements (Brower et al., 1977) compiled at stations near Region C for maximum fetch conditions.

Hs (m)	1	2	3	4	5	6	7	8	9	10	11	12	13	TOTAL %
N	4	0	8	10	9	6	3	+	+					40
NE	1	0	3	3	1	0	1	+						9
E	2	1	2	1	+	0	+							6
SE	1	1	+	0	1	+	1	+						5
S	7	3	2	0	1	1	1	1	+					16
SW	5	1	+	+	+	0	+	+						7
W	2	1	1	0	+	+								5
NW	1	0	1	2	1	1	+	+	+					7
CALM	5													5
TOTAL%	28	7	18	16	14	9	7	1	+					100

Table 6a. The predicted frequency of significant wave heights (Hs) in meters for waves from eight specified directions in October. These data were derived from wind velocity histograms (Brower et al., 1977) compiled at stations near Region C for maximum fetch conditions.

Tp(S)	2	4	6	8	10	12	14	16	TOTAL %
N	+	1	3	8	19	9	+		40
NE	+	+	4	3	1	1	+		9
E	+	2	1	3	+	+			6
SE	+	1	1	+	1	1			5
S	1	6	3	2	2	2	+		16
SW	1	4	1	+	+	+			7
W	+	2	1	1	+	+			5
NW	+	+	1	1	2	2	+		7
CALM	5								5
TOTAL%	9	17	15	19	25	15	+		100

Table 6b. The predicted frequency of peak wave periods (Tp) in seconds for waves coming from eight specified directions in October. These data were derived from wind velocity measurements (Brower et al., 1977) compiled at stations near Region C for maximum fetch conditions.

H _s (m)	1	2	3	4	5	6	7	8	9	10	11	12	13	TOTAL	%
N	4	6	0	6	6	0	3	2	0	+				27	
NE	1	3	3	0	3	2	0	1	0	+	+			13	
E	1	2	2	2	+	0	1	+	+					8	
SE	+	+	+	0	+	+	0	+	+	+				2	
S	7	2	2	0	2	1	0	2	1	1				18	
SW	5	1	+	+	+	0	+	+	+					8	
W	2	2	1	0	1	+	+	0	+					7	
NW	3	3	2	1	0	1	1	0	+					11	
CALM	6													6	
TOTAL%	29	19	10	9	13	5	6	6	2	1	+			100	

Table 7a. The predicted frequency of significant wave heights (H_s) in meters for waves from eight specified directions in November. These data were derived from wind velocity histograms (Brower et al., 1977) compiled at stations near Region C for maximum fetch conditions.

T _p (S)	2	4	6	8	10	12	14	16	TOTAL	%
N	+	1	6	6	9	2	+		27	
NE	+	1	3	3	5	1	+	+	14	
E	+	1	2	4	1	+	+		9	
SE	+	+	+	+	+	+	+		2	
S	1	6	2	2	3	3	1		18	
SW	1	4	1	+	+	+	+		7	
W	+	2	2	1	1	+			6	
NW	+	3	3	3	1	1			11	
CALM	6								6	
TOTAL%	8	18	23	20	21	8	2	+	100	

Table 7b. The predicted frequency of peak wave periods (T_p) in seconds for waves coming from eight specified directions in November. These data were derived from wind velocity measurements (Brower et al., 1977) compiled at stations near Region C for maximum fetch conditions.

Hs (m)	1	2	3	4	5	6	7	8	9	10	11	12	13	TOTAL %
N	16	6	3	1	+									26
NE	8	1	+	+	+									9
E	5	1	+											6
SE	+	+	+	+	+	+	+							1
S	10	7	6	4	2	0	1	+	+					30
SW	4	2	1	1	+	+								8
W	+	0	0	0	+									1
NW	2	2	1	+	+									5
CALM	14													14
TOTAL%	60	19	11	6	3	+	1	+	+					100

Table 8a. The predicted frequency of significant wave heights (Hs) in meters for waves from eight specified directions in June. These data were derived from wind velocity histograms (Brower et al., 1977) compiled at stations near Region C for mean fetch conditions.

Tp(S)	2	4	6	8	10	12	14	16	TOTAL %
N	3	13	6	4	+				26
NE	1	7	1	+	+				9
E	+	5	1	+					6
SE	+	+	+	+	+	+			1
S	2	8	7	10	3	+			30
SW	1	3	2	2	+				8
W	+	+	0	0	+				1
NW	+	2	2	1	+				5
CALM	14								14
TOTAL%	22	38	19	18	3	+			100

Table 8b. The predicted frequency of peak wave periods (Tp) in seconds for waves coming from eight specified directions in June. These data were derived from wind velocity measurements (Brower et al., 1977) compiled at stations near Region C for mean fetch conditions.

H _s (m)	1	2	3	4	5	6	7	8	9	10	11	12	13	TOTAL %
N	4	1	0	+	+									5
NE	8	3	1	0	+									12
E	19	2	+	+	+	0	+							22
SE	6	1	+	0	+	+	0	+						8
S	4	4	3	0	2	1	1	0	+	+				15
SW	3	5	4	3	1	0	+	+	+					16
W	3	1	+	0	+	+								4
NW	5	1	0	+	+									6
CALM	12													12
TOTAL%	64	18	9	4	3	1	1	+	+	+				100

Table 9a. The predicted frequency of significant wave heights (H_s) in meters for waves from eight specified directions in July. These data were derived from wind velocity histograms (Brower et al., 1977) compiled at stations near Region C for mean fetch conditions.

T _p (S)	2	4	6	8	10	12	14	16	TOTAL %
N	1	1	3	+	+				5
NE	1	7	3	1	+				12
E	3	16	2	+	+				22
SE	1	5	1	+	+	+			8
S	+	4	4	3	3	1	+		15
SW	+	3	5	7	1	+	+		16
W	+	3	1	+	+				4
NW	1	2	3	+	+				6
CALM	12								12
TOTAL%	19	41	22	12	5	1	+		100

Table 9b. The predicted frequency of peak wave periods (T_p) in seconds for waves coming from eight specified directions in July. These data were derived from wind velocity measurements (Brower et al., 1977) compiled at stations near Region C for mean fetch conditions.

Hs (m)	1	2	3	4	5	6	7	8	9	10	11	12	13	TOTAL %
N	8	0	6	4	2	1								21
NE	5	3	0	2	1	1	+							12
E	4	2	1	1	+	+								8
SE	4	3	1	0	+	+								8
S	4	4	4	0	2	+	+							14
SW	5	2	1	1	+	0	+	+	+					10
W	4	2	1	0	1	+	+							9
NW	7	0	3	2	1	+	0	+						13
CALM	5													5
TOTAL%	46	16	17	10	8	3	+	+	+					100

Table 10a. The predicted frequency of significant wave heights (Hs) in meters for waves from eight specified directions in August. These data were derived from wind velocity histograms (Brower et al., 1977) compiled at stations near Region C for mean fetch conditions.

TP(S)	2	4	6	8	10	12	14	16	TOTAL %
N	1	3	10	4	2	1			21
NE	1	2	5	2	2	+			12
E	+	4	2	2	+	+			8
SE	1	3	4	+	+				8
S	+	4	4	4	2	+			14
SW	1	4	2	2	+	+	+		10
W	1	3	2	1	1	+			9
NW	1	3	6	2	1	+			13
CALM	5								5
TOTAL%	11	26	35	17	9	2	+		100

Table 10b. The predicted frequency of peak wave periods (Tp) in seconds for waves coming from eight specified directions in August. These data were derived from wind velocity measurements (Brower et al., 1977) compiled at stations near Region C for mean fetch conditions.

Hs (m)	1	2	3	4	5	6	7	8	9	10	11	12	13	TOTAL	%
N	5	0	5	4	3	0	1	0	1					19	
NE	6	0	3	2	2	0	1							14	
E	6	3	1	1	+									11	
SE	5	2	2	+	+									9	
S	5	2	3	0	1	+	0	+						11	
SW	3	2	1	0	1	0	+	+	+	+				7	
W	4	2	1	0	1	+	+							8	
NW	6	0	5	3	2	0	1	0	1					18	
CALM	3													3	
TOTAL%	43	11	21	10	10	+	3	+	2	+				100	

Table 11a. The predicted frequency of significant wave heights (Hs) in meters for waves from eight specified directions in September. These data were derived from wind velocity histograms (Brower et al., 1977) compiled at stations near Region C for mean fetch conditions.

Tp(S)	2	4	6	8	10	12	14	16	TOTAL	%
N	1	1	8	4	3	2			19	
NE	1	2	6	2	2	1	+		14	
E	1	5	3	1	1				11	
SE	1	4	2	1	1	+	+		9	
S	1	4	2	3	1	+			11	
SW	+	3	2	1	1	+			7	
W	1	3	2	1	1	+			8	
NW	+	3	8	3	2	2			18	
CALM	3								3	
TOTAL%	9	25	33	16	12	5	+		100	

Table 11b. The predicted frequency of peak wave periods (Tp) in seconds for waves coming from eight specified directions in September. These data were derived from wind velocity measurements (Brower et al., 1977) compiled at stations near Region C for mean fetch conditions.

H _s (m)	1	2	3	4	5	6	7	8	9	10	11	12	13	TOTAL %
N	4	8	0	10	9	6	3	+						40
NE	1	3	3	0	1	1	+	+						9
E	2	1	2	1	+	0	+							6
SE	1	1	+	0	1	+	1	+						5
S	7	3	2	0	1	1	1	1	+					16
SW	5	1	+	+	+	0	+	+						7
W	2	1	1	0	+	+								5
NW	1	0	1	2	1	1	+	+						7
CALM	5													5
TOTAL%	28	18	10	13	14	10	6	1	+					100

Table 12a. The predicted frequency of significant wave heights (H_s) in meters for waves from eight specified directions in October. These data were derived from wind velocity histograms (Brower et al., 1977) compiled at stations near Region C for mean fetch conditions.

T _p (S)	2	4	6	8	10	12	14	16	TOTAL %
N	+	1	11	19	9	+			40
NE	+	1	3	3	2	+			9
E	+	2	1	3	+	+			6
SE	+	1	1	+	1	1			5
S	1	6	3	2	2	2	+		16
SW	1	4	1	+	+	+			7
W	+	2	1	1	+	+			5
NW	+	+	2	2	2	+			7
CALM	5								5
TOTAL%	10	17	23	31	16	3	+		100

Table 12b. The predicted frequency of peak wave periods (T_p) in seconds for waves coming from eight specified directions in October. These data were derived from wind velocity measurements (Brower et al., 1977) compiled at stations near Region C for mean fetch conditions.

H _s (m)	1	2	3	4	5	6	7	8	9	10	11	12	13	TOTAL %
N	4	12	6	5	+									27
NE	1	3	3	3	2	1	+							13
E	1	4	2	1	+									8
SE	+	+	+	+	+									2
S	7	2	2	2	1	3	1							18
SW	5	1	+	+	+	+	+							8
W	2	3	1	+										7
NW	3	5	2	1										11
CALM	6													6
TOTAL%	29	30	18	13	4	4	2							100

Table 13a. The predicted frequency of significant wave heights (H_s) in meters for waves from eight specified directions in November. These data were derived from wind velocity histograms (Brower et al., 1977) compiled at stations near Region C for mean fetch conditions.

T _p (S)	2	4	6	8	10	12	14	16	TOTAL %
N	+	4	12	11	+				27
NE	+	1	3	6	3	+			14
E	+	1	4	3	+				9
SE	+	+	+	+	+				2
S	1	6	2	4	4	1			18
SW	1	4	1	+	+	+			7
W	+	2	3	1					6
NW	+	3	5	3					11
CALM	6								6
TOTAL%	8	2	31	29	9	2			100

Table 13b. The predicted frequency of peak wave periods (T_p) in seconds for waves coming from eight specified directions in November. These data were derived from wind velocity measurements (Brower et al., 1977) compiled at stations near Region C for mean fetch conditions.

southwest in September (Tables 5 and 11). Since H_s is independent of T_p , the joint probability of occurrence $p(H_s, T_p) = p(H_s) \cdot p(T_p)$ (Guttman and Wilks, 1965). As an example, using the percentage frequency from Table 3 (a, b) or Table 5 (a, b) for H_s and T_p their joint occurrence probability is $+ \cdot + = \sim (5 \times 10^{-3}) \cdot (5 \times 10^{-3})$ or .0025% in Region C for July or September. The largest possible H_s and T_p found were 11 m and 16 s respectively for waves from the northeast at maximum fetch in November (Table 7, Fig. 8a). This maximum fetch condition has a 1% probability of occurrence in Region C and is also independent of H_s and T_p . Therefore, the joint probability of all three occurring is $1 \cdot + \cdot + = \sim (1 \times 10^{-2}) \cdot (5 \times 10^{-3})^2$ or .00000025%. Region C usually has limited open water in November (Fig. 8b) which also eliminates the chances for large waves (Table 13).

Most potentially destructive wave directions are from the south for the months of May to July and from the north to northeast for the months of August to November which correspond to the change in vector mean winds and fetch for these months (Brower et al., 1977).

Region B

This region is just above C and has a shorter open water period. The minimum ice edge position in the Chukchi Sea for June through November can be seen in Figs. 3a-8a. The mean Chukchi Sea ice edge position from July until October (shorter open water period) is shown in Figs. 4b-7b. Tables 14-19 and Tables 20-23 show H_s and T_p for maximum and mean fetch respectively. The months with the greatest amount of open water for Region B are August and September. They show little difference between the corresponding maximum fetch Tables 16-17 and the mean fetch Tables 21-22 since the ice edge is far away from Region B for both cases.

Hs (m)	1	2	3	4	5	6	7	8	9	10	11	12	13	TOTAL %
N	12	2	+											14
NE	14	5	4	1	+									24
E	6	4	3	2										15
SE	2	+	+	+										3
S	3	+	+	0	+	+	0	+						4
SW	8	0	2	1	+	0	+	0	+					12
W	10	+	+	0	+									11
NW	9	+												9
CALM	8													8
TOTAL%	72	12	10	4	1	1	+	+	+					100

Table 14a. The predicted frequency of significant wave heights (Hs) in meters for waves from eight specified directions in June. These data were derived from wind velocity histograms (Brower et al., 1977) compiled at stations near Region B for maximum fetch conditions.

Tp(S)	2	4	6	8	10	12	14	16	TOTAL %
N	1	11	2	+					14
NE	1	13	5	5	+				24
E	+	6	4	5					15
SE	+	2	+	+					3
S	1	2	+	+	+	+			4
SW	1	7	2	1	+	+			12
W	1	8	1	+	+				11
NW	1	8	+						9
CALM	8								8
TOTAL%	15	57	15	12	1	+			100

Table 14b. The predicted frequency of peak wave periods (Tp) in seconds for waves coming from eight specified directions in June. These data were derived from wind velocity measurements (Brower et al., 1977) compiled at stations near Region B for maximum fetch conditions.

Hs (m)	1	2	3	4	5	6	7	8	9	10	11	12	13	TOTAL %
N	4	1	+	0	+									5
NE	8	3	1	+										12
E	19	2	+	0	+	+	+							22
SE	6	1	+	+	+	0	+							8
S	4	4	0	3	2	1	0	1	0	+	+			15
SW	3	0	5	4	3	0	1	0	+	0	+	+		16
W	3	0	1	+	+	0	+							4
NW	5	1	+	0	+									6
CALM	12													12
TOTAL%	64	12	8	8	5	1	1	1	+	+	+	+		100

Table 15a. The predicted frequency of significant wave heights (Hs) in meters for waves from eight specified directions in July. These data were derived from wind velocity histograms (Brower et al., 1977) compiled at stations near Region B for maximum fetch conditions.

Tp(S)	2	4	6	8	10	12	14	16	TOTAL %
N	1	3	1	+	+				5
NE	1	7	3	1					12
E	3	16	2	+	+	+			22
SE	1	5	1	+	+				8
S	+	1	7	3	3	1	+	+	15
SW	+	1	7	4	3	1	+	+	16
W	+	1	3	+	+	+			4
NW	1	4	1	+	+				12
CALM	12								12
TOTAL%	19	38	25	9	7	2	+	+	100

Table 15b. The predicted frequency of peak wave periods (Tp) in seconds for waves coming from eight specified directions in July. These data were derived from wind velocity measurements (Brower et al., 1977) compiled at stations near Region B for maximum fetch conditions.

Hs (m)	1	2	3	4	5	6	7	8	9	10	11	12	13	TOTAL	%
N	8	1	+	0	+									9	
NE	14	5	0	1	+	+								20	
E	11	5	2	0	1	+								19	
SE	5	1	+	+	+									6	
S	4	1	0	1	1	0	+							7	
SW	7	0	3	1	1	0	+	0	+					12	
W	7	0	1	1	1	0	+							10	
NW	7	0	1	+	+	0	0	0	+					8	
CALM	9													9	
TOTAL%	72	13	7	4	4	+	+	0	+					100	

Table 16a. The predicted frequency of significant wave heights (Hs) in meters for waves from eight specified directions in August. These data were derived from wind velocity histograms (Brower et al., 1977) compiled at stations near Region B for maximum fetch conditions.

Tp(S)	2	4	6	8	10	12	14	16	TOTAL	%
N	1	7	1	+	+				9	
NE	1	5	13	1	+				20	
E	1	10	5	2	1				19	
SE	1	4	1	+	+				6	
S	+	2	3	1	1				7	
SW	+	3	7	1	1	+			12	
W	1	3	4	1	1	+			10	
NW	1	3	4	+	+	+			8	
CALM	9								9	
TOTAL%	15	37	38	6	4	+			100	

Table 16b. The predicted frequency of peak wave periods (Tp) in seconds for waves coming from eight specified directions in August. These data were derived from wind velocity measurements (Brower et al., 1977) compiled at stations near Region B for maximum fetch conditions.

H _s (m)	1	2	3	4	5	6	7	8	9	10	11	12	13	TOTAL %
N	7	1	0	+	+									8
NE	16	0	6	4	+									26
E	12	6	5	2	0	+	+							25
SE	6	1	+	+	0	+								7
S	5	1	0	1	+	0	+							7
SW	5	0	2	1	+	0	+							8
W	3	0	2	+	+	+								6
NW	3	1	0	1	+	0	+							6
CALM	7													7
TOTAL%	64	10	15	10	1	+	+							100

Table 17a. The predicted frequency of significant wave heights (H_s) in meters for waves from eight specified directions in September. These data were derived from wind velocity histograms (Brower et al., 1977) compiled at stations near Region B for maximum fetch conditions.

T _p (S)	2	4	6	8	10	12	14	16	TOTAL %
N	1	3	4	+	+				8
NE	1	6	15	3	1	+			26
E	1	11	6	5	2	+			25
SE	1	5	1	+	+				7
S	+	5	1	1	+				7
SW	1	1	5	1	+	+			8
W	+	1	4	+	+	+			6
NW	+	1	3	1	+	+			6
CALM	7								7
TOTAL%	12	33	39	12	4	+			100

Table 17b. The predicted frequency of peak wave periods (T_p) in seconds for waves coming from eight specified directions in September. These data were derived from wind velocity measurements (Brower et al., 1977) compiled at stations near Region B for maximum fetch conditions.

Hs (m)	1	2	3	4	5	6	7	8	9	10	11	12	13	TOTAL %
N	2	1	0	+	+									3
NE	14	7	0	4	2	+								27
E	14	6	4	0	2	+								26
SE	12	1	+	+	+									13
S	7	2	0	1	+	0	+							10
SW	3	0	2	1	+	0	+	0	+					7
W	2	1	0	+	+									4
NW	2	0	1	+	+									3
CALM	7													7
TOTAL%	63	18	7	7	5	+	1	0	+					100

Table 18a. The predicted frequency of significant wave heights (Hs) in meters for waves from eight specified directions in October. These data were derived from wind velocity histograms (Brower et al., 1977) compiled at stations near Region B for maximum fetch conditions.

Tp(S)	2	4	6	8	10	12	14	16	TOTAL %
N	+	1	2	+	+				3
NE	1	6	14	4	2				27
E	1	13	6	4	2				26
SE	2	10	1	+	+				13
S	1	3	5	1	+				10
SW	+	1	4	1	+	+			7
W	+	1	2	+	+				4
NW	+	1	2	+	+				3
CALM	7								7
TOTAL%	12	36	36	11	5	+			100

Table 18b. The predicted frequency of peak wave periods (Tp) in seconds for waves coming from eight specified directions in October. These data were derived from wind velocity measurements (Brower et al., 1977) compiled at stations near Region B for maximum fetch conditions.

Hs (m)	1	2	3	4	5	6	7	8	9	10	11	12	13	TOTAL %
N	2	1	+	+	+									3
NE	11	7	7	3	0	2	+							30
E	10	6	6	3	0	2	+							27
SE	8	1	1	+	+									11
S	4	1	0	1	+	0	+	+						7
SW	3	1	0	2	1	0	1	+	0	0	+			9
W	2	1	0	1	+	+	0	+						5
NW	2	1	+	0	+	+								3
CALM	5													5
TOTAL%	47	19	15	11	2	5	1	+	0	0	+			100

Table 19a. The predicted frequency of significant wave heights (Hs) in meters for waves from eight specified directions in November. These data were derived from wind velocity histograms (Brower et al., 1977) compiled at stations near Region B for maximum fetch conditions.

Tp(S)	2	4	6	8	10	12	14	16	TOTAL %
N	+	2	1	+	+				3
NE	1	10	7	10	2	+			30
E	1	9	6	9	2				27
SE	1	7	1	1	+				11
S	+	2	3	1	+	+			7
SW	+	1	3	3	1	+	0	+	9
W	+	+	3	1	+	+			5
NW	+	2	1	+	+				3
CALM	5								5
TOTAL%	11	34	25	25	5	+	0	+	100

Table 19b. The predicted frequency of peak wave periods (Tp) in seconds for waves coming from eight specified directions in November. These data were derived from wind velocity measurements (Brower et al., 1977) compiled at stations near Region B for maximum fetch conditions.

H _s (m)	1	2	3	4	5	6	7	8	9	10	11	12	13	TOTAL %
N	4	1	+	+										5
NE	8	3	1	+										12
E	19	2	+	0	+	+	+							22
SE	6	1	+	+	+	0	+							8
S	4	4	0	3	2	1	0	1	0	+	+			15
SW	3	5	0	4	3	1	0	+	0	+	+			16
W	3	1	+	0	+	+								4
NW	5	1	+	+										6
CALM	12													12
TOTAL%	64	18	2	8	5	2	0	1	0	+	+			100

Table 20a. The predicted frequency of significant wave heights (H_s) in meters for waves from eight specified directions in July. These data were derived from wind velocity histograms (Brower et al., 1977) compiled at stations near Region B for mean fetch conditions.

T _p (S)	2	4	6	8	10	12	14	16	TOTAL %
N	1	3	1	+					5
NE	1	7	3	1					12
E	3	16	2	+	+	+			22
SE	1	5	1	+	+				8
S	+	1	7	3	3	1	+	+	15
SW	+	1	7	4	4	+	+	+	16
W	+	3	1	+	+				4
NW	1	4	1	+					
CALM	12								12
TOTAL%	19	40	23	9	5	1	+	+	100

Table 20b. The predicted frequency of peak wave periods (T_p) in seconds for waves coming from eight specified directions in July. These data were derived from wind velocity measurements (Brower et al., 1977) compiled at stations near Region B for mean fetch conditions.

H _s (m)	1	2	3	4	5	6	7	8	9	10	11	12	13	TOTAL %
N	8	1	+	+										9
NE	14	5	1	+	0	+								20
E	11	5	2	0	1	+								19
SE	5	1	+	+	+									6
S	4	1	0	1	1	0	+							7
SW	7	0	3	1	1	0	+	0	+					12
W	7	1	0	1	1	0	+							10
NW	7	1	+	0	+	0	+							8
CALM	9													9
TOTAL%	72	15	6	3	4	+	+	0	+					100

Table 21a. The predicted frequency of significant wave heights (H_s) in meters for waves from eight specified directions in August. These data were derived from wind velocity histograms (Brower et al., 1977) compiled at stations near Region B for mean fetch conditions.

T _p (S)	2	4	6	8	10	12	14	16	TOTAL %
N	1	7	1	+					9
NE	1	13	5	1	+				20
E	1	10	5	2	1				19
SE	1	4	1	+	+				6
S	+	2	3	1	1				7
SW	+	3	7	1	1	+			12
W	1	3	4	1	1				10
NW	1	6	1	+	+	+			8
CALM	9								9
TOTAL%	15	48	27	6	4	+			100

Table 21b. The predicted frequency of peak wave periods (T_p) in seconds for waves coming from eight specified directions in August. These data were derived from wind velocity measurements (Brower et al., 1977) compiled at stations near Region B for mean fetch conditions.

H _s (m)	1	2	3	4	5	6	7	8	9	10	11	12	13	TOTAL %
N	7	1	+	0	+									8
NE	16	6	4	0	+									26
E	12	6	5	2	0	+	+							25
SE	6	1	+	+	0	+								7
S	5	1	0	1	+	0	+							7
SW	5	0	2	1	+	0	+							8
W	3	0	2	+	+	+								6
NW	3	1	1	0	+	+								6
CALM	7													7
TOTAL%	64	16	14	5	1	+	+							100

Table 22a. The predicted frequency of significant wave heights (H_s) in meters for waves from eight specified directions in September. These data were derived from wind velocity histograms (Brower et al., 1977) compiled at stations near Region B for mean fetch conditions.

T _p (S)	2	4	6	8	10	12	14	16	TOTAL %
N	1	6	1	+	+				8
NE	1	15	6	3	1	+			26
E	1	11	6	5	2	+			25
SE	1	5	1	+	+				7
S	+	5	1	1	+				7
SW	1	1	5	1	+	+			8
W	+	1	4	+	+	+			6
NW	+	3	1	1	+	+			6
CALM	7								7
TOTAL%	12	47	25	12	4	+			100

Table 22b. The predicted frequency of peak wave periods (T_p) in seconds for waves coming from eight specified directions in September. These data were derived from wind velocity measurements (Brower et al., 1977) compiled at stations near Region B for mean fetch conditions.

H _s (m)	1	2	3	4	5	6	7	8	9	10	11	12	13	TOTAL %
N	2	1	+	+										3
NE	14	7	4	2	+									27
E	14	6	4	2	0	+								26
SE	12	1	+	+	+									13
S	7	2	0	1	+	0	+							10
SW	3	2	0	1	+	+	0	+						7
W	2	1	0	+	+									4
NW	2	1	+	0	+									3
CALM	7													7
TOTAL%	63	21	8	7	1	+	+	+						100

Table 23a. The predicted frequency of significant wave heights (H_s) in meters for waves from eight specified directions in October. These data were derived from wind velocity histograms (Brower et al., 1977) compiled at stations near Region B for mean fetch conditions.

T _p (S)	2	4	6	8	10	12	14	16	TOTAL %
N	+	2	1	+					3
NE	1	13	7	6	+				27
E	1	13	6	6	+				26
SE	2	10	1	+	+				13
S	1	3	5	1	+				10
SW	+	1	4	1	+				7
W	+	1	2	+	+				4
NW	+	2	1	+	+				3
CALM	7								7
TOTAL%	12	45	27	15	1				100

Table 23b. The predicted frequency of peak wave periods (T_p) in seconds for waves coming from eight specified directions in October. These data were derived from wind velocity measurements (Brower et al., 1977) compiled at stations near Region B for mean fetch conditions.

The maximum Hs and Tp found in the major open water months were 9 m and 12 s respectively (Tables 16 and 21, August) for waves coming from the southwest and northwest. Using the percentage frequency from Table 16 (a, b) or Table 21 (a, b) the joint probability of occurrence for Hs and Tp is $+ \cdot + = \sim (5 \times 10^{-3}) \cdot (5 \times 10^{-3})$ or .0025% in Region B for August. The largest possible Hs and Tp found were 12 m and 16 s respectively for waves from the southwest at maximum fetch in July (Table 15, Fig. 4a). This maximum fetch condition also has a 1% probability of occurrence in Region C and is independent of Hs and Tp. Therefore, the joint probability of the largest wave, calculated as for Region C (above), will equal $\sim .00000025\%$. Region B usually has the ice edge on its northern border (Fig. 4b) which means that winds from the south will create the largest waves.

Most potentially destructive wave directions are from the south and southwest for all the months of open water in Region B. This is generally due to the sea ice edge at it's northern boundary reducing the total fetch for northerly winds.

Region A

This is the farthest north of the three regions studied and, therefore, has the shortest open water season. It also has no complicating coastal areas so that the deep water statistics will apply to the entire region. The minimum ice edge position in the Chukchi Sea for July through November can be seen in Figs. 4a-8a. In November (Fig. 8a) the minimum sea ice position still covers more than 50% of the region. The mean Chukchi Sea ice edge position from August to October is shown in Figs. 5b-7b. Tables 24-28 and Tables 29-31 show Hs and Tp for maximum and mean fetch respectively. Due to the proximity of the ice edge there is considerable difference between corresponding maximum and mean fetch tables in all months.

Hs (m)	1	2	3	4	5	6	7	8	9	10	11	12	13	TOTAL %
N	4	1	+	+										5
NE	8	3	1	+										12
E	19	2	0	+	+	0	+	+						22
SE	6	1	+	+	0	+	+							8
S	4	0	4	3	2	0	1	0	1	0	+	+		15
SW	3	0	5	4	3	0	1	0	+	0	+	+		16
W	3	1	0	+	+	+								4
NW	5	1	+	+										6
CALM	12													12
TOTAL%	64	9	11	8	5	+	2	+	1	0	+	+		100

Table 24a. The predicted frequency of significant wave heights (Hs) in meters for waves from eight specified directions in July. These data were derived from wind velocity histograms (Brower et al., 1977) compiled at stations near Region A for maximum fetch conditions.

Tp(S)	2	4	6	8	10	12	14	16	TOTAL %
N	1	3	1	+					5
NE	1	7	3	1					12
E	3	9	9	+	+	+			22
SE	1	5	1	+	+	+			8
S	+	1	7	3	2	2	+	+	15
SW	+	1	7	4	3	1	+	+	16
W	+	1	3	+	+				4
NW	1	4	1	+					6
CALM	12								12
TOTAL%	19	31	32	9	6	3	+	+	100

Table 24b. The predicted frequency of peak wave periods (Tp) in seconds for waves coming from eight specified directions in July. These data were derived from wind velocity measurements (Brower et al., 1977) compiled at stations near Region A for maximum fetch conditions.

Hs (m)	1	2	3	4	5	6	7	8	9	10	11	12	13	TOTAL %
N	8	1	+	+										9
NE	14	5	1	+	0	+								20
E	11	5	0	2	1	0	+							19
SE	5	1	+	0	+	+								6
S	4	0	1	1	1	0	+							7
SW	7	0	3	1	1	0	+	0	+					12
W	7	0	1	1	1	0	+							10
NW	7	1	+	+	0	0	+							8
CALM	9													9
TOTAL%	72	13	6	5	4	+	+	0	+					100

Table 25a. The predicted frequency of significant wave heights (Hs) in meters for waves from eight specified directions in August. These data were derived from wind velocity histograms (Brower et al., 1977) compiled at stations near Region A for maximum fetch conditions.

Tp(S)	2	4	6	8	10	12	14	16	TOTAL %
N	1	7	1	+					9
NE	1	13	5	1	+				20
E	1	3	12	2	1				19
SE	1	4	1	+	+				6
S	+	2	3	1	1	+			7
SW	+	3	7	1	1	+			12
W	1	3	4	1	1	+			10
NW	1	6	1	+	0	+			8
CALM	9								9
TOTAL%	15	41	34	6	4	+			100

Table 25b. The predicted frequency of peak wave periods (Tp) in seconds for waves coming from eight specified directions in August. These data were derived from wind velocity measurements (Brower et al., 1977) compiled at stations near Region A for maximum fetch conditions.

H _s (m)	1	2	3	4	5	6	7	8	9	10	11	12	13	TOTAL %
N	7	1	+	+										8
NE	16	6	3	0	1	+								26
E	12	6	0	5	2	+	0	+						25
SE	6	1	0	+	+	+								7
S	5	0	1	1	+	0	+							7
SW	5	0	2	1	+	0	+							8
W	3	0	2	+	+	+								6
NW	3	1	1	0	+	+								6
CALM	7													7
TOTAL%	64	15	9	8	4	+	+	+						100

Table 26a. The predicted frequency of significant wave heights (H_s) in meters for waves from eight specified directions in September. These data were derived from wind velocity histograms (Brower et al., 1977) compiled at stations near Region A for maximum fetch conditions.

T _p (S)	2	4	6	8	10	12	14	16	TOTAL %
N	1	6	1	+					8
NE	1	15	6	3	1	+			26
E	1	4	13	5	2	+			25
SE	1	3	3	+	+	+			7
S	+	3	3	1	+	+			7
SW	1	1	5	1	+	+			8
W	+	1	4	+	+				6
NW	+	3	1	1	+	+			6
CALM	7								7
TOTAL%	12	36	36	12	4	+			100

Table 26b. The predicted frequency of peak wave periods (T_p) in seconds for waves coming from eight specified directions in September. These data were derived from wind velocity measurements (Brower et al., 1977) compiled at stations near Region A for maximum fetch conditions.

H _s (m)	1	2	3	4	5	6	7	8	9	10	11	12	13	TOTAL %
N	2	1	+	0	+									3
NE	14	7	4	0	2	+								27
E	14	6	0	4	2	0	+							26
SE	12	1	+	0	+	+								13
S	7	0	2	1	+	0	+							10
SW	3	0	2	1	+	0	+	0	+					7
W	2	0	1	+	+									4
NW	2	1	+	0	+									3
CALM	7													7
TOTAL%	63	16	9	6	5	1	+	0	+					100

Table 27a. The predicted frequency of significant wave heights (H_s) in meters for waves from eight specified directions in October. These data were derived from wind velocity histograms (Brower et al., 1977) compiled at stations near Region A for maximum fetch conditions.

T _p (S)	2	4	6	8	10	12	14	16	TOTAL %
N	+	2	1	+	+				3
NE	1	13	7	4	2	+			27
E	1	5	14	4	2				26
SE	2	10	1	+	+				13
S	1	3	3	3	+	+			10
SW	+	1	4	1	+	+			7
W	+	1	2	+	+				4
NW	+	2	1	+	+				3
CALM	7								7
TOTAL%	12	37	33	13	5	+			100

Table 27b. The predicted frequency of peak wave periods (T_p) in seconds for waves coming from eight specified directions in October. These data were derived from wind velocity measurements (Brower et al., 1977) compiled at stations near Region A for maximum fetch conditions.

Hs (m)	1	2	3	4	5	6	7	8	9	10	11	12	13	TOTAL %
N	2	1	+											3
NE	11	7	10	2	+									30
E	10	6	6	3	2	+								27
SE	8	1	1	+	0	+								11
S	4	0	1	1	+	0	+	0	+					7
SW	3	1	0	2	1	1	0	+	0	0	+			9
W	2	1	1	+	0	+	+							5
NW	2	1	+											3
CALM	5													5
TOTAL%	47	18	19	9	4	2	1	+	+	0	+			100

Table 28a. The predicted frequency of significant wave heights (Hs) in meters for waves from eight specified directions in November. These data were derived from wind velocity histograms (Brower et al., 1977) compiled at stations near Region A for maximum fetch conditions.

Tp(S)	2	4	6	8	10	12	14	16	TOTAL %
N	+	2	1	+					3
NE	4	7	14	5	+				30
E	1	9	6	9	2	+			27
SE	1	7	1	1	+				11
S	+	2	3	1	+	+			7
SW	+	1	3	2	1	1			9
W	+	2	1	1	+				5
NW	+	2	1	+					3
CALM	5								5
TOTAL%	14	32	30	20	3	1			100

Table 28b. The predicted frequency of peak wave periods (Tp) in seconds for waves coming from eight specified directions in November. These data were derived from wind velocity measurements (Brower et al., 1977) compiled at stations near Region A for maximum fetch conditions.

Hs (m)	1	2	3	4	5	6	7	8	9	10	11	12	13	TOTAL %
N	8	1	+											9
NE	14	5	1	+										20
E	11	5	2	0	1	+								19
SE	5	1	+	+	+									6
S	4	1	0	1	1	0	+							7
SW	7	0	3	1	1	0	+	0	+					12
W	7	1	1	0	1	+								10
NW	7	1	+	+										8
CALM	9													9
TOTAL%	72	15	7	2	4	+	+	0	+					100

Table 29a. The predicted frequency of significant wave heights (Hs) in meters for waves from eight specified directions in August. These data were derived from wind velocity histograms (Brower et al., 1977) compiled at stations near Region A for mean fetch conditions.

Tp(S)	2	4	6	8	10	12	14	16	TOTAL %
N	1	7	1	+					9
NE	1	13	6	+					20
E	1	10	5	2	1				19
SE	1	4	1	+	+				6
S	+	2	3	1	1				7
SW	+	3	7	1	1	+			12
W	1	6	1	1	1				10
NW	1	6	1	+					8
CALM	9								9
TOTAL%	15	51	25	5	4	+			100

Table 29b. The predicted frequency of peak wave periods (Tp) in seconds for waves coming from eight specified directions in August. These data were derived from wind velocity measurements (Brower et al., 1977) compiled at stations near Region A for mean fetch conditions.

H _s (m)	1	2	3	4	5	6	7	8	9	10	11	12	13	TOTAL	%
N	7	1	+	+										8	
NE	16	6	3	1	+									26	
E	12	6	5	2	+	+								25	
SE	6	1	+	+	0	+								7	
S	5	1	1	+	0	+								7	
SW	5	0	2	1	+	0	+							8	
W	3	2	0	+	+	+								6	
NW	3	1	1	+	+									6	
CALM	7													7	
TOTAL%	64	18	13	5	+	+	+							100	

Table 30a. The predicted frequency of significant wave heights (H_s) in meters for waves from eight specified directions in September. These data were derived from wind velocity histograms (Brower et al., 1977) compiled at stations near Region A for mean fetch conditions.

T _p (S)	2	4	6	8	10	12	14	16	TOTAL	%
N	1	6	1	+					8	
NE	1	15	6	3	1				26	
E	1	11	6	5	2	+			25	
SE	1	5	1	+	+				7	
S	+	5	2	+					7	
SW	1	1	5	1	+	+			8	
W	+	1	4	+	+	+			6	
NW	+	3	1	1	+				6	
CALM	7								7	
TOTAL%	12	47	26	11	4	+			100	

Table 30b. The predicted frequency of peak wave periods (T_p) in seconds for waves coming from eight specified directions in September. These data were derived from wind velocity measurements (Brower et al., 1977) compiled at stations near Region A for mean fetch conditions.

H _s (m)	1	2	3	4	5	6	7	8	9	10	11	12	13	TOTAL %
N	2	1	+											3
NE	14	11	2											27
E	14	6	4	2										26
SE	12	1	+											13
S	7	3	+											10
SW	3	2	1	0	+	+	0	+						7
W	2	1	+	0	+	+								4
NW	2	1	+											3
CALM	7													7
TOTAL%	63	26	8	2	1	+	0	+						100

Table 31a. The predicted frequency of significant wave heights (H_s) in meters for waves from eight specified directions in October. These data were derived from wind velocity histograms (Brower et al., 1977) compiled at stations near Region A for mean fetch conditions.

T _p (S)	2	4	6	8	10	12	14	16	TOTAL %
N	+	2	1	+					3
NE	1	13	11	2					27
E	1	13	10	2					26
SE	2	10	1	+					13
S	1	6	3	+					10
SW	+	3	2	1	+	+			7
W	+	2	1	+	+				4
NW	+	2	1	+					3
CALM	7								7
TOTAL%	12	51	30	6	1	+			100

Table 31b. The predicted frequency of peak wave periods (T_p) in seconds for waves coming from eight specified directions in October. These data were derived from wind velocity measurements (Brower et al., 1977) compiled at stations near Region A for mean fetch conditions.

The maximum Hs and Tp found for maximum fetch conditions (1% probability) were 12 m and 16 s respectively for waves generally from the south to southwest in July, (Table 24). The joint probability of this large wave in July is \sim .00000025%. The maximum Hs and Tp found for average fetch conditions were 9 m and 12 s respectively for waves from the southwest in August (Table 29). The joint probability of occurrence for this wave is .0025%.

Most potentially destructive large wave directions are from the south and southwest for all the months of open water in Region A. This is due to the sea ice edge, which usually exists at or within its northern boundary, reducing the total fetch for northerly and northeasterly winds which are the most common.

Five Percent Highest Waves

The maximum Hs for Regions A, B and C was 12 m. The height of the 5% highest waves (H5) conversion factor (1.73) applied to 12 m, results in a 20.8 m wave. The probability of this large wave is, however, less than .00000025% (see above) in any month.

WAVE BREAKING STATISTICS

The five shoreline orientations (Wise et al., 1981) included in this section (Fig. 1) are contained in Region C (2-5) and Region B(1). Frequency tables of breaking wave height (H), breaking water depth (D) and wave run-up (R) were derived from equations in the WAVE BREAKING CRITERIA and WAVE RUN-UP sections above and additional considerations of the joint probabilities of Hs, Tp and wave direction. Table 32 shows the beach slope, appropriate region statistics (A, B or C), and major wave directions contributing to the

TABLE 32

Coastline	1	2	3	4	5
Beach Slope	1/65	1/65	1/100	1/100	1/130
Regional Wave Statistics Used in Deep Water Basin	B	C	C	C/local waves	C
Wave Direction Contributing to H, D and R	N,SW W,NW	W,SW S,SE	NW	E	N,NW W

Table 32. The beach slope, appropriate region statistics (A, B, or C) and major wave directions contributing to the calculation of H, D and R.

calculation of H, D and R. The beach slopes were taken from standard nautical charts (NOS 16003, 1975 and DMA 16002, 1977) and computed by taking the minimum distance of the 10 fathom curve to the coast. This results in maximum slopes which give worst possible run-up conditions. The typical demarcation lines between the nearshore (breaker zone) and offshore regions are characterized by the water depth contours of 5 m, 5 m, 3 m, 3 m and 5 m for coastlines 1, 2, 3, 4, and 5 respectively. These contours are generally parallel to and inside the 10 m contour lines shown in Fig. 1. For some unusually large waves, however, a maximum breaking wave height of 10 m and breaking water depth of 16 m was calculated. The relatively shallower breaking water depths for coastline 3 and 4 (Fig. 1) are due to their short fetches and smaller locally generated waves.

The monthly and combined average (all possible months) frequency tables of H, D and R for maximum and mean fetches involving coastlines 1-5 are presented in Tables 33-42. The wave run-up in all tables is less than 1 m due to the relatively gentle beach slopes found. This 1 m run-up means that structures in these shore areas will be relatively safe. However, a pollutant such as oil may be washed far inland if the terrain slope is also gentle.

Coastline 1

This is the farthest north and longest coastline in the study (Fig. 1) and it is open to wave impingement from June through November (Fig. 3a-8a) under minimum ice edge conditions (Table 33). Table 32 shows that the main wave directions contributing to H, D and R are from the N, SW, W and NW. Table 33f shows that November would be the most destructive month with 28% of its wave breaking heights equal to 3 m or greater and 23% of its breaking wave depths, 4 m or greater. November also shows a remote possibility

(M)	1	2	3	4	5	6	7	8	9	10	11	12	13	14	15	16	%
H	85	10	5	+	+												100
D	83	5	10	2	+	+	+	+									100
R	100																100

Table 33a. Frequency table of breaking wave height (H), breaking water depth (D), and wave run-up (R) for coastline 1 in June under maximum fetch conditions.

(M)	1	2	3	4	5	6	7	8	9	10	11	12	13	14	15	16	%
H	76	16	7	1	+	+	+	+									100
D	74	14	9	2	1	+	+	+	+								100
R	100																100

Table 33b. Frequency table of breaking wave height (H), breaking water depth (D), and wave run-up (R) for coastline 1 in July under maximum fetch conditions.

(M)	1	2	3	4	5	6	7	8	9	10	11	12	13	14	15	16	%
H	78	17	3	2	1	+	+	+	+	+							100
D	75	18	3	2	1	1	+	+	+	+	+	+					100
R	100																100

Table 33c. Frequency table of breaking wave height (H), breaking water depth (D), and wave run-up (R) for coastline 1 in August under maximum fetch conditions.

(M)	1	2	3	4	5	6	7	8	9	10	11	12	13	14	15	16	%
H	75	15	5	3	2	+	+										100
D	74	14	4	3	2	2	1	+									100
R	100																100

Table 33d. Frequency table of breaking wave height (H), breaking water depth (D), and wave run-up (R) for coastline 1 in September under maximum fetch conditions.

(M)	1	2	3	4	5	6	7	8	9	10	11	12	13	14	15	16	%
H	88	10	2	+	+	+											100
D	88	8	3	1	+	+	+	+	+								100
R	100																100

Table 33e. Frequency table of breaking wave height (H), breaking water depth (D), and wave run-up (R) for coastline 1 in October under maximum fetch conditions.

(M)	1	2	3	4	5	6	7	8	9	10	11	12	13	14	15	16	%
H	55	17	12	10	3	2	1	+	+	+							100
D	54	10	13	8	8	3	2	1	1	+	+	+	+				100
R	100	+															

Table 33f. Frequency table of breaking wave height (H), breaking water depth (D), and wave run-up (R) for coastline 1 in November under maximum fetch conditions.

(M)	1	2	3	4	5	6	7	8	9	10	11	12	13	14	15	16	%
H	76	14	6	3	1	+	+	+	+	+							100
D	74	12	7	3	2	1	1	+	+	+	+	+	+				100
R	100																100

Table 33g. Average of Tables 33(a-f) under maximum fetch conditions for Coastline 1.

(M)	1	2	3	4	5	6	7	8	9	10	11	12	13	14	15	16	%
H	78	15	6	1	+	+	+										100
D	74	15	9	2	+	+	+	+	+								100
R	100	+															100

Table 34a. Frequency table of breaking wave height (H), breaking water depth (D), and wave run-up (R) for coastline 1 in July under mean fetch conditions.

(M)	1	2	3	4	5	6	7	8	9	10	11	12	13	14	15	16	%
H	78	18	2	1	1	+	+	+									100
D	75	18	4	1	1	1	+	+	+	+							100
R	100																100

Table 34b. Frequency table of breaking wave height (H), breaking water depth (D), and wave run-up (R) for coastline 1 in August under mean fetch conditions.

(M)	1	2	3	4	5	6	7	8	9	10	11	12	13	14	15	16	%
H	85	10	4	1	+												100
D	84	8	5	2	1	+	+										100
R	100																100

Table 34c. Frequency table of breaking wave height (H), breaking water depth (D), and wave run-up (R) for coastline 1 in September under mean fetch conditions.

(M)	1	2	3	4	5	6	7	8	9	10	11	12	13	14	15	16	%
H	89	9	1	1	+	+											100
D	88	8	4	+	+	+	+										100
R	100																100

Table 34d. Frequency table of breaking wave height (H), breaking water depth (D), and wave run-up (R) for coastline 1 in October under mean fetch conditions.

(M)	1	2	3	4	5	6	7	8	9	10	11	12	13	14	15	16	%
H	83	13	3	1	+	+	+	+									100
D	80	12	6	1	1	+	+	+	+	+							100
R	100																100

Table 34e. Average of Tables 34(a-d) under mean fetch conditions for coastline 1.

(M)	1	2	3	4	5	6	7	8	9	10	11	12	13	14	15	16	%
H	86	9	4	1	+	+	+	+									100
D	84	8	4	2	2	+	+	+	+	+							100
R	100																100

Table 35a. Frequency table of breaking wave height (H), breaking water depth (D), and wave run-up (R) for coastline 2 in June under maximum fetch conditions.

(M)	1	2	3	4	5	6	7	8	9	10	11	12	13	14	15	16	%
H	67	11	11	7	3	1	+	+	+	+							100
D	65	10	10	5	6	3	1	+	+	+	+	+	+	0	+	+	100
R	100																100

Table 35b. Frequency table of breaking wave height (H), breaking water depth (D), and wave run-up (R) for coastline 2 in July under maximum fetch conditions.

(M)	1	2	3	4	5	6	7	8	9	10	11	12	13	14	15	16	%
H	65	15	10	5	4	1	+	+	+								100
D	63	14	9	6	5	2	1	+	+	+							100
R	100																100

Table 35c. Frequency table of breaking wave height (H), breaking water depth (D), and wave run-up (R) for coastline 2 in August under maximum fetch conditions.

(M)	1	2	3	4	5	6	7	8	9	10	11	12	13	14	15	16	%
H	78	7	6	9	1	+	+	+	+								100
D	77	6	5	8	3	1	+	+	+	+							100
R	100																100

Table 35d. Frequency table of breaking wave height (H), breaking water depth (D), and wave run-up (R) for coastline 2 in September under maximum fetch conditions.

(M)	1	2	3	4	5	6	7	8	9	10	11	12	13	14	15	16	%
H	83	12	3	2	+	+	+	+									100
D	81	10	4	3	1	1	+	+	+	+							100
R	100																100

Table 35e. Frequency table of breaking wave height (H), breaking water depth (D), and wave run-up (R) for coastline 2 in October under maximum fetch conditions.

(M)	1	2	3	4	5	6	7	8	9	10	11	12	13	14	15	16	%
H	73	14	4	4	2	2	1	+	+	+							100
D	70	13	6	3	2	2	1	1	1	1	+	+	+				100
R	100																100

Table 35f. Frequency table of breaking wave height (H), breaking water depth (D), and wave run-up (R) for coastline 2 in November under maximum fetch conditions.

(M)	1	2	3	4	5	6	7	8	9	10	11	12	13	14	15	16	%
H	67	14	10	6	2	1	+	+	+	+							100
D	68	12	8	5	4	2	1	+	+	+							100
R	100																100

Table 35g. Average of Tables 35(a-f) under maximum fetch conditions for coastline 2.

(M)	1	2	3	4	5	6	7	8	9	10	11	12	13	14	15	16	%
H	67	11	11	7	3	1	+	+	+	+							100
D	65	10	10	5	6	3	1	+	+	+	+	+	+	0	+	+	100
R	100																100

Table 36a. Frequency table of breaking wave height (H), breaking water depth (D), and wave run-up (R) for coastline 2 in July under mean fetch conditions.

(M)	1	2	3	4	5	6	7	8	9	10	11	12	13	14	15	16	%
H	65	15	10	5	4	1	+	+	+								100
D	63	14	9	6	5	2	1	+	+	+							100
R	100																100

Table 36b. Frequency table of breaking wave height (H), breaking water depth (D), and wave run-up (R) for coastline 2 in August under mean fetch conditions.

(M)	1	2	3	4	5	6	7	8	9	10	11	12	13	14	15	16	%
H	78	7	6	9	1	+	+	+	+								100
D	77	6	5	8	3	1	+	+	+	+							100
R	100																100

Table 36c. Frequency table of breaking wave height (H), breaking water depth (D), and wave run-up (R) for coastline 2 in September under mean fetch conditions.

(M)	1	2	3	4	5	6	7	8	9	10	11	12	13	14	15	16	%
H	83	12	3	2	+	+	+	+									100
D	81	10	4	3	1	1	+	+	+	+							100
R	100																100

Table 36d. Frequency table of breaking wave height (H), breaking water depth (D), and wave run-up (R) for coastline 2 in October under mean fetch conditions.

(M)	1	2	3	4	5	6	7	8	9	10	11	12	13	14	15	16	%
H	72	11	8	6	2	1	+	+	+	+	+	+	+	0	+	+	100
D	70	10	7	6	4	2	1	+	+	+							100
R	100																100

Table 36e. Average of Tables 36(a-d) under mean fetch conditions for coastline 2.

(M)	1	2	3	4	5	6	7	8	9	10	11	12	13	14	15	16	%
H	96	3	1	+	+	+											100
D	95	3	1	1	+	+	+										100
R	100																100

Table 37a. Frequency table of breaking wave height (H), breaking water depth (D), and wave run-up (R) for coastline 3 in June under maximum fetch conditions.

(M)	1	2	3	4	5	6	7	8	9	10	11	12	13	14	15	16	%
H	96	3	1	+	+												100
D	95	4	1	+	+	+											100
R	100																100

Table 37b. Frequency table of breaking wave height (H), breaking water depth (D), and wave run-up (R) for coastline 3 in July under maximum fetch conditions.

(M)	1	2	3	4	5	6	7	8	9	10	11	12	13	14	15	16	%
H	90	5	4	1	+	+	+	+	+								100
D	88	4	3	3	2	+	+	+	+	+	+	+					100
R	100																100

Table 37c. Frequency table of breaking wave height (H), breaking water depth (D), and wave run-up (R) for coastline 3 in August under maximum fetch conditions.

(M)	1	2	3	4	5	6	7	8	9	10	11	12	13	14	15	16	%
H	95	4	1	+	+	+											100
D	93	5	1	1	+	+	+	+	+	+							100
R	100																100

Table 37d. Frequency table of breaking wave height (H), breaking water depth (D), and wave run-up (R) for coastline 3 in September under maximum fetch conditions.

(M)	1	2	3	4	5	6	7	8	9	10	11	12	13	14	15	16	%
H	65	14	10	8	3	+	+										100
D	62	12	11	6	4	3	2	+	+	+	+						100
R	100																100

Table 37e. Frequency table of breaking wave height (H), breaking water depth (D), and wave run-up (R) for coastline 3 in October under maximum fetch conditions.

(M)	1	2	3	4	5	6	7	8	9	10	11	12	13	14	15	16	%
H	90	4	3	2	1	+	+	+									100
D	89	4	3	2	1	1	+	+	+	+	0	+					100
R	100																100

Table 37f. Frequency table of breaking wave height (H), breaking water depth (D), and wave run-up (R) for coastline 3 in November under maximum fetch conditions.

(M)	1	2	3	4	5	6	7	8	9	10	11	12	13	14	15	16	%
H	87	6	4	2	1	+	+	+	+								100
D	87	5	4	2	1	1	+	+	+	+	+	+					100
R	100																100

Table 37g. Average of Tables 37(a-f) under maximum fetch conditions for coastline 3.

(M)	1	2	3	4	5	6	7	8	9	10	11	12	13	14	15	16	%
H	96	3	1	+	+												100
D	95	4	1	+	+	+											100
R	100																100

Table 38a. Frequency table of breaking wave height (H), breaking water depth (D), and wave run-up (R) for coastline 3 in July under mean fetch conditions.

(M)	1	2	3	4	5	6	7	8	9	10	11	12	13	14	15	16	%
H	90	5	4	1	+	+	+	+	+								100
D	88	4	3	3	2	+	+	+	+	+	+	+					100
R	100																100

Table 38b. Frequency table of breaking wave height (H), breaking water depth (D), and wave run-up (R) for coastline 3 in August under mean fetch conditions.

(M)	1	2	3	4	5	6	7	8	9	10	11	12	13	14	15	16	%
H	95	4	1	+	+	+											100
D	93	5	1	1	+	+	+	+	+	+	+	+					100
R	100																100

Table 38c. Frequency table of breaking wave height (H), breaking water depth (D), and wave run-up (R) for coastline 3 in September under mean fetch conditions.

(M)	1	2	3	4	5	6	7	8	9	10	11	12	13	14	15	16	%
H	70	15	8	5	2	+	+	+									100
D	68	14	7	6	3	2	+	+	+	+							100
R	100																100

Table 38d. Frequency table of breaking wave height (H), breaking water depth (D), and wave run-up (R) for coastline 3 in October under mean fetch conditions.

(M)	1	2	3	4	5	6	7	8	9	10	11	12	13	14	15	16	%
H	86	7	4	2	1	+	+	+	+								100
D	85	7	3	3	1	1	+	+	+	+	+	+					100
R	100																100

Table 38e. Average of Table 38(a-d) under mean fetch conditions for coastline 3.

(M)	1	2	3	4	5	6	7	8	9	10	11	12	13	14	15	16	%
H	98	2	+														100
D	94	5	1														100
R	100																100

Table 39a. Frequency table of breaking wave height (H), breaking water depth (D), and wave run-up (R) for coastline 4 in June under maximum fetch conditions.

(M)	1	2	3	4	5	6	7	8	9	10	11	12	13	14	15	16	%
H	96	4	+	+	+												100
D	82	17	1	+	+												100
R	100																100

Table 39b. Frequency table of breaking wave height (H), breaking water depth (D), and wave run-up (R) for coastline 4 in July under maximum fetch conditions.

(M)	1	2	3	4	5	6	7	8	9	10	11	12	13	14	15	16	%
H	95	3	2	+	+												100
D	93	5	2	+	+												100
R	100																100

Table 39c. Frequency table of breaking wave height (H), breaking water depth (D), and wave run-up (R) for coastline 4 in August under maximum fetch conditions.

(M)	1	2	3	4	5	6	7	8	9	10	11	12	13	14	15	16	%
H	85	12	3	+	+	+											100
D	82	10	5	3	+	+	+										100
R	100																100

Table 39d. Frequency table of breaking wave height (H), breaking water depth (D), and wave run-up (R) for coastline 4 in September under maximum fetch conditions.

(M)	1	2	3	4	5	6	7	8	9	10	11	12	13	14	15	16	%
H	90	8	2	+	+	+											100
D	85	10	3	2	+	+	+										100
R	100																100

Table 39e. Frequency table of breaking wave height (H), breaking water depth (D), and wave run-up (R) for coastline 4 in October under maximum fetch conditions.

(M)	1	2	3	4	5	6	7	8	9	10	11	12	13	14	15	16	%
H	92	1	5	1	1	+	+										100
D	92	1	4	2	1	+	+	+	+	+							100
R	100																100

Table 39f. Frequency table of breaking wave height (H), breaking water depth (D), and wave run-up (R) for coastline 4 in November under maximum fetch conditions.

(M)	1	2	3	4	5	6	7	8	9	10	11	12	13	14	15	16	%
H	93	5	2	+	+	+	+										100
D	88	8	3	1	+	+	+	+	+	+							100
R	100																100

Table 39g. Average of Tables 39(a-f) under maximum fetch conditions in coastline 4.

(M)	1	2	3	4	5	6	7	8	9	10	11	12	13	14	15	16	%
H	96	4	+	+	+												100
D	82	17	1	+	+												100
R	100																100

Table 40a. Frequency table of breaking wave height (H), breaking water depth (D), and wave run-up (R) for coastline 4 in July under mean fetch conditions.

(M)	1	2	3	4	5	6	7	8	9	10	11	12	13	14	15	16	%
H	95	3	2	+	+												100
D	93	5	2	+	+												100
R	100																100

Table 40b. Frequency table of breaking wave height (H), breaking water depth (D), and wave run-up (R) for coastline 4 in August under mean fetch conditions.

(M)	1	2	3	4	5	6	7	8	9	10	11	12	13	14	15	16	%
H	87	12	1	+	+												100
D	85	10	3	2	+	+											100
R	100																100

Table 40c. Frequency table of breaking wave height (H), breaking water depth (D), and wave run-up (R) for coastline 4 in September under mean fetch conditions.

(M)	1	2	3	4	5	6	7	8	9	10	11	12	13	14	15	16	%
H	95	3	2	+	+	+											100
D	90	8	1	1	+	+	+										100
R	100																100

Table 40d. Frequency table of breaking wave height (H), breaking water depth (D), and wave run-up (R) for coastline 4 in October under mean fetch conditions.

(M)	1	2	3	4	5	6	7	8	9	10	11	12	13	14	15	16	%
H	93	6	1	+	+	+											100
D	87	10	2	1	+	+	+										100
R	100																100

Table 40e. Average of Tables 40(a-d) under mean fetch conditions for coastline 4.

(M)	1	2	3	4	5	6	7	8	9	10	11	12	13	14	15	16	%
H	80	15	4	1	+	+											100
D	70	20	7	2	1	+	+	+									100
R	100																100

Table 41a. Frequency table of breaking wave height (H), breaking water depth (D), and wave run-up (R) for coastline 5 in June under maximum fetch conditions.

(M)	1	2	3	4	5	6	7	8	9	10	11	12	13	14	15	16	%
H	90	8	2	+	+	+											100
D	86	11	2	1	+	+	+										100
R	100																100

Table 41b. Frequency table of breaking wave height (H), breaking water depth (D), and wave run-up (R) for coastline 5 in July under maximum fetch conditions.

(M)	1	2	3	4	5	6	7	8	9	10	11	12	13	14	15	16	%
H	70	15	6	7	2	+	+	+	+	+							100
D	65	12	8	7	6	2	+	+	+	+	+	+	+				100
R	100																100

Table 41c. Frequency table of breaking wave height (H), breaking water depth (D), and wave run-up (R) for coastline 5 in August under maximum fetch conditions.

(M)	1	2	3	4	5	6	7	8	9	10	11	12	13	14	15	16	%
H	65	18	12	3	2	+	+	+	+								100
D	63	16	11	5	3	2	+	+	+	+	+						100
R	100																100

Table 41d. Frequency table of breaking wave height (H), breaking water depth (D), and wave run-up (R) for coastline 5 in September under maximum fetch conditions.

(M)	1	2	3	4	5	6	7	8	9	10	11	12	13	14	15	16	%
H	75	15	5	3	2	+	+	+	+								100
D	73	14	4	5	2	2	+	+	+	+	+						100
R	100																100

Table 41e. Frequency table of breaking wave height (H), breaking water depth (D), and wave run-up (R) for coastline 5 in October under maximum fetch conditions.

(M)	1	2	3	4	5	6	7	8	9	10	11	12	13	14	15	16	%
H	57	12	11	8	7	3	1	1	+								100
D	56	10	10	5	7	6	3	2	1	+	+	+	0	+			100
R	100																100

Table 41f. Frequency table of breaking wave height (H), breaking water depth (D), and wave run-up (R) for coastline 5 in November under maximum fetch conditions.

(M)	1	2	3	4	5	6	7	8	9	10	11	12	13	14	15	16	%
H	72	14	7	4	2	1	+	+	+	+							100
D	69	14	7	4	3	2	1	+	+	+	+	+	+	+			100
R	100																100

Table 41g. Average of Tables 41(a-f) under maximum fetch conditions for coastline 5.

(M)	1	2	3	4	5	6	7	8	9	10	11	12	13	14	15	16	%
H	80	15	5	+	+	+											100
D	70	20	7	2	1	+	+										100
R	100																100

Table 42a. Frequency table of breaking wave height (H), breaking water depth (D), and wave run-up (R) for coastline 5 in June under mean fetch conditions.

(M)	1	2	3	4	5	6	7	8	9	10	11	12	13	14	15	16	%
H	91	8	1	+	+	+											100
D	86	12	2	+	+	+	+										100
R	100																100

Table 42b. Frequency table of breaking wave height (H), breaking water depth (D), and wave run-up (R) for coastline 5 in July under mean fetch conditions.

(M)	1	2	3	4	5	6	7	8	9	10	11	12	13	14	15	16	%
H	70	15	7	6	2	+	+	+	+	+							100
D	65	12	8	7	6	2	+	+	+	+	+	+	+				100
R	100																100

Table 42c. Frequency table of breaking wave height (H), breaking water depth (D), and wave run-up (R) for coastline 5 in August under mean fetch conditions.

(M)	1	2	3	4	5	6	7	8	9	10	11	12	13	14	15	16	%
H	65	18	12	3	2	+	+	+	+								100
D	63	16	11	5	3	2	+	+	+	+	+						100
R	100																100

Table 42d. Frequency table of breaking wave height (H), breaking water depth (D), and wave run-up (R) for coastline 5 in September under mean fetch conditions.

(M)	1	2	3	4	5	6	7	8	9	10	11	12	13	14	15	16	%
H	79	16	4	1	+	+	+										100
D	76	15	5	2	2	+	+	+	+								100
R	100																100

Table 42e. Frequency table of breaking wave height (H), breaking water depth (D), and wave run-up (R) for coastline 5 in October under mean fetch conditions.

(M)	1	2	3	4	5	6	7	8	9	10	11	12	13	14	15	16	%
H	77	14	6	2	1	+	+	+	+	+							100
D	72	15	7	3	2	1	+	+	+	+	+	+	+				100
R	100																100

Table 42f. Average of Tables 42(a-e) under mean fetch conditions for coastline 5.

for a 10 m breaking wave in 13 m of water depth (< .5%). The joint probability of this occurrence is $(5 \times 10^{-3}) \cdot (1 \times 10^{-2})$ or .005% since the minimum ice edge position has a 1% probability of existence. The run-up should never exceed 1 m during the study months (Table 33g).

Coastline 1 will normally (Table 34, mean sea ice conditions) be open to destructive waves from only July through October (Figs. 4b-7b). The main wave directions are from N, SW, W, NW (Table 32). July is the month (Table 34a) where most damage can be done with 7% of the breaking wave heights at 3 m or above and 2% of its breaking wave depths at 4 m or greater. An 8 m breaking wave in 10 m water depth has a .5% probability during mean ice edge conditions. Again, the run-up should never exceed 1 m for all the study months (Table 34e).

Coastline 2

Table 32 shows that the main wave directions contributing to H, D and R are from the W, SW, S and SE for this coastline (Fig. 1). Table 35 was constructed for maximum fetch conditions (minimum sea ice extent) which have open water from June through November (Figs. 3a-8a). July waves have the most potential destruction along coastline 2. Table 35b shows that 23% of the wave breaking heights are 3 m or greater and 15% break in 4 m depths or greater. It is also possible (July) for a 10 m high wave to break in 16 m water depths. The probability of this wave occurring is .5% since the coastline orientation precludes wave impingement from fetch dependent directions to the north and July will always have open water to the south and southwest of this coastline (Fig. 4).

Coastline 2 will normally (Table 36, mean sea ice edge) be open to destructive waves from July through October (Figs. 4b-7b). The main wave directions are from the W, SW, S and SE (Table 32). Tables 36a and 35b are

identical for July since the major wave propagation directions are unaffected by sea ice in this month. Again, July is the month with greatest potential for destruction (see above paragraph). The combined average (Table 36e) statistics for the open water months affecting this coastline reflect the influence of July on the maximum wave breaking height (10 m) and breaking water depth (16 m).

Coastline 3

The wave direction (Table 32) contributing to H, D and R is from the NW for this coastline (Fig. 1). Table 37 was constructed for maximum fetch conditions (minimum sea ice extent) which have open water from June through November (Figs. 3a-8a). Table 38 (mean sea ice extent) was constructed for mean fetch conditions which have open water from July through October (Figs. 4b-7b). October is the most potentially destructive month for either maximum (Table 37e) or mean (Table 38d) fetch conditions. These maximum and mean tables show 21% and 15% breaking wave heights at 3 m or greater with 26% and 18% breaking in 3m depth or greater (respectively). The largest wave breaking height (9 m) and breaking depth (12 m) is seen in August for both fetch conditions also (Tables 37c and 38b). Their occurrence probability is .5% since the maximum fetch and mean fetch conditions do not affect the statistics in these months with large expanses of open water. The run-up in all months studied should be less than 1 m (Tables 37g and 38e).

Coastline 4

This coastline is the most protected (Fig. 1) of the five examined in this study. The major destructive wave direction is from the east thereby making land boundaries the primary reasons for limited fetch as long as sea

ice is not present. Table 39 (minimum sea ice extent) statistics are for maximum fetch conditions which have open water from June through November (Figs. 3a-8a). Table 40 (mean sea ice extent) statistics are for mean fetch conditions which have open water from July through October (Figs. 4b-7b). September waves are most severe under both maximum and mean fetch conditions. For maximum fetch, 15% of breaking wave heights and 18% of breaking wave depths equal 2 m or more (Table 39d). For mean fetch, 13% of breaking wave heights and 15% of breaking wave depths equal 2 m or more (Table 40c). November statistics (maximum fetch only, Table 39f) show a remote possibility (.005%) for a wave breaking height of 7 m and a breaking depth of 10 m. Again the run-up does not exceed 1 m in any of the study months (summarized in Tables 39g and 40e).

Coastline 5

This is the farthest south coastline (Fig. 1) in the study and it is open to wave impingement from June through November (Figs. 3a-8a) under minimum ice edge conditions. Table 32 shows that the main wave directions contributing to H, D and R are from the N, NW and W. Destructive wave impingement can exist in the months of June through October for mean ice edge conditions (Figs. 3b-7b). The statistics for July through October are almost identical (Tables 41b-e and 42b-e) for maximum or mean fetch conditions since coastline 5 is so far from the ice edge during these months. September is potentially the most destructive of these typical open water months (Table 41d or 42d). It has 17% of its wave breaking heights and 21% of its wave breaking depths greater than or equal to 3 m. For the typical open water months, the highest breaking wave (10 m) and greatest breaking wave depth (13 m) also occurs in August with a probability of .5%. November statistics

(maximum fetch only, Table 41f) show a remote chance (.005%) of a wave breaking height of 9 m and a breaking depth of 14 m. The run-up does not exceed 1 m in any study month (summarized in Table 41g and 42f).

SUMMARY

A wave hindcast technique was used to determine the months and locations of highest risk to oil and gas development in the Chukchi Sea area. Parameters required were fetch, wind duration, wind velocity, water depth and beach slope. From these, significant deep water wave heights and periods were tabulated for Chukchi regions A, B and C (Fig. 1.). The tabulations were used later to produce statistics of breaking wave heights and depths for five coastline orientations (Fig. 1). as defined by Wise et al. (1981).

Fetch conditions were controlled by both sea ice cover (Kozo, 1985) and coastlines thereby becoming highly directionally dependent. Wind duration and velocity data were taken (Brower et al., 1977) from designated land stations bordering the Chukchi study regions and/or designated marine areas. Water depths and beach slope were obtained from standard nautical charts and worst cases (steepest) used for slopes.

Deep water significant wave heights in Region C (Fig. 1) can reach 10 m coming from the south in July and from the northeast and southwest in September. The large waves coming from the northeast direction are due to the increased September fetch (Fig. 6b). The most potentially destructive wave directions are from the south in May (minimum sea ice extent) through July and from the north to northeast in August through November. Region B can have 9 m (Hs) waves in August, from both the southwest and northwest. The waves from the northwest are due to a larger fetch distance in the latter direction by August (Fig. 5b). Most potentially destructive wave directions are from the south and southwest for July through October. Region A, the farthest north of the three regions, can have 9 m waves (Hs) from the

southwest in August during average sea ice conditions. The most destructive wave directions are from the south and southwest for August through October, the main months of possible open water. The height of the 5% highest waves is $1.73 \times$ (significant wave height), therefore extreme waves of 15.5-17 m are possible in the three study regions.

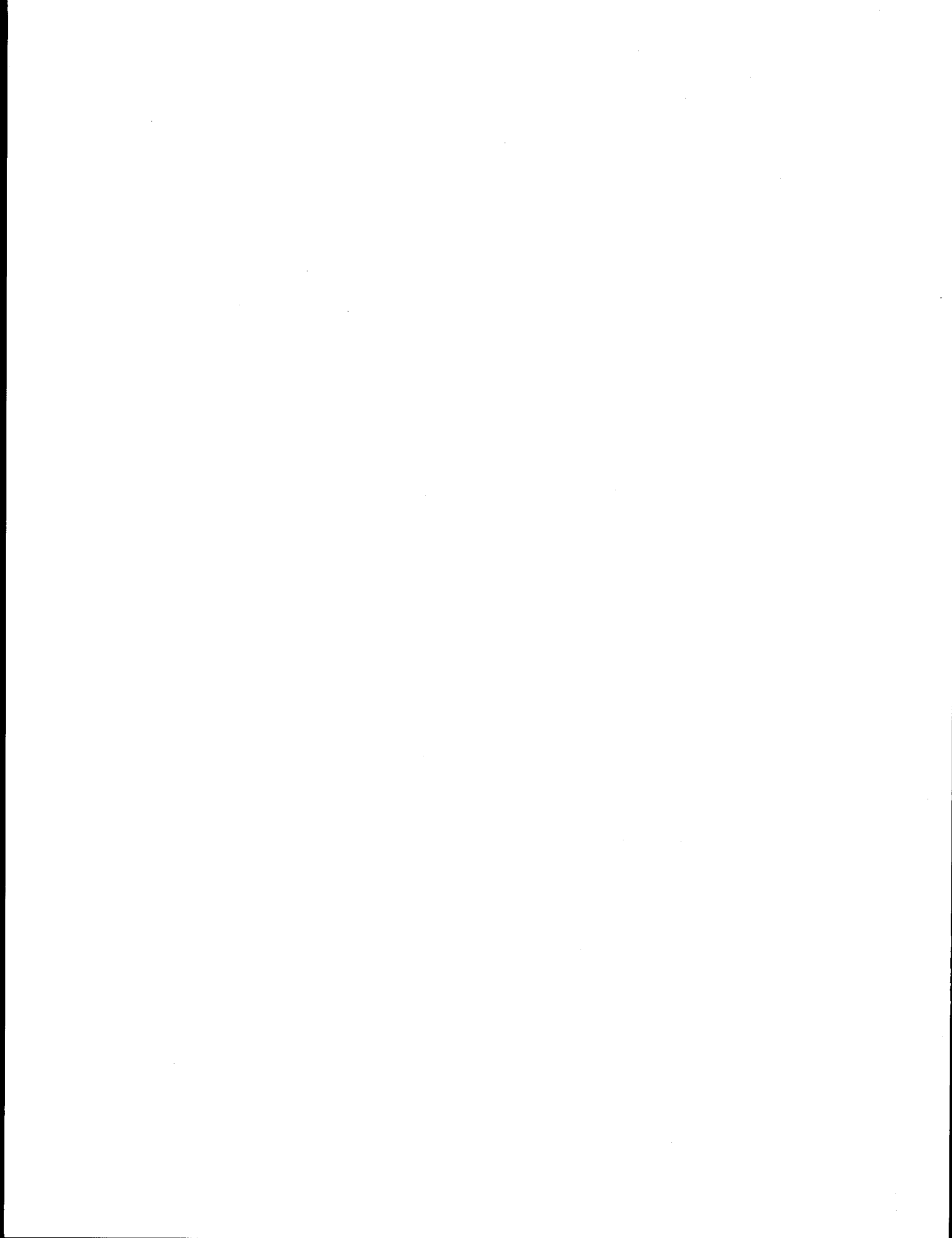
Wave breaking statistics were compiled for five coastlines (Fig. 1). Coastline 5, the farthest south (greatest fetch) is the one facing the most probable damage from waves. The main wave impingement directions are from the N, NW and W. September appears as the most severe of the typical open water months with a 17% probability of breaking wave heights at 3 m or above and a maximum height of 9 m possible. Wave run-up will be 1 m or less on all five coasts in all months, which implies limited damage on structures, but possible inland inundation for gentle sloping topography.

FURTHER STUDY

A summer wave parameter study through deployment of floating buoys in deep water offshore from the five coastlines should be started. Geostrophic wind histograms from historical data should be developed for the three regions on a monthly basis. Since many of the arctic coastal wind sites are affected by orography, the geostrophic directions and a modified wind speed (Kozo, 1984) would be a better input to the wave hindcast model.

ACKNOWLEDGEMENTS

This study was funded by the Minerals Management Service, U.S. Department of the Interior, through interagency agreement with the National Oceanic and Atmospheric Administration, U. S. Department of Commerce, as part of the Outer Continental Shelf Environmental Assessment Program.

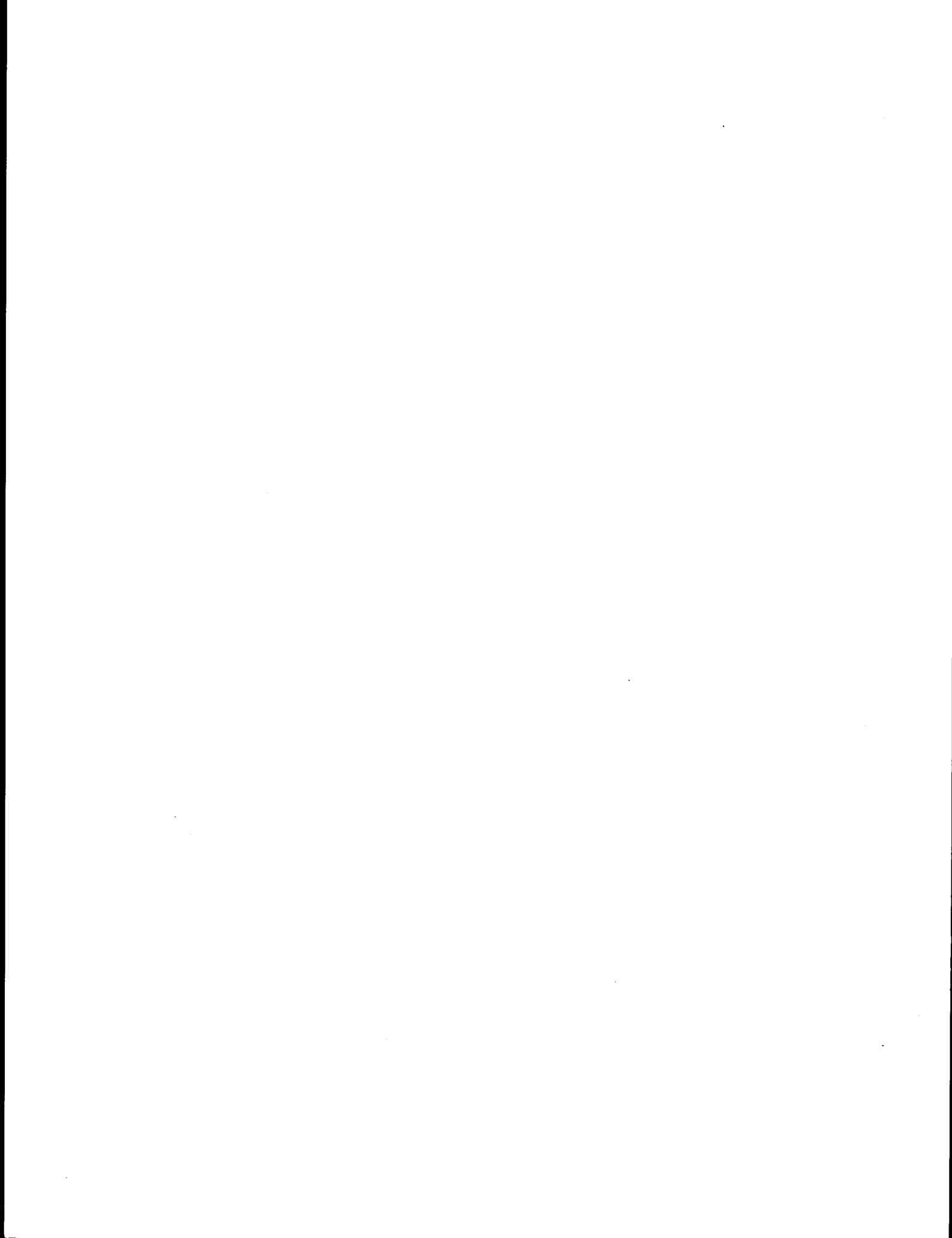


REFERENCES

- Battjes, J. A. 1974. Computation of set-up, longshore currents run-up and overtopping due to wind-generated waves. Communications on Hydraulics, Department of Civil Engineering, Delft University of Technology, Report 74-2.
- Brower, W. A., H. F. Diaz, A. S. Prechtel, H. W. Searby and J. L. Wise. 1977. Climatic atlas of the outer continental shelf waters and coastal regions of Alaska. NOAA, NCC, EDS, Ashville, North Carolina. 409 p.
- Collins, J. I. 1972. Prediction of shallow-water spectra. *J. Geophys. Res.* 77, 11:2693-2707.
- DMA, 16002, 1977. Approaches to Bering Strait, Defense Mapping Agency Hydrographic Center, Washington, D. C.
- Goda, Y. 1970. A synthesis of breaker indices. *Transactions of JSCE*, Vol. 2, Part 2, 227-230.
- Guttman, I. and S. S. Wilks, 1965. *Introductory Engineering Statistics*. John Wiley and Sons, Inc. New York, p. 87.
- Hasselmann, K. et al. 1973. Measurements of wind-wave growth and swell decay during the Joint North Sea Wave Project, Deutsches Hydrographisches Institut, Hamburg.
- Hasselmann, K. 1976. A parametric wave prediction model. *J. Phys. Ocean.* 6:200-228.
- Kitaigorodskii, S. A., V. P. Krasitskii and M. M. Zaslavskii. 1975. On Phillips' theory of equilibrium range in the spectra of wind-generated waves. *J. Phys. Ocean.* 5:410-420.

- Kozo, T. L. 1984. Mesoscale wind phenomena along the Alaska Beaufort Sea Coast, in *The Alaska Beaufort Sea: Ecosystems and Environment*. (Ed. by P. W. Barnes, D. M. Schell and E. Reimnitz). Academic Press, New York. pp. 23-45.
- Kozo, T. L. 1985. Superstructure icing in the North Chukchi, South Chukchi and Hope Basin areas. NOAA-OCS contract #NA84-ABC-00174 (Task 2). VANTUNA Research Group, Occidental College, Los Angeles. 46 pp.
- LeMehaute, B. and R. C. Y. Koh. 1967. On the breaking of waves arriving at an angle to the shore. *J. Hydraul. Res.*, 5, No. 1.
- Longuet-Higgins, M. S. 1957. On the transformation of a continuous spectrum by refraction. *Proceedings, Cambridge Phil. Soc.* 53:226-229.
- Longuet-Higgins, M. S., and R. W. Steward. 1960. Changes in the form of short gravity waves on long waves and tidal currents. *J. Fluid Mechan.* 8:565-583.
- NOS, 16003, 1975. Arctic Coast of Alaska, National Ocean Survey, U. S. Department of Commerce Nautical Chart, Washington, D.C.
- Phillips, O. M. 1958. The equilibrium range in the spectrum of wind-generated waves. *J. Fluid Mechan.* 4:426-434.
- Pierson, W. J., G. Newmann, and R. W. James. 1971. *Practical Methods of Observing and Forecasting Ocean Waves*. U. S. Naval Oceanographic Office Publ. #603. 283 pp.
- Stringer, W. J., 1984. Sea ice occurrence probability study. Geophysical Institute, University of Alaska, Fairbanks (unpublished).
- Thorton, E. B. 1977. Rederivation of the saturation range in the frequency spectrum of wind-generated gravity waves. *J. Phys. Ocean.*, Vol. 7, 1:137-140.

- Weggel, J. R. 1972. Maximum breaker height. *Journal of the Waterways, Harbors and Coastal Engineering Directory*, WW4, 529-548.
- Wise, J. L., A. L. Comiskey, and R. Becker. 1981. *Storm surge climatology and forecasting in Alaska*. Alaska Council on Science and Technology, Alaskan Natural Hazards Research. 45 pp.
- Wu, H. Y., E. Y. Hsu, and R. L. Street. 1979. Experimental study of non-linear wave-wave interaction and white-cap dissipation of wind-generated waves. *J. Dynam. Atmos. and Oceans* 3:55-78.
- Wu, H. Y., J. I. Collins and D. Divoky. 1980. Spectral wave set-up and run-up. National symposium on Urban Storm Water Management in Coastal Area. Blacksburg, Virginia, May 26-28.



HEADLAND MODELING APPLIED TO THE EASTERN
BEAUFORT SEA COAST

by

Thomas L. Kozo, Ph.D.

VANTUNA Research Group

Occidental College

Final Report
Outer Continental Shelf Environmental Assessment Program
Research Unit 519

1984

259

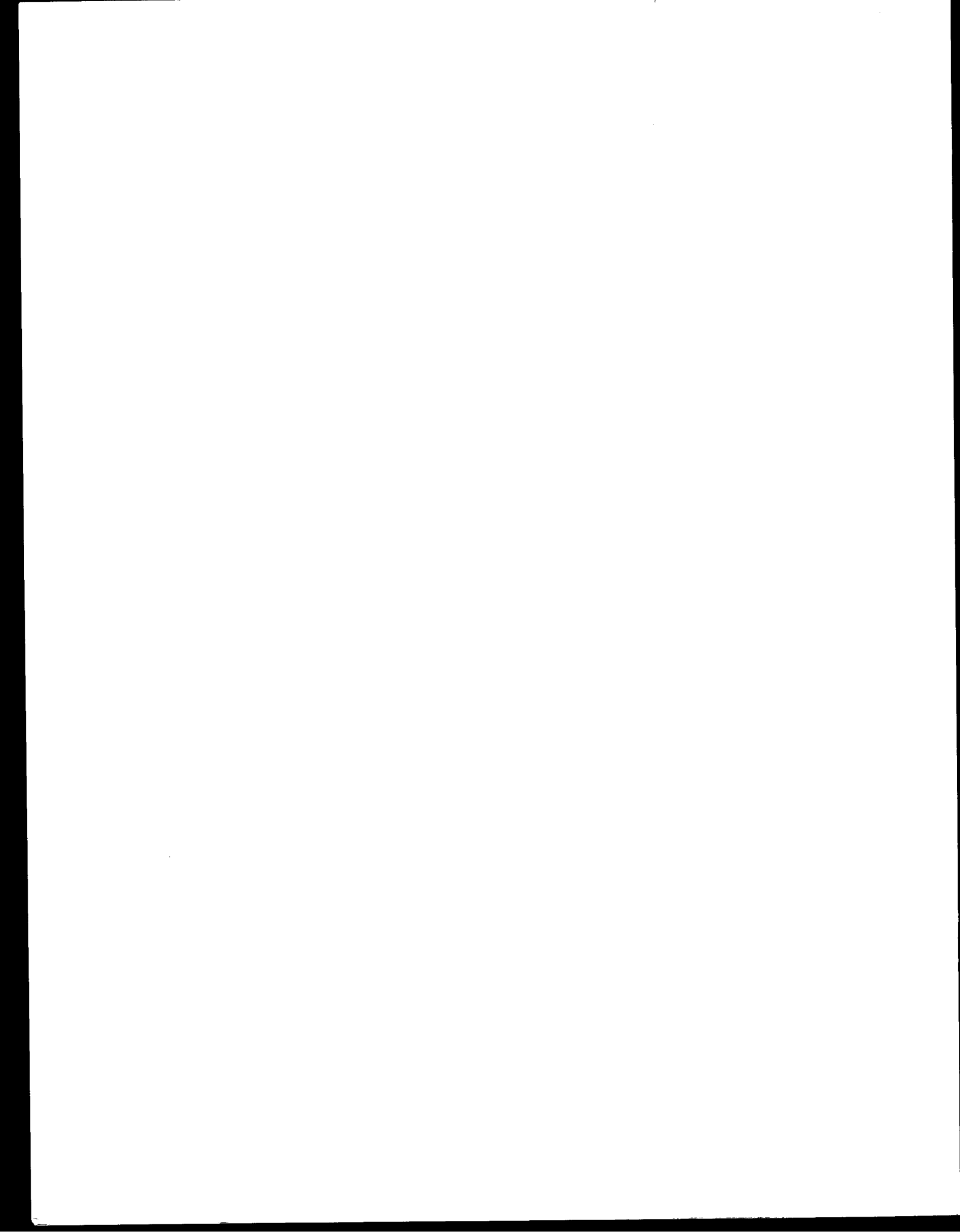


TABLE OF CONTENTS

LIST OF FIGURES.....	
LIST OF TABLES.....	
ABSTRACT.....	
INTRODUCTION.....	
STUDY AREA.....	
DATA.....	
PRESSURE DATA.....	
GEOSTROPHIC WIND DATA.....	
BUOY POSITION DATA.....	
RESULTS WITH DISCUSSION.....	
MODEL DESCRIPTION-WINDS.....	
MODEL DESCRIPTION-BUOY TRAJECTORIES.....	
SUMMARY AND CONCLUSIONS.....	
FUTURE WORK.....	
ACKNOWLEDGMENTS.....	
REFERENCES.....	
FIGURES (1-13).....	
TABLES (1-3).....	



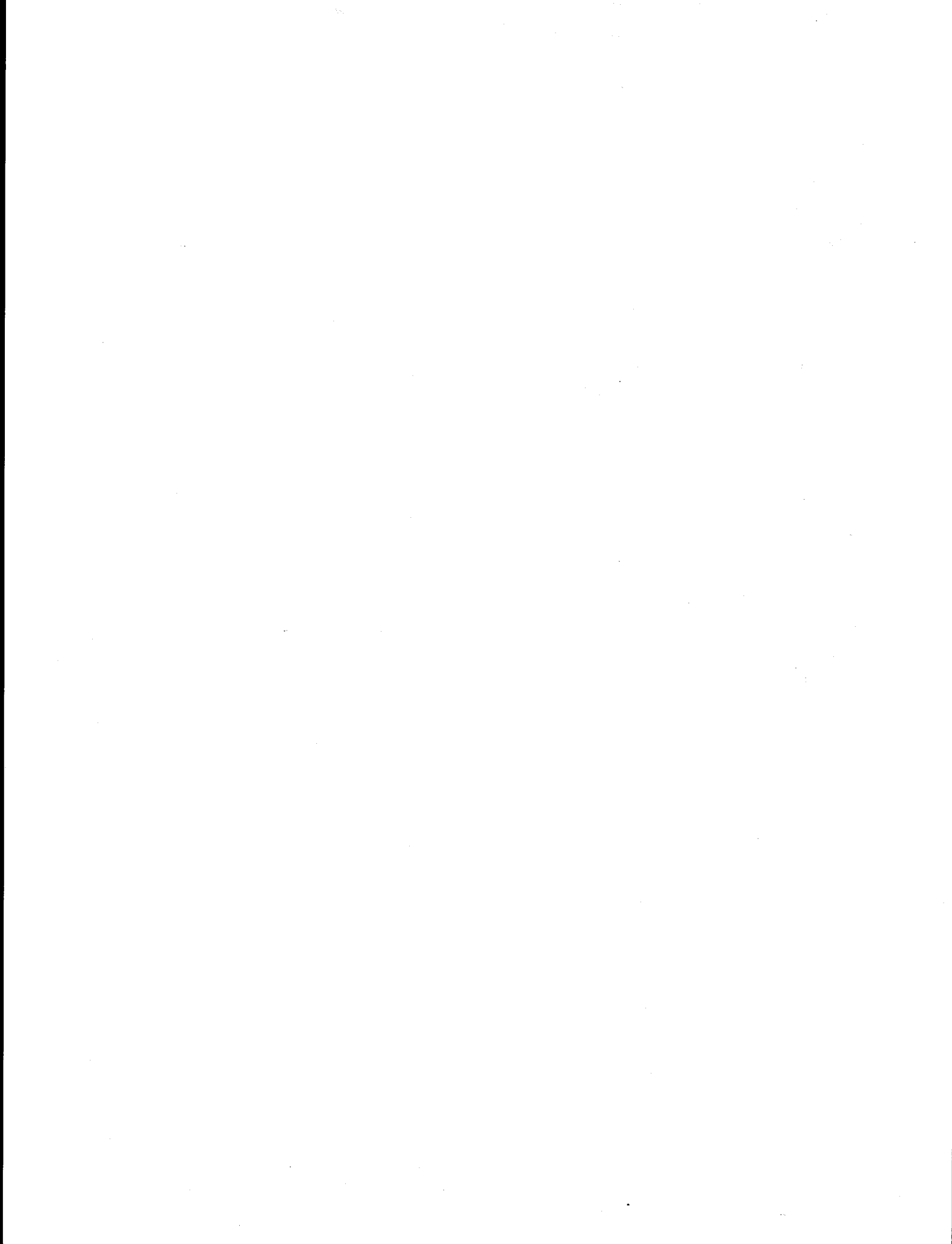
LIST OF FIGURES

- Figure 1. Topographic chart of northern Alaska (after Dickey, 1961) showing the 600 m contour of the Brooks Range approximated as a circular arc. Its radius (a) is computed to be 274 km and its hypothetical center is Z. The distance from Z to Barter Island is 322 km.....
- Figure 2. Pressure triangles used to compute geostrophic winds for August (ABC), September (CDE), and October (CFD) 1983. Data stations are Barrow (A), Franklin Bluffs (B), Barter Island (C), Inuvik (D), Tuktoyaktuk (E) and Sachs Harbor (F). 0 \equiv Buoy 4519, D \equiv 4518 (died 24 September 1983, position #3). Buoy position numbers 1-2 (August), 2-4 (September), 4-5 (October) indicate positions relative to pressure triangles. The dashed arc is the probable distance seaward of major orographic influence from the 600 m contour (cross hatched). Z \equiv hypothetical center of the circle matching the arc.....
- Figure 3. Surface pressure weather map (from Henry, 1975) showing resulting surface winds at shore stations. (Short flags $\sim 1.5-3.5 \text{ ms}^{-1}$; long flags $\sim 4.0-6.0 \text{ ms}^{-1}$).....
- Figure 4. Streamlines and velocity field around a fixed cylindrical barrier (Dickey, 1961) for irrotational, non-divergent flow of V_G . Numbers at points along the streamlines are wind speeds in multiples of the V_G . The B zones indicate higher than normal speeds and the A zones indicate reduced speeds.....
- Figure 5. Model generated U velocities in multiples of V_G magnitudes for V_G 's from the west.....
- Figure 6. Model generated U velocities in multiples of V_G magnitudes for V_G 's from the northwest.....
- Figure 7. Model generated U velocities in multiples of V_G magnitudes for V_G 's from the north.....
- Figure 8. Model generated U velocities in multiples of V_G magnitudes for V_G 's from the northeast.....
- Figure 9. Model generated U velocities in multiples of V_G magnitudes for V_G 's from the east.....

- Figure 10. Trajectories of buoys 4518 and 4519 (U.S. Coast Guard) during unimpeded drift. Parts of surrounding pressure triangles, and the average ice edge (greater than 50% coverage) for August, September and October 1983 are shown. The combined trajectory for September is designated x. The buoys were deployed 18 August 1983. Starting west and moving eastward, days 18-30 represent August positions, days 1-30 represent September positions and days 3-18 represent October positions.....
- Figure 11. The combined 4518 and 4519 drift compared to the model drift. Again the pressure triangles are shown in part. The buoys were deployed 18 August 1983 (ST) and were locked into the sea ice by 18 October 1983 (EM \equiv last model buoy position; EB \equiv last actual buoy position).....
- Figure 12. The bathymetry in the Mackenzie Bay area and its effect on wind driven surface currents (after MacNeill and Garrett, 1975). Actual buoy drift for 21-27 September 1983 shown as 0-0-0.....
- Figure 13. Flow chart for the wind-driven model.....

LIST OF TABLES

- Table 1. Calculated geostrophic wind speed (ms^{-1}) vs. direction
for August 1983.....
- Table 2. Calculated geostrophic wind speed (ms^{-1}) vs. direction
for September 1983.....
- Table 3. Calculated geostrophic wind speed (ms^{-1}) vs. direction
for October 1983.....



ABSTRACT

The United States Coast Guard deployed a cluster of satellite-transmitting, surface-drifting buoys in the Beaufort Sea north of Prudhoe Bay, Alaska on 17 August 1983. The surface currents in this coastal area are predominantly wind driven. An unusual stand of westerly winds led to eastward drift with the surviving buoys moving into an area north of Mackenzie Bay (Canada) by mid-October. The buoy motion suggested that they were driven by the geostrophic wind modified by the orographic "umbrella" of the Brooks Range. The mountain influence was seen to cover an arcuate zone at least 100 km seaward of the coast from Camden Bay (Alaska) to Mackenzie Bay. This is a headland effect on the wind of major proportions creating changes in direction and regions of super and subgeostrophic speeds over the coastal zone.

A simple model was developed to predict the wind modifications in this headland zone and the resultant wind-driven buoy drift. The initial wind velocity input to this model is a calculated geostrophic wind derived from triangular-shaped mesoscale atmospheric pressure networks. These networks were chosen because their boundaries alternately contained the trajectories of the eastward-moving buoys. The model then used this network velocity to generate the wind field at the buoy location and appropriate offshore area north of the Brooks Range. The mountain barrier was taken to have approximate cylindrical geometry and atmospheric flow conditions were assumed to be irrotational and non-divergent.

The actual buoy drift during the open water season covered 650 km in 60 days with the final model-predicted buoy-drift position in error by less than

50 km. The major error occurred when the buoys moved into shallow water in the Mackenzie Bay on 21 September 1983. One buoy was destroyed and the other was constrained to move parallel to the 10 m bottom contour. The Brooks Range influence did not appear to affect the October buoy drift which was north of Richards Island (Canada) above 70°N and east of 135°N.

INTRODUCTION

A headland or promontory (Crossley, 1938) of sufficient height and lateral dimensions will modify the large scale wind and pressure fields. Flow around an obstacle requires less energy than flow over the same obstacle in a stable atmospheric boundary layer, which often exists in arctic regions in all seasons (Kozo, 1984a, 1982). Zones of accelerated and decelerated, diverted flow will reach offshore from headlands for distances equal to the lateral dimensions of the obstacle (usually mesoscale effects). The exact positions of these stagnation or acceleration zones will shift with the direction of the incoming large-scale wind. Since ocean surface pollutant residence times the trajectories are of major concern in coastal zones, a model predicting the lateral extent and location of "abnormal" winds can be very useful. The utility is magnified in coastal zones such as found in the Alaskan Beaufort where the surface currents are primarily wind driven (Aagaard, 1984).

A simple model utilizing combinations of mesoscale atmospheric pressure networks (Kozo, 1980, 1982, 1984a) to calculate high resolution calculated geostrophic winds for initial input has been developed. This model then computes a new wind velocity for designated offshore areas as modified by flow around the Brooks Range. The method was pioneered by Dickey (1961) but extends his concepts spatially from land to offshore and temporally from winter to summer. Dickey (1961) approximated the 600 m contour of the Brooks Range (see Fig. 1) as a cylindrical barrier and calculated the velocity field around this barrier using basic hydrodynamical equations (i.e., Batchelor, 1967). His analysis was then used to explain the supergeostrophic

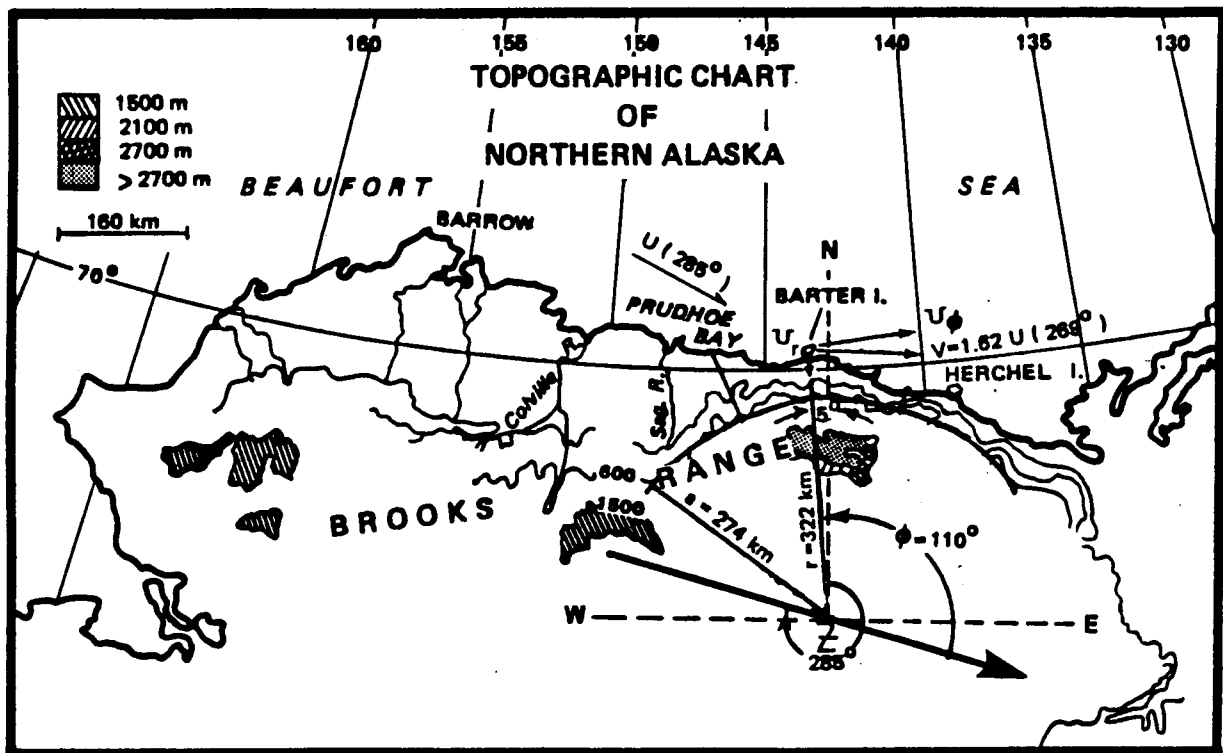


Figure 1. Topographic chart of northern Alaska (after Dickey, 1961) showing the 600 m contour of the Brooks Range approximated as a circular arc. Its radius (a) is computed to be 274 km and its hypothetical center is Z. The distance from Z to Barter Island is 322 km.

winds at Barter Island (Fig. 1), a main observation point on the Alaskan Beaufort coast. Twenty-four years later NOAA/MMS field work has expanded the data base offshore (Kozo, 1980, 1984a). In addition, the United States Coast Guard (Robe *et al.* 1984) has recently obtained buoy drift data (position and time) which have shown open-water movement characteristics that could only be explained by Dickey's (1961) original hypothesis. Therefore, matching the empirical buoy drift positions with model buoy drift positions has provided a means of predicting wind modification zones and buoy movement as well.

STUDY AREA

Figure 1 shows the Beaufort Sea coast of Alaska and Canada with the 600 m contour of the Brooks Range approximated as a cylinder with a 274 km radius (z-axis vertical). Moving eastward, this contour approaches to within 40 km of the coast and stays even closer until well past Herschel Island (Canada). The coastal zones offshore from this encroaching mountain range will be subject to stable boundary layer induced orographic effects in winter or summer (Kozo, 1984a; see summer temperature profiles) which can dominate winds at least 100 km seaward (Kozo 1984b). Orographic effects several 100 km offshore have been documented in the Antarctic (Schwerdtfeger, 1979).

The mid-shelf (~ 50 m isobath) surface currents along the Alaskan Beaufort Sea coast are mainly wind driven (Aagaard, 1984). The typical wind direction at most surface data stations (Brower *et al.*, 1977) is from the northeast resulting in a net westward drift. Sea ice dominates this same coastal zone, covering it for at least nine months each year (open water season, about mid-July to mid-October). Again, it is the winds that play a major role in the sea ice edge position in these open water months (Kozo, 1984a). Results of Arctic research since the 1970's have shown that large

scale (synoptic-scale) weather map analyses have been inadequate for predicting surface winds or ice edge motion in the Alaskan Beaufort coast region (Rogers, 1978; Albright, 1978; Kozo, 1980). The main reason was the lack of National Weather Service (NWS) stations with only Barrow and Barter Island (Fig. 1) covering 540 km of coastline. There were none north of the coast, on a continuous basis, until the Arctic Basin Buoy Project (National Science Foundation) was begun in February 1979. The other reasons are the arctic sea breeze (Kozo, 1982) and the orographic modifications on the large scale wind produced by the Brooks Range for at least 50% of the Alaskan Beaufort coast. For the purposes of this study the sea breeze effect has been shown to be minimal 20 km seaward of the coast (Kozo 1982) and cannot be evaluated by examination of the Coast Guard buoy tracks.

DATA

PRESSURE DATA

Barometric pressure data reduced to sea level and temperature data were taken simultaneously from three-station weather networks and used to compute hypothetical geostrophic winds for the area enclosed by each network (Fig. 2). The stations A (Barrow), C (Barter Island), D (Inuvik, Canada) and E (Tuktoyaktuk, Canada) are part of a global weather network (first order stations) and transmit real-time data to the National Meteorological Center (NMC). The accuracies of their pressure and temperature data are better than $\pm .25$ mb and $\pm 1^\circ\text{C}$ respectively. Station B (Franklin Bluffs) was an unmanned satellite-transmitting pressure, temperature and position platform operating through System ARGOS and manufactured by Polar Research Laboratory in Santa Barbara, California. ARGOS is a cooperative project between Center National d' Etudes Spatiales (NES, France), National Aeronautics and Space

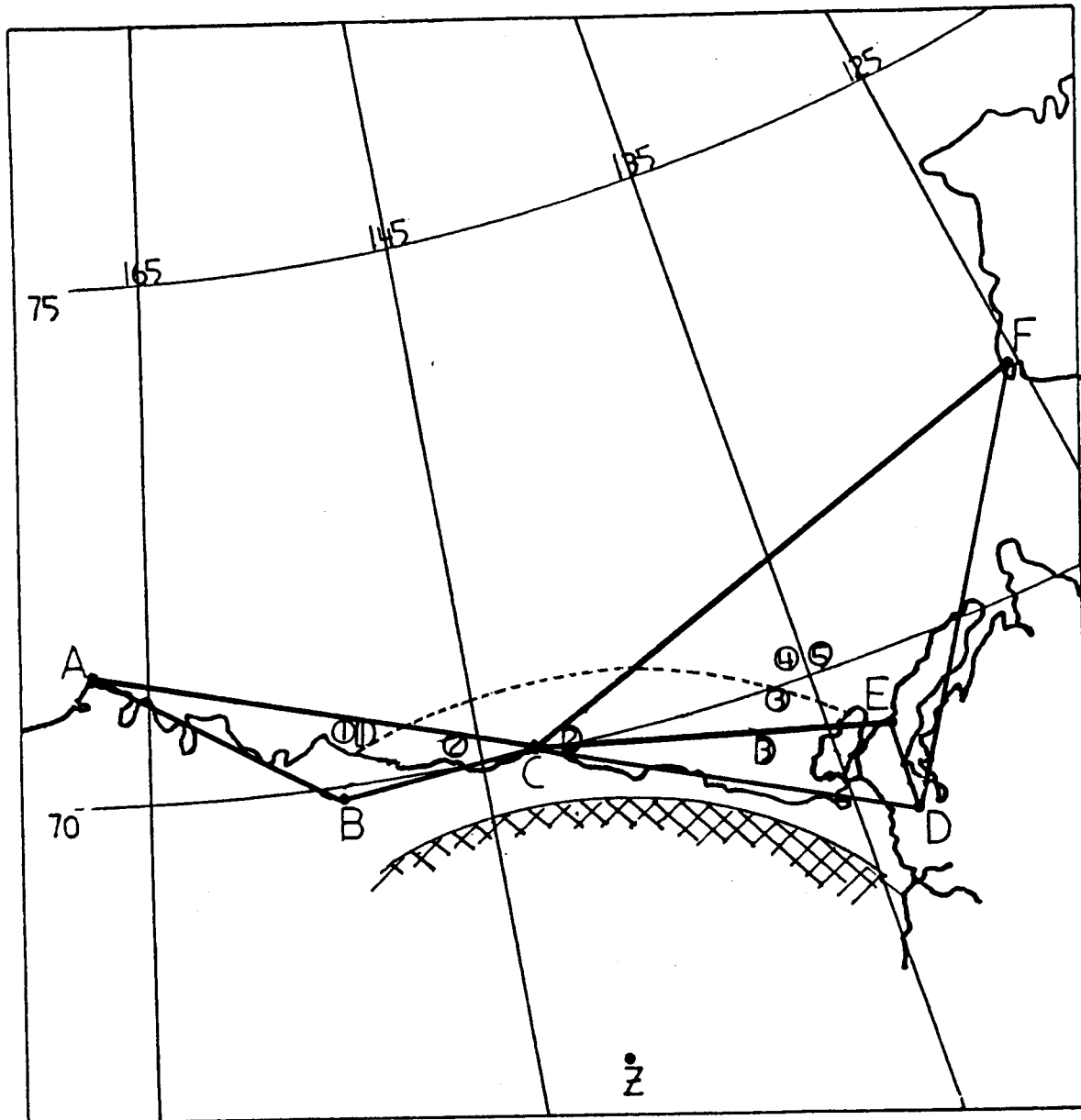


Figure 2.

Pressure triangles used to compute geostrophic winds for August (ABC), September (CDE), and October (CFD) 1983. Data stations are Barrow (A), Franklin Bluffs (B), Barter Island (C), Inuvik (D), Tuktoyaktuk (E) and Sachs Harbor (F). 0 ≡ Buoy 4519. D ≡ 4518 (died 24 September 1983, position #3). Buoy position numbers 1-2 (August), 2-4 (September), 4-5 (October) indicate positions relative to pressure triangles. The dashed arc is the probable distance seaward of major orographic influence from the 600 m contour (cross hatched). Z ≡ hypothetical center of the circle matching the arc.

Administration (NASA, U.S.) and the National Oceanic and Atmospheric Administration NOAA, U.S.). The pressure and temperature data accuracies were also better than $\pm .25$ mb and $\pm 1^\circ\text{C}$ respectively since both were comparison calibrated to the Barrow and Barter Island station instruments. Station F (Sachs Harbor) is an airport weather station that reports four times a day (six-hourly). No check has been made on its data accuracy. The eastward buoy trajectories made it a necessary network input, however.

GESTROPHIC WIND DATA

These data were computed from the pressure and temperature data triangles shown in Figure 2. Three triangles were chosen from five (original ones) because they fit certain criteria: buoy trajectory coverage, output compatibility with buoy motion, and availability of data.

The atmospheric flow was assumed to be in geostrophic balance (1):

$$f(\mathbf{k} \times \mathbf{V}_G) + \frac{\nabla P}{\rho} = 0 \quad (1)$$

The first term is the Coriolis force, and the second is the pressure gradient force with f the Coriolis parameter ($1.37 \times 10^{-4} \text{ sec}^{-1}$ at 70° N), \mathbf{k} the vertical unit vector, \mathbf{V}_G the geostrophic velocity vector, ∇P the gradient of the atmospheric pressure, and ρ the air density. Using the station combination of triangle ABC (Fig. 2) for example, and noting that pressure can be represented as a function of latitude (y) and longitude (x) on a plane surface:

$$\begin{aligned} P_A(x,y) &= ax_A + by_A + c \\ P_B(x,y) &= ax_B + by_B + c \\ P_C(x,y) &= ax_C + by_C + c \end{aligned} \quad (2)$$

Here the subscripts A, B, C denote their respective stations. Cramer's rule

or a least squares fitting technique (Kozo, 1982) can be applied to (2) to solve for unknowns a, b, c. Since $\frac{dP}{dx} = a$ and $\frac{dP}{dy} = b$, the pressure gradient ∇P can be determined. Use of (1) results in V_G since f is known and ρ for dry air can be determined from station temperatures.

Station errors of $\pm 1^\circ\text{C}$ can cause errors of .34% in the velocity magnitude since they effect ρ estimates. Calculated geostrophic winds less than 2 ms^{-1} are suspect since pressure errors (see above) can create maximum speed errors (Kozo, 1982) greater than $\pm 1.35 \text{ ms}^{-1}$ and direction errors greater than $\pm 40^\circ$ for triangle ABC. The error will be approximately the same for triangle CED and less for large triangle CFD if station F is reliable (see Fig. 2).

Bivariate distributions of calculated geostrophic wind speeds versus wind directions are shown for the months of August (Table 1, ΔABC), September (Table 2, ΔCDE) and October (Table 3, ΔCDF). It can be seen that the dominant wind directions were from the NW-W in August, September, and October, which accounted for the observed eastward buoy drift.

BUOY POSITION DATA

The data buoys deployed in open water on August 1983 by the U. S. Coast Guard were tracked by NOAA polar orbiting satellites through use of a position transponder called an ARGOS Data Acquisition Platform (ADAP), Model 901. Each ADAP platform position is received 8-12 times per day with an accuracy of approximately 300 m (Bessis, 1981). The buoy hulls have a ratio of submerged area to exposed area of at least 2:1. Therefore wind stress on the hull itself does not dominate buoy motion. The best assumption is that the buoys follow the wind-driven currents in the upper 1-2 m of the water column.

Table 1. Calculated geostrophic wind speed (ms^{-1}) vs. direction for August 1983.

WIND DIR. °	WIND VEL. (M/S)															TOTA.	PER
	0-2	2-4	4-6	6-8	8-10	10-12	12-14	14-16	16-18	18-20	20-22	22-24	24-25	25-28	28-30		
326.0-348.5	1	2	0	1	0	0	0	0	0	0	0	0	0	0	0	4	1.0
303.5-326.0	3	4	0	1	1	0	0	0	0	0	0	0	0	0	0	9	3.0
281.0-303.5	4	3	7	3	6	7	1	0	0	0	0	0	0	0	0	31	12.0
258.5-281.0	2	7	11	5	15	3	0	0	0	0	0	0	0	0	0	43	17.0
236.0-258.5	0	5	2	4	4	9	3	2	1	1	0	0	0	0	0	31	12.0
213.5-236.0	1	3	2	1	1	5	1	0	0	0	0	0	0	0	0	14	5.0
191.0-213.5	1	4	4	3	0	0	0	0	0	0	0	0	0	0	0	12	4.0
168.5-191.0	0	1	0	1	1	0	0	0	0	0	0	0	0	0	0	11	4.0
146.0-168.5	1	3	5	4	1	1	0	0	0	0	0	0	0	0	0	15	6.0
123.5-146.0	0	0	2	0	3	1	1	1	0	2	0	0	0	0	0	10	4.0
101.0-123.5	0	1	4	4	5	9	2	1	1	1	0	0	0	0	0	28	11.0
78.5-101.0	2	2	0	3	0	0	2	3	1	0	1	0	0	0	0	14	5.0
56.0-78.5	1	2	1	0	1	2	0	0	0	0	0	0	0	0	0	7	2.0
33.5-56.0	0	3	0	1	0	0	0	0	0	0	0	0	0	0	0	4	1.0
11.0-33.5	4	3	4	1	0	0	0	0	0	0	0	0	0	0	0	12	4.0
348.5-11.0	0	1	1	1	0	0	0	0	0	0	0	0	0	0	0	3	1.0

Table 2. Calculated geostrophic wind speed (ms^{-1}) vs. direction for September 1983.

WIND DIR. °	WIND VEL. (M/S)															TOTAL	PER
	0-2	2-4	4-6	6-8	8-10	10-12	12-14	14-16	16-18	18-20	20-22	22-24	24-26	26-28	28-30		
326.0-348.5	1	4	3	4	7	2	1	0	0	0	0	0	0	0	0	22	9.0
303.5-326.0	1	3	3	3	2	0	1	0	2	0	0	0	0	0	0	15	6.0
281.0-303.5	3	5	5	0	0	0	0	0	0	0	0	0	0	0	0	13	5.0
258.5-281.0	3	3	6	4	0	0	0	0	0	0	0	0	0	0	0	16	6.0
236.0-258.5	2	2	3	5	1	0	0	0	0	0	0	0	0	0	0	13	5.0
213.5-236.0	2	2	2	2	2	0	0	0	0	0	0	0	0	0	0	10	4.0
191.0-213.5	3	5	7	4	2	1	1	0	0	0	0	0	0	0	0	23	9.0
168.5-191.0	7	4	9	4	1	0	0	0	0	0	1	0	0	0	0	26	10.0
146.0-168.5	3	5	2	3	2	3	2	1	1	1	2	0	0	0	0	25	10.0
123.5-146.0	2	0	4	1	2	1	0	0	0	0	0	0	0	0	0	10	4.0
101.0-123.5	3	4	1	0	0	0	0	0	0	0	0	0	0	0	0	8	3.0
78.5-101.0	3	5	1	0	0	0	0	0	0	0	0	0	0	0	0	9	3.0
56.0-78.5	3	2	2	0	0	0	0	0	0	0	0	0	0	0	0	7	2.0
33.5-56.0	3	2	1	2	0	0	0	0	0	0	0	0	0	0	0	8	3.0
11.0-33.5	2	2	1	3	4	1	0	0	0	0	0	0	0	0	0	13	5.0
348.5-11.0	3	1	10	3	2	0	1	1	1	0	0	0	0	0	0	22	9.0

Table 3. Calculated geostrophic wind speed (ms^{-1}) vs. direction for October 1983.

WIND DIR. °	WIND VEL. (M/S)															TOTAL	PER
	0-2	2-4	4-6	6-8	8-10	10-12	12-14	14-16	16-18	18-20	20-22	22-24	24-26	26-28	28-30		
325.0-348.5	0	2	4	1	2	0	0	0	0	0	0	0	0	0	0	9	7.0
303.5-326.0	0	3	7	5	3	1	0	0	0	0	0	0	0	0	0	19	15.0
281.0-303.5	0	2	1	3	2	2	0	0	0	0	0	0	0	0	0	10	8.0
258.5-281.0	0	0	1	1	0	0	0	0	0	0	0	0	0	0	0	2	1.0
236.0-258.5	1	2	0	1	0	0	0	0	0	0	0	0	0	0	0	4	3.0
213.5-236.0	0	1	0	1	0	1	0	0	0	0	0	0	0	0	0	3	2.0
191.0-213.5	3	1	1	0	1	0	1	0	0	0	0	0	0	0	0	7	5.0
168.5-191.0	2	2	2	1	0	0	1	0	0	0	0	0	0	0	0	8	6.0
146.0-168.5	1	0	0	3	0	1	0	0	0	0	0	0	0	0	0	5	4.0
123.5-146.0	1	0	1	2	1	1	0	1	0	0	0	0	0	0	0	7	5.0
101.0-123.5	2	6	3	3	3	0	0	0	0	0	0	0	0	0	0	17	13.0
78.5-101.0	0	2	2	0	2	1	0	0	1	0	0	0	0	0	0	8	6.0
56.0-78.5	4	0	1	0	1	0	0	0	1	0	0	0	0	0	0	7	5.0
33.5-56.0	2	1	3	0	0	0	0	0	1	0	0	0	0	0	0	7	5.0
11.0-33.5	1	1	5	1	0	0	0	0	0	0	0	0	0	0	0	8	6.0
348.5-11.0	0	1	2	0	0	0	0	0	0	0	0	0	0	0	0	3	2.0

The open-water buoy trajectory chosen to match the model output was a composite of the two longest surviving buoy trajectories for periods free of interference from offshore islands or shoaling areas. The air temperatures near the coast reached -20°C by 18 October 1983 and remained at or below this level for the rest of the month. This coincided with greatly reduced buoy motion for relatively strong wind fields, characteristic of buoy motion for conditions of total ice cover. Therefore, this became the last date for comparison to the open-water, wind-drift model.

RESULTS WITH DISCUSSION

MODEL DESCRIPTION-WINDS

The geostrophic wind velocities computed from the appropriate surface pressure networks (discussed above) are used as initial input to the model. The model given this velocity (V_G) and a buoy latitude and longitude will compute a new wind velocity (U) based on this position relative to the center (Z) of the hypothetical cylinder approximating the 600 m contour of the Brooks Range (Fig. 1). To get this orographically modified wind the expressions for the velocity distribution around a cylinder in steady, horizontal, irrotational frictionless flow of an incompressible fluid are (Dickey, 1961; see Fig. 1):

$$\text{Radial velocity component} \quad U_r = V_G(1-a^2/r^2) \cos\phi \quad (3)$$

$$\text{Directional velocity component} \quad U_\phi = -V_G(1+a^2/r^2) \sin\phi \quad (4)$$

$$\text{Magnitude} \quad U = (U_r^2 + U_\phi^2)^{\frac{1}{2}} \quad (5)$$

where a is the radius of the cylinder (274 km), r is the distance to a measuring station or buoy from Z and ϕ is the angle from the head of V_G to r . For example, to obtain the probable effects at Barter Island upon a westerly V_G from 285° : let $a = 274$ km, $r = 322$ km and $\phi = 110^\circ$. From (3-5), $U_r = -.095 V_G$ $U_\phi = -1.619V_G$ and the modified wind vector $U = 1.62V_G$ from 269° .

The input velocity used in this model differs from that of Dickey (1961). He did not use V_G in (3-5), but a surface wind (V_S) taken as $.9V_G$ with a cross isobaric angle (α) of 25° . Taking Barter Island as his main observation point, he matched derived synoptic wind fields from data-limited NWS charts to measured surface winds at land stations. In relatively flat

areas free from orographic influences on the Arctic pack ice, Albright (1980) showed V_S to be $.585 V_G$ with $\alpha = 25.9^\circ$. Dickey's (1961) main data site was contaminated by interaction with orography and should not have been used. It was surprising that his cross isobaric angle was so close to the more recent work, but the surface speed was obviously affected. This investigator recognizes that adequate information regarding the stability of the boundary layer over the Arctic Ocean is rare and that the primary area of the study will be contaminated by orographic influence. Also, counterclockwise geostrophic departure of the wind due to surface friction in the atmospheric Ekman layer is usually counteracted by clockwise departure from the applied wind stress direction in the oceanic Ekman layers. Therefore, V_G is used directly with no speed reduction or cross isobaric angle applied prior to insertion in (3-5). U is considered the approximate orographically-modified surface wind.

This assumption was tested on some more recent land data shown in Figure 3 (Henry, 1975). Sites L (Lonely) and O (Oliktok) show surface winds from the northeast to east while C (Barter Island), I (Inuvik) and T (Tuktoyaktuk) show surface winds from the northwest. This is obvious evidence for some type of redirected flow around an approximately cylindrical object. V_G can be estimated from the isobaric spacing (Fig. 3) as 17.9 ms^{-1} from 340° . Remembering Figures 1 and 2, $r = 480 \text{ km}$, $\phi = 195^\circ$ and $r = 322 \text{ km}$, $\phi = 165^\circ$ for sites O and C, respectively. Since $a = 274 \text{ km}$ for both sites, application of (3-5) results in $U = .52V_G$ from 296° for C and $U = .73V_G$ from 27.2° for O. The surface wind flags at C and O show (Fig. 3) a speed of $.55V_G$ from 315° and a speed of $.42V_G$ from 40° , respectively. The directional fit is close with only the speed at O exhibiting large error. This result is very encouraging since the change in direction along the

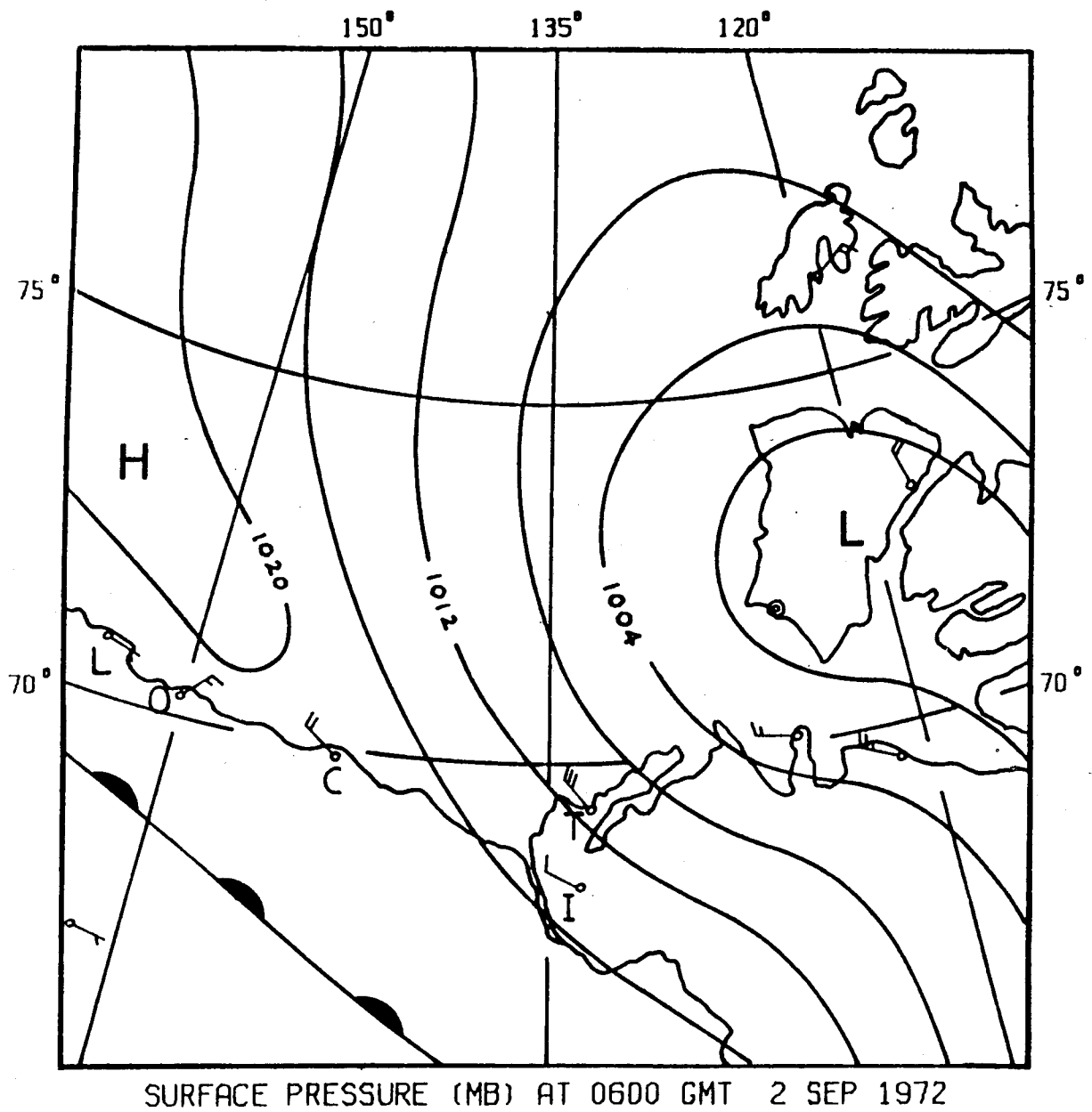


Figure 3. Surface pressure weather map (from Henry, 1975) showing resulting surface winds at shore stations. (Short flags $\sim 1.5-3.5 \text{ ms}^{-1}$; long flags $\sim 4.0-6.0 \text{ ms}^{-1}$).

coastline is explained and the speeds are of the correct magnitudes despite the gross approximation of V_G from the weather map.

Figure 4 (Dickey, 1961) displays the streamlines and the velocity field around a cylindrical barrier for conditions of irrotational, non-divergent flow of an undisturbed velocity (V_G in the case of this model) from 285° . The numbers at points along the streamlines (showing direction) are wind speeds in multiples of V_G . Zones A and B are areas of subgeostrophic and supergeostrophic speeds, respectively. The major influence on the winds is seen to extend approximately one radius (theoretically) away from the hypothetical cylinder. The A zones cover 30° of arc and the B zones cover 60° of arc. The 600 m elevation does not represent a complete cylinder (see Fig. 1), therefore, V_G 's from 120° to 270° are not operated on by the model since they would be coming from behind the mountain range. However, these V_G 's are obtained from triangular networks which indicate the mesoscale pressure field north of the Brooks Range so they are preserved at the original calculated velocities. Use of a NWS synoptic surface chart to "guess" at the surface wind for headings from 120° to 270° would also be unwise due to blockage effects on winds from behind the mountains (Kozo, 1984c).

Figures 5-9 show model generated U velocities in multiples of V_G magnitudes as they apply to the Alaska Arctic in a theoretical coastal zone 200 km wide for V_G 's from the west, northwest, north, northeast and east, respectively. It should be remembered that a different wind is "created" at each buoy location or study site for a given V_G . Examination of Figures 1 and 2 shows that if a given V_G direction is greater than 180° (direction from site to Z), the site will be subject to counterclockwise (CCW) flow around the mountain barrier or a westward push. Also, if a given V_G direction is

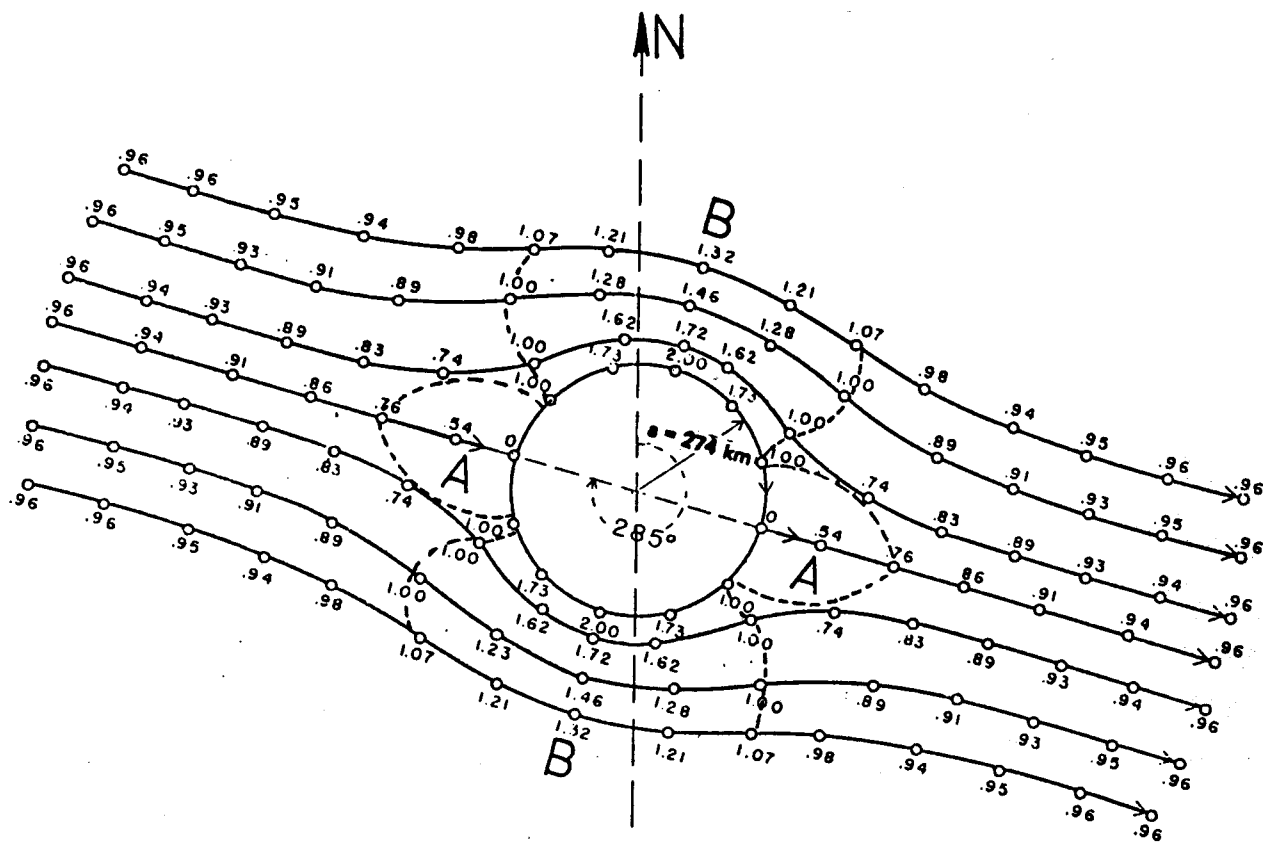


Figure 4. Streamlines and velocity field around a fixed cylindrical barrier (Dickey, 1961) for irrotational, non-divergent flow of V_G . Numbers at points along the streamlines are wind speeds in multiples of the V_G . The B zones indicate higher than normal speeds and the A zones indicate reduced speeds.

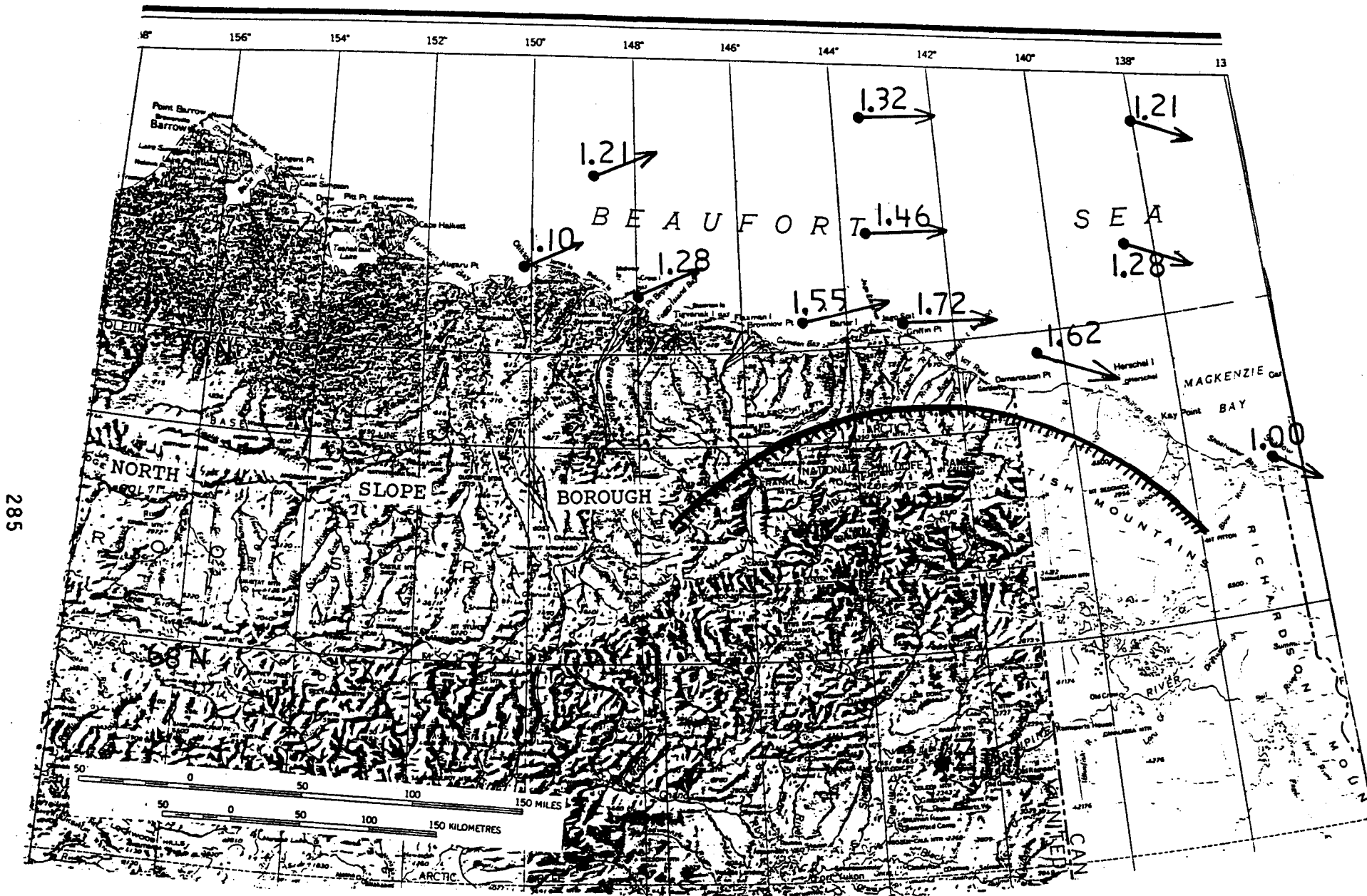


Figure 5. Model generated U velocities in multiples of V_G magnitudes for V_G 's from the west.

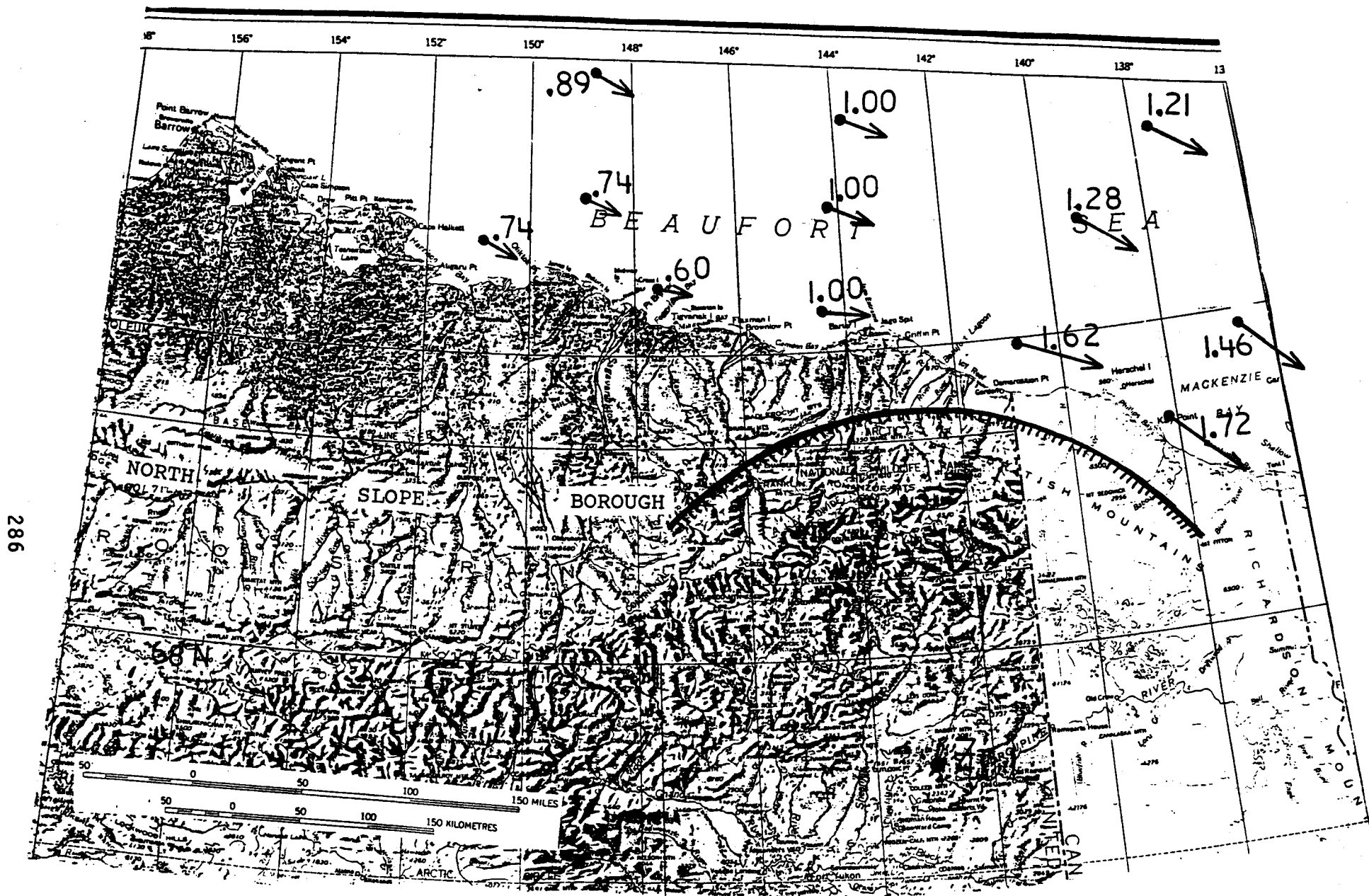


Figure 6. Model generated U velocities in multiples of V_G magnitudes for V_G 's from the northwest.

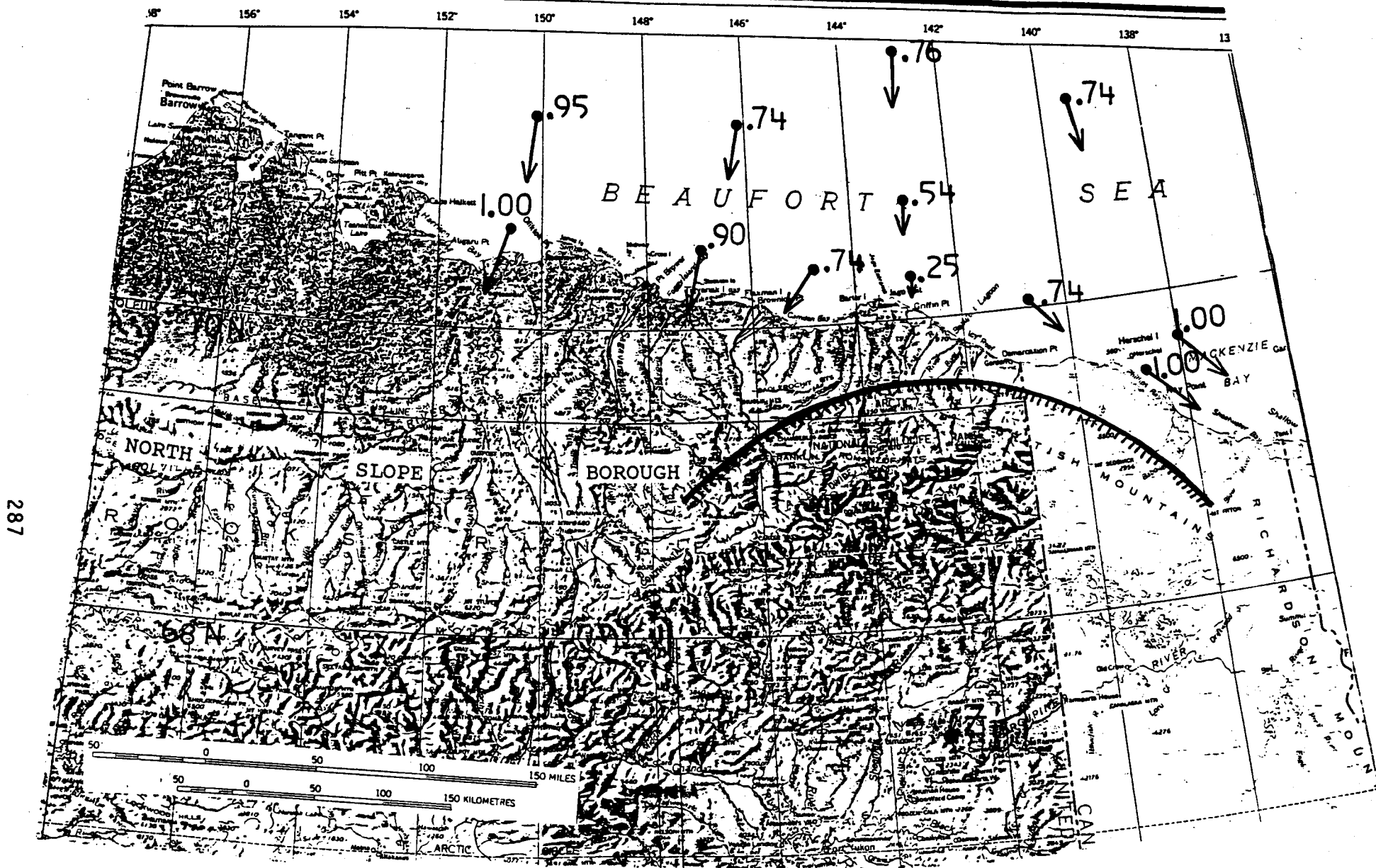


Figure 7. Model generated U velocities in multiples of V_G magnitudes for V_G 's from the north.

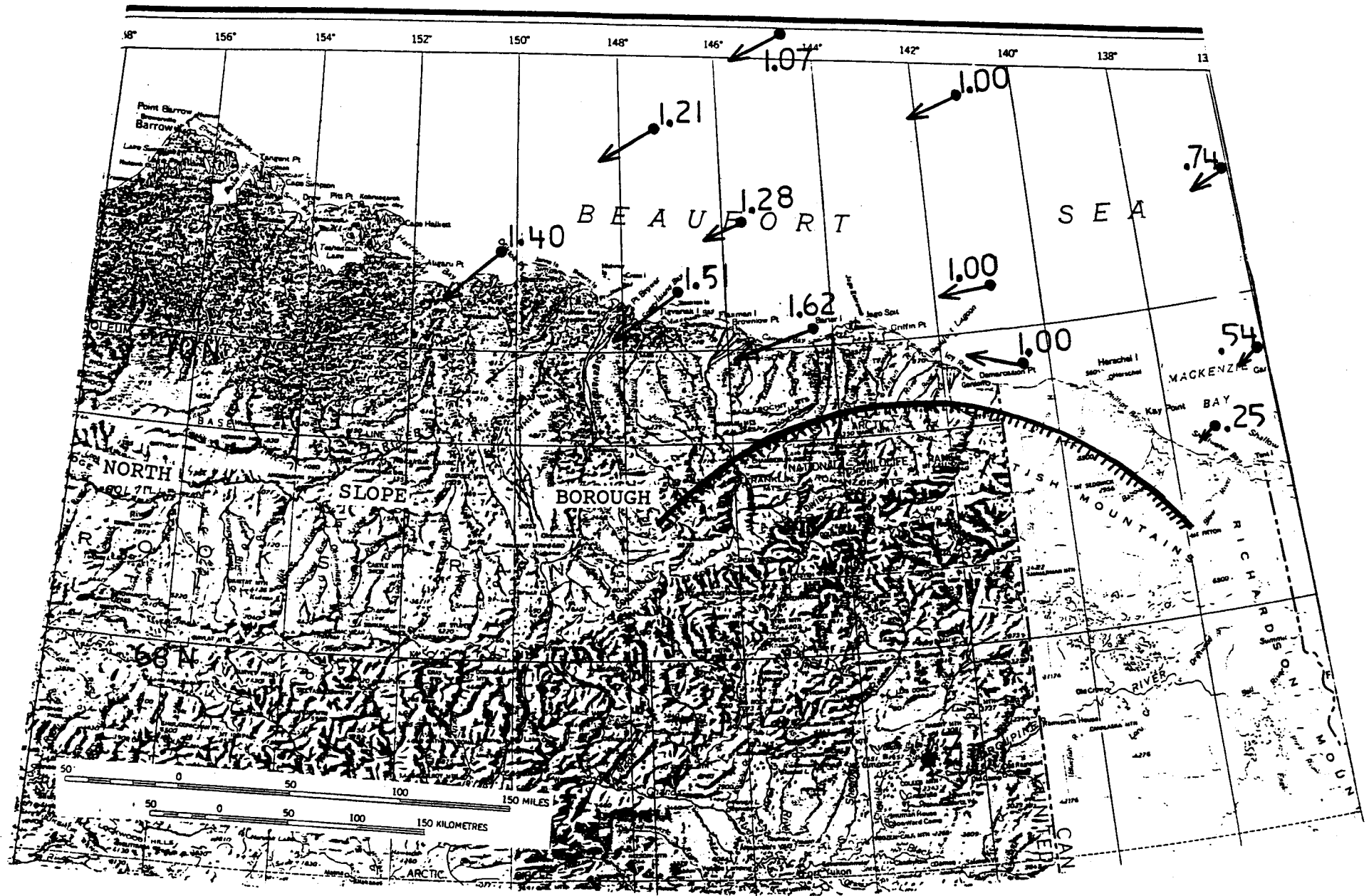


Figure 8. Model generated U velocities in multiples of V_G magnitudes for V_G 's from the northeast.

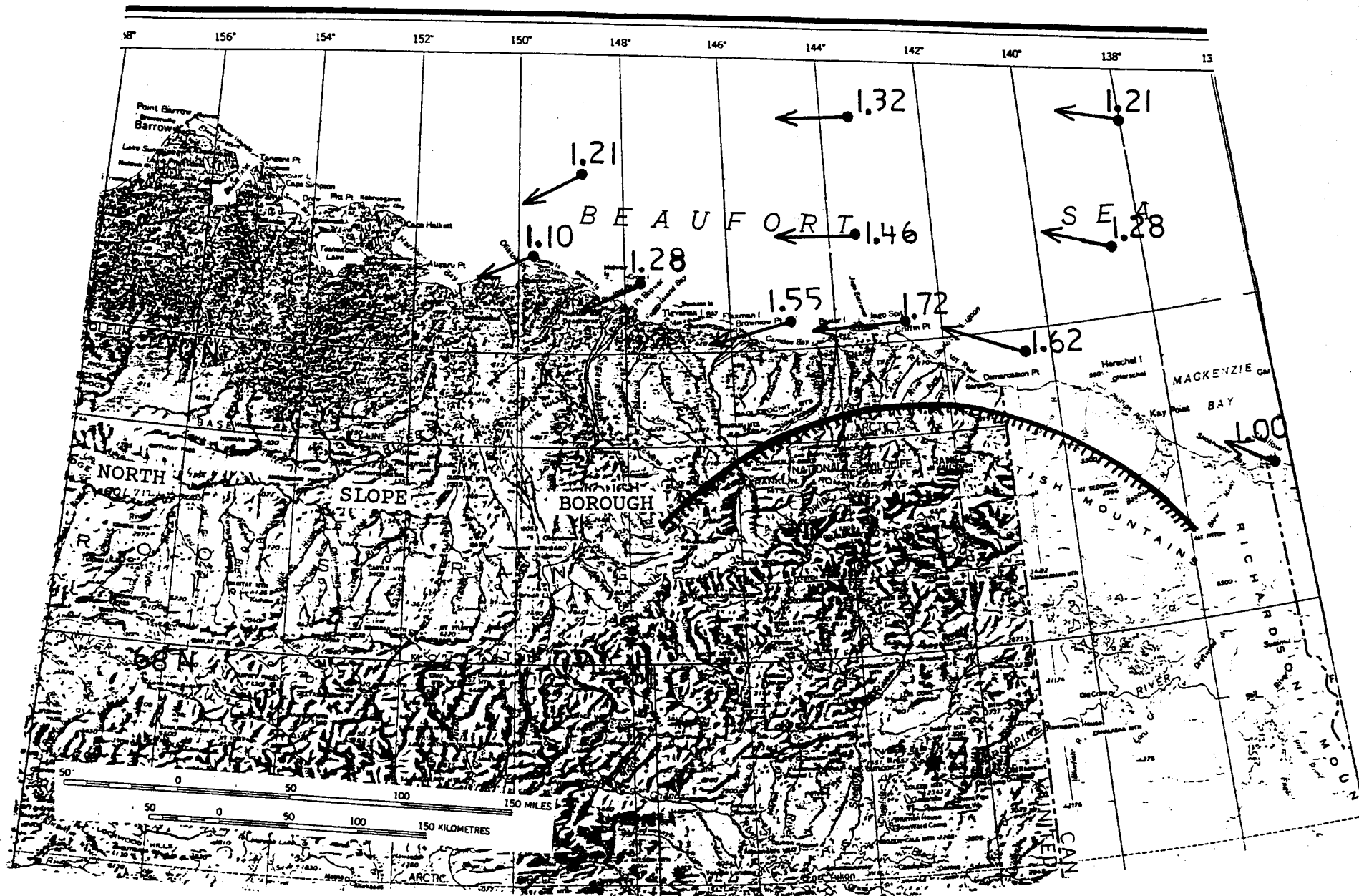


Figure 9. Model generated U velocities in multiples of V_G magnitudes for V_G 's from the east.

less than 180° (direction to Z), the site will be subject to clockwise (cw) flow around the mountain barrier or an eastward push.

Figure 5 shows the theoretical winds in multiples of a westerly V_G . The nearshore winds are supergeostrophic from Prudhoe Bay to Herschel Island and decrease in magnitude seaward. Figure 6 shows theoretical winds in multiples of a northwesterly V_G . The coastal winds from Harrison Bay to Camden Bay are subgeostrophic and increase in magnitude as distance from the Brooks Range increases. The nearshore winds from Barter Island to Mackenzie Bay are supergeostrophic and decrease in magnitude seaward. Figure 7 shows the wind pattern that evolves from a northerly wind. The nearshore winds from Harrison Bay to Herschel Island are now all subgeostrophic with velocities approaching geostrophic to the north. This is an example of "split" flow with winds west of Barter Island having an easterly heading and winds east of Barter Island having a westerly heading. The nearshore zone from Camden Bay to Demarcation Pt. will have drastically reduced winds. Figure 8 shows the wind pattern for an initial northeasterly wind. The coastal winds from Barter Island to Harrison Bay are supergeostrophic with little directional change but they diminish seaward. The nearshore winds from Barter Island to Herschel Island maintain their original speed but show directional changes which diminish seaward. The winds in the Mackenzie Bay area are greatly reduced. Figure 9 is the pattern caused by an initial easterly wind. The nearshore winds are supergeostrophic from Herschel Island west to Harrison Bay and their magnitudes diminish seaward.

Figure 2 shows the coastal coverage of pressure network CED. This coastal zone will undergo supergeostrophic winds for V_G 's from the east, northeast, west and northwest and will be subject to reduced winds for only northerly winds (see Figures 5-9) which are rare.

MODEL DESCRIPTION-BUOY TRAJECTORIES

Due to the unusual predominance of westerly winds along the Beaufort coast from August through October 1983, the average Coast Guard buoy motion was eastward. The V_G data was calculated from three different pressure triangles (Fig. 2, chosen from six possible combinations). These triangles alternately contained the buoy trajectories (4518 and 4519) during most of their eastward drift. Triangles ABC, CED, and CDF were used in August, September, and October, respectively. Figure 10 shows the actual trajectories of buoys 4518 and 4519 (two longest lasting buoys) from August through October with the average monthly ice edges superimposed (NOAA/U.S. Navy Joint Ice Center, 1983). Buoy 4519 ran into shoals in August which caused it to stop movement for several days. It later "caught up" with buoy 4518 by 9 September and moved in a similar trajectory until 4518 ran into shallow water on 21 September ("died" 24 September). Buoy 4519 continued drifting in open water until 18 October when it was apparently frozen in or attached to pack ice. For comparison to the model derived buoy trajectories: buoy 4518 positions are used in August up to 6 September, the combined trajectories (Fig. 10) of 4519 and 4518 are used until 21 September, and the trajectory of buoy 4519 is used until 18 October.

As a preliminary model run, the initial buoy deployment position (4518) was used in conjunction with unmodified V_G 's generated by the appropriate pressure triangles (Fig. 2). This hypothetical buoy was advanced in the direction of $V_G + 180^\circ$ (standard rhumbline navigational algorithm) at 3, 4, 5 and 6% of V_G . All of these trial runs without modification for flow around an obstacle resulted in the model buoy running into the shore after a month of drift. This inevitable fact and the actual individual buoy tracks

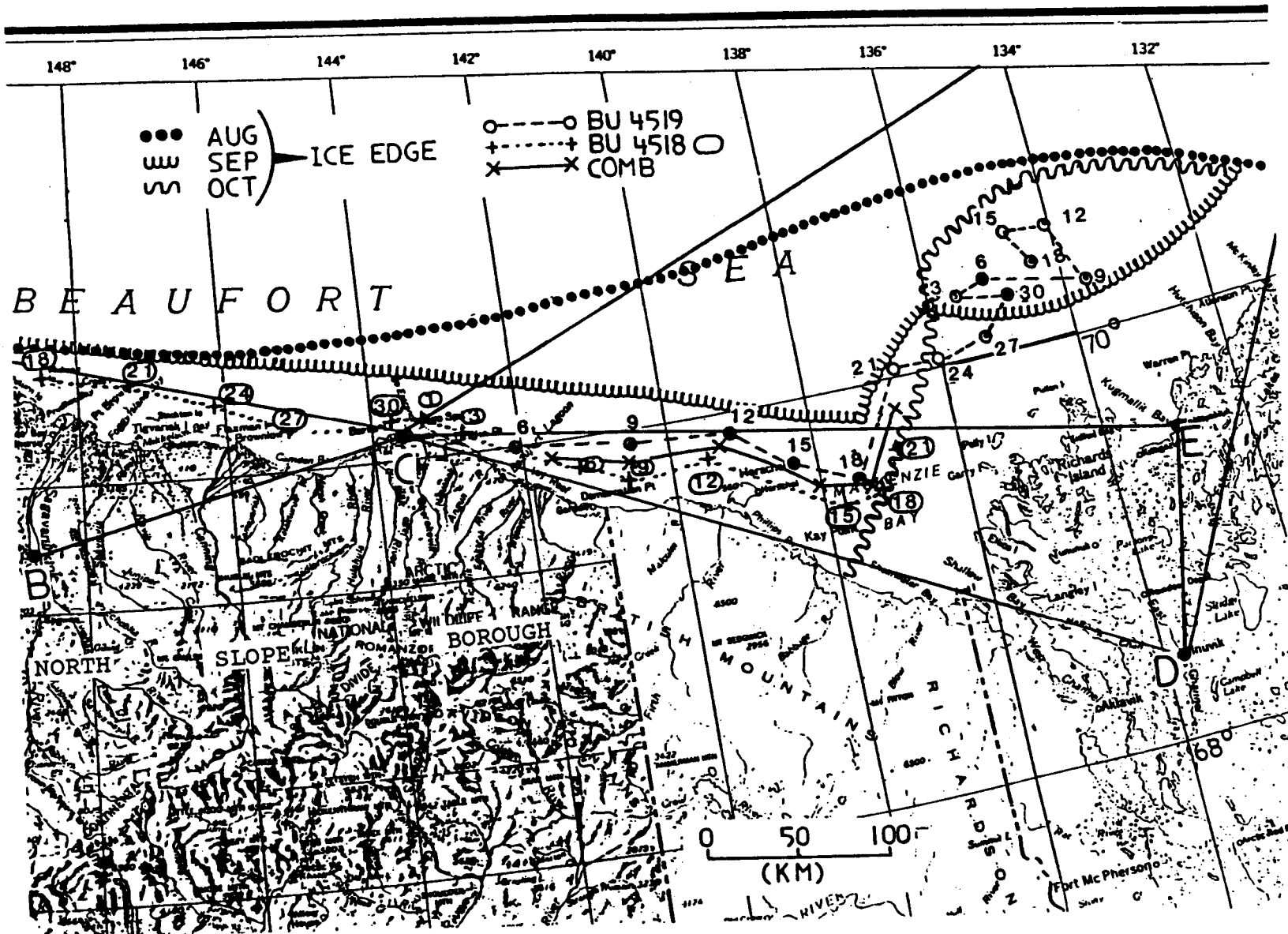


Figure 10. Trajectories of buoys 4518 and 4519 (U.S. Coast Guard) during unimpeded drift. Parts of surrounding pressure triangles, and the average ice edge (greater than 50% coverage) for August, September and October 1983 are shown. The combined trajectory for September is designated x. The buoys were deployed 18 August 1983. Starting west and moving eastward, days 18-30 represent August positions, days 1-30 represent September positions and days 3-18 represent October positions.

indicating periods of increased and decreased drift speeds relative to each other for the same large scale wind, pointed to some position-dependent mesoscale headland effect operating along the eastern Alaskan Arctic coast.

The next set of model runs were those in which a hypothetical buoy was advanced with a V_G modified by orography, except when from 120° to 270° (see Model Description-Winds above). Therefore, modified flow U (see 3-5) or unmodified flow V_G (if direction is from 120° to 270°) is used to advance a hypothetical buoy in the U or $V_G + 180^\circ$ direction at 3, 4, 5 and 6% of their respective magnitudes.

A third set of runs used the same procedure as above, but geostrophic winds were smoothed in speed and direction before the orographic modification was applied. This was tried because large changes in speed and direction within the basic model interval of 3 hrs do not represent geostrophic balance conditions. In these cases, the effects of the rapidly changing wind field are not transmitted instantaneously to the actual buoys.

The best fit to the actual buoy trajectories (combined tracks of 4518 and 4519) can be seen in Figure 11. This was obtained by using the modified wind scheme without smoothing for August and September and the unmodified V_G for October. The simple October fit was probably due to several causes: the real buoy was in a location that was probably not affected by orography; the real buoy was in deeper water (> 100 m) and not affected by bathymetry, and the model buoy was farther south and would have been (theoretically) affected by orography. The percentage of the modified or unmodified wind speeds used to advance the model buoy was 4% for trajectories (see Figs. 2 and 11) contained in triangle ABC (August), 2% for trajectories contained in triangle CED (September), and 4% for trajectories governed by CDF (October). Reynolds *et al.* (1985) recently found that ice floes in the southern Bering Sea

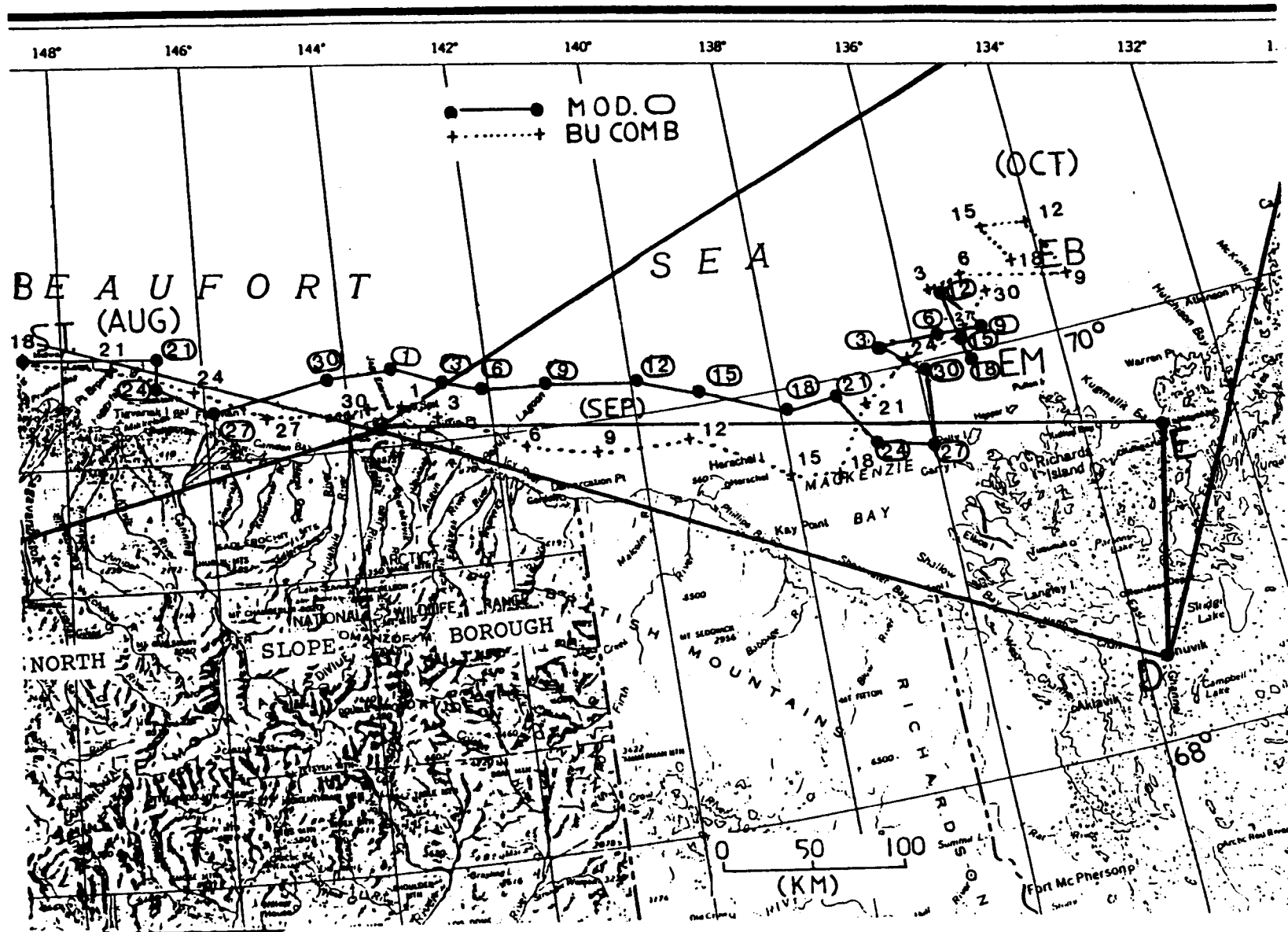


Figure 11. The combined 4518 and 4519 drift compared to the model drift. Again the pressure triangles are shown in part. The buoys were deployed 18 August 1983 (ST) and were locked into the sea ice by 18 October 1983 (EM \equiv last model buoy position; EB \equiv last actual buoy position).

marginal ice zone (MIZ) drifted at 4% of the surface wind speed (away from orographic effects). A main reason that only 2% of the speed was needed to drive the model buoy in September was that the triangle CED covers a coastal area subject to supergeostrophic enhancement of winds (see Figs. 5, 6, 8, 9). The major discrepancy between the purely wind driven model buoy motion and the actual buoy motion occurred during the 21-27 September period. Figure 12 shows the bathymetry in the Mackenzie Bay area and its effect on wind driven surface currents under a large scale wind from the northwest (MacNeill and Garrett, 1975). The model buoy drift from 21-27 September reflects a net wind from the northwest pushing the hypothetical buoy to the southeast. Figure 12 shows that the actual buoy was in shallow water between 10 m and 50 m. The piling up of water in this shallow area would produce a northeast to east contour-following water movement which did not allow the real buoy to move southeast. If the wind driven surface currents were in deeper water, out of the effects of the bottom, the actual buoy and model buoy would be less than 20 km apart after 60 days instead of 50 km apart. In either case, the technique appears to work quite well and explains 90% of the actual motion (on a distance basis). This success adds to the belief that the model describes the winds accurately in this area of the Beaufort Sea.

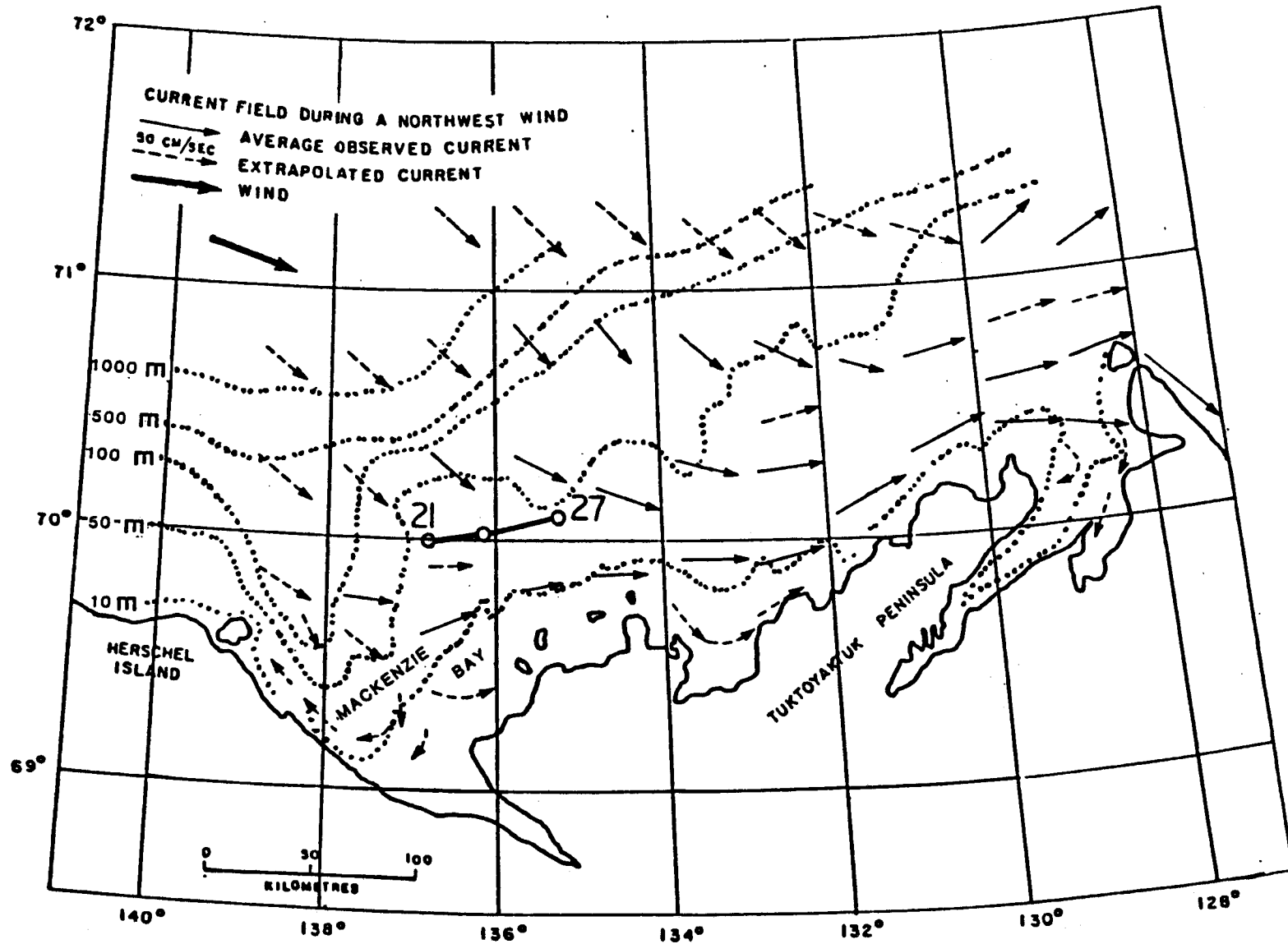


Figure 12.

The bathymetry in the Mackenzie Bay area and its effect on wind driven surface currents (after MacNeill and Garrett, 1975). Actual buoy drift for 21-27 September 1983 shown as 0-0-0.

SUMMARY AND CONCLUSIONS

The effect of a large headland on the wind field in a coastal zone has been modeled and carried one step beyond in an effort at "ground truthing". Actual buoy trajectories along a coastal zone which has predominant wind driven surface currents were compared with model generated buoy trajectories driven by headland modified winds. The model and buoy trajectories were very similar. After 60 days and 650 km of total drift, they were 50 km apart. The main discrepancy occurred when the actual buoy moved into a shallow part of the Mackenzie Bay. There the surface current in response to a northwesterly wind was constrained to flow to the northeast instead of the southeast.

The model uses high resolution mesoscale atmospheric pressure networks to define the pressure gradient wind V_G offshore which becomes its initial input. These networks are land based and, therefore, do not require drifting satellite-transmitting pressure buoys with a low life expectancy (~ 6 months) in arctic offshore environs. A simple extension of Dickey's (1961) work to offshore areas and the open water season allows basic hydrodynamic considerations to be applied. The network V_G is modified by flow around the 600 m contour of the Brooks Range. Areas of supergeostrophic and subgeostrophic flows are easily delineated in designated offshore areas.

In using the model, a number of parameters can be varied from which new insight may be gained. For example, the simple act of changing the percentages of the driving wind speed allows the user to check on the degree of coupling between the wind and ocean. This could be an indirect check on stability of the atmosphere. The time between onset of a wind velocity and

application of this wind to drive the buoy can also be changed. This allows for calculation of the lag time between onset of a pressure pattern and the actual flow realized. Figure 13 is a simple flow chart for the model.

WIND-DRIVEN MODEL FLOW CHART

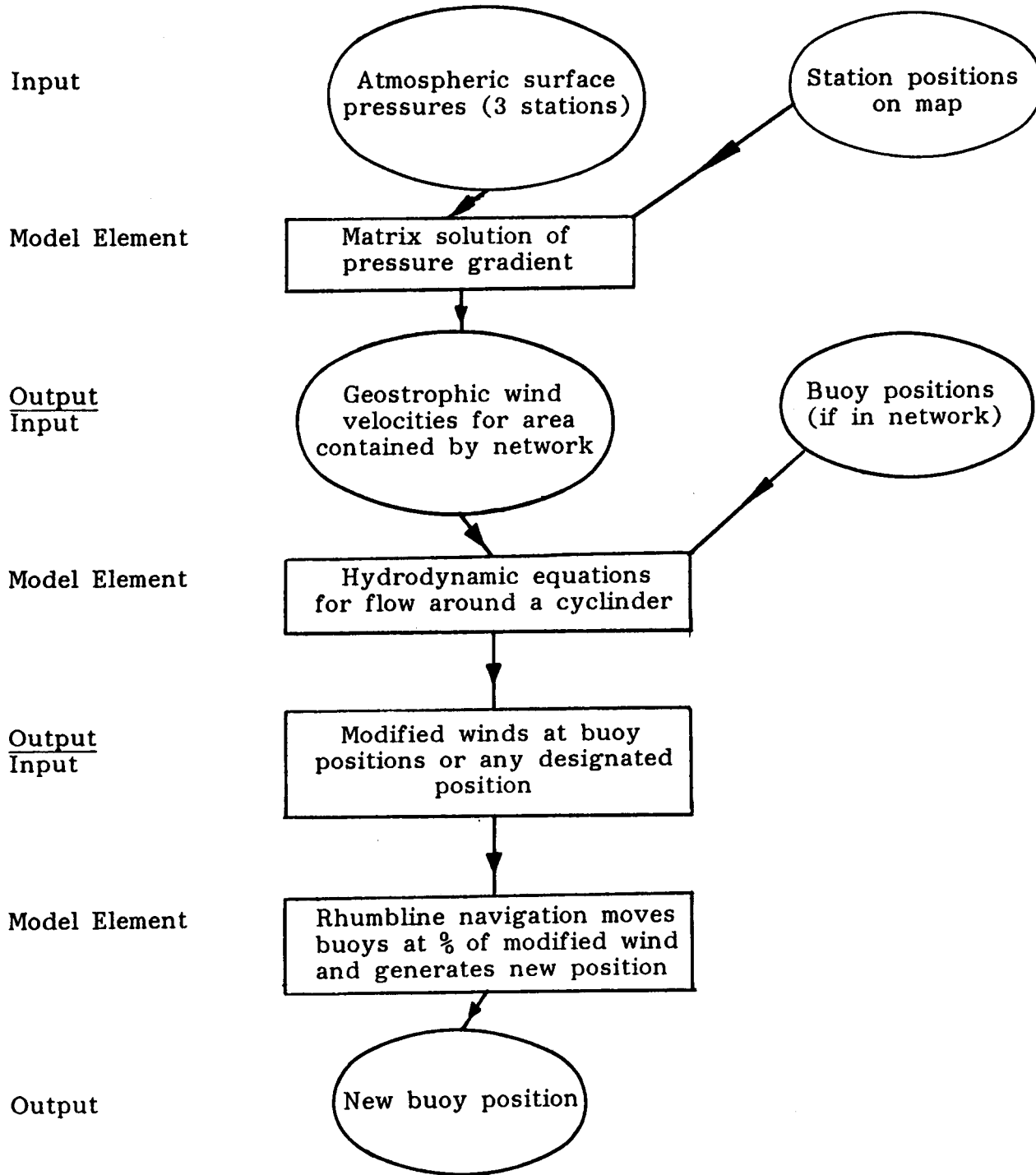


Figure 13. Flow chart for the wind-driven model.

FUTURE WORK

The degree of coupling between the atmosphere and the ocean from July through October can be examined through use of buoy deployment within one fixed pressure network. The amount of buoy drift for a given network V_G and atmospheric sounding can be compared. Atmospheric blockage by the Brooks Range can also be assessed. For a given large scale wind direction from 120° to 270° , coastal surface winds can be measured, mesoscale network winds can be derived and actual buoy movement at varying distances offshore recorded. A comparison of the large scale wind computed from NWS maps, mesoscale network winds, surface winds and actual buoy movement should provide many answers.

ACKNOWLEDGMENTS

This study was funded by the Minerals Management Service, U.S. Department of the Interior, through interagency agreement with the National Oceanic and Atmospheric Administration; U.S. Department of Commerce, as part of the Outer Continental Shelf Environmental Assessment Program. I wish to also thank R. Q. Robe of the U.S. Coast Guard R & D Center, Avery Point, Connecticut, for the use of his buoy data.

REFERENCES

- Aagaard, K. 1984. The Beaufort Undercurrent, in *The Alaska Beaufort Sea: Ecosystems and Environment*. Edited by P. Barnes, D. Schell and E. Reimnitz. Academic Press, New York, pp. 47-71
- Albright, M. 1978. Construction of atmospheric surface pressure maps from the AIDJEX data set. *AIDJEX Bull.*, 39:111-120. University of Washington, Seattle
- Albright, M. 1980. Geostrophic wind calculations for AIDJEX, in *A symposium on sea ice processes and models*. Edited by R. S. Pritchard. Proc. Intern. Comm. on Snow and Ice/Arctic Ice Dynamics Joint Experiment. University of Washington Press, Seattle, pp. 402-409
- Batchelor, G. K. 1967. *An Introduction to Fluid Dynamics*. University Press, Cambridge, Mass. 615 pp.
- Bessis, J. L. 1981. Operational data collection and platform location by satellite. *Remote Sensing of Environment*. 11:93-111.
- Brower, W. A., H. D. Diaz, A. S. Prechtel, H. W. Searby and J. L. Wise. 1977. *Climatic Atlas of the Outer Continental Shelf Waters and Coastal Regions of Alaska*. Vol. III. AEIDC, University of Alaska, Anchorage and U.S. National Climatic Center, Asheville, NC., 409 pp.
- Crossley, A. F. 1938. Note on the variation of pressure accompanying a distortion of air flow. *Quart. J. Royal Meteorol. Soc.*, Vol. 64, p. 477.
- Dickey, W. W. 1961. A study of a topographic effect on wind in the Arctic. *J. Meteorol.* 18:790-803.
- Henry, R. F. 1975. Storm surges. Beaufort Sea Tech. Rpt. #19, Beaufort Sea Proj., Dept. of the Environment, 512 Federal Bldg., 1230 Government St., Victoria, B. C. V8W1Y4, 41 pp.
- Kozo, T. L. 1980. Mountain barrier baroclinity effects on surface winds along the Alaskan Arctic Coast. *Geophys. Res. Ltrs.* 7:377-380.
- Kozo, T. L. 1982. An observational study of sea breezes along the Alaskan Beaufort Sea coast. Part 1. *J. Appl. Meteorol.* 12:891-905.
- Kozo, T. L. 1984a. Mesoscale wind phenomena along the Alaskan Beaufort Sea coast, in *The Alaskan Beaufort Sea: Ecosystems and Environments*. Edited by P. Barnes, D. Schell and E. Reimnitz. Academic Press, New York, pp. 23-45

- Kozo, T. L. 1984b. Mountain barrier baroclinicity effects on surface winds along the Alaskan Arctic coast and offshore. Abstract in the 1984 Arctic Science Conf. (35th Alaskan Conf.), Oct. 2-5, 1984, Anchorage, sponsored by Amer. Ass. for Adv. of Sci-Arctic Div., Amer. Meteorol. Soc. and Arctic Inst. of North America, 109 pp.
- Kozo, T. L. 1984c. Mesoscale meteorology, in *Environmental Characterization and Biological Use of Lagoons in the Eastern Beaufort Sea*. Edited by J. C. Truett. Final Reports of Principal Investigators, 24:129-579, NOAA-OMA-OAD, Alaska Office, 701 C St., P.O. Box 56, Anchorage, pp. 469-500.
- MacNeill, M. R. and J. F. Garrett. 1975. Open water surface currents in the southern Beaufort Sea. Beaufort Sea Tech. Rpt. #17, Dept. of the Environment, 512 Federal Bldg., 1240 Government St., Victoria, B.C. V8W1Y4, 113 pp.
- NOAA/U.S. Navy Joint Ice Center. 1983. Eastern-western Arctic sea ice analysis. Naval Polar Oceanogr. Ctr., Navy Dept., 4301 Suitland Rd., Washington, D.C. 20390
- Reynolds, M., C. H. Pease and J. E. Overland. 1985. Ice drift and regional meteorology in the southern Bering Sea: Results from MIZEX West. J. Geophys. Res. 90:11,967-11,981.
- Robe, R. Q., I. J. Lissauer, and T. L. Kozo. 1984. Beaufort Sea coastal currents. 1983 Abstract in 1984 Arctic Science Conf. (35th Alaskan Conf.), Oct. 2-5, 1984, Anchorage, Alaska, sponsored by Amer. Ass. for Adv. of Sci-Arctic Div., Amer. Meteorol. Soc. and Arctic Inst. of North America. 109 pp.
- Rogers, J. C. Meteorological factors affecting Inter-annual variability of summertime ice extent in the Beaufort Sea. Mon. Weather Rev., 106:890-897.
- Schwerdtfeger, W. 1979. Meteorological aspects of the drift of ice from the Weddell Sea toward the mid-latitude westerlies. J. Geophys. Res. 84:6321-6328.

SUPERSTRUCTURE ICING IN THE NORTH CHUKCHI,
SOUTH CHUKCHI AND HOPE BASIN AREAS

by

Thomas L. Kozo, Ph.D.

VANTUNA Research Group

Occidental College

Final Report
Outer Continental Shelf Environmental Assessment Program
Research Unit 519

1984

303

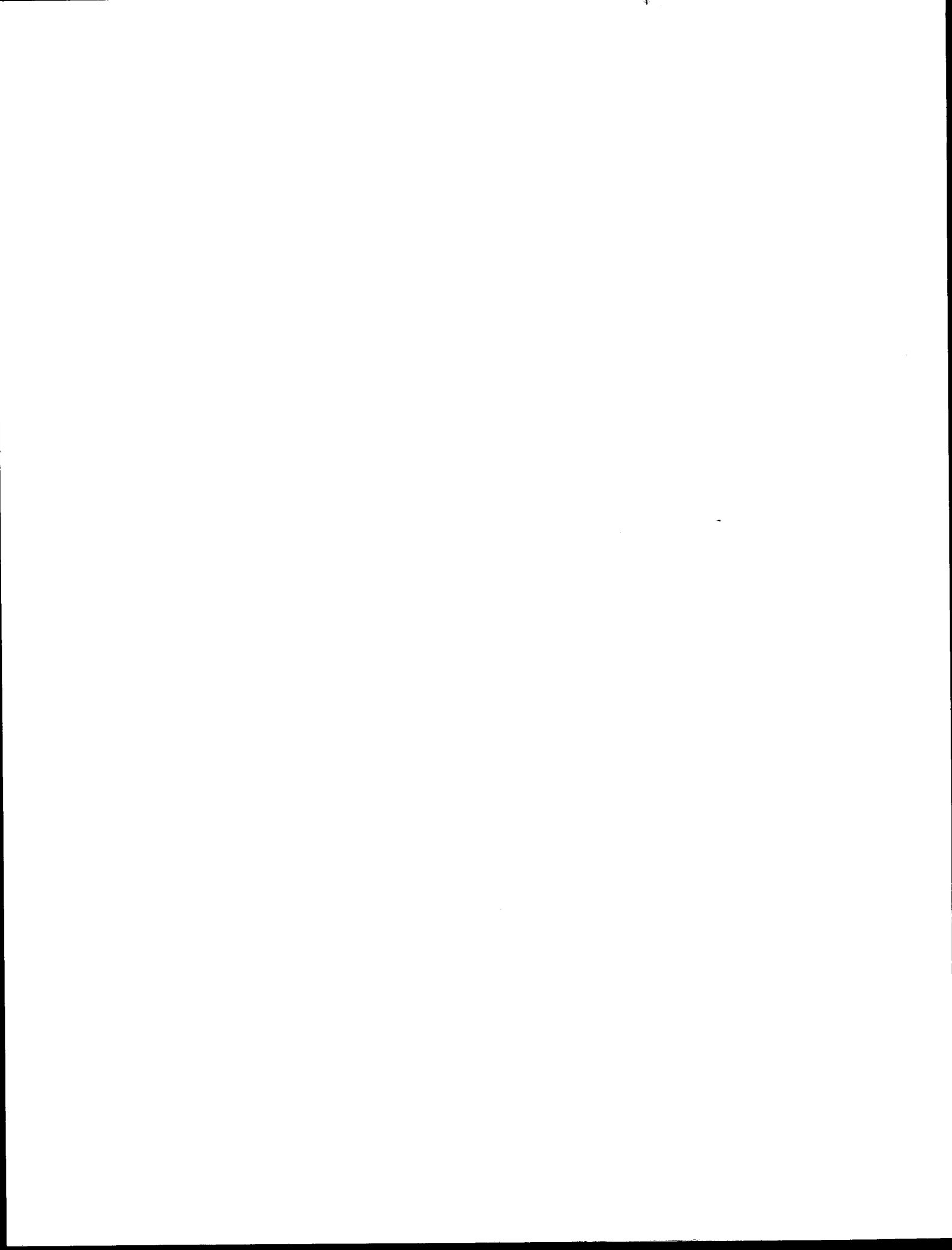
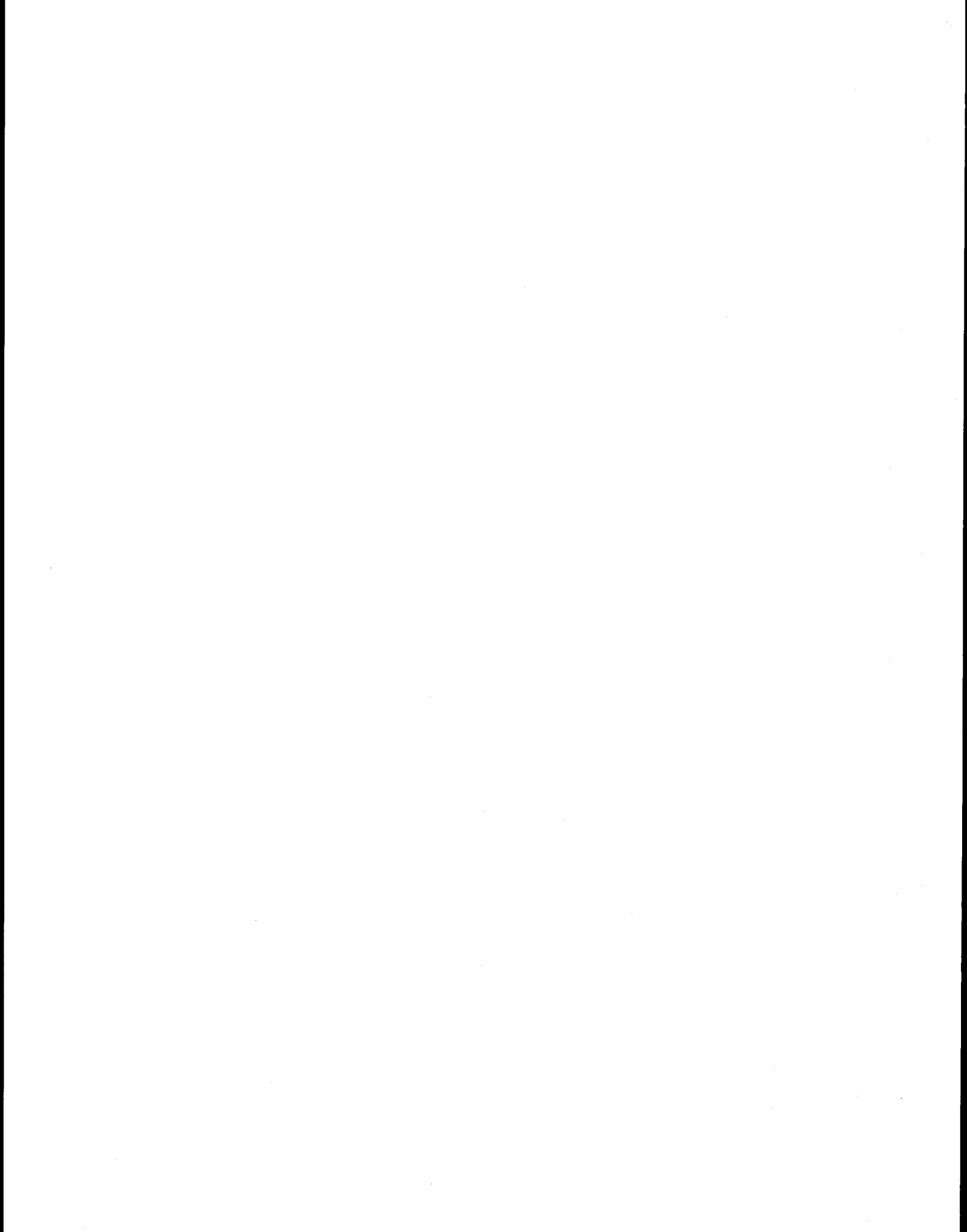


TABLE OF CONTENTS

LIST OF FIGURES.....	
LIST OF TABLES.....	
INTRODUCTION.....	
EFFECTS ON SHIPS.....	
ICING ON OFFSHORE STATIONARY PLATFORMS.....	
METEOROLOGY AND SEA CONDITIONS	
Freezing Rain and Snow.....	
Arctic Sea-smoke.....	
"Sea Ice".....	
Freezing Spray.....	
Air Temperature.....	
Wind.....	
Effect of the Ice Pack.....	
Sea Temperature.....	
CONSTRUCTION OF ICING MAPS.....	
DESCRIPTIONS OF ICING MONTHS.....	
May.....	
June.....	
July.....	
August.....	
September.....	
October.....	
November.....	
SUMMARY.....	
FURTHER STUDY.....	
REFERENCES.....	
FIGURE COVER PAGE.....	
FIGURES.....	

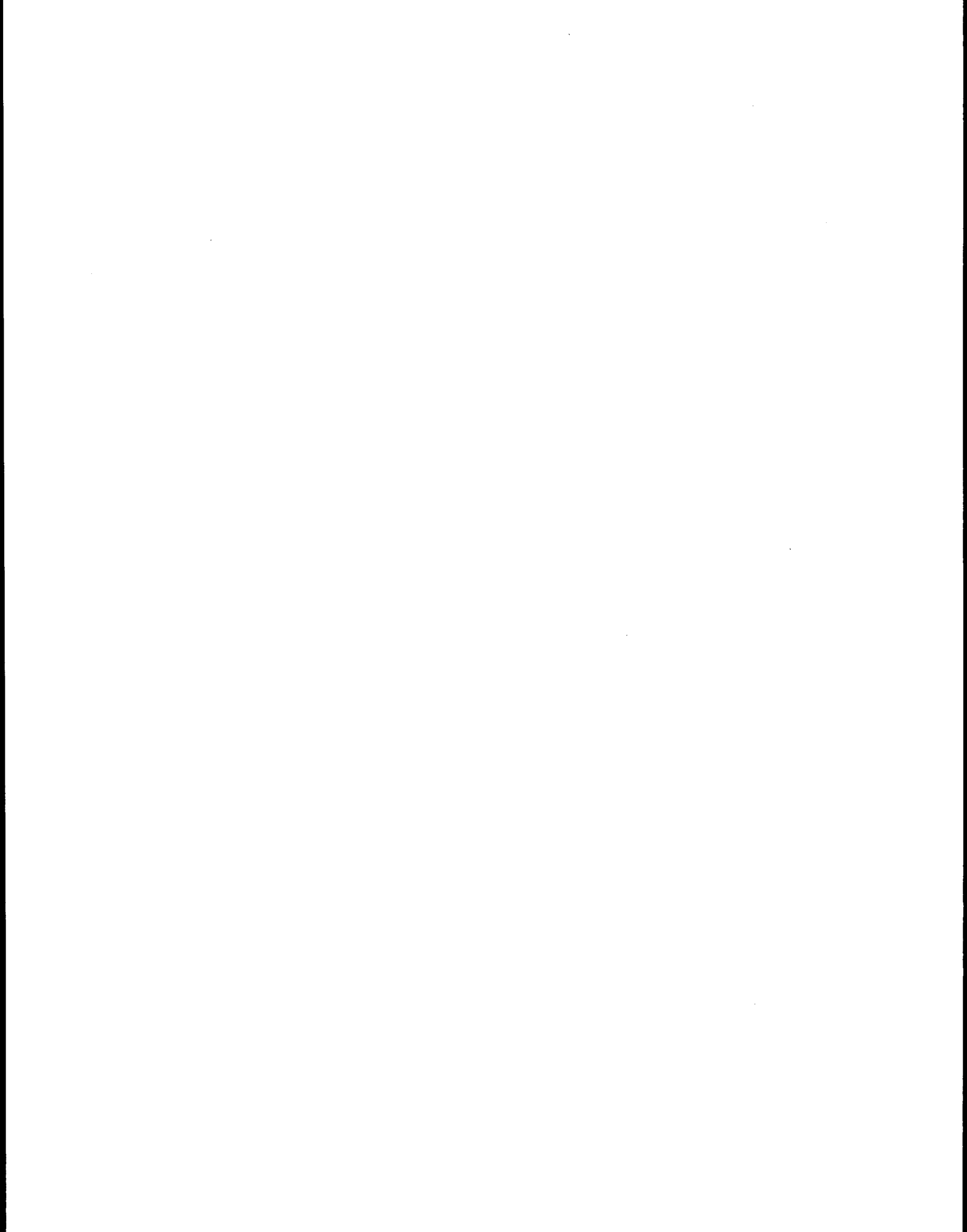


LIST OF FIGURES

- Figure 1a. May superstructure icing (SI) for conditions of minimum sea ice extent, maximum sea surface temperatures, mean air temperatures, and 28 knot winds.
- Figure 1b. May SI for the above conditions except with 50 knot winds.
- Figure 2a. May SI for conditions of minimum sea ice extent, maximum sea surface temperatures, minimum air temperatures, and 28 knot winds.
- Figure 2b. May SI for the above conditions except with 50 knot winds.
- Figure 3a. June SI for conditions of mean sea ice extent, mean sea surface temperatures, minimum air temperatures, and 28 knot winds.
- Figure 3b. June SI for the above conditions except with 50 knot winds.
- Figure 4a. June SI for conditions of minimum sea ice extent, maximum sea surface temperatures, minimum air temperatures, and 28 knot winds.
- Figure 4b. June SI for the above conditions except with 50 knot winds.
- Figure 5a. July SI for conditions of mean sea ice extent, mean sea surface temperatures, minimum air temperatures, and 28 knot winds.
- Figure 5b. July SI for the above conditions except with 50 knot winds.
- Figure 6a. July SI for conditions of maximum sea ice extent, minimum sea surface temperatures, minimum air temperatures, and 28 knot winds.
- Figure 6b. July SI for the above conditions except with 50 knot winds.
- Figure 7a. July SI for conditions of minimum sea ice extent, maximum sea surface temperatures, minimum air temperatures, and 28 knot winds.
- Figure 7b. July SI for the above conditions except with 50 knot winds.
- Figure 8a. August SI for conditions of mean sea ice extent, mean sea surface temperatures, minimum air temperatures, and 28 knot winds.
- Figure 8b. August SI for the above conditions except with 50 knot winds.
- Figure 9a. August SI for conditions of maximum sea ice extent, minimum sea surface temperatures, minimum air temperatures, and 28 knot winds.

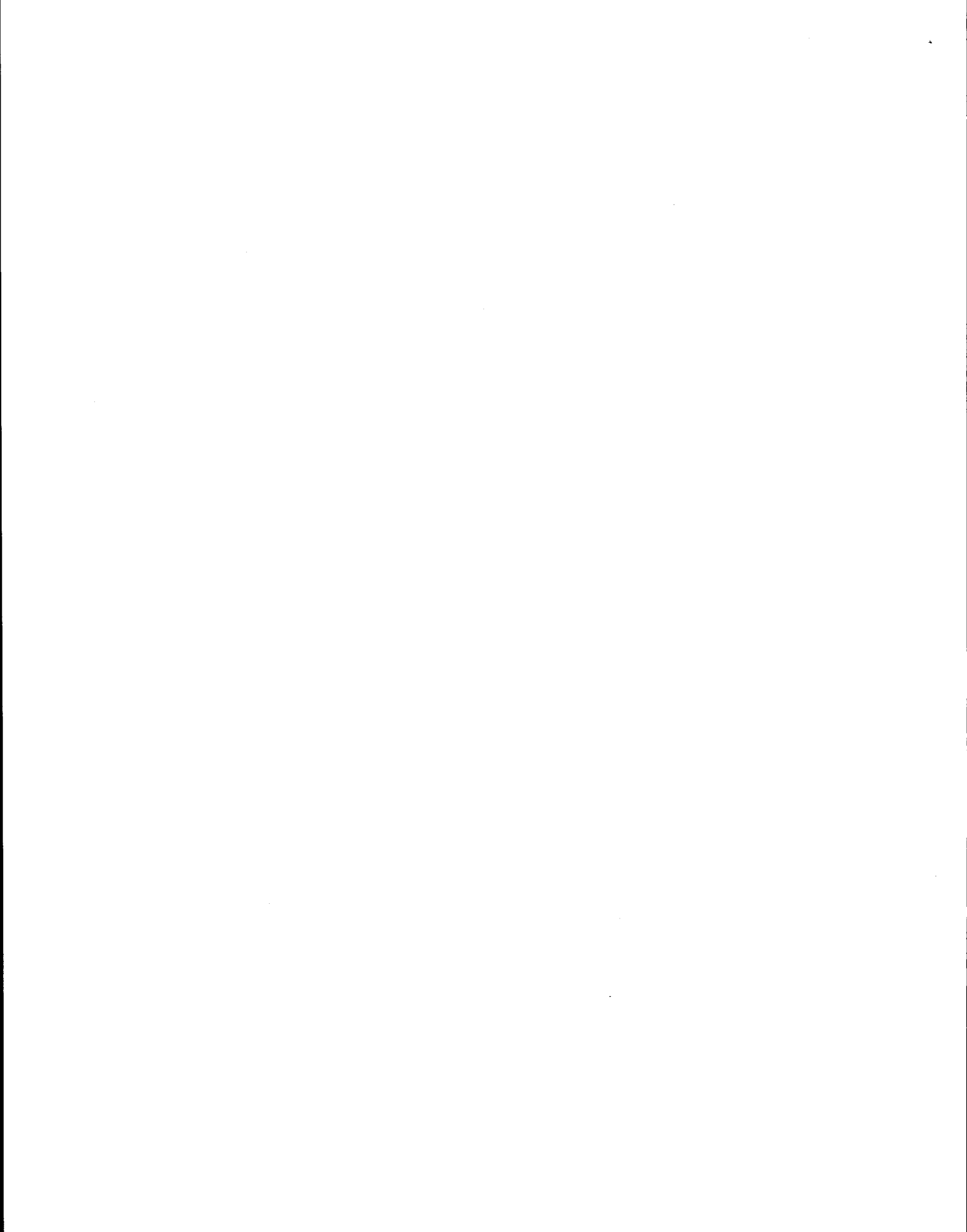
- Figure 9b. August SI for the above conditions except with 50 knot winds.
- Figure 10a. August SI for conditions of minimum sea ice extent, maximum sea surface temperatures, minimum air temperatures, and 28 knot winds.
- Figure 10b. August SI for the above conditions except with 50 knot winds.
- Figure 11a. September SI for conditions of mean sea ice extent, mean sea surface temperatures, minimum air temperatures, and 28 knot winds.
- Figure 11b. September SI for the above conditions except with 50 knot winds.
- Figure 12a. September SI for conditions of mean sea ice extent, mean sea surface temperatures, mean air temperatures, and 28 knot winds.
- Figure 12b. September SI for the above conditions except with 50 knot winds.
- Figure 13a. September SI for conditions of maximum sea ice extent, minimum sea surface temperatures, minimum air temperatures, and 28 knot winds.
- Figure 13b. September SI for the above conditions except with 50 knot winds.
- Figure 14a. September SI for conditions of minimum sea ice extent, maximum sea surface temperatures, minimum air temperatures, and 28 knot winds.
- Figure 14b. September SI for the above conditions except with 50 knot winds.
- Figure 15a. September SI for conditions of minimum sea ice extent, maximum sea surface temperatures, mean air temperatures, and 28 knot winds.
- Figure 15b. September SI for the above conditions except with 50 knot winds.
- Figure 16a. October SI for conditions of mean sea ice extent, mean sea surface temperatures, minimum air temperatures, and 28 knot winds.
- Figure 16b. October SI for the above conditions except with 50 knot winds.
- Figure 17a. October SI for conditions of mean sea ice extent, mean sea surface temperatures, mean air temperatures, and 28 knot winds.
- Figure 17b. October SI for the above conditions except with 50 knot winds.
- Figure 18a. October SI for conditions of maximum sea ice extent, minimum sea surface temperatures, minimum air temperatures, and 28 knot winds.
- Figure 18b. October SI for the above conditions except with 50 knot winds.

- Figure 19a. October SI for conditions of maximum sea ice extent, minimum sea surface temperatures, mean air temperatures, and 28 knot winds.
- Figure 19b. October SI for the above conditions except with 50 knot winds.
- Figure 20a. October SI for conditions of minimum sea ice extent, maximum sea surface temperatures, maximum air temperatures, and 28 knot winds.
- Figure 20b. October SI for the above conditions except with 50 knot winds.
- Figure 21a. October SI for conditions of minimum sea ice extent, maximum sea surface temperatures, minimum air temperatures, and 28 knot winds.
- Figure 21b. October SI for the above conditions except with 50 knot winds.
- Figure 22a. October SI for conditions of minimum sea ice extent, maximum sea surface temperatures, mean air temperatures, and 28 knot winds.
- Figure 22b. October SI for the above conditions except with 50 knot winds.
- Figure 23a. November SI for conditions of mean sea ice extent, mean sea surface temperatures, mean air temperatures, and 28 knot winds.
- Figure 23b. November SI for the above conditions except with 50 knot winds.
- Figure 24a. November SI for conditions of minimum sea ice extent, maximum sea surface temperatures, maximum air temperatures, and 28 knot winds.
- Figure 24b. November SI for the above conditions except with 50 knot winds.
- Figure 25a. November SI for conditions of minimum sea ice extent, maximum sea surface temperatures, mean air temperatures, and 28 knot winds.
- Figure 25b. November SI for the above conditions except with 50 knot winds.



LIST OF TABLES

- Table 1a. Characteristics of structural icing months for the North Chukchi (Region A). (See Figure Cover Page).....
- Table 1b. Characteristics of structural icing months for the Hope Basin (Region C). (See Figure Cover Page).....
- Table 2. Environmental conditions capable of producing structural icing from May through November in the Hope Basin (C), North Chukchi (A) and South Chukchi (B) regions. (See Figure Cover Page).....



INTRODUCTION

Icing is mainly a function of the amount of water which remains liquid after striking a ship's or fixed platform's surface and the elapsed time before this water freezes. There are two types of ice accumulation, rime ice and glaze ice. Rime is rough, milky, opaque ice with minimal adhesion and is formed when small, super-cooled drops of water freeze on contact with a surface. It does not spread and can form at any temperature in the icing range. Glaze is formed on slow freezing of large super-cooled drops. It can spread over a larger surface and is harder to remove than rime icing (the preceding paragraph has been paraphrased from Berry et al., 1975).

Ice accretion depends on many factors. Meteorology and sea conditions are paramount (see below). However, vessel size, navigational peculiarities, structural design, kinematic and thermodynamic interaction at the surface of a design member and water droplets (stagnation zones on a surface, Ackley and Templeton, 1979) also become critical.

EFFECTS ON SHIPS

Ships such as fishing trawlers, smaller merchant ships, and Coast Guard Cutters are most vulnerable to icing due to less freeboard and the increased amount of travel time through an area experiencing icing conditions. It should be noted that the right combination of events can produce icing on large vessels also. Icing on a vessel increases its weight, changes its trim, elevates its center of gravity, decreases its metacentric height and increases its sail area and heeling moment leading to extreme handling difficulties (Berry et al. 1975).

ICING ON OFFSHORE STATIONARY PLATFORMS

As on ships, a coating of ice on external surfaces can elevate the platform's center of gravity. In addition, the ice will usually form in stagnation zones on the windward side (Ackley and Templeton, 1979) causing an imbalanced weight distribution on a platform. Vertical and horizontal members of offshore structures are designed to meet oscillatory stresses due to wave action. The forces on the structure are made up of hydrodynamic drag and inertial (mass) components. Icing changes the physical characteristics of structure members, such as diameter, surface roughness, mass and flexural response (Ippen 1966). Therefore, a fixed structure's ability to withstand a design wave is questionable after and during an extreme ice accumulation.

Depending on freezing rates, the ice forming on structures due to sea spray will generally have a salt content much less than the sea salinity and may even approach 0 ‰ salinity. The maximum pressure produced by water freezing in a confined space is 30,000 lb in⁻². This stress on a structure or ship occurring during a freezing sea spray condition can drastically weaken support members.

METEOROLOGY AND SEA CONDITIONS

(the following subsections have been paraphrased from Berry et al., 1975)

FREEZING RAIN AND SNOW

Freezing rain itself seldom reaches large enough accumulations to be the sole source of danger to a ship. However, combined with freezing salt spray

(see below) it becomes dangerous since, as freshwater, it freezes faster than salt water and can act as a nucleus for faster ice accumulation from salt spray. Snow is not considered a threat due to inherent lack of adhesion.

ARCTIC SEA-SMOKE

Arctic sea-smoke forms when extremely cold air flows over much warmer water. The water vapor that results from the ensuing evaporation condenses immediately in the cold air and super-cooled droplets become visible as rising columns of "steam". Weight of ice deposited is only a problem if the condition exists for a long time since it is a low wind phenomenon.

"SEA ICE"

Water taken over the side of the ship will not freeze readily unless trapped by ice chocked rails and ports. This is considered a minimal hazard.

FREEZING SPRAY

This report has been developed mainly for freezing spray conditions. This is the most common and dangerous form of icing, resulting in glaze ice characterized by high density and great adhesion power. This type of icing is a function of several simultaneously occurring variables:

Air Temperature

The critical range for this study is from 0°F to 32°F (-18°C to 0°C). At temperatures below 0°F the water striking the structure will usually be in the form of non-adhering small dry ice crystals (Berry et al., 1975).

Wind

Sea spray generation depends on the wave height and period of waves. Waves in turn depend on the duration of the wind and fetch. Generally, the higher the wind speed for the above temperature range, the greater the ice accumulation. The range of wind speeds covered in this study are from 25 knots (12.5 ms^{-1}) to 60 knots (30 ms^{-1}). Data indicate that wind speeds below 25 knots do not produce icing, while wind speeds in excess of 60 knots are rare. Wu (1982) mentions that a wind speed of 12.5 ms^{-1} is considered the incipient velocity for entrainment of water particles in air (without need of waves).

Effect of the Ice Pack

When the ice pack concentration reaches 50% areal coverage, superstructure icing is thought to be minimal since wave formation is reduced and freezing spray is eliminated.

Sea Temperature

The critical range of sea surface temperatures are 28° F (-2.2° C) to 48° F (8.9° C). Seawater of normal salinities is generally frozen below 28° F . The upper value of 48° F is not an impediment to freezing since sea spray can be cooled rapidly when air temperatures are below 28° F .

A dangerous layer of ice accumulation occurs at 3.9 in (10 cm, Berry et al., 1975). Of the five icing categories used in this study, extreme icing would produce this thickness in 4.5 hours, heavy icing would produce this thickness in 8 hours, and light icing would produce this thickness in one day.

CONSTRUCTION OF ICING MAPS

To construct icing contours for the figures discussed below (see end of text), two data sources were used. The monthly positions of the northern, southern and mean 5/8 areal coverage sea ice edge are shown in Brower et al. (1977) for the Chukchi Sea. Their ice edge positions were derived from 17 years of aerial, ship and satellite observations of the pack ice edge (1954 through 1970). Recently Dr. William Stringer (University of Alaska) completed a sea ice occurrence probability study (as yet unpublished) using satellite data collected from 1973 to 1984. His study was based on sea ice of any concentration appearing in designated map grid areas during weekly time periods from June through November. As a result, Stringer's 50% ice frequency position (over each month) was more "conservative" (appeared farther south) than the mean 5/8 areal coverage position of Brower et al. (1977) but had the same general shape except for November. The same description fits the monthly comparisons of the northern limits of 5/8 areal coverage position (Brower et al., 1977) with the 100% sea ice probability ice edge (Stringer) and the southern limit of the 5/8 areal coverage position (Brower et al., 1977) with the 0% sea ice (open water) probability ice edge (Stringer). Despite differences in data types and length of the studies, the results seemed quite consistent. Therefore, the position of the mean, maximum (southernmost) and minimum (northernmost) sea ice edge used below were taken as the average of the corresponding edges from the above two data sources. Average and extreme contours of sea surface and air temperatures for map construction came from Brower et al. (1977).

The wind speed and temperature data in Table 1a (North Chukchi) and Table 1b (Hope Basin) came from the nearest marine areas and least orographically modified shore stations (when marine area data was unavailable) shown in Brower et al. (1977). There is no evidence of any area in the Chukchi having monthly mean winds of 25 knots (12.5 ms^{-1}). Therefore mean wind contours were not useful in constructing icing maps. The World Meteorological Organization (W.M.O.) lists 28 knots (14 ms^{-1}) as the onset of dangerous wind speeds (gale level winds) and 50 knots (25 ms^{-1}) as the onset of real storm level winds. Hence, these levels were used as the critical winds for mean and extreme icing. Table 1 shows the % time of occurrence of gale and storm level winds during possible icing months. In addition the % of air temperatures below 0° F (18° C), which generally preclude superstructure icing, are shown. It must be noted that while the percentages are low for the total time of occurrence of these wind speeds, the probability of these speeds existing in each month is 100% and the duration of these speeds is sufficient to produce severe icing provided the other environmental conditions are met. Therefore, fixed structures which remain in place in one location over many months will be more susceptible to icing than vessels which may move in and out of a given area.

A new nomogram for superstructure icing in Alaskan waters has been used which is similar to but replaces that of Wise and Comiskey (1980). The nomogram, also developed by Comiskey, was discussed by L. D. Leslie (Arctic Environmental Information and Data Center) at the "Symposium on Meteorology and Oceanography of the High Northern Latitudes" (October, 1984, Anchorage). It has icing rates double those of the previous nomogram.

Five rates of ice accumulation are used in icing maps (Figs. 1-25) constructed for this study. The codes for these rates are shown on the

Table 1a. Characteristics of Structural Icing Months for the North Chukchi (Region A).

Icing Months	% Winds		% air temperature <-18° C
	>28 kn (14 ms ⁻¹) W.M.O.* Gale	>50 kn (25 ms ⁻¹) W.M.O.* Storm	
June	5	0	0
July	3	0	0
August	4	0	0
September	6	<1	0
October	6	0	4
November	~5**	0**	~50**

Note: Under conditions of mean sea ice extent, the North Chukchi area has some open water for the months of August, September and October only.

Table 1b. Characteristics of Structural Icing Months for the Hope Basin (Region C).

Icing Months	% Winds		% air temperature <-18° C
	>28 kn (14 ms ⁻¹) W.M.O.* Gale	>50 kn (25 ms ⁻¹) W.M.O.* Storm	
May	10	0	0
June	3	0	0
July	5	<1	0
August	5	<1	0
September	7	<1	0
October	14	<1	8
November	~14**	1**	~40**

*W.M.O. ≡ World Meteorological Organization.

**Data average from three coastal sites with least amount of orographic modification

These tables were compiled from Brower et al. (1977). It is assumed that the south Chukchi (Region B) has statistics that are a mean of the statistics of Region A and C. The Regions A, B, and C are defined on the Figure Cover Page at the end of the text (page 335).

Figure Cover Page along with map outlines of the North Chukchi (A), South Chukchi (B), and Hope Basin (C) area locations. The dividing line between the North Chukchi and South Chukchi areas is roughly the 50 m isobath. The most common waves in any ocean are gravity waves which range in periods from 1 to 30 S (Kinsman, 1965). The 50 m isobath represents a transition depth from deep to shallow water for a majority of these very common waves. As waves move from deep to shallow water, they slow down, shorten in length, become higher and less stable making it easier for the wind to blow their tops off. Therefore, a given swell type (wind waves that have traveled out of their generating area) will produce more icing in the shallower South Chukchi area than the North Chukchi for similar wind speeds.

Superstructure icing is precluded above the ice edge line shown on the Figures below (see end of text). It must be remembered that sea ice edge positions, whether mean, minimum, or maximum, will have corresponding sea surface temperatures which have "adjusted" to the edge position with the lowest sea temperatures adjacent to the ice. These sea surface temperatures will have a much greater thermal inertia than the atmosphere above them. Therefore, even on minimum sea ice extent years with higher than average sea surface temperatures, a sudden cold front with high winds can move into the Chukchi Sea and produce severe icing. For the time scales important to superstructure icing, atmospheric conditions will generally change quicker than oceanic conditions and appear to be the most critical variable in the "puzzle".

DESCRIPTIONS OF ICING MONTHS

The Chukchi Sea conditions presented monthly are for mean, maximum and minimum sea ice edges with corresponding sea surface temperature fields. Each of these three edge positions is in turn matched to mean, maximum and minimum recorded air temperature fields. The resulting nine possible environmental combinations are subjected to wind speeds of 28 knots (14 ms^{-1}) and 50 knots (25 ms^{-1}). Eighteen environmental combinations have been evaluated for each icing month. Despite this extensive study, real icing conditions will fall somewhere between the conditions shown on the maps below. Table 1 shows that gale force winds average 5% and 8% of each month in the North Chukchi and Hope Basin regions, respectively. This is a time period of at least 36 hours. Even light icing conditions produce a dangerous ice accumulation of 3.9 inches (10 cm) in under 24 hours (see Meteorology and Sea Conditions Section). Table 2 catalogs these combinations from May through November in the North Chukchi (A), South Chukchi (B) and Hope Basin (C) regions. The Figure Cover Page shows the area designations and superstructure icing (SI) codes. The months with the greatest chance for superstructure icing in all three regions are September and October.

MAY

Four out of the 18 chosen environmental combinations for SI exist (see Table 2). This month shows the A and B regions to be completely covered by sea ice and C, only partially uncovered with the sea ice edge at its minimum

Table 2. Possible Structural Icing Months for Hope Basin, North Chukchi and South Chukchi Regions.

May	June	July	August	September	October	November	Environmental Conditions	
							28 Knot (14 ms ⁻¹) Gale Class Winds Sea Ice Extent	
I I I	TH M(C)† TH	TH L(B),L(C)† TH	TH L(A),L(B),L(C)† TH	TH H(A),M(B),L(C)† L(A),L(B)†	TH H(B),H(C)† H(A),H(B),M(C)†	TH TL M(C)†	Mean**	Max. Air Temp. (1%) Min. Air Temp. (1%) Mean Air Temp.
I I I	I I I	TH L(C)† TH	TH L(B),L(C)† TH	TH M(B),M(C)† TH	TH VH(C)† M(C)†	I I I	Max.**	Max. Air Temp. (1%) Min. Air Temp. (1%) Mean Air Temp.
TH VH† M(C)†	TH M(C),M(B)† TH	TH L(A),L(B)† TH	TH L(A),L(B)† TH	TH M(A),L(B),L(C)† L(A),L(B)†	TH M(B),M(C)† H(A),M(B),L(C)†	M(A),L(B),L(C)† TL VH(A),VH(C)†	Min.**	Max. Air Temp. (1%) Min. Air Temp. (1%) Mean Air Temp.
I I I	TH VH(C)† TH	TH M(B),L(C)† TH	TH H(A),M(B),L(C)† TH	TH VH(A),VH(B),H(C)† M(A),L(B)†	TH E(A),E(B),E(C)† VH(A),VH(B),H(C)†	TH TL E(C)†	Mean**	Max. Air Temp. (1%) Min. Air Temp. (1%) Mean Air Temp.
I I I	I I I	TH M(C)† TH	TH H(B),H(C)† TH	TH VH(B),VH(C)† TH	TH E(C)† VH(C)†	I I I	Max.**	Max. Air Temp. (1%) Min. Air Temp. (1%) Mean Air Temp.
TH E(C)† VH(C)†	TH VH(B),VH(C)† TH	TH H(A),L(B)† TH	TH H(A),M(B)† TH	TH VH(A),H(B),M(C)† M(A),L(B)†	TH E(A),E(B),VH(C)† E(A),VH(B),H(C)†	VH(A),H(B),M(C)† TL E(A),E(B),E(C)†	Min.**	Max. Air Temp. (1%) Min. Air Temp. (1%) Mean Air Temp.

Factors Precluding Icing

I = Sea ice covering area
 TL = Air temperature too low
 TH = Air temperature too high
 SS = Sea surface temperature too high

† = Icing Possible

Worst Icing Possible

E = Extreme
 VH = Very heavy
 H = Heavy
 M = Moderate
 L = Light

Regions

C = Hope Basin
 A = North Chukchi
 B = South Chukchi

**Mean, max. and min. sea ice extent also corresponds to mean, max. and min. sea surface temperatures

recorded extent (Figs. 1 and 2). Figure 1 shows SI under mean air temperatures with (a) for 28 knot winds and (b) for 50 knot winds. The 50 knot case can result in very heavy icing in Region C. Figure 2 shows SI under minimum recorded air temperatures for conditions of 28 and 50 knot winds. In Figure 2b for 50 knot winds, extreme icing conditions will occur. It should be noted that the combined probability of finding any open water in Region C along with extreme minimum air temperatures and 50 knot winds in May is almost negligible (less than .01%).

JUNE

Four out of the 18 chosen environmental combinations for SI exist (see Table 2). With the sea ice edge at its mean extent, only Region C is uncovered (Fig. 3). A mean or maximum recorded air temperature field is too warm for icing. Under minimum air temperatures, moderate (Fig. 3a) and very heavy (Fig. 3b) icing levels are reached for 28 knot and 50 knot winds, respectively. The minimum extent of sea ice recorded shows Regions B and C open (Fig. 4). Only minimum air temperatures produce SI at levels up to moderate and very heavy for wind speeds of 28 knots (Fig. 4a) and 50 knots (Fig. 4b), respectively. SI chances in June are greater than in May, but Region B has a less than .01% probability and Region A has 0 probability.

JULY

Only six out of 18 chosen environmental combinations for SI exist (see Table 2). Mean or maximum air temperature fields are too warm for icing. For a mean sea ice edge and minimum recorded air temperatures, light SI (Fig. 5A) and up to moderate SI (Fig. 5b) can be seen for 28 knots and 50

knots, respectively in Region B. Region A is completely covered by sea ice and most of Region C has air temperatures above freezing, precluding icing (Fig. 5). Maximum sea ice extent with minimum air temperatures show light SI (Fig. 6a) and up to moderate SI (Fig. 6b) in Region C only, since sea ice covers Regions A and B. Minimum recorded sea ice extent uncovers Regions A, B and C (Fig. 7). The sea surface temperatures associated with minimum sea ice extent preclude SI in Region C, however. Region B would suffer light SI under 28 to 50 knot winds, but Region A would reach heavy icing conditions under 50 knot winds (see Fig. 7a and b). SI chances in July are greater than in June, but Region C conditions will never get beyond light icing and chances in Region A are less than .01%. Typical July temperatures would preclude any icing. This is a month of high ship traffic in the study area.

AUGUST

SI can exist for six out of 18 chosen environmental combinations (see Table 2). As in July, mean or maximum air temperature fields are too warm for icing. A mean sea ice edge coupled with a minimum air temperature field produces light SI in Regions A, B, and C for 28 knot winds (Fig. 8a). Fifty knot winds will produce heaving icing in Region A, moderate icing in Region B, and light icing in Region C (Fig. 8b). It should be noted that most of Region A is covered while most of Region C is too warm for icing (Fig. 8).

Maximum sea ice extent with a minimum air temperature field precludes SI in Region A due to sea ice extent and eliminates SI in most of Region C due to temperatures above freezing (Fig. 9). SI can change from light to heavy in both Regions B and C under wind conditions of 28 knots (Fig. 9a) and 50 knots (Fig. 9b), respectively.

Minimum sea ice extent and a minimum air temperature field precludes SI in Region C and most of B because the sea surface temperatures associated with this edge position would be too warm (Fig. 10). All region A would be susceptible to SI with conditions of light changing to heavy if wind speeds changed from 28 knots (Fig. 10a) to 50 knots (Fig. 10b).

SI chances in August are greater than in July because there is more open water under average ice edge conditions. However, chances of heavy icing in Region B or C are less than .01%. Typical August temperatures would preclude icing. Ship traffic in August is typically high.

SEPTEMBER

SI can exist for 10 of 18 selected environmental combinations (see Table 2). Maximum air temperature fields were too warm for SI (Table 2). A mean sea ice edge coupled with a minimum air temperature field (1% probability) can produce SI in all Regions, A-C (Fig. 11). A change in wind speed from 28 knots (Fig. 11a) to 50 knots (Fig. 11b) can produce very heavy icing conditions in Region A which is closest to the mean ice edge.

A mean sea ice edge subjected to a mean air temperature field is the most probable situation that would be encountered (Fig. 12). SI is not encountered in Region C and most of Region B due to air temperatures above freezing (Fig. 12). Region A can reach moderate SI at wind speeds of 50 knots (Fig. 12b) which have a less than 1% chance of occurring in September (Table 1a).

A maximum sea ice extent condition precludes SI in Region A (Fig. 13) and is far enough south that a mean or maximum air temperature field would produce air temperatures above freezing for open water areas in Regions B and C. Condition of a minimum air temperature field with winds of 28 knots (Fig.

13a) and 50 knots (Fig. 13b) will produce moderate and very heavy SI, respectively, in Regions B and C. However, the chance for this set of events occurring is less than .01%.

A combination of minimum sea ice extent and a minimum air temperature field (less than .01% probability) will produce SI in Regions A-C (Fig. 14). However, the sea surface temperature field associated with this sea ice edge will have ocean temperatures too high (SS) for icing in most of Region C. Under 28 knot winds only moderate icing levels are reached in Region A (Fig. 14a), while 50 knot winds produce very heavy icing in a portion of Region A (Fig. 14b).

Minimum sea ice extent coupled with mean air temperatures will result in no SI in most of Regions B and C due to air temperature above freezing (TH) (Fig. 15). A change from 28 knot winds (Fig. 15a) to 50 knot winds (Fig. 15b) will increase the SI from light to moderate in part of Region A.

SI chances in September are greater than August because the average temperatures are lower and there is more open water under average ice edge conditions. Ship traffic would be high during this month. Typical September conditions would preclude icing in Region B or C with moderate icing at 50 knot wind speeds (not common, see Table 1a) in Region A.

OCTOBER

SI can exist for 14 of 18 selected environmental combinations (see Table 2). This month is the one with the greatest probability of icing. It is fortunate that ship traffic is not as high as July, August or September in Regions A-C at this time of year.

A mean sea ice edge and minimum air temperature field (Fig. 16) will produce extreme SI under 50 knot winds in Regions A-C (Fig. 16b). It must be

noted that at wind speeds of 28 knots (Fig. 16a) sea spray would freeze before striking a structure and not adhere. This condition is designated TL and covers most of Region B and the open water portion of Region A.

The most typical conditions are those of a mean sea ice edge and mean air temperature field (Fig. 17). They can produce heavy icing in the same regions under 50 knot winds (Fig. 17b). Gale force winds have a 10% probability (mean of statistics for Regions A and C in Tables 1a and b) of occurrence in Region B.

A maximum sea ice edge extent will cover Regions A and B precluding SI there. In combination with minimum air temperatures over Region C, SI will range from very heavy (Fig. 18a) to extreme (Fig. 18b) under winds of 28 knots and 50 knots, respectively. In combination with mean air temperatures over Region C, SI will range from moderate (Fig. 19a) to very heavy (Fig. 19b) under wind speeds of 28 knots and 50 knots, respectively.

A minimum sea ice edge extent combined with maximum recorded air temperatures (less than .01% probability) will result in SI in Region A only (Fig. 20). These conditions will result in light SI and heavy SI Region A under winds of 28 knots (Fig. 20a) and 50 knots (Fig. 20b), respectively.

A minimum sea ice edge and minimum air temperatures (less than .01% probability) will produce moderate SI in Region C under 28 knot winds (Fig. 21a). However, the low temperatures (TL) would cause spray to freeze before striking the ship, resulting in no SI in Region A and most of Region B. At 50 knots, Region A and most of Region B would be subjected to extreme SI (Fig. 21b), while most of Region C would reach very heavy icing.

A minimum sea ice edge with mean air temperatures results in some kind of SI over all three regions (Fig. 22). The most dominant SI changes from

light to moderate in Region C, moderate to heavy in Region B, and moderate to very heavy in Region A as wind speeds change from 28 knots (Fig. 22a) to 50 knots (Fig. 22b), respectively.

Typical October conditions would have Region A mostly ice covered precluding SI there. However, gale force winds in Region B (10% chance, Table 1a and b combined) and Region C (14% chance, Table 1b) could produce moderate SI and light SI, respectively.

NOVEMBER

SI can exist for six out of 18 selected environmental combinations (see Table 2). A maximum recorded sea ice edge precludes open water in Regions A-C so SI would be non-existent.

A mean sea ice edge will have open water in a portion of Region C only (Fig. 23). Maximum air temperatures are too warm and minimum air temperatures are too cold for icing in Region C. Mean air temperatures will produce heavy icing and extreme icing under 28 knot winds (Fig. 23a) and 50 knot winds (Fig. 23b), respectively. Gale force winds under these typical conditions can be expected 14% of the time (Table 1b).

Conditions of a minimum sea ice edge and maximum air temperatures (less than .01% chance) can produce SI levels up to very heavy in Regions A and B under 50 knot winds (Fig. 24b). Most of Region C would have air temperatures above freezing (Fig. 24) under these conditions, eliminating a chance for SI.

A minimum sea ice edge and mean air temperatures (combined 1% chance) would produce very heavy and extreme SI under 28 knots (Fig. 25a) and 50 knots (Fig. 25b) winds respectively. It should be noted that a minimum air temperature field produces temperatures too low for SI.

If open water exists in Region A, B, or C in November, there is a better than 10% chance of heavy icing under gale force winds (see Table 1b).

SUMMARY

Remember that real icing conditions will fall somewhere between the environmental combinations chosen for Figures 1-25 and Table 2. Ocean thermal inertia will make atmospheric changes, which operate on a shorter time scale, the most dangerous for evolving SI conditions. For example, sudden cold fronts with high winds can move into the Chukchi Sea under average sea ice edge extent and produce heavy icing in the "warm" months of July and August. September and October are the months with the greatest chance for SI. Table 2 shows that they have the most possible combinations for SI (10 September, 14 October). All conditions other than mean conditions have a 1% chance of occurrence. Therefore, any two independent combinations of these 1% probability conditions have a .01% chance of occurrence. However, sea ice extent and sea surface temperatures are not independent.

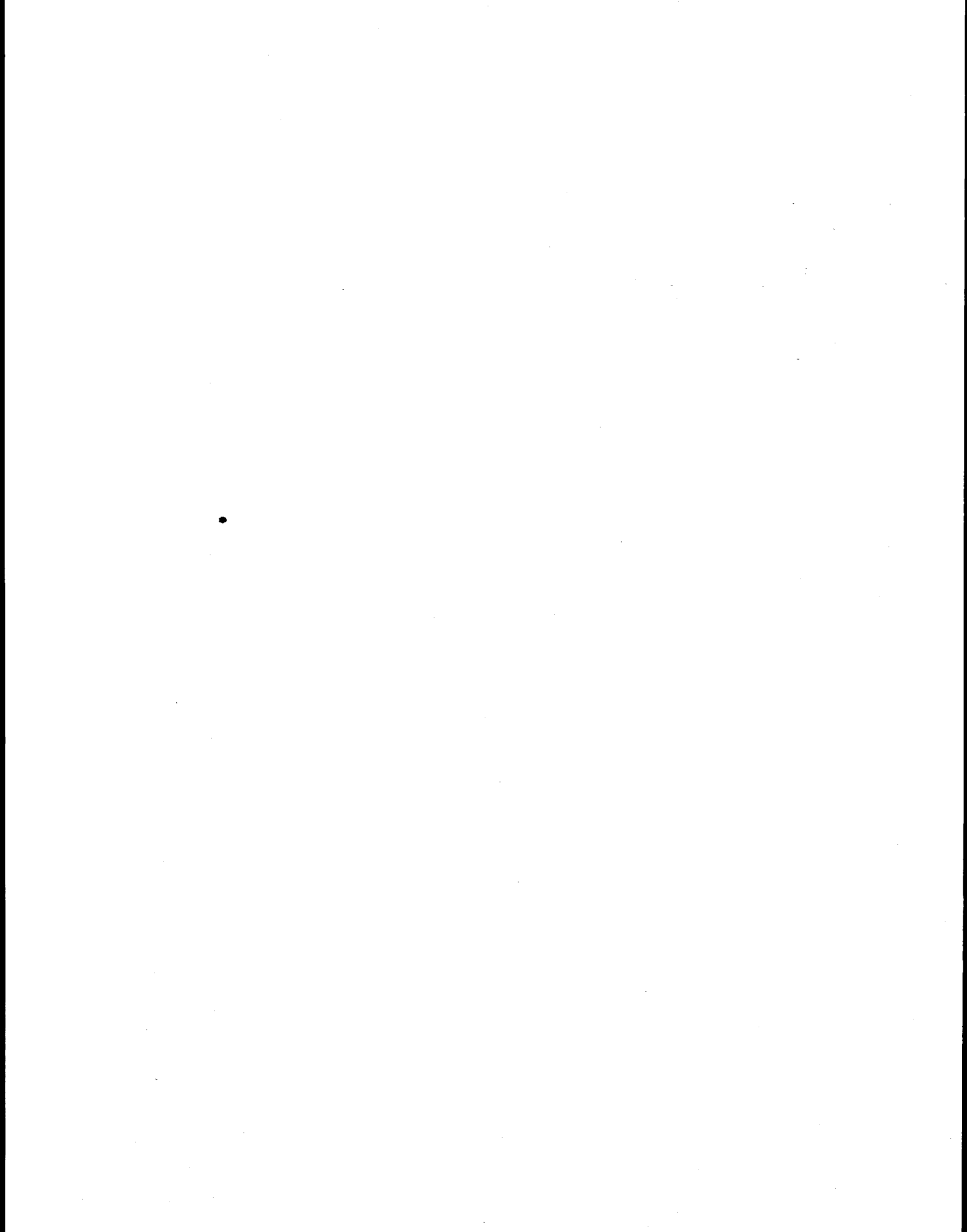
A polynya exists along the Alaskan Chukchi coast between Pt. Barrow and Pt. Hope in the months of February to April when the study area is usually ice covered (Stringer, 1982). Stringer's study (eight years of data) has shown that this polynya is closed 77% of the time in February and averages 12 km wide. In April, it is closed 62% of the time and averages 1 km wide. This would not be a corridor for major ship traffic and would have limited fetch for wave production.

FURTHER STUDY

A data gathering program should be initiated for the North Chukchi, South Chukchi, and Hope Basins. Among the parameters measured during icing events should be salinity of adhering ice, materials with or without coatings adhered to, percentage due to sea spray, ship size, ship speed, types of waves, wave directionality and thickness of ice. Also, some type of meteorological early warning system should be studied.

ACKNOWLEDGEMENTS

This study was funded by the Minerals Management Service, U. S. Department of the Interior, through interagency agreement with the National Oceanic and Atmospheric Administration, U. S. Department of Commerce, as part of the Outer Continental Shelf Environmental Assessment Program.



REFERENCES

- Ackley, S. F. and M. K. Templeton, 1979: Computer modeling of atmospheric ice accretion, CRREL Rpt. #79-4. Hanover, New Hampshire, 36 pp.
- Berry, M.O., P. M. Dutchak, M. E. Lalonde, J. A. W. McCulloch and I. Savdie, 1975: Weather, waves and icing in the Beaufort Sea, Technical Rpt. #21. Meteorological Applications Branch, Atmospheric Environment Service, Ottawa, Ontario. 57 pp.
- Brower, W. A., H. F. Diaz, A. S. Prechtel, H. W. Searby and J. L. Wise, 1977: Climatic Atlas of the Outer Continental Shelf Waters and Coastal Regions of Alaska. Volume III Chukchi-Beaufort Sea, NOAA, NCC, EDS. Asheville, North Carolina. 409 pp.
- Ippen, A. T., 1966: Estuary and Coastline Hydrodynamics. McGraw-Hill, New York, 744 pp.
- Kinsman, B. 1965: Wind Waves. Prentice-Hall, Inc. New Jersey. 676 pp.
- Stringer, W. J. 1982. Width and persistence of the Chukchi polynya. NOAA-OCS Contract #81-RAC00147. Geophysical Institute, University of Alaska, Fairbanks. 22 pp.
- Webster, B. D., 1981: A climatology of the ice extent in the Bering Sea, NOAA Technical memo, NWS AR-33, Anchorage, Alaska, 38 pp.
- Wise, J. L. and A. L. Comiskey, 1980: Superstructure icing in Alaskan Waters, NOAA Special Rpt. Pacific Marine Environmental Laboratory, Seattle, Washington, 30 pp.
- Wu, H. Y., E. Y. Hsu, and R. L. Street, 1979: Experimental study of non-linear wave-wave interaction and white cap dissipation of wind-generated waves, J. of Dynamics of Atmospheres and Oceans, 3, 55-78.
- Wu, J., 1982: Sea Spray: A further look, J. Geophys. Res., 87, 8905-8912.

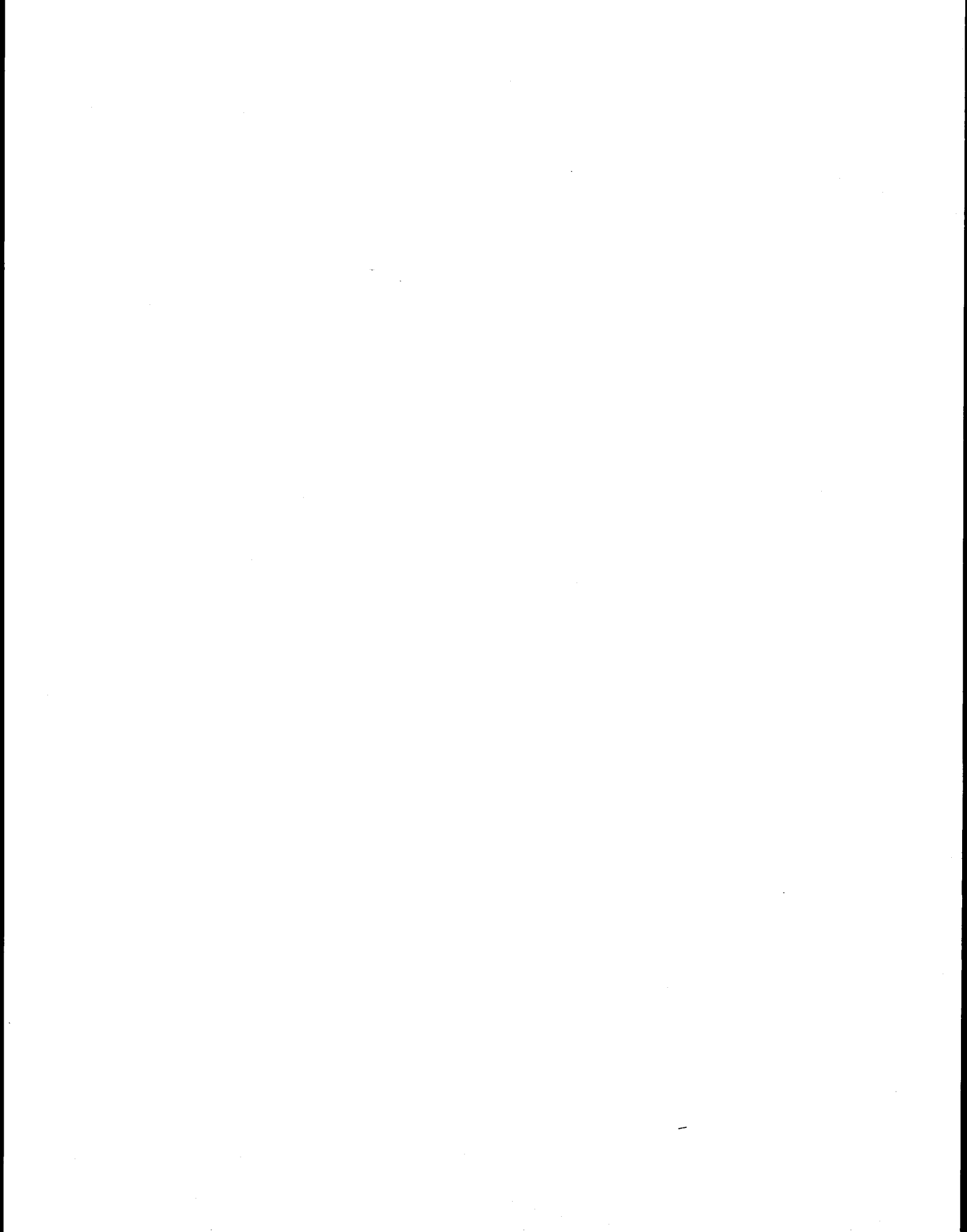
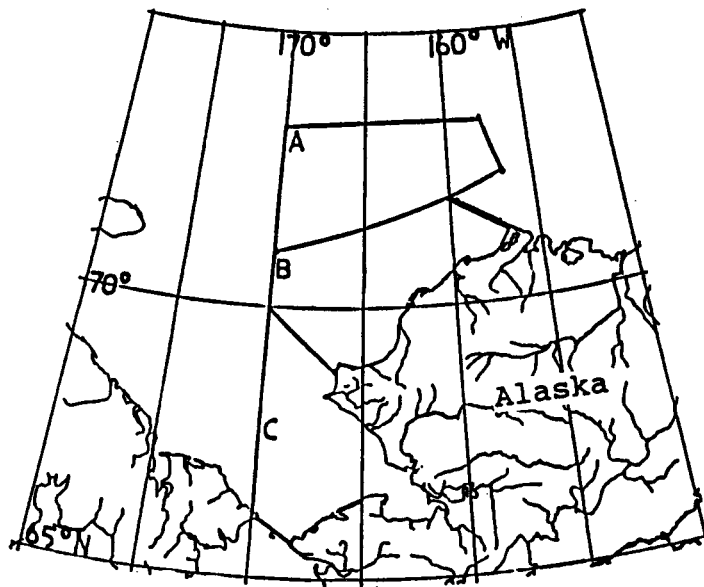


FIGURE COVER PAGE



STUDY REGIONS

- A ≡ North Chukchi
- B ≡ South Chukchi
- C ≡ Hope Basin

 (Sea Ice Edge)

(Icing Categories)		Extreme	2.50 +
		Very Heavy	1.50 to 2.49
		Heavy	1.00 to 1.49 (Inches per 3 hours)
		Moderate	.50 to .99
		Light	0 to .49

(Factors Precluding Superstructure Icing)	I	≡	Sea ice covering area
	TL	≡	Air temperature too low
	TH	≡	Air temperature too high
	SS	≡	Sea surface temperature too high

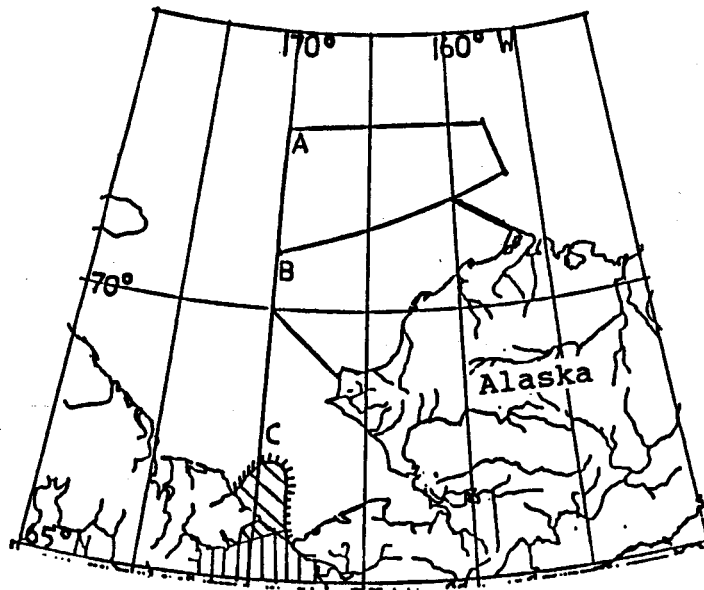


Figure 1a. May superstructure icing (SI) for conditions of minimum sea ice extent, maximum sea surface temperatures, mean air temperatures, and 28 knot winds.

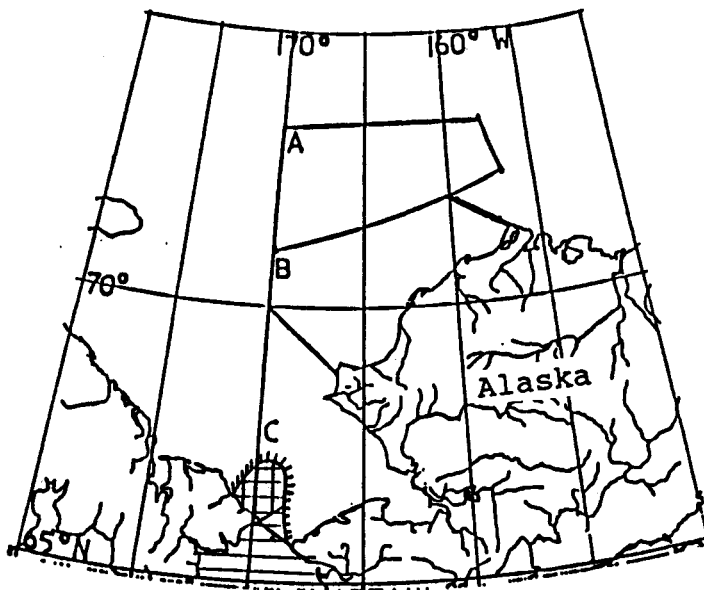


Figure 1b. May SI for the above conditions except with 50 knot winds.

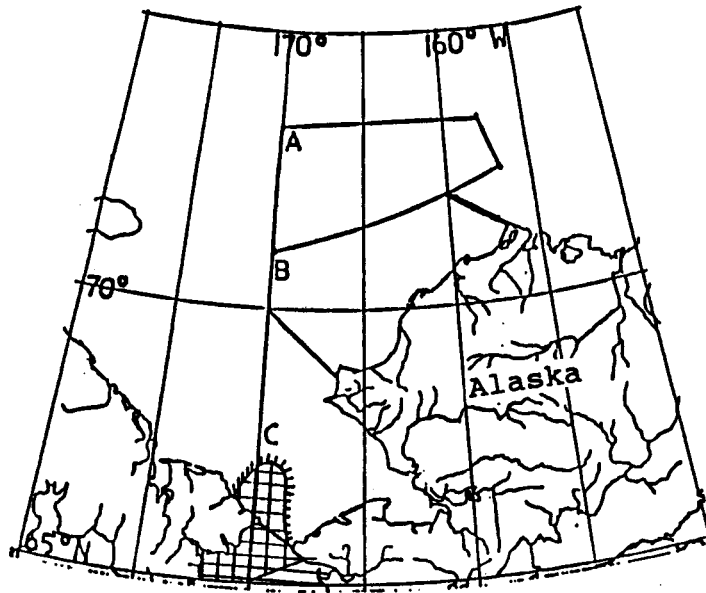


Figure 2a. May SI for conditions of minimum sea ice extent, maximum sea surface temperatures, minimum air temperatures, and 28 knot winds.

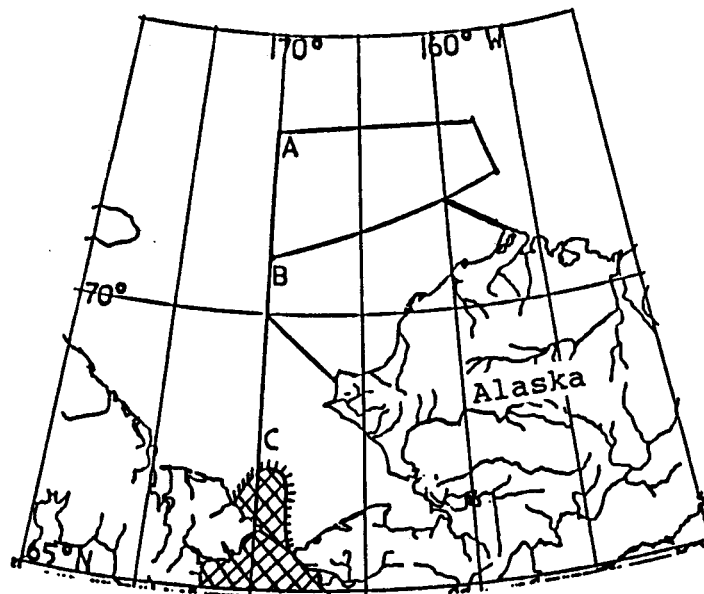


Figure 2b. May SI for the above conditions except with 50 knot winds.

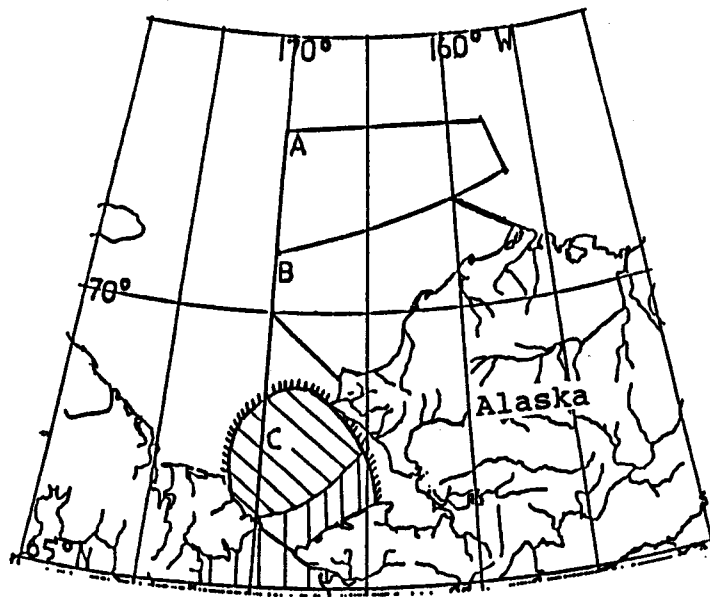


Figure 3a. June SI for conditions of mean sea ice extent, mean sea surface temperatures, minimum air temperatures, and 28 knot winds.

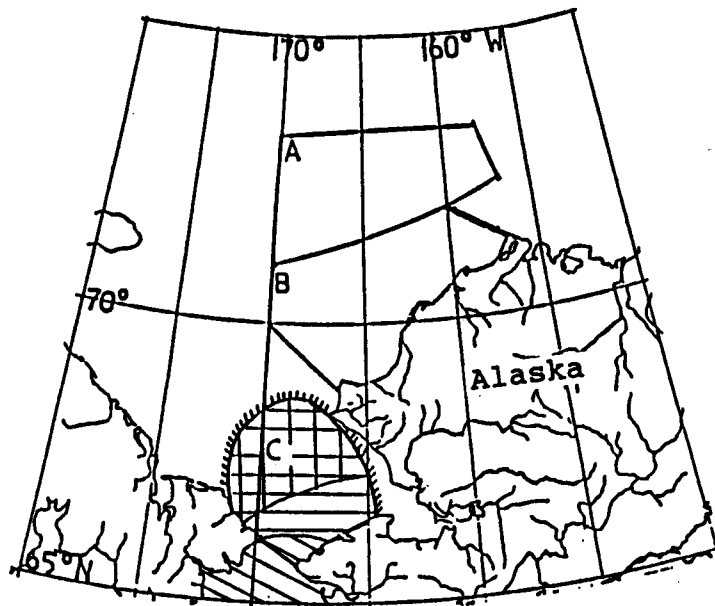


Figure 3b. June SI for the above conditions except with 50 knot winds.

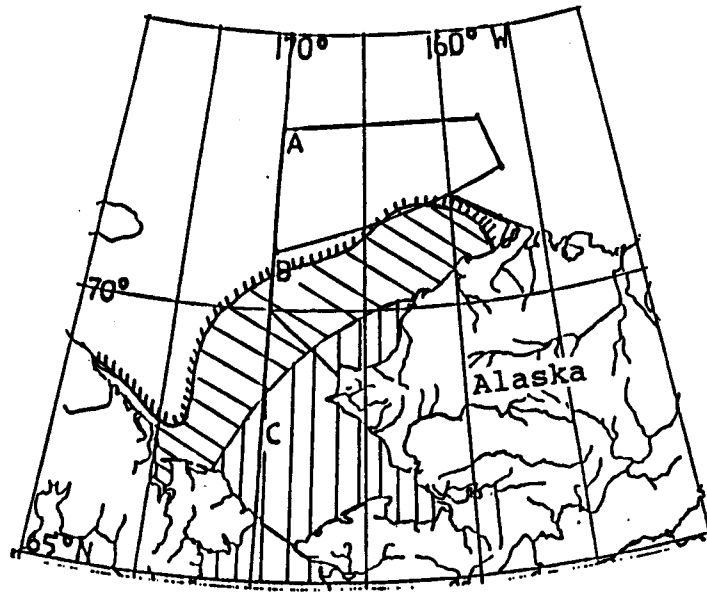


Figure 4a. June SI for conditions of minimum sea ice extent, maximum sea surface temperatures, minimum air temperatures, and 28 knot winds.

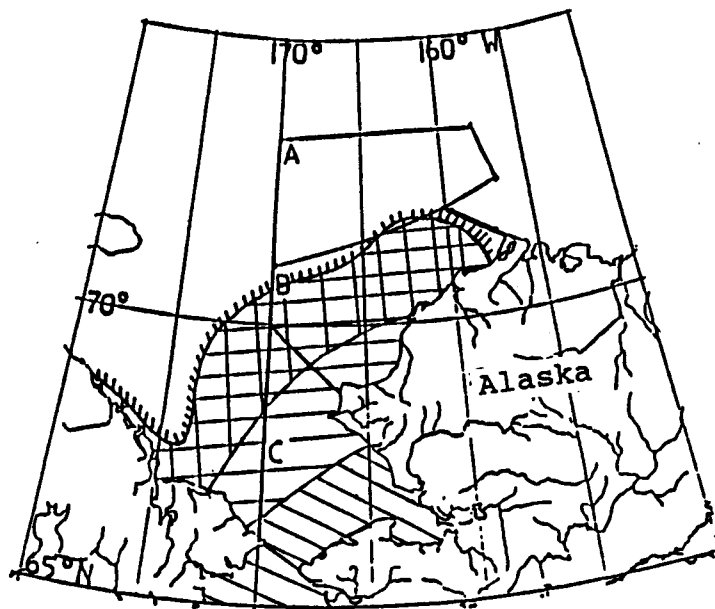


Figure 4b. June SI for the above conditions except with 50 knot winds.

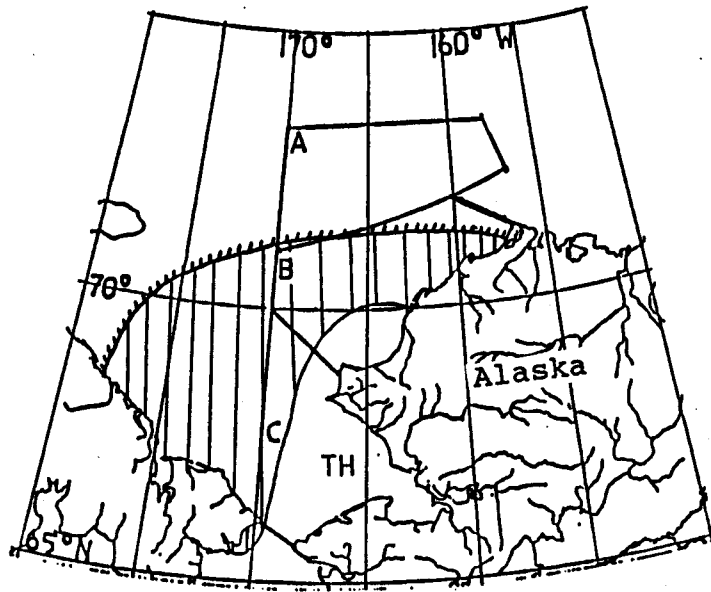


Figure 5a. July SI for conditions of mean sea ice extent, mean sea surface temperatures, minimum air temperatures, and 28 knot winds.

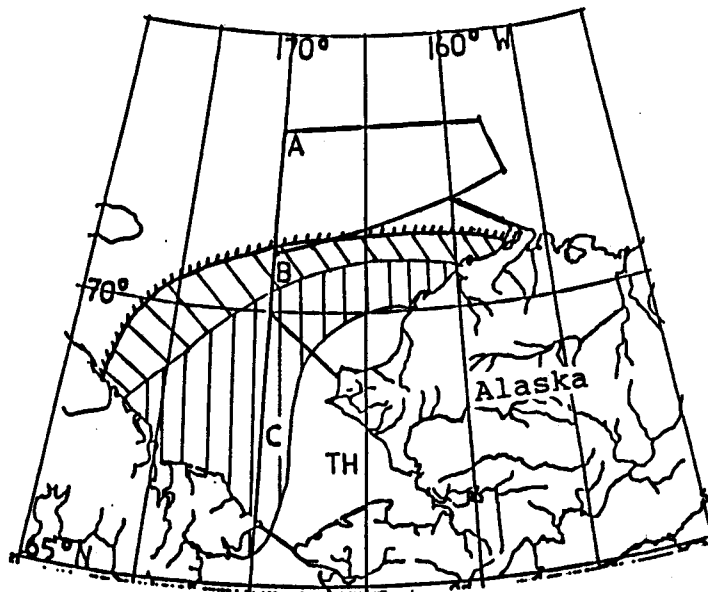


Figure 5b. July SI for the above conditions except with 50 knot winds.

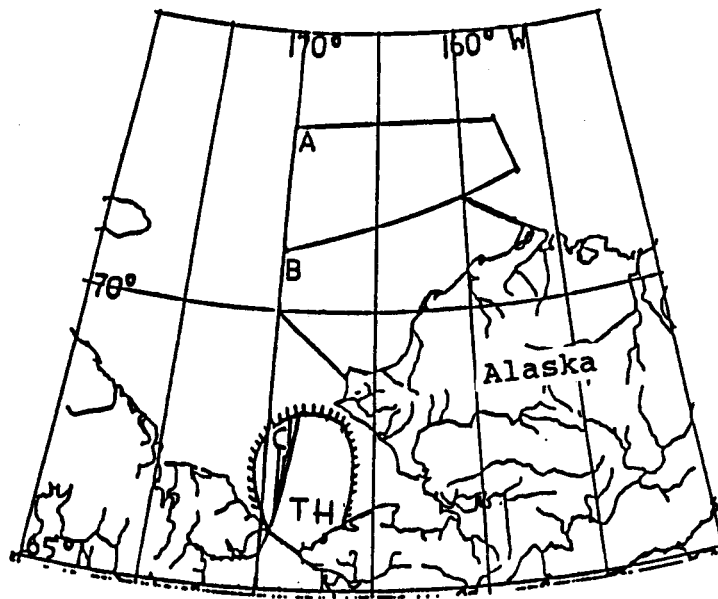


Figure 6a. July SI for conditions of maximum sea ice extent, minimum sea surface temperatures, minimum air temperatures, and 28 knot winds.

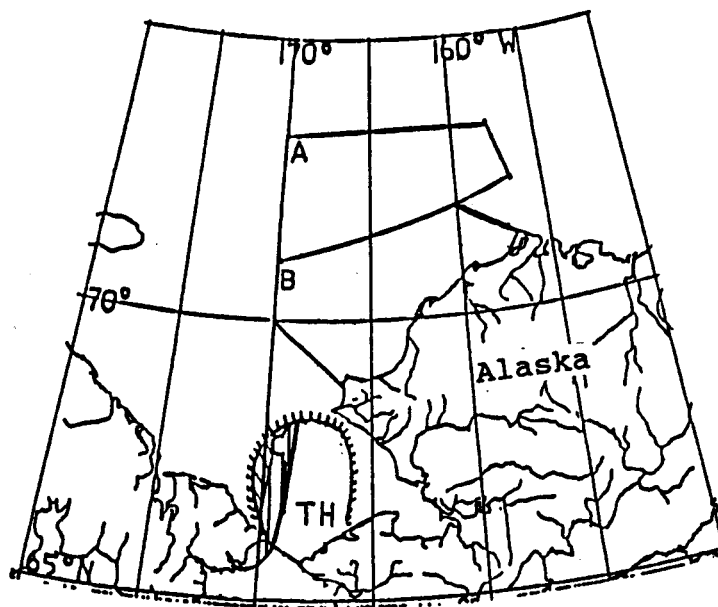


Figure 6b. July SI for the above conditions except with 50 knot winds.

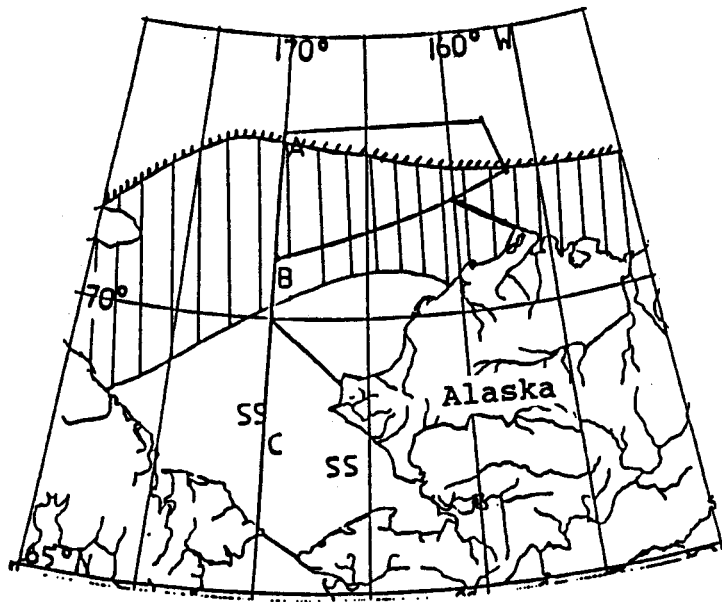


Figure 7a. July SI for conditions of minimum sea ice extent, maximum sea surface temperatures, minimum air temperatures, and 28 knot winds.

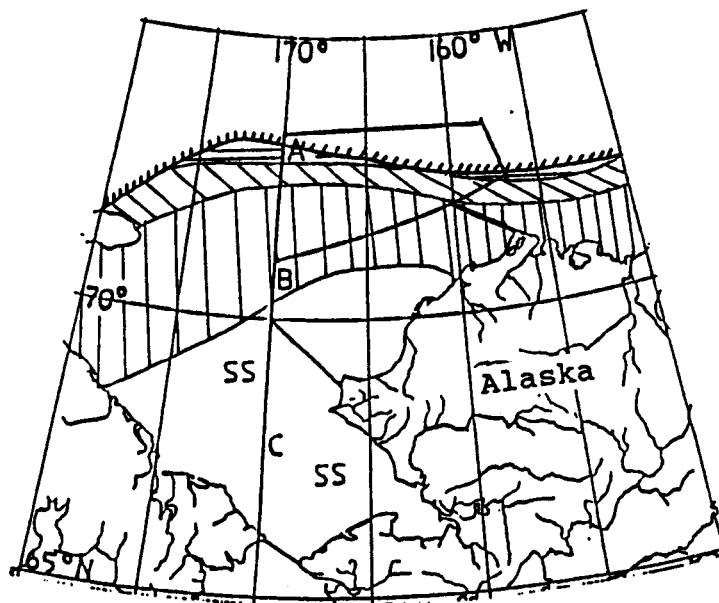


Figure 7b. July SI for the above conditions except with 50 knot winds.

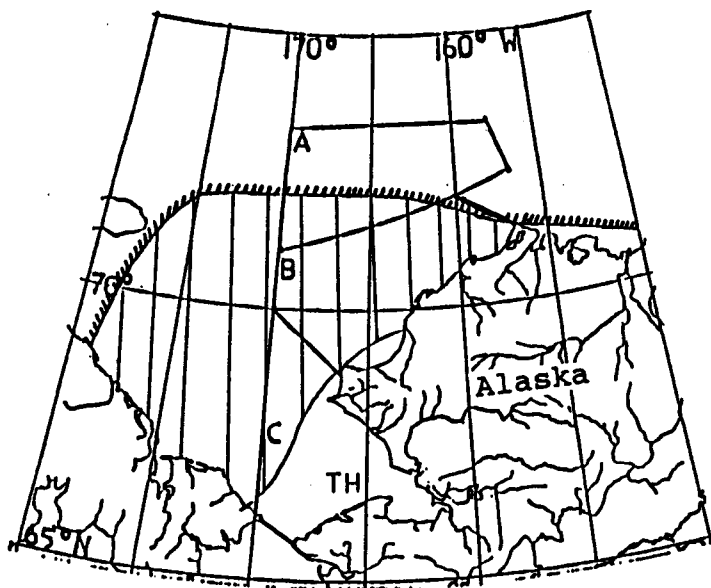


Figure 8a. August SI for conditions of mean sea ice extent, mean sea surface temperatures, minimum air temperatures, and 28 knot winds.

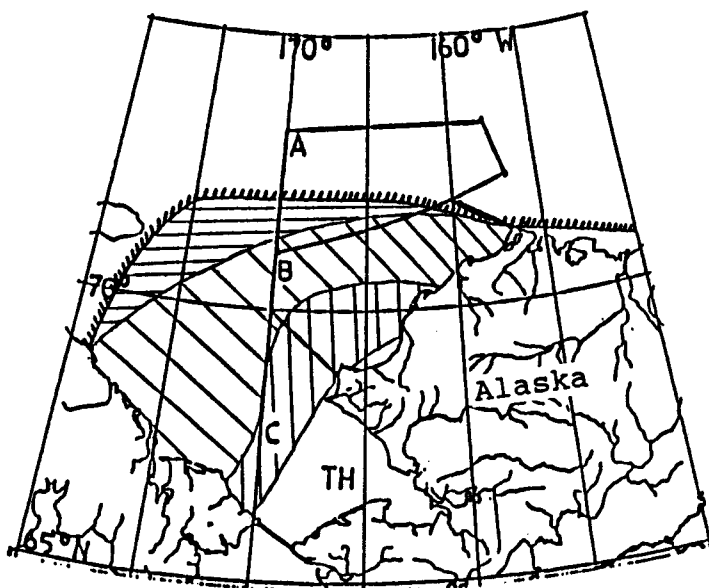


Figure 8b. August SI for the above conditions except with 50 knot winds.

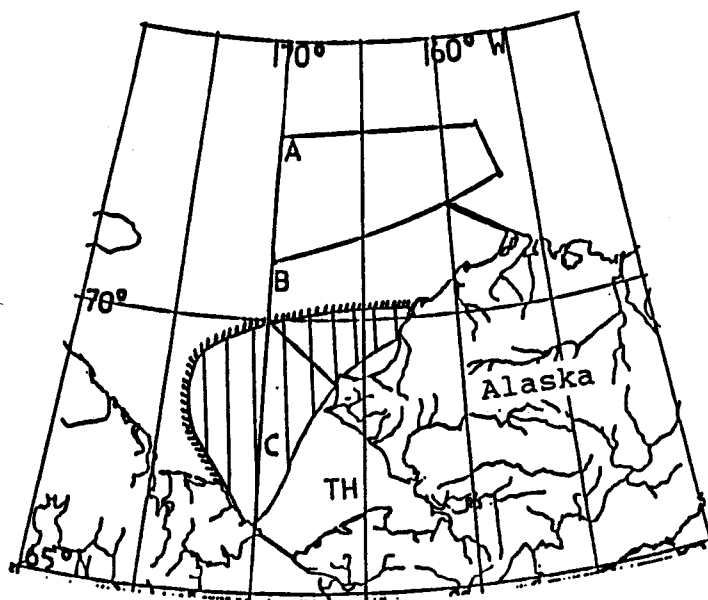


Figure 9a. August SI for conditions of maximum sea ice extent, minimum sea surface temperatures, minimum air temperatures, and 28 knot winds.

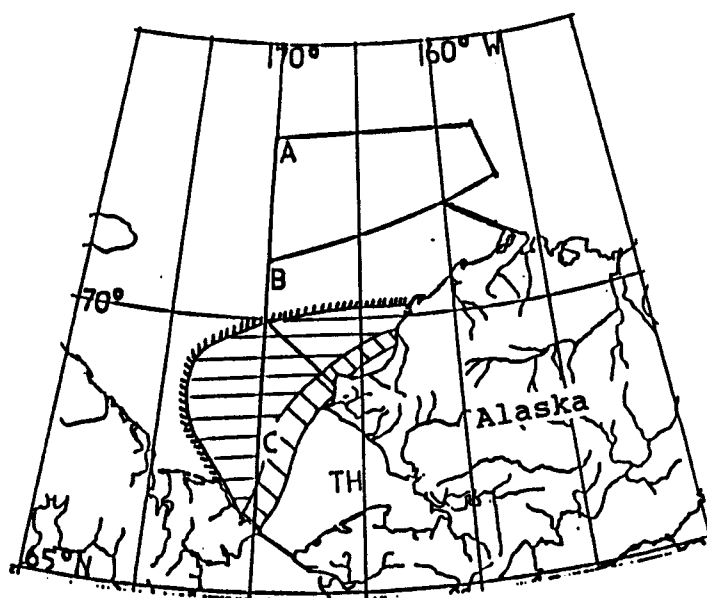


Figure 9b. August SI for the above conditions except with 50 knot winds.

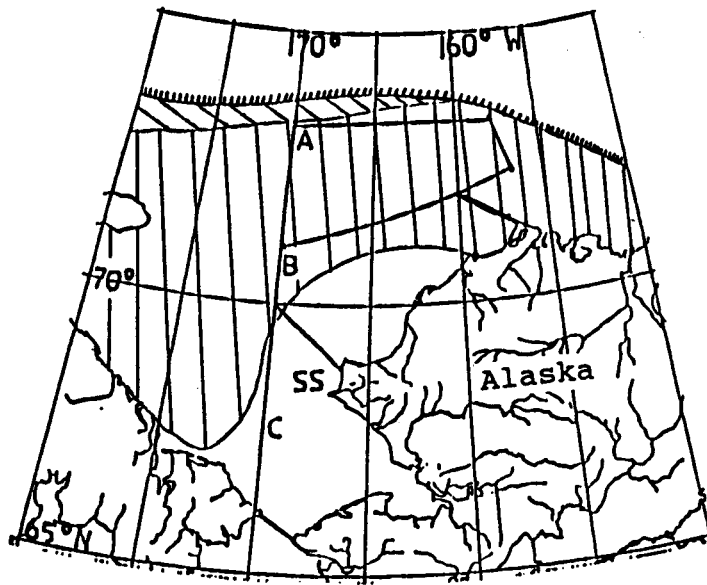


Figure 10a. August SI for conditions of minimum sea ice extent, maximum sea surface temperatures, minimum air temperatures, and 28 knot winds.

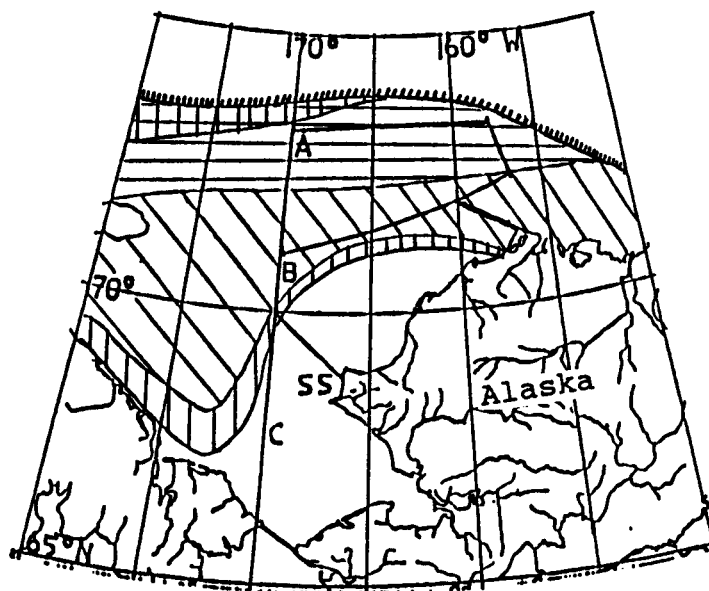


Figure 10b. August SI for the above conditions except with 50 knot winds.

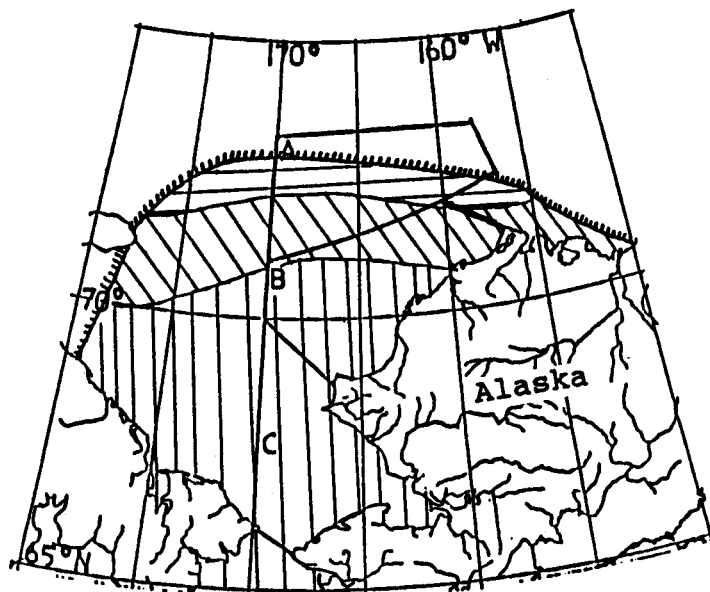


Figure 11a. September SI for conditions of mean sea ice extent, mean sea surface temperatures, minimum air temperatures, and 28 knot winds.

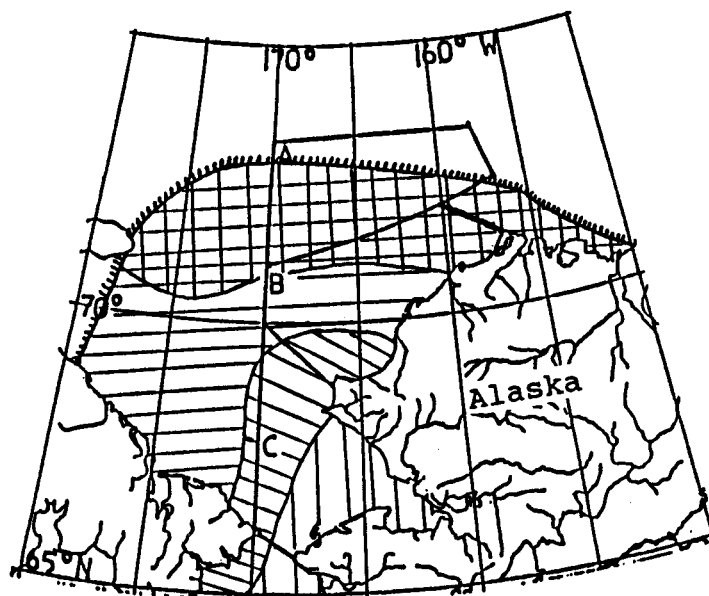


Figure 11b. September SI for the above conditions except with 50 knot winds.

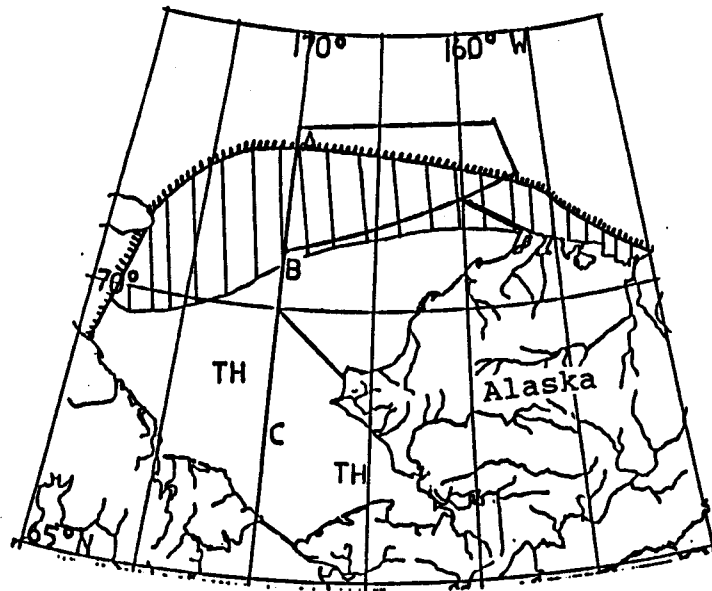


Figure 12a. September SI for conditions of mean sea ice extent, mean sea surface temperatures, mean air temperatures, and 28 knot winds.

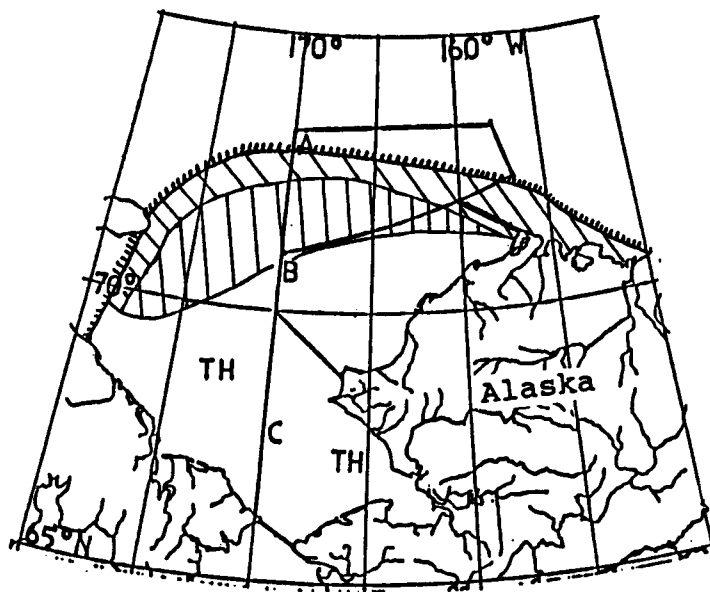


Figure 12b. September SI for the above conditions except with 50 knot winds.

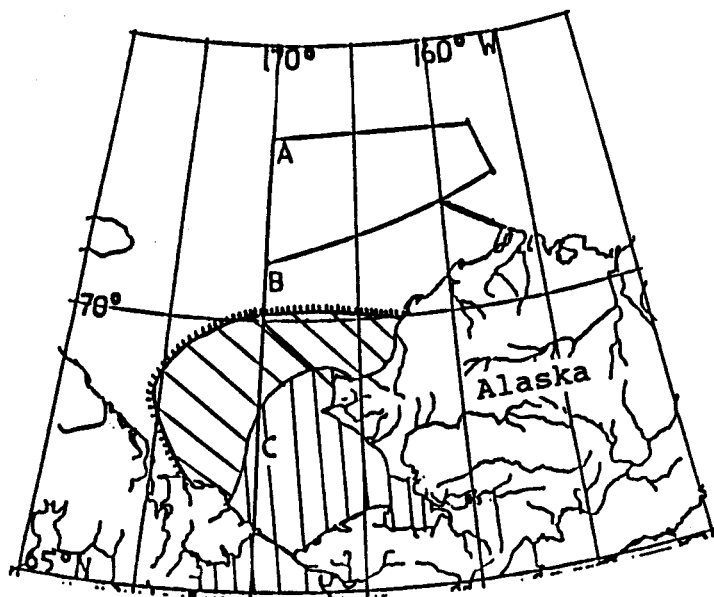


Figure 13a. September SI for conditions of maximum sea ice extent, minimum sea surface temperatures, minimum air temperatures, and 28 knot winds.

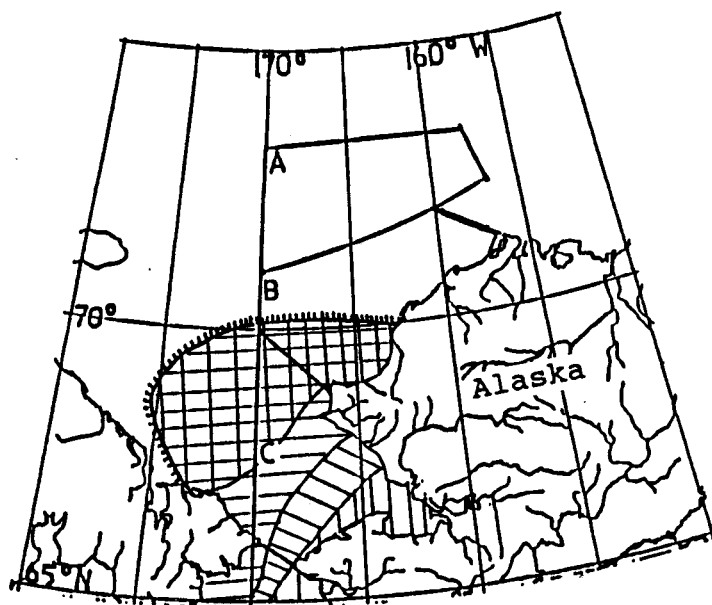


Figure 13b. September SI for the above conditions except with 50 knot winds.

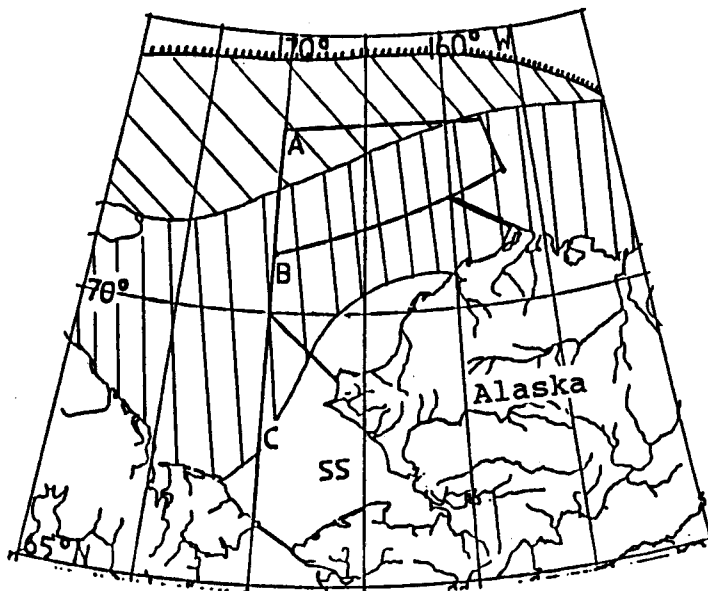


Figure 14a. September SI for conditions of minimum sea ice extent, maximum sea surface temperatures, minimum air temperatures, and 28 knot winds.

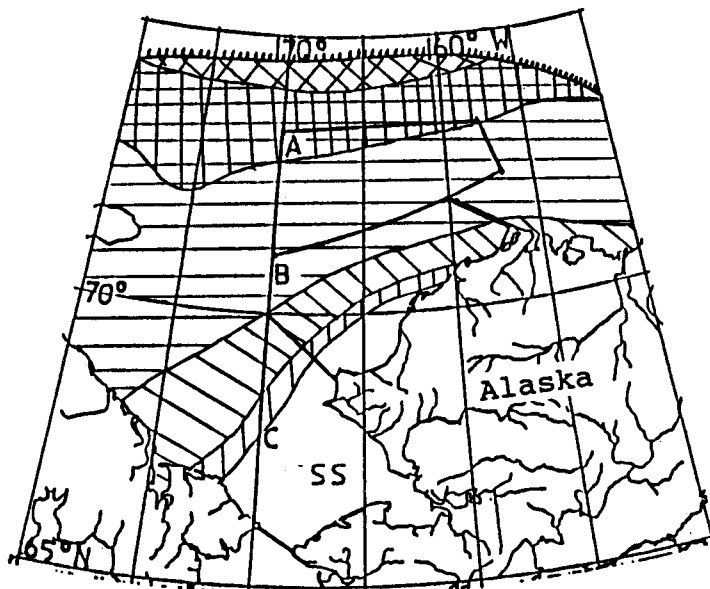


Figure 14b. September SI for the above conditions except with 50 knot winds.

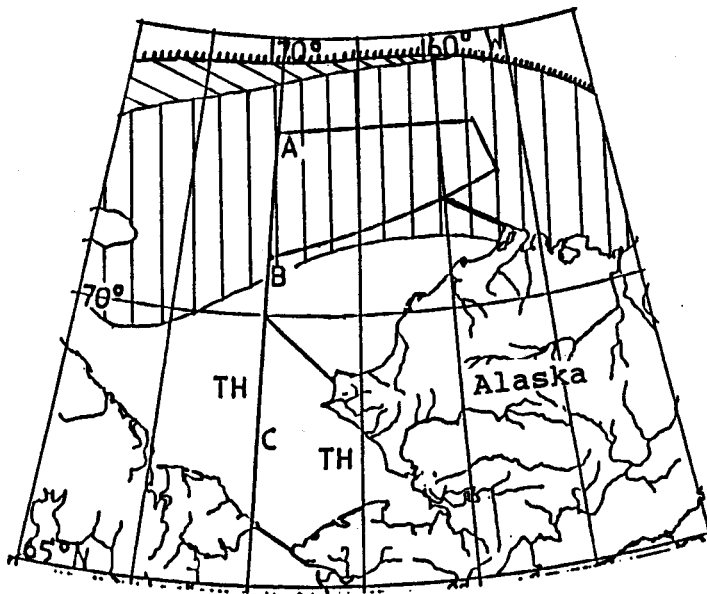


Figure 15a. September SI for conditions of minimum sea ice extent, maximum sea surface temperatures, mean air temperatures, and 28 knot winds.

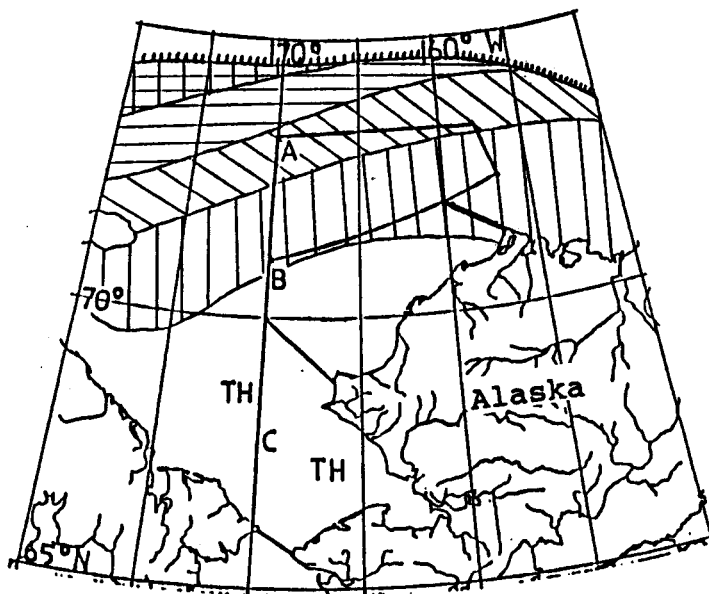


Figure 15b. September SI for the above conditions except with 50 knot winds.

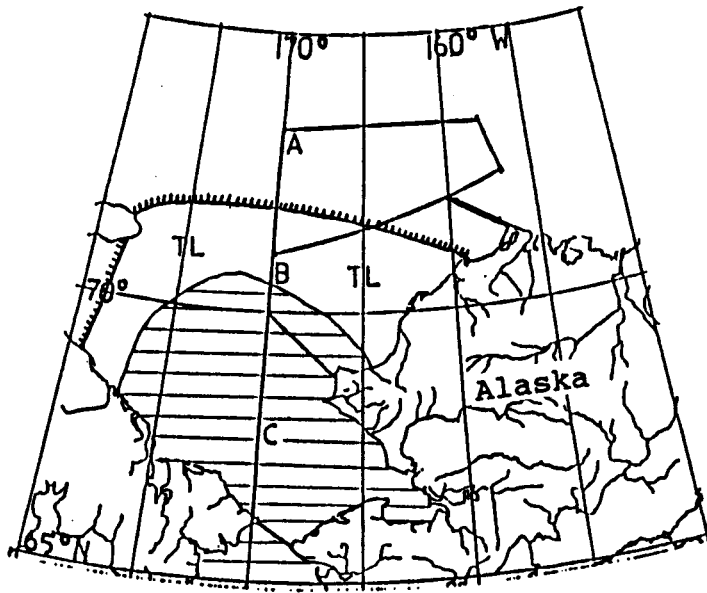


Figure 16a. October SI for conditions of mean sea ice extent, mean sea surface temperatures, minimum air temperatures, and 28 knot winds.

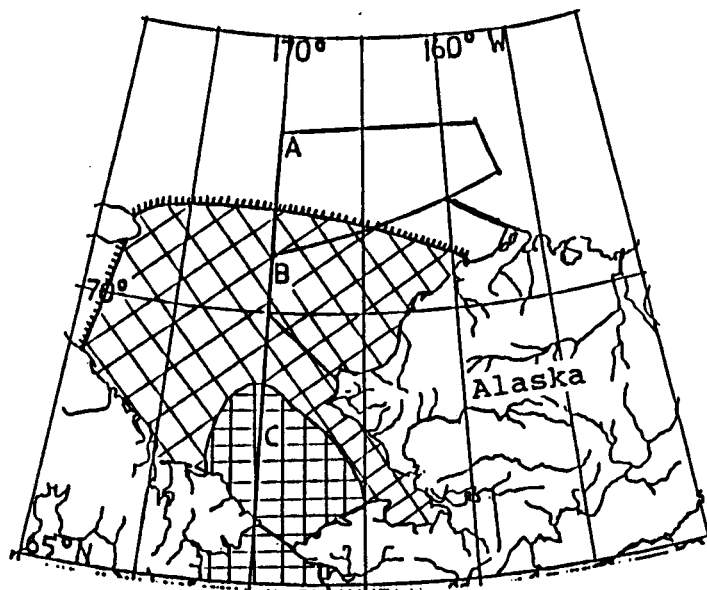


Figure 16b. October SI for the above conditions except with 50 knot winds.

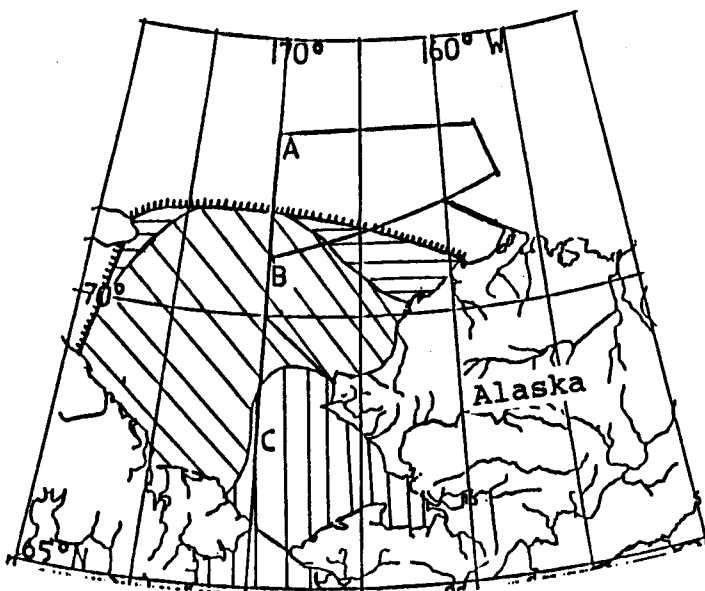


Figure 17a. October SI for conditions of mean sea ice extent, mean sea surface temperatures, mean air temperatures, and 28 knot winds.

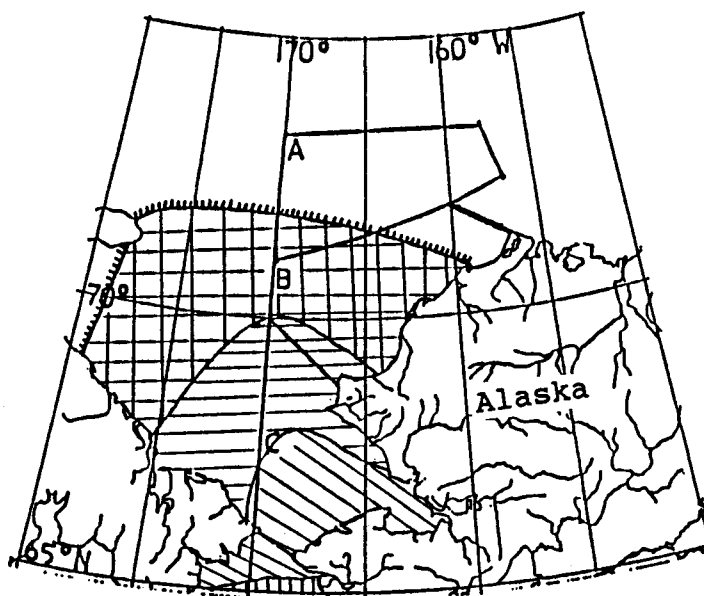


Figure 17b. October SI for the above conditions except with 50 knot winds.

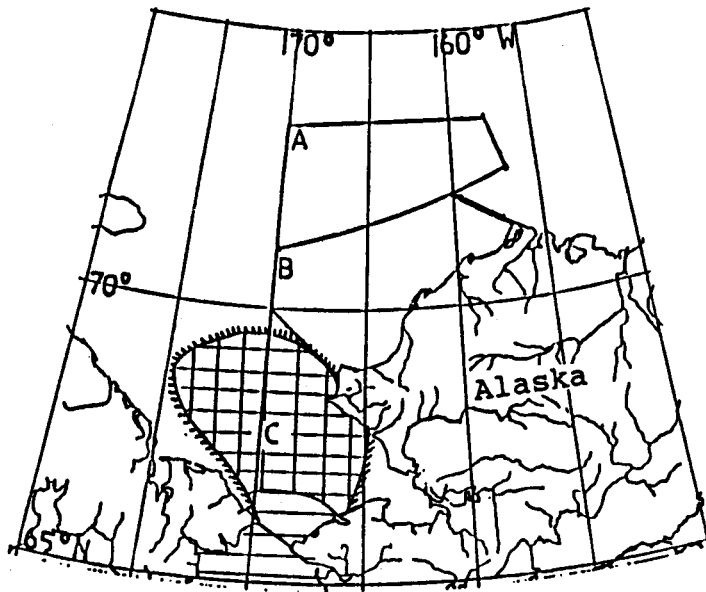


Figure 18a. October SI for conditions of maximum sea ice extent, minimum sea surface temperatures, minimum air temperatures, and 28 knot winds.

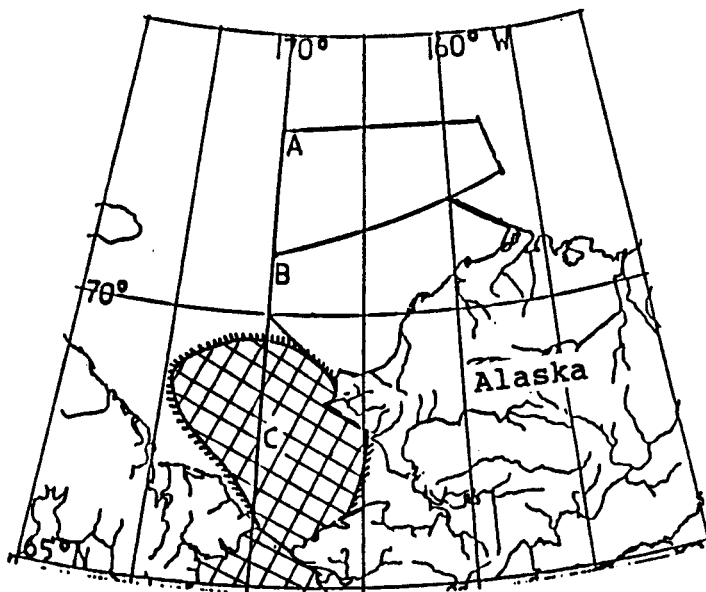


Figure 18b. October SI for the above conditions except with 50 knot winds.

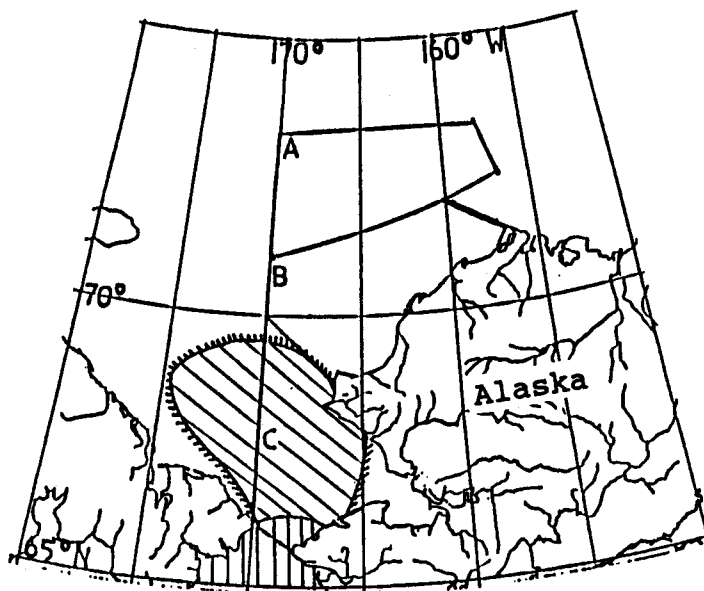


Figure 19a. October SI for conditions of maximum sea ice extent, minimum sea surface temperatures, mean air temperatures, and 28 knot winds.

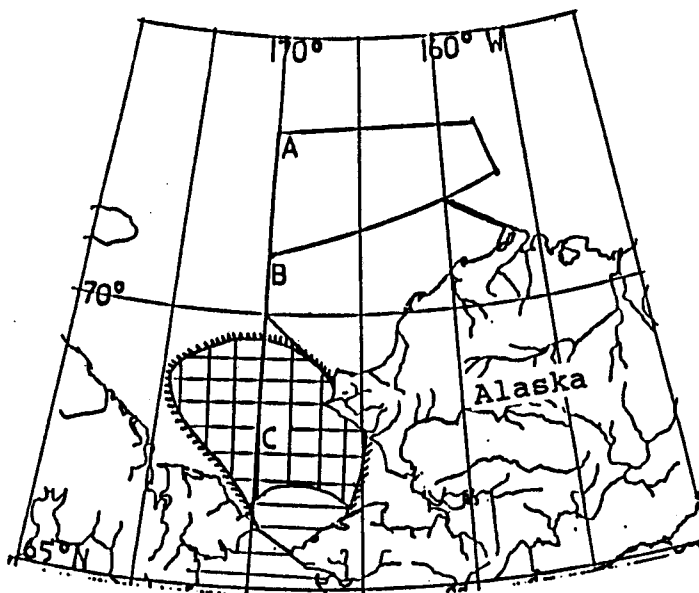


Figure 19b. October SI for the above conditions except with 50 knot winds.

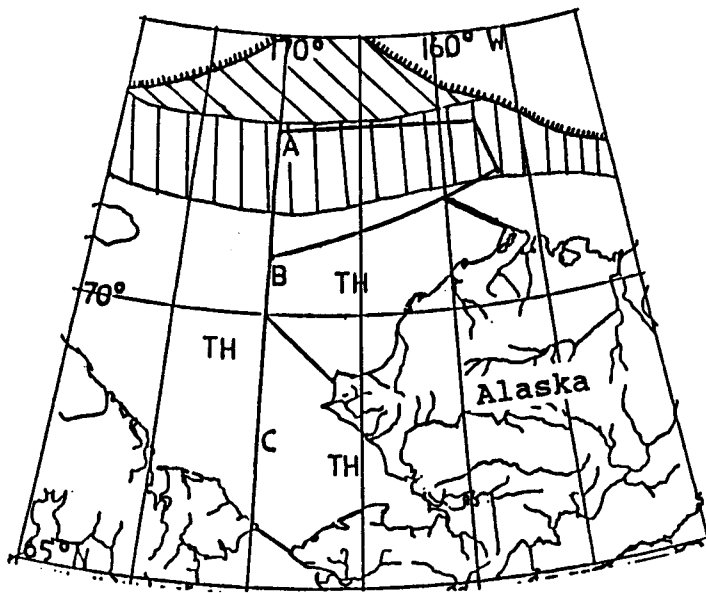


Figure 20a. October SI for conditions of minimum sea ice extent, maximum sea surface temperatures, maximum air temperatures, and 28 knot winds.

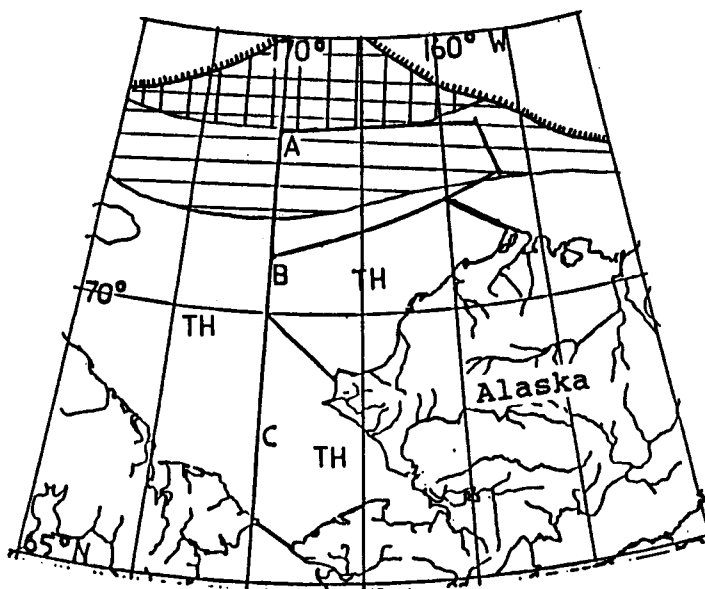


Figure 20b. October SI for the above conditions except with 50 knot winds.

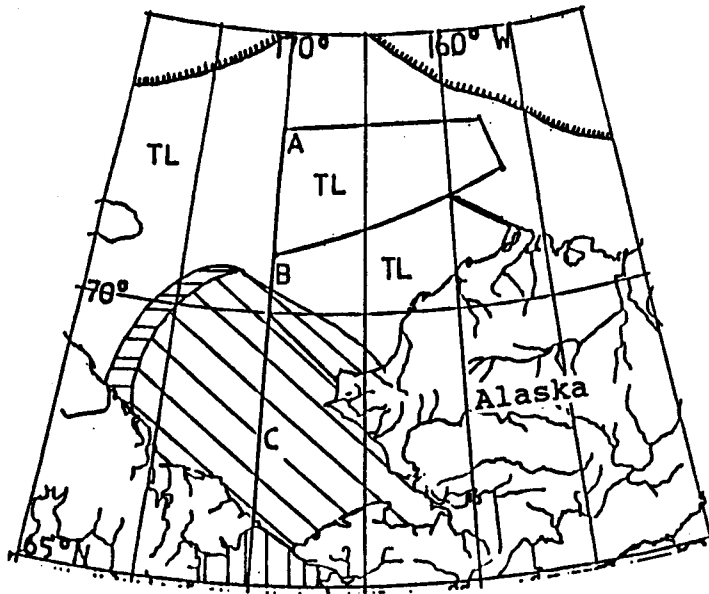


Figure 21a. October SI for conditions of minimum sea ice extent, maximum sea surface temperatures, minimum air temperatures, and 28 knot winds.

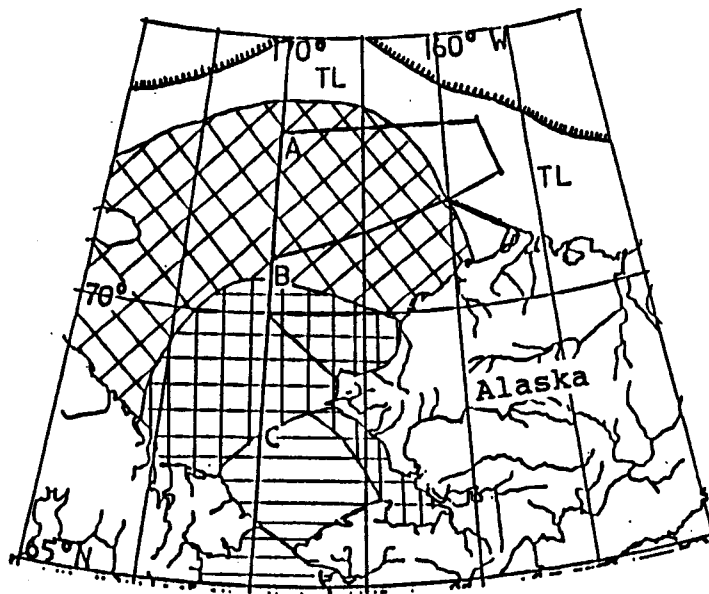


Figure 21b. October SI for the above conditions except with 50 knot winds.

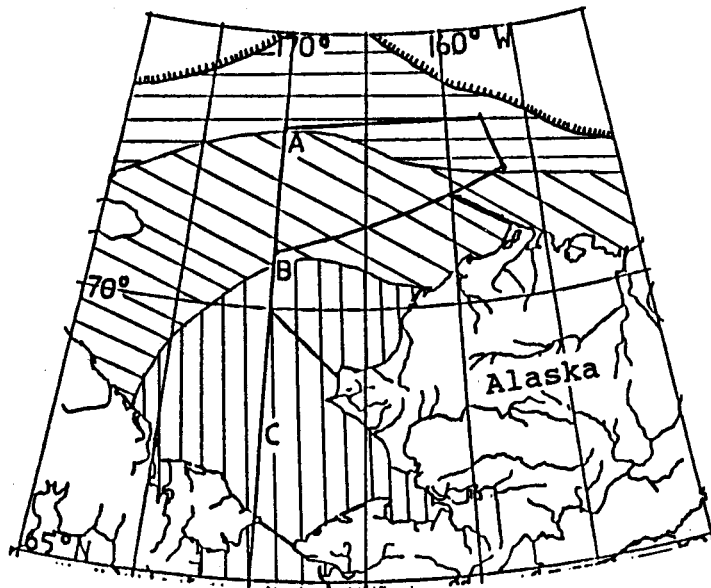


Figure 22a. October SI for conditions of minimum sea ice extent, maximum sea surface temperatures, mean air temperatures, and 28 knot winds.

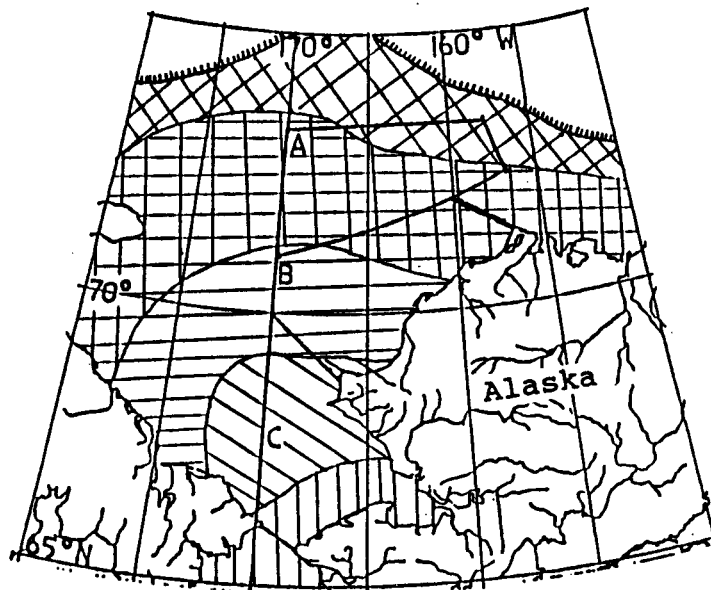


Figure 22b. October SI for the above conditions except with 50 knot winds.

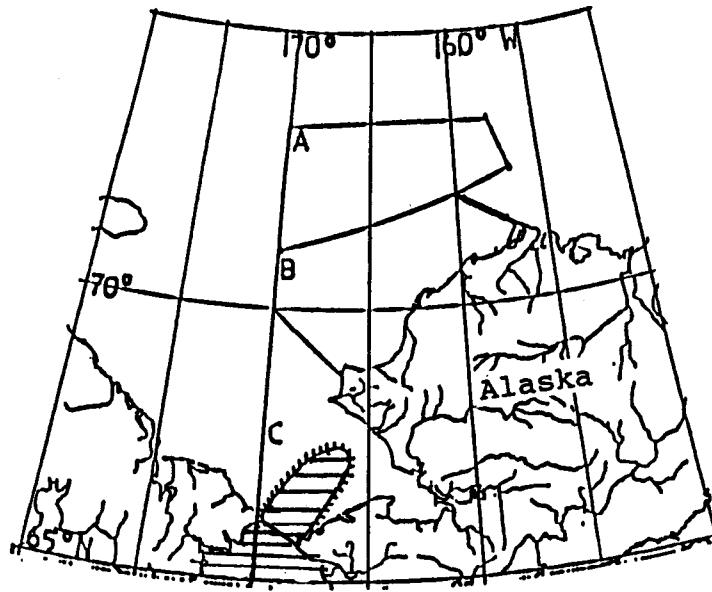


Figure 23a. November SI for conditions of mean sea ice extent, mean sea surface temperatures, mean air temperatures, and 28 knot winds.

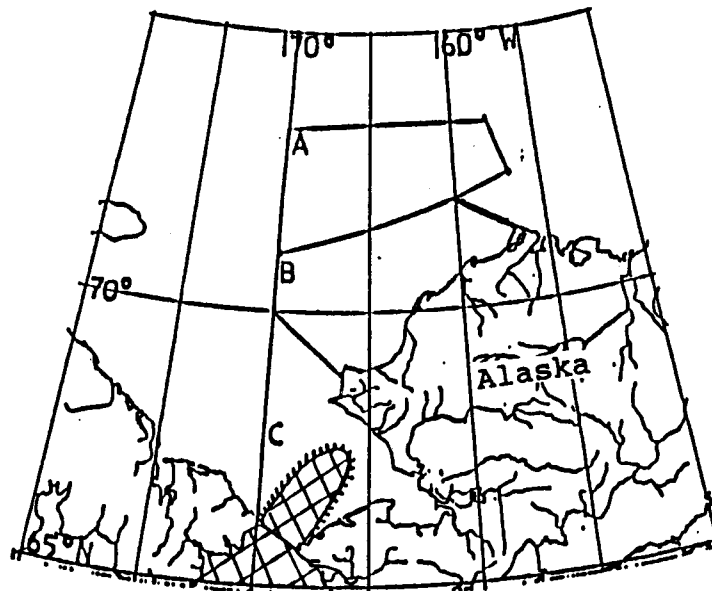


Figure 23b. November SI for the above conditions except with 50 knot winds.

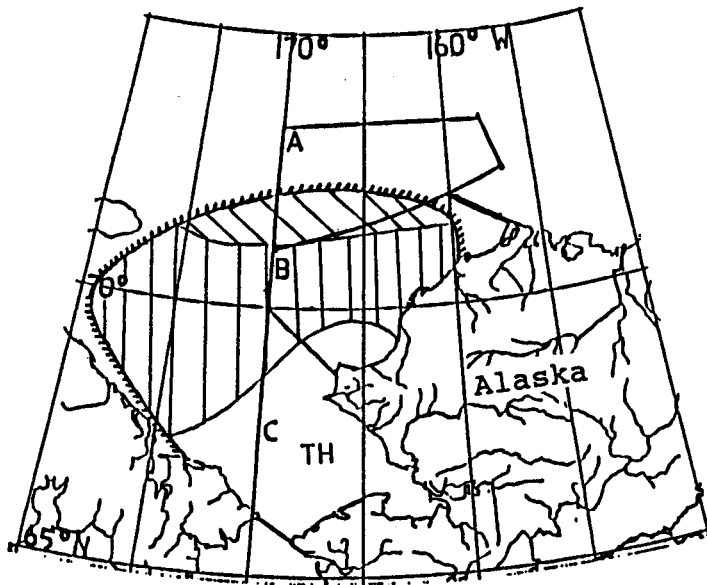


Figure 24a. November SI for conditions of minimum sea ice extent, maximum sea surface temperatures, maximum air temperatures, and 28 knot winds.

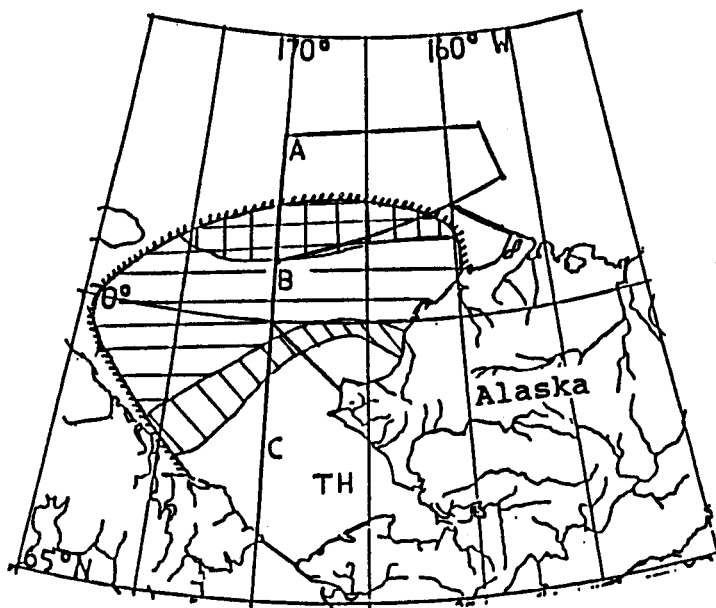


Figure 24b. November SI for the above conditions except with 50 knot winds.

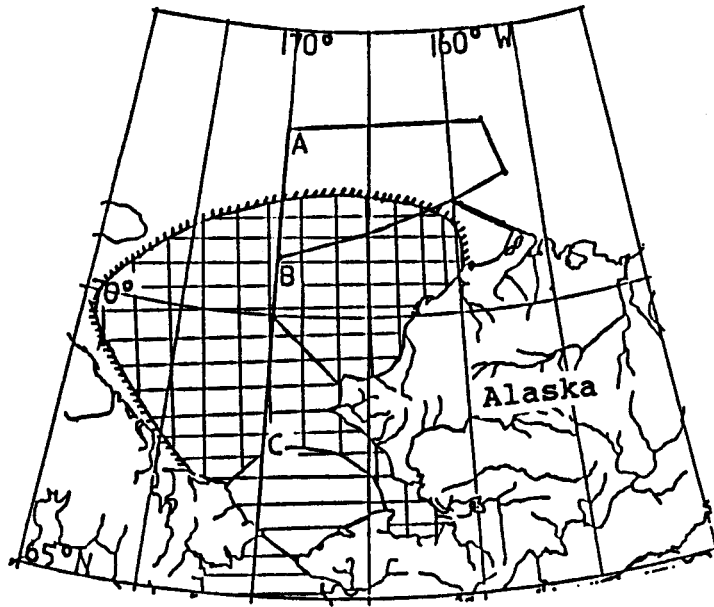


Figure 25a. November SI for conditions of minimum sea ice extent, maximum sea surface temperatures, mean air temperatures, and 28 knot winds.

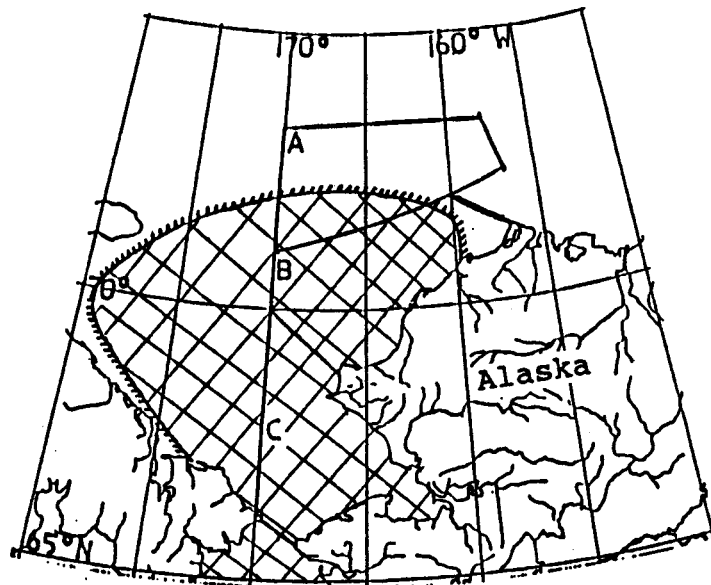


Figure 25b. November SI for the above conditions except with 50 knot winds.

U.S. DEPARTMENT OF COMMERCE
NATIONAL OCEANIC AND ATMOSPHERIC
ADMINISTRATION
NATIONAL OCEAN SERVICE
701 C Street
Box 56
Anchorage, Alaska 99513

OFFICIAL BUSINESS
PENALTY FOR PRIVATE USE \$300

POSTAGE AND FEES PAID
U.S. DEPARTMENT OF COMMERCE
COM-210



PRINTED MATTER

CLASS OF POSTAL SERVICE

BARBARA J. SOKOLOV
ARCTIC ENVIRON INFO AND DATA CTR
UNIVERSITY OF ALASKA
707 A STREET
ANCHORAGE, AK 99501

NOAA FORM 61-13
(9-84)